Physical and Mechanical Behavior of Amorphous Poly(arylene ether)ketone and Poly(arylene ether)ketone Modified Bismaleimides

by

James S. Senger

Dissertation submitted to the Faculty of the

Virginia Polytechnic Institute and State University

in partial fulfillment of the requirements for the degree of

Doctor of Philosophy

in

Materials Engineering Science

APPROVED:

J. E. McGrath, Chairman

G. L. Wilkes

D. A. Dillard

L. T. Taylor

W. W. Stinchcomb

September 28, 1990

Blacksburg, Virginia

Physical and Mechanical Behavior of Amorphous Poly(arylene ether)ketone and Poly(arylene ether)ketone Modified Bismaleimides

by

James S. Senger

J. E. McGrath, Chairman

Materials Engineering Science

(ABSTRACT)

Bisphenol-A based poly(arylene ether)ketones (PAEKs) are tough, amorphous processable thermoplastics possessing a glass transition temperature of approximately 160 °C. In the form of a thermoset, these polymers have potential usages as structural engineering matrix resins or adhesives, as well as modifiers for existing engineering polymers. Thermosets of PAEKs can be prepared through the incorporation of amine, maleimide, or nadimide groups onto the ends of the polymer chains followed by the curing of the materials at elavated temperatures. Plates for mechanical testing, 1/8 inch in thickness or greater, were prepared by first degassing the polymeric powder under vacuum at temperatures 10-50 °C above the Tg of the respective oligomer for short periods of time, followed by compression molding of the resulting material. The networks exhibited high fracture toughness values, as determined by 3 point bend measurements, Tg's around 160 °C as well as a stable rubbery modulus to above 350 °C, as determined by dynamic mechanical measurements. Toughness of these networks increased dramaticly with increasing Mc up to the chain entanglement molecular weight. Tg and rubbery modulus were only slightly altered by Mc. The swelling of these networks in chloroform reveals a two stage increase in solvent absorption. The two stages are believed to be related to the viscoelastic extension of the chains followed by subsequent disentanglement of dangling ends allowing further extension. The toughness behavior of thermoplastic PAEK oligomers versus molecular weight was found to parallel the oligomer's melt viscosity behavior. As a modifier, PAEK cocured with bismaleimide produces network substantially tougher than the unmodified bismaleimide network. Control experiments with non-reactive PAEK oligomers demonstrated the necessity to functionalize the oligomers to

produce the toughening effect. Cocured systems were found to possess a homogeneous morphology while physically blended systems phase separated. Swelling occurred in a single stage, possibly due to the high concentration of functional groups which eliminated dangling ends from the network. These networks possess a Tg at 160 °C, associated with the relaxation of PAEK, and stable rubber modulus of above 350 °C whose absolute value was a function of the BMI/PAEK ratio.

Acknowledgements

Looking back over the past 11 years of my life which I have spent as a student at Virginia Tech, there have been dozens of people who have, in one way or another, given me the support I've needed to get my Ph D. Certainly, this list not only includes my coworkers and professors, but my family and friends as well. I would like to acknowledge them all separately here so that I could highlight the support they have provided, but that would be impractical. Therefore instead, and since I have a sentimental streak in me, I prefer to acknowledge some of those places and events which I will remember my years at Virginia Tech by: Hokie basketball games at the coliseum; movies and chili dogs at Stig's; unit operations lab; Saturday morning basketball; after dinner ping-pong; 5th floor AJ; doughnut eating contests during group meetings; Friday night basketball with the chemistry graduate students; lunch time basketball with the faculty; "burn in hell!";"one more slide"; "hey you"; short courses; summer afternoons on the Tech golf course; Friday nights at Pizza Hut; Saturday nights at Macado's; compression molding; vapor phase osometry; purification of methyl methacrylate; summer evening ice cream breaks; bike rides through Ellite Valley; Dave and Mary Ward's housegroup; Blacksburg Christian Fellowship.

Dedication

During my fifth year as a graduate student, I felt I had just about stomached all of Virginia Tech I could take. After 9 years of school here, with probably several more to go, I had lost hope that there was a light at the end of the tunnel. And even if that light did exist, I saw no reason for trying to reach it. Part of this hopeless feeling came from the sense, that as a scientist, I just did not measure up to those around me. I tried to overcome this feeling by trying to work harder than anyone else; by doing more than what was required from me. This only depressed me further however, when I saw those around me get much credit, while I got none. It was not that I wanted or needed to be best, I just wanted to be appreciated. To make matters worse, over a period of a year, I saw all my friends who I had started school with, some of who I felt very close to, graduate and move away, leaving me behind. I was angry, frustrated, but most of all I felt alone. I considered quitting school.

Then something happened to me that changed my life. I found God. You might ask what do I mean by "I found God". I can only tell you that while I was growing up I always considered myself a good Christian. I went to church religiously, I stayed out of trouble, I believed in God (or at least I thought I did). After I came to college though, I stopped going to church. I guess I stopped going because my religious beliefs really did not mean that much to me. It was then someone told me that for Christianity to mean something, you had to believe in God not only

in your mind, but in your heart as well; and the only way to do that was to ask God to come in and take over your life. I really did not like the thought of doing that at the time because I wanted to run my own life. It was not till this hard time in graduate school that I realized that if I was running my own life, I was doing a pretty rotten job considering how terrible I felt. So I decided to fire myself as the one in charge of my life and ask God to come in and take over. That was the best decision I've ever made, because He has turned my life around. Some people call it being "born again". I can see why, because it was like getting a new start on life. Because upon making my decision to follow God, came a belief in my heart that God really does exist. And once you truely believe that God exists, you are given a hope and a purpose to your life that nothing can take away. It's really a fantastic feeling.

Therefore, I would like to dedicate this thesis to my savior, Jesus Christ, who gave me the opportunity of finding God by dying for me on the cross. Not only did He start a spark in my soul, He placed people in my life who have kindled that spark into a flame, so that they can also find God. I am forever grateful.

Table of Contents

List of Illustrations

List of Tables

Chapter 1 Introduction

The use of high performance engineering thermoplastics and thermosets in such applications as structural composites and electrical equipment has been increasing rapidly over the past 10 years. One category of these materials which is of interest are poly(arylene ether)ketones. Poly(arylene ether)ketones, sold commercially, are semi-crystalline thermoplastics possessing the advantages of toughness, rigidity and thermal stability as well as solvent and creep resistance. They however have the disadvantages of having a melting point greater than 330 °C, making them hard to process, and only a moderately high glass transition temperature (140 to 180 °C), which limits some of their applications as high temperature materials.

The goals of this reasearch were to examine the physical and mechanical properties of two amorphous poly(arylene ether)ketones, polyetherketoneethers, PEKE, and polyetherketoneketoneether, PEKKE, thermosets, cured from fuctionally terminated oligomers, and their analogous thermoplastics. These systems would possess the advantages over the commercial polymers of; ease of processing, due to their amorphous morphology, and higher Tg due to their crosslinked topology. This work also included the thermal and mechanical characterization of bismaleimides modified with maleimide terminated PEKE oligomers. PEKE modified bismaleimides offered the possibility of combining the high rigidity, ease of proc-

essing and high glass transition temperature of the bismaleimides with the toughness of PEKE.

The work required with both research goals included synthesis and chemical characterization of functionalized PEKE and PEKKE oligomers, molding, curing and fabrication of the resulting oligomers into test specimen, and finally physical and mechanical characterization of the resulting thermosets and thermoplastics. A special emphasis was placed on the analysis and understanding of the toughening mechanisms involved in these systems. A chapter is included presenting a systematic examination of the possible molecular scale motions and interactions which might possibly affect fracture toughness.

The literature review presented below discusses some of the basics of mechanics of materials as well as some of the theories behind mechanical behavior of polymers. This is included to act as a foundation for arguments used in the results and discussion chapters. Poly(arylene ether)ketones and bismaleimides are also reviewed.

Chapter 2 Mechanics

This section will review the principles of mechanics and fracture mechanics so as to define the terms and concepts which will be used in later discussions. This is not meant as an all inclusive presentation of these materials, but rather an overview. The interested reader should refer to one or more of these texts [1,2,3,4] for a more indepth study of these subjects.

2.1 Mechanics of Materials

The science of mechanics deals with the reaction of a body to an applied force. A force, when applied to a body which is free to float in space, induces an acceleration inversely proportional to the body's mass,

$$\text{FORCE} = \text{MASS} \times \text{ACCELERATION} \qquad [2.1]$$

A force which is applied to a fixed body must be counterbalanced by an equal but opposite force for that body to remain stationary. The sum of the forces is therefore equal to zero. However, these forces do cause the body to undergo deformation and, possibly, fracture. The

science of mechanics of materials predicts the magnitude of deformation and the force at failure of materials under load.

2.1.1 Stress and Strain

Two concepts exist which are the foundation for all of mechanics of materials, stress and strain. When a load is placed on a body, it acts only over a given area of that body. Stress is defined as the magnitude of the applied load per unit area of the affected surface,

$$\text{STRESS} = \frac{\text{FORCE}}{\text{AREA}} \qquad [2.2]$$

Strain is defined as the magnitude of elongation or distortion of the body caused by the load. Both stress and strain can be broken down into components acting normal and tangential to the body's surface (Figure 1). These components are referred to as normal and shear stress and strain.

2.1.1.1 Normal Stress and Strain

Normal stress, σ_i, acts perpendicular to the surface causing either an elongation (positive stress) or a compression (negative stress) of the body along the direction of the normal stress. The axis along which the stress is applied is denoted by the subscript i. The normal strain is equal to the change in length of the body along the normal axis divided by its original length,

$$\varepsilon_i = \frac{\Delta L}{L} \qquad [2.3]$$

2.1.1.2 Shear

Shear stress, denoted by τ_{ij}, acts parallel to the surface causing a distortion of the body

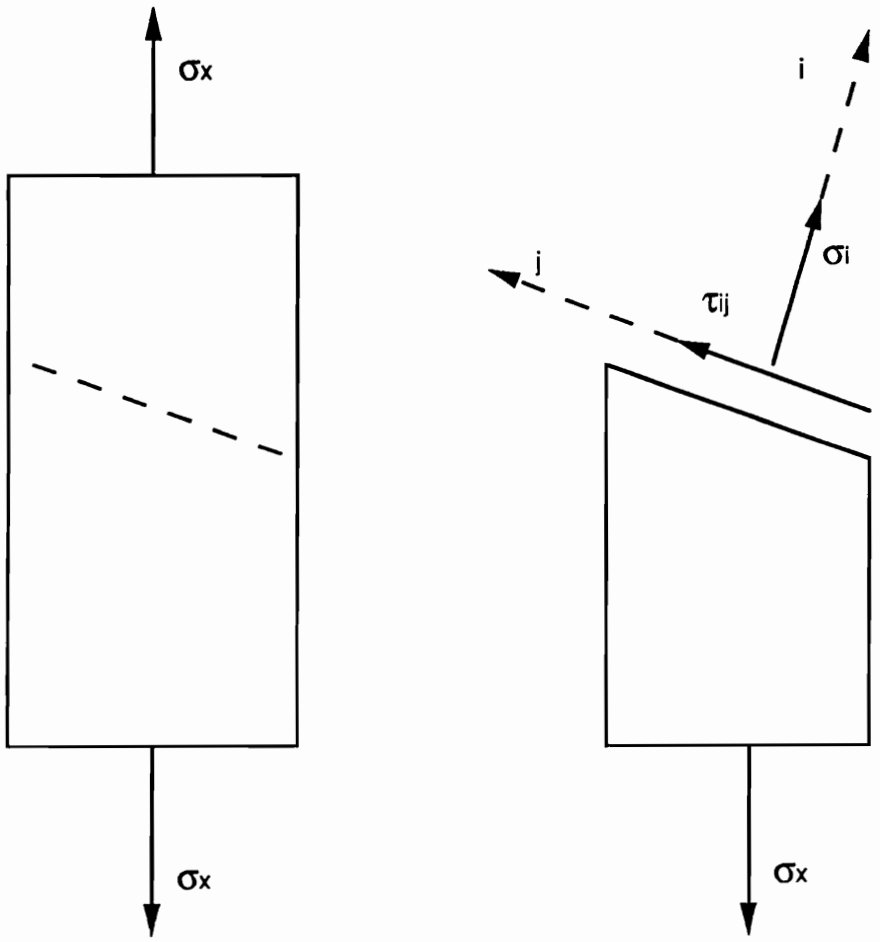

Figure 1. Normal and shear stress components of an applied load

by shifting the cross-sections which lie parallel to the surface, relative to one another (Figure 2). The subscripts i and j denote the axis normal to the plane of the stress and the axis parallel to the stress, respectively. Strain due to shear, denoted by γ_{ij} is not measured as a change in length, but rather it is defined as the angle of distortion.

2.1.1.3 Poisson's Ratio

A normal tensile and compressive stress not only can induce deformation along its own axis, but also along the two transverse coordinate directions perpendicular to the stress axes. The magnitudes of strain along the two perpendicular axes are proportional to and opposite in sign to the strain in the stress direction. For example, if a tensile stress lies along the x axis, then a negative strain will occur along the y and z axis (Figure 3). The proportionality constant which relates the magnitude of the strains is referred to as Poisson's ratio, μ_{ij}, a material property,

$$\varepsilon_j = -\mu_{ij}\varepsilon_i \qquad [2.4]$$

where i denotes the direction of the axial strain and j denotes the direction of the resultant transverse strain.

2.1.2 Stress versus Strain

A relationship between stress and strain for a given material is usually obtained by subjecting a test specimen to a range of strains and then calculating the resulting stresses from the measured loads. The result can vary for a given material depending on the mode of loading which is applied. For example, concrete exhibits a stress at fracture which is nearly 15 times greater under a compressive load than under a tensile load.

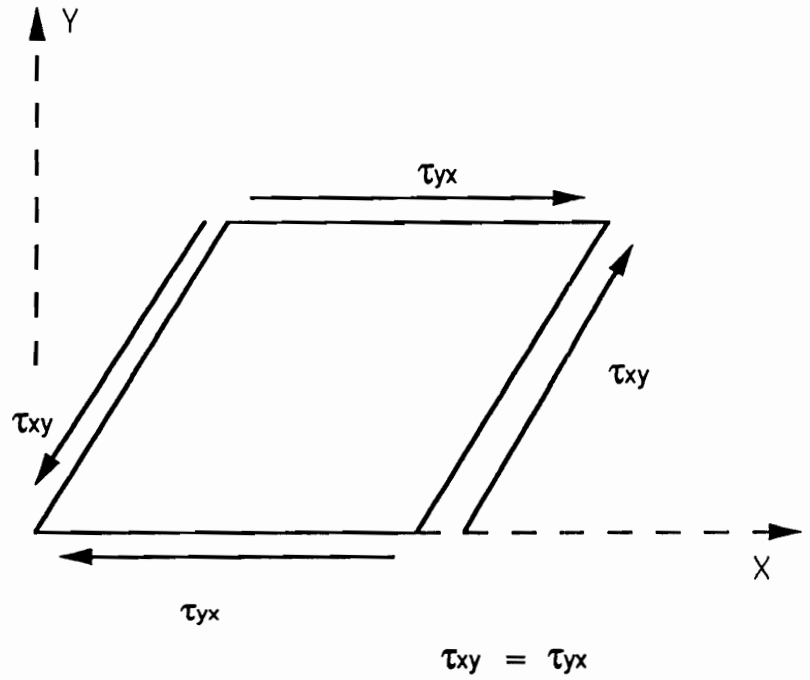

Figure 2. Effect of shear stress

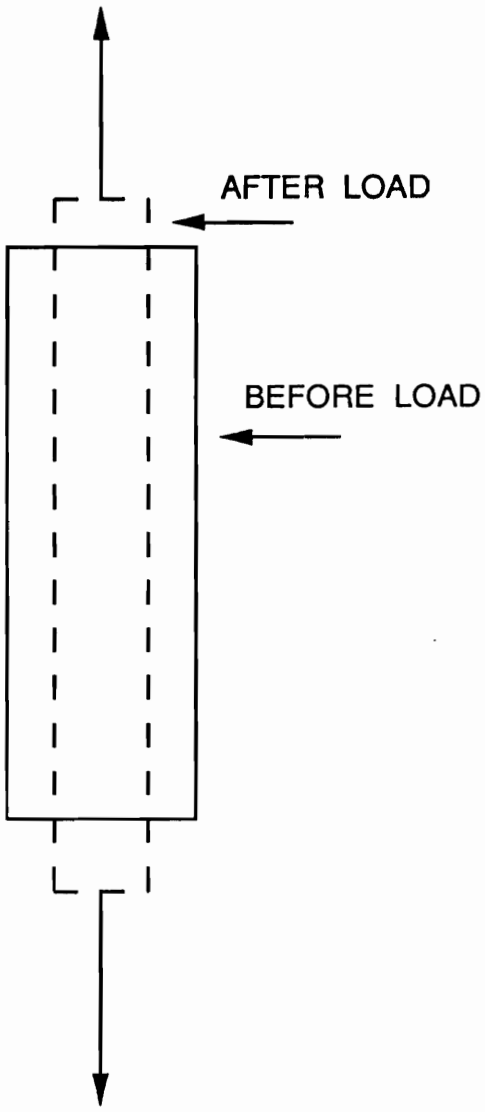

Figure 3. Induced strain transverse to an applied normal load

2.1.2.1 Tensile Testing

Tensile tests are usually considered the quickest and experimentally most feasible method to obtain a one dimensional stress-strain relationship. Therefore, they are typically the method used to compare the mechanical responses for different materials. The specimen which is used for tensile testing is shaped as either a flat dogbone or a tapered cylinder. It is clamped at each end to the crossheads of a mechanical testing machine such as an Instron. The crossheads are displaced in opposite directions at a constant displacement rate with the applied tensile force measured by a load cell. The stress that is caused by this displacement is calculated by dividing the applied load by the cross sectional area of the tapered region. The cross sectional area, however, decreases during the test thereby creating two means of reporting stress. Engineering stress is defined as the applied load divided by the original cross sectional area while true stress is equal to the load divided by actual area.

2.1.2.2 Elastic Plastic Response

The tensile response of a theoretical elastic plastic material can be described through the combined responses of a Hookean spring connected in series to two boards which are prevented from sliding past one another due to friction (Figure 4). The Hookean spring represents the inital response of the material which is referred to as elastic behavior (Figure 5). Stress increases proportionally with strain with the slope of the line defined as the material's tensile or Young's modulus, denoted by E,

$$\sigma = E\varepsilon \qquad [2.5]$$

The modulus is a measure of the stiffness of the material and has the units of force per unit area. Equation [2.5] applies for a linear elastic isotropic homogeneous material under one dimensional loading.

The material alters its response when stress is increased to a critical level known as the yield stress. Friction between the two boards is overcome, allowing them to slide past one

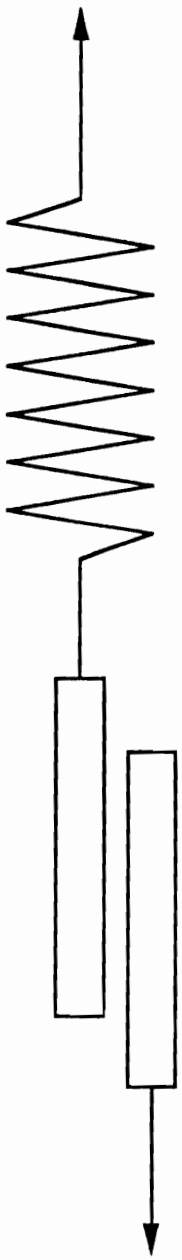

Figure 4. Model of an elastic plastic material

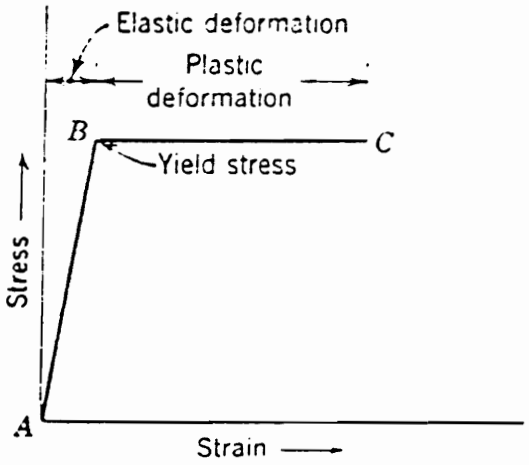

Figure 5. Tensile test of a perfect elastic plastic material [5]

another under a constant stress. This region of response is referred to as plastic behavior. The boards continue to slide past one another until failure.

The total strain of the combined elements is equal to the sum of the elastic and plastic strains. The removal of the stress before failure causes the loss of the elastic strain as the spring attempts to return to its original length. The plastic portion is retained, however, since friction prevents the boards from sliding back over one another. The residual plastic strain is referred to as permanent plastic deformation, or sometimes as permanent set.

2.1.2.3 Strain Energy

The retention of plastic strain in actual materials is related to the loss of strain energy. As a material is strained, energy is transferred from the surroundings to the material. This energy is either stored in the form of elastic strain energy or lost as heat during plastic deformation. Since energy is equal to force multiplied by displacement, the magnitude of the elastic and plastic energy components is equal to the integrated area under a stress-strain curve,

$$U_T = U_E + U_P = \int_0^{\varepsilon_T} \sigma \, d\varepsilon \qquad [2.6]$$

where:

U_T = total energy per unit of volume

U_E = elastic strain energy per unit of volume

U_P = plastic energy per unit of volume

ε_T = total strain

σ = applied stress = function of strain

For the case of an ideal elastic plastic material (Figure 5),

$$U_E = \frac{1}{2} \sigma_o \varepsilon_E \qquad [2.7]$$

$$U_P = \sigma_o(\varepsilon_T - \varepsilon_E) \qquad [2.8]$$

where:

σ_o = yield stress

ε_E = elastic strain

Upon removal of the stress, the material must dissipate an equal amount of energy in order to regain its original dimensions. Since, only the elastic portion of the energy is available, only the elastic portion of the strain is lost.

2.1.3 Stress Transformation

The tensile force, which is transmitted through each of the specimen's cross sections, produces a normal stress on those cross sections lying perpendicular to it and a shear stress to those cross sections lying at an angle to it (Figure 1). The magnitude of these stresses, varies with the angle between the cross section and the force (Figure 6)

$$\sigma_x = \frac{\sigma_x}{2} + \frac{\sigma_x}{2}\cos 2\theta \qquad [2.9]$$

$$\tau_{xy} = -\frac{\sigma_x}{2}\sin 2\theta \qquad [2.10]$$

where:

θ = the angle between the cross section and the tensile load

σ_x = the normal stress to the cross section

τ_{xy} = the shear stress to the cross section

The planes of maximum and minimum normal and shear stresses can be determined by differentiating equations 2.9 and 2.10 with respect to θ, and setting the resulting equations equal to zero,

$$- \sigma_x \sin 2\theta = 0 \qquad \text{NORMAL STRESS} \qquad [2.11]$$

$$- \sigma_x \cos 2\theta = 0 \qquad \text{SHEAR STRESS} \qquad [2.12]$$

Normal stress reaches a maximum at 0 and 180 degrees, perpendicular to the load, and a minimum at 90 degrees, parallel to the load. Shear stress reaches its maximum in magnitude at 45 and 135 degrees with its minimum of zero at 0, 90 and 180 degrees. The plane where the shear is zero are referred to as principal planes. The normal stresses acting on these planes are referred to as principal stresses. These principal stresses, for the case of a tensile test, coincide with the normal stresses along the x, y and z axes,

$$\sigma_1 = \sigma_x \qquad [2.13]$$

$$\sigma_2 = \sigma_y = 0 \qquad [2.14]$$

$$\sigma_3 = \sigma_z = 0 \qquad [2.15]$$

where, σ_1, σ_2 and σ_3 are principal stresses. The principal and coordinate stresses, however, usually do not coincide for more complex loading conditions.

Figure 7 shows an example of an elemental body under a two dimensional complex state of stress. The magnitude of the normal and shear stresses along with their maximums and minimums are given by equations,

$$\sigma_x' = \frac{\sigma_x + \sigma_y}{2} + \frac{\sigma_x - \sigma_y}{2} \cos 2\theta + \tau_{xy} \sin 2\theta \qquad [2.16]$$

$$\sigma_y' = \frac{\sigma_x + \sigma_y}{2} - \frac{\sigma_x - \sigma_y}{2} \cos 2\theta - \tau_{xy} \sin 2\theta \qquad [2.17]$$

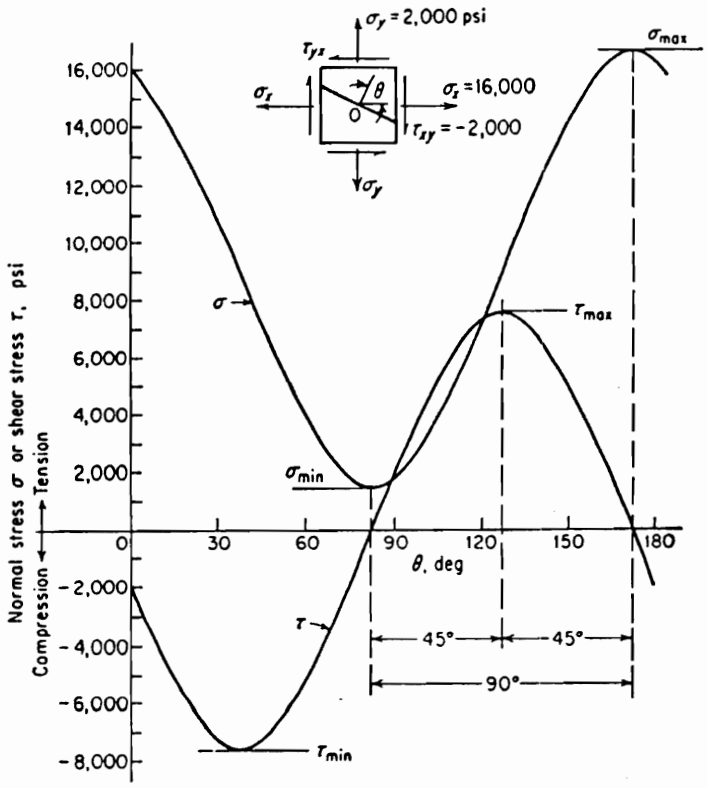

Figure 6. Normal and shear stresses vs. angle of cross section [2]

$$\tau_{xy}' = -\frac{\sigma_x - \sigma_y}{2} \sin 2\theta + \tau_{xy} \cos 2\theta \qquad [2.18]$$

$$\sigma_x', \sigma_y' \begin{matrix}\max \\ \min\end{matrix} = \frac{\sigma_x + \sigma_y}{2} \pm \sqrt{\left(\frac{\sigma_x - \sigma_y}{2}\right)^2 + \tau_{xy}^2} \qquad [2.19]$$

$$\tau_{xy}' \begin{matrix}\max \\ \min\end{matrix} = \pm \left[\left(\frac{\sigma_x - \sigma_y}{2}\right)^2 + \tau_{xy}^2\right] \qquad [2.20]$$

2.1.4 Hydrostatic and Deviatoric Stress

It can be concluded from equations 2.19 and 2.20 that the applied normal and shear stresses act together to produce the normal and shear stresses acting on any of the various cross sections of the material. This combined stress state can produce two mechanical responses from the material, elastic volume change and plastic deformation.

Elastic volume change is created by a hydrostatic stress. Hydrostatic stress, sometimes referred to as the mean stress, can be defined as an uniform normal stress field surrounding a body (Figure 8). Its magnitude is equal to the average of the normal stresses,

$$\sigma_h = \sigma_m = \frac{\sigma_x + \sigma_y}{2} \qquad \text{2D case} \qquad [2.21]$$

where:

σ_h = hydrostatic stress

σ_m = mean stress

The hydrostatic stress equals the minimum normal stress which can act on a cross section and is represented by the first term in equations 2.9, 16, 17, 19. No plastic deformation is

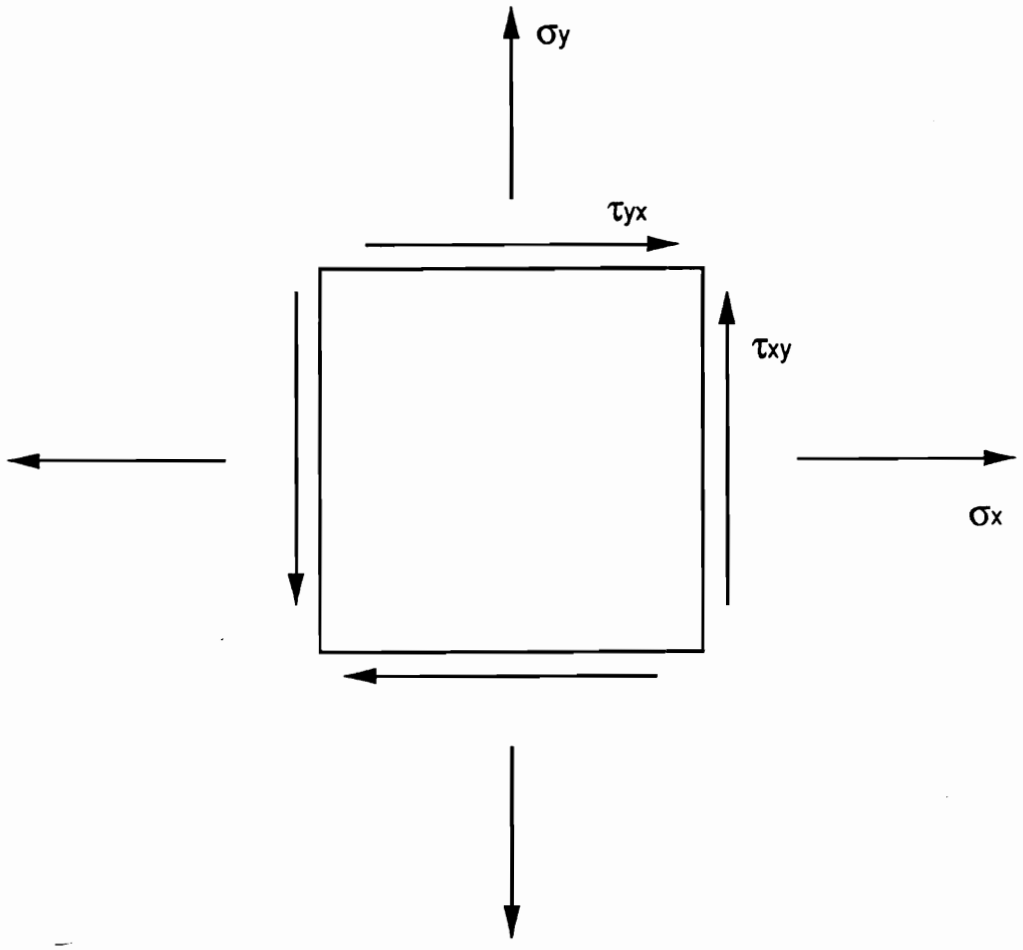

Figure 7. Elemental cube subjected to a complex biaxial stress state

produced by a hydrostatic stress, therefore, at critical stress levels the material fails in a brittle mode without undergoing any plastic deformation.

Plastic deformation is produced through a deviatoric stress. The deviatoric stress is a combination of the applied shear stress plus the transformable portions of the normal stresses. These transformable portions are equal to each normal stress minus the hydrostatic stress,

$$\sigma_{xd} = \frac{\sigma_x - \sigma_y}{2} \qquad [2.22]$$

$$\sigma_{yd} = \frac{\sigma_y - \sigma_x}{2} \qquad [2.23]$$

where:

σ_{xd} = deviatoric normal stress in the x-direction

σ_{yd} = deviatoric normal stress in the y-direction

These stresses produce a shear as shown in Figure 9. The deviatoric normal stresses are represented by the second terms in equations 2.9, 16, 17, 19 and the first terms in equations 2.18 and 2.20, while deviatoric shear stresses are represented by the last terms in equations 2.16-20. It should be noted that the equations for normal stresses (Equations 2.9,16,17,19) *all* contain a hydrostatic and a deviatoric stress term. The equations for shear stresses (Equations 2.10,18,20), however, only possess a deviatoric term. This means that normal stresses can produce plastic deformation but shear stresses cannot produce brittle fracture.

2.1.5 Plane Stress and Strain

Figure 7 shows an elemental cube subjected to a biaxial stress state. All the stresses are contained within the xy plane with the stresses lying in the z direction equal to zero.

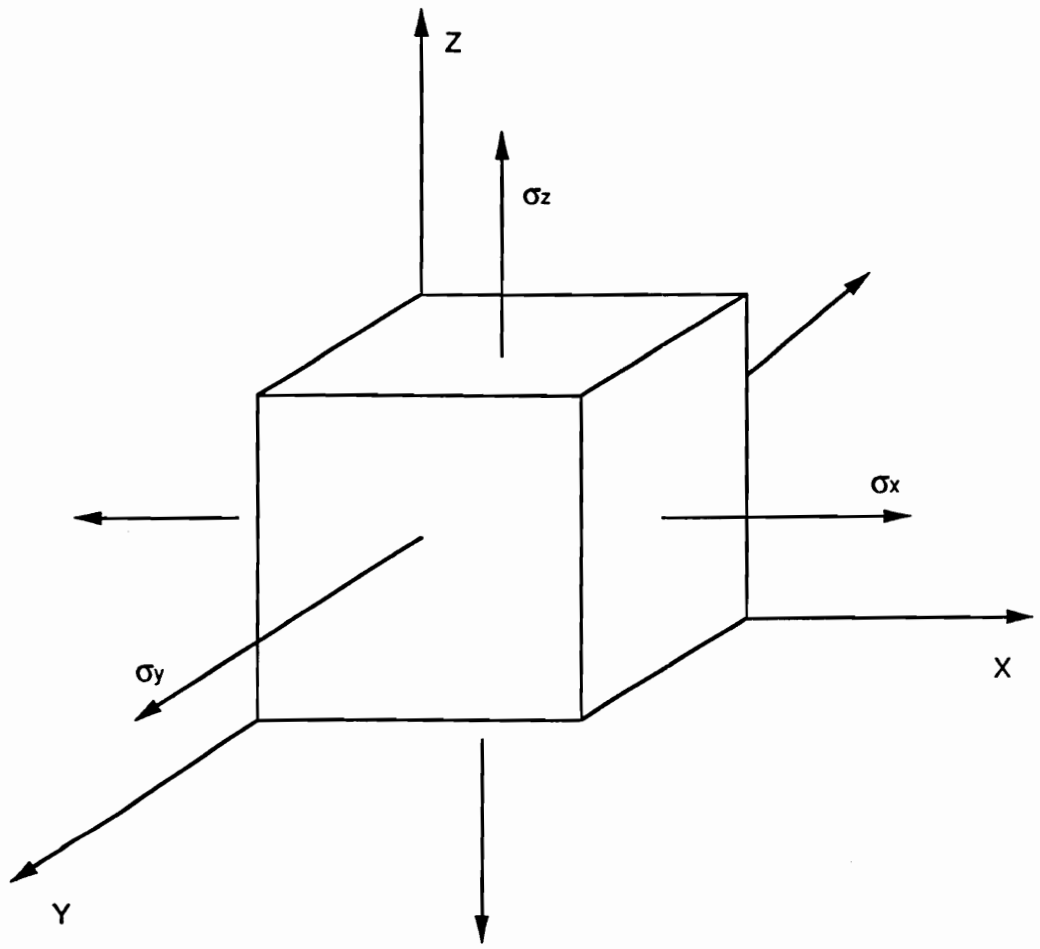

Figure 8. Elemental cube subjected to a hydrostatic stress

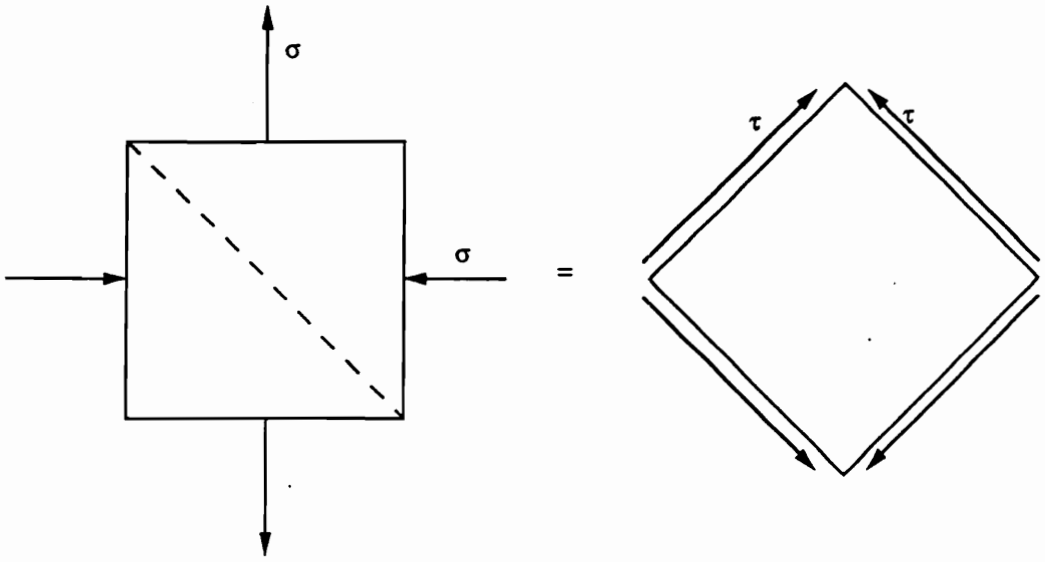

Figure 9. Transformation of normal stresses to shear stresses

$$\sigma_z = \tau_{xz} = \tau_{yz} = 0 \qquad [2.24]$$

This condition is referred to as plane stress. The surface normal to the z axis is free to elongate or contract in accordance to poisson's ratio,

$$\varepsilon_z = -\frac{\mu}{E}(\sigma_x + \sigma_y) \qquad [2.25]$$

The strain in this direction is eliminated, however, if an opposing normal stress equal to $\mu(\sigma_x + \sigma_y)$ is applied along it. This condition, plane strain, only permits strain in the xy plane. Plane strain is a more restricted state of stress due to the restriction of strain. Materials therefore will behave with less ductility.

2.1.6 Stress Concentration

The magnitude of the stress acting on a cross section of a material often is not constant due to the presence of stress concentrators. These concentrators exist as inhomogenities such as voids, notches or small particles. Since they are incapable of carrying a load, the material surrounding them is forced to compensate during an applied stress by accepting a greater level of stress. This concentration effect decreases rapidly when moving away from the inhomogeneity.

The level of stress around a concentrator is dependent on its shape as well as the applied stress,

$$\sigma_{conc} = \sigma(1 + 2a/b) \qquad [2.26]$$

where:

σ_{conc} = concentrated stress

σ = applied elastic stress

a = length of the concentrator

b = width of the concentrator at its tip

It can be concluded from this equation that long, narrow inhomogeneities produce the highest stress concentrations.

2.2 Fracture Mechanics

Fracture can be defined as the physical separation or splitting of a material into two or more parts. It is caused by the propagation of one or more cracks through a material, usually driven by some external load. Cracks typically start out as some type of inhomogeneity such as a notch or a void. As a load is applied, stress and strain develop throughout the material. The magnitude of the stress and strain energy surrounding these inhomogeneities becomes magnified due to stress concentration effects. At a critical stress or energy level, the material surrounding the inhomogeneities begins to fail. A crack develops which then propagates as long as sufficient stress and energy is maintained in front of the crack tip. If the stress drops below the level needed to support propagation, the crack propagation is terminated. However, if termination does not occur the crack propagates until the material is fractured. This is referred to as critical crack propagation with the applied stress referred to as the critical stress.

2.2.1 Fracture Energy

In 1920, Griffith[6] set forth the first theory to predict the stress necessary to cause critical failure of a material. Griffith knew that as a crack propagated through a staticly loaded material, the strain energy stored in the material decreases. He proposed that critical failure occurred when the rate at which this energy was lost equaled or exceeded the energy required to create new surface area generated by the crack propagation,

$$\frac{2\pi\sigma^2 at}{E} \geq 4t\gamma_s \qquad [2.27]$$

where:

$2\pi\sigma^2 at/E$ = strain energy release per unit of crack extension

$4t\gamma_s$ = created surface energy per unit of crack extension

σ = applied stress

a = one half the crack length

t = plate thickness

E = Young's modulus

γ_s = surface tension

The applied stress at failure was equal to the critical stress, therefore,

$$\sigma_c = \sqrt{\frac{2E\gamma_s}{\pi a}} \qquad [2.28]$$

where, σ_c = critical stress. This equation for critical stress was found to be nearly identical to the equation for the cohesive stress needed to separate two adjacent atoms in a crystalline material, considering $(2/\pi) \simeq 1$;

$$\sigma_{coh} = \sqrt{\frac{E\gamma_s}{a_o}} \qquad [2.29]$$

where:

σ_{coh} = cohesive stress

γ_s = surface energy

a_o = equilbrium atomic distance

The predicted critical stresses, however, fell significantly short of the stresses required to fracture actual materials. Plastics, for example, exhibited critical stresses several orders of magnitude greater than predicted. Griffith had assumed that materials undergoing fracture

exhibited pure linear elastic behavior. Actual materials, however, were found to undergo varying degrees of plastic deformation. This deformation which occurred as crack tip blunting, absorbed significant amounts of strain energy.

Orowan[7], to account for plastic deformation, modified Griffith's results by adding a plastic energy term similar to the surface energy term,

$$\sigma_c = \sqrt{\left(\frac{2E\gamma_s}{\pi a}\right)\left(1+\frac{\gamma_p}{\gamma_s}\right)} \qquad [2.30]$$

where γ_p = plastic deformation energy. For $\gamma_p >> \gamma_s$, the equation is simplified:

$$\sigma_c \simeq \sqrt{\frac{2E\gamma_p}{\pi a}} \qquad [2.31]$$

This relationship found little application since γ_p could not be measured separately.

2.2.2 Strain Energy Release Rate

Irwin[8,9] decided to combine both γ_s and γ_p into a single term which he referred to as the strain energy release rate, denoted by G,

$$G = 2(\gamma_s + \gamma_p) \qquad [2.32]$$

G represented the total change in stored strain energy per increment of crack surface area,

$$G = \frac{\partial U}{\partial a} \qquad [2.33]$$

The critical stress at failure was therefore reached at a critical energy release rate,

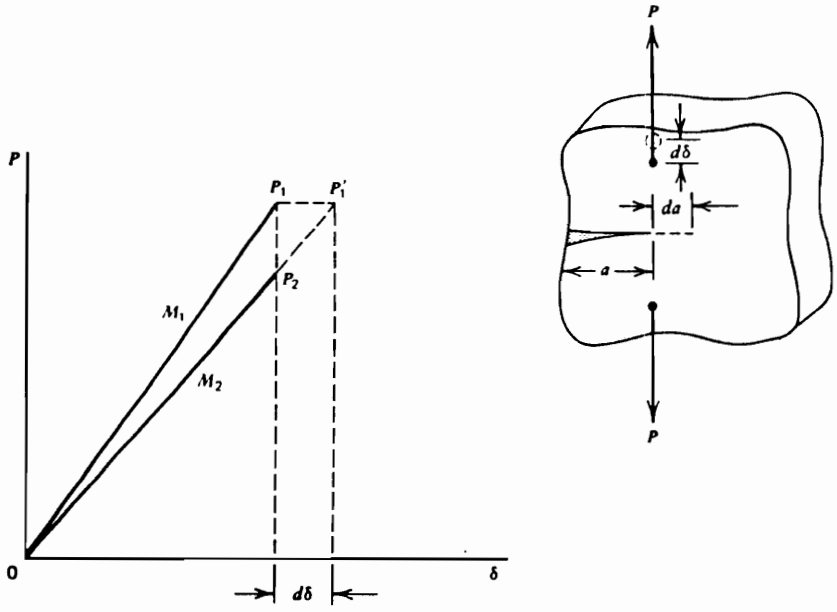

Figure 10. Stiffness versus crack length [3]

$$\sigma_c = \sqrt{\frac{EG_c}{\pi a}} \qquad [2.34]$$

where, G_c = critical strain energy release rate.

G_c could be determined by measuring the stored elastic strain energy at various crack lengths (Figure 10). Irwin proposed that the total energy change of a specimen, for an incremental increase in crack length, was equal to the energy transferred to the material by an external load, P, minus the loss of strain energy denoted by V:

$$G = \frac{\partial U}{\partial a} = P\frac{d\delta}{da} - \frac{dV}{da} \qquad [2.35]$$

where, δ = displacement. The stored strain energy for an elasticity loaded body is equal to one half the load multiplied by the displacement:

$$V = \frac{P\delta}{2} = \frac{P^2}{2m} \qquad [2.36]$$

where, m = δ/P = stiffness of the material. As the crack extends, the stiffness of the material decreases making the product of stiffness and displacement a constant for a constant load,

$$\frac{P_1}{m_1} = \frac{P_2}{m_2} \qquad [2.37]$$

Substituting P and V into equation 2.35, the energy release rate for a constant load can be determined:

$$\left(\frac{\partial U}{\partial a}\right)_p = P\frac{\partial \delta}{\partial a} - \frac{1}{2}P\frac{\partial \delta}{\partial a} \qquad [2.38]$$

$$\text{or} \quad G = \frac{1}{2}P^2\left(\frac{\partial 1/m}{\partial a}\right)$$

where, 1/m = material compliance. The change of compliance with respect to crack length

is always positive, making G positive.

Instability is reached when the load is increased to a level where the strain energy release rate reaches a critical magnitude;

$$G_c = \frac{1}{2} P_{max}^2 \left(\frac{\partial 1/m}{\partial a} \right) \qquad [2.39]$$

where, P_{max} = load at failure. The limitation of this equation is that the plastic deformation which occurs adjacent to the crack tip must be small enough in magnitude so that it does not influence the overall elastic material behavior.

2.2.3 Stress Intensity

Irwin[10] re-examined the fracture problem using the concepts of elastic theory. Utilizing an analytical method proposed by Westergaard[11], he determined the magnitude of the various stresses surrounding an atomically sharp crack within an infinitely wide elastic plate under a tensile load (Figure 11).

$$\sigma_x = \sigma\sqrt{a/2r}\left[\cos\frac{\theta}{2}\left(1 - \sin\frac{\theta}{2}\sin\frac{3\theta}{2}\right)\right] \qquad [2.40]$$

$$\sigma_y = \sigma\sqrt{a/2r}\left[\cos\frac{\theta}{2}\left(1 + \sin\frac{\theta}{2}\sin\frac{3\theta}{2}\right)\right] \qquad [2.41]$$

$$\tau_{xy} = \sigma\sqrt{a/2r}\left[\sin\frac{\theta}{2}\cos\frac{\theta}{2}\cos\frac{3\theta}{2}\right] \qquad [2.42]$$

where;

σ = applied normal stress

τ = applied shear stress

ρ = crack tip radius

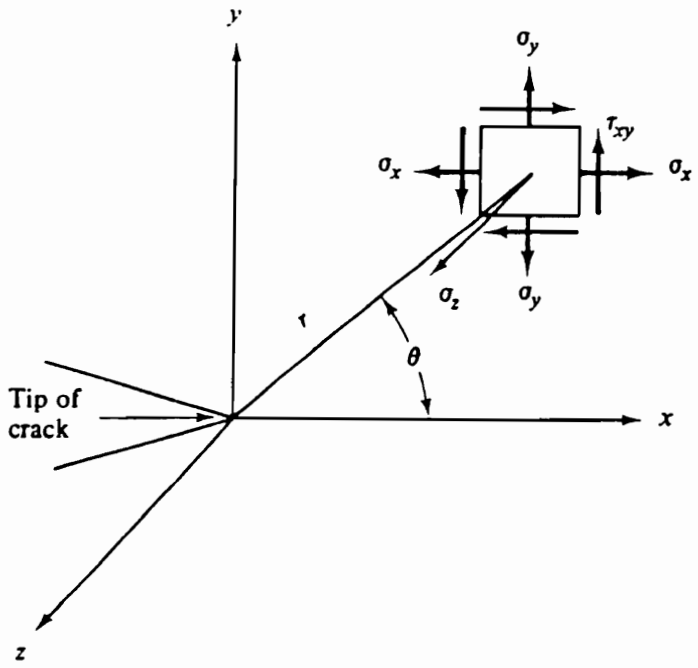

Figure 11. Stress coordinates surrounding a crack tip [4]

r = distance from the crack tip, $a > r > \rho$

a = one half the crack length

θ = angle between the crack plane and the vector r

Irwin recognized that the magnitude of each stress was directly proportional to the product of the applied stress and the square root of the crack length. He referred to this product as stress intensity, denoted by K,

$$K = \sigma\sqrt{\pi a} \quad \text{INFINITELY WIDE PLATE} \qquad [2.43]$$

$$K = f(\sigma, a) \quad \text{OTHER GEOMETRIES} \qquad [2.44]$$

From equation 2.43, the applied stress can be related to the stress intensity divided by the square root of the crack length,

$$\sigma = \frac{K}{\sqrt{\pi a}} \quad \text{INFINITELY WIDE PLATE} \qquad [2.45]$$

This result paralled Irwin's relationship between the applied stress and the strain energy release rate,

$$\sigma = \sqrt{\frac{EG}{\pi a}} \qquad [2.34]$$

This implied that stress intensity could be related to the strain energy release rate,

$$K^2 = GE \quad \text{PLANE STRESS} \qquad [2.46]$$

$$K^2 = \frac{GE}{1-\mu^2} \quad \text{PLANE STRAIN} \qquad [2.47]$$

Critical failure occurred not only at G_c but also at a critical value of K, denoted by K_c. Both G_c and K_c are thus defined as intrinsic material parameters.

2.2.4 Crack Tip Stresses

Westergaard's equations for the stresses surrounding a crack tip applied only for infinitely wide materials exhibiting pure elastic behavior. These equations become invalid for actual samples due to thickness effects as well as localized plastic deformation which controls the material's mechanical response.

Consider first the cross section of an elastic material which contains a notch or a crack running in the x direction along the xz plane with an applied tensile load in the y direction (Figure 12a). The stress in the y direction is greatest closest to the notch due to the stress concentration effect. This concentration effect can magnify the applied stress by several orders of magnitude. However, it decreases quickly as the distance from the notch in the positive x direction increases.

The presence of the notch not only concentrates the stress in the y direction, but also creates stresses in the x and z directions. Dieter[2] explained this by comparing the material in front of the notch to a series of tensile specimens lined up running from the notch in the x direction, with their lengths in y direction and their widths equal to the width of the material along the z axis parallel to the notch tip.

As each specimen is elongated in the y direction due to the normal tensile stress in y direction, σ_y, it attempts to contract in the x direction by a quantity equal to the strain in the y direction multiplied by Poisson's ratio. The tensile specimen next to the notch is free to contract without restraint since the normal tensile stress in the x direction, σ_x, is equal to zero. σ_x is equal to zero here since the notch forms a free surface. The tensile specimens in from the notch however, are not free to contract since each is sandwiched between other specimens who also desire to contract. The opposing tendencies of the adjacent specimens to contract generates a normal stress in the x direction thus preventing them from splitting apart. Close to the notch σ_x is relatively small, but it increases rapidly as the distance from the notch increases. This increase in σ_x is caused by the decreasing influence of the free surface.

At a certain distance, σ_x begins to decrease again. This is caused by the decreasing tendency to contract, due to σ_y decreasing, finally overshadowing the increasing restriction to contract.

The magnitude of stress in the z direction is dependent on the thickness of the specimen. Comparing the material to a series of tensile specimens were now lined up in the z direction along the notch tip, each specimen would now contract in the z direction as it was elongated in the y direction. The two end specimens positioned along the free surfaces of the material would be free to contract since σ_z for them would be equal to zero. Stress would however increase rapidly away from the ends and plateau off in the middle of the sample (Figure 12c). For thin samples, this plateau level is never reached thus producing a condition equivalent to plane stress. For thick samples, the surface effect becomes negligible with respect to the mechanical behavior of the entire material thus producing a condition equivalent to plane strain. The effect of thickness on σ_x and σ_y is usually less than 10 percent in metals.

Figure 12b shows the dependence of σ_z on the distance from the notch tip in the x direction. The z directional stress is not influenced by the free surface of the notch, therefore, it shows a maximum at the tip and decreases similarly to σ_y with increasing distance.

2.2.5 Plastic Zone

In the above discussion, the distribution of stresses in front of a notch for a material exhibiting purely elastic behavior was described. The distribution of stresses for a material capable of elastic and plastic behavior is different. For a purely elastic material, the magnitude of σ_y of the notch tip is equal to the applied stress multiplied by the stress concentration factor. Depending on the length and sharpness of the crack, the stress can be magnified by several orders of magnitude or more. The high concentration of stress is often prevented from occurring in an actual material however, due to the formation of a region of plastic deforma-

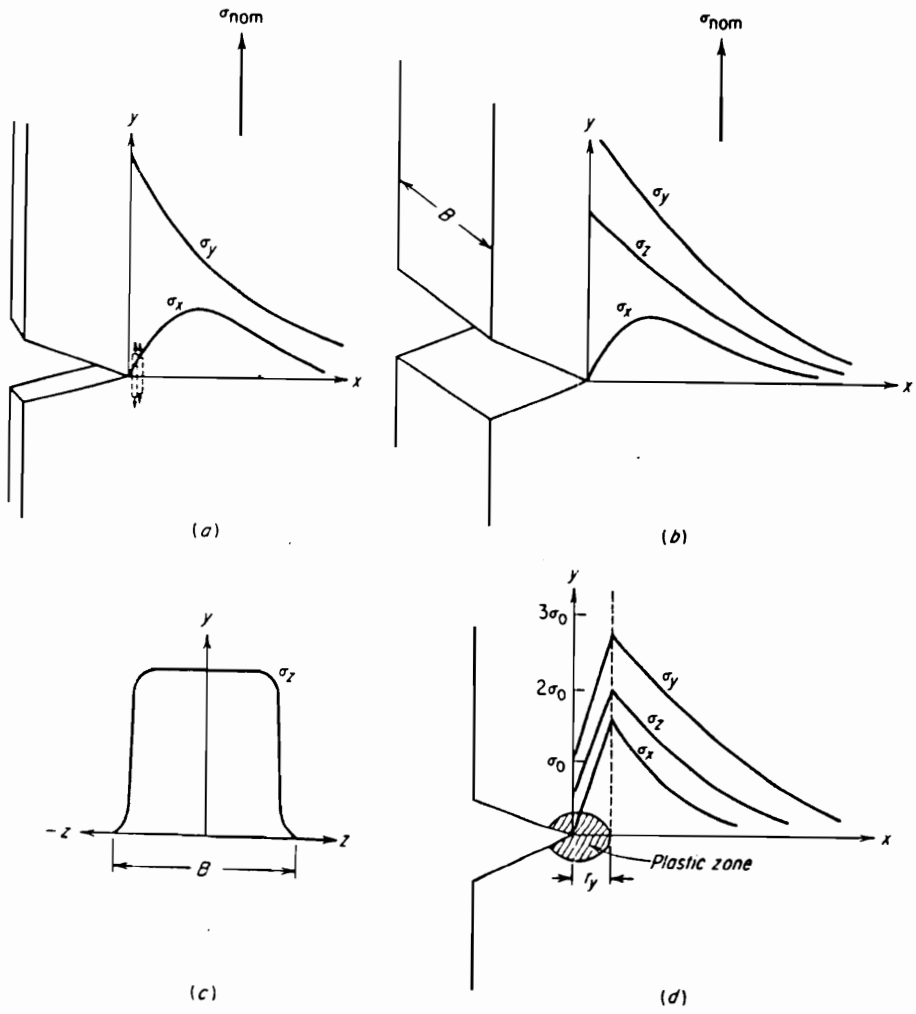

Figure 12. Stresses surrounding an atomically sharp crack: a) elastic stresses beneath a notch in a thin plate(plane stress); b) elastic stresses beneath a notch in a plane strain; c) distribution of σ_z with z at x=0 (plane strain); d) distribution of stresses during local yielding (plane strain) [2]

tion in front of the notch tip, referred to as the plastic zone. The plastic defromation acts as a relieve valve to the high stresses thereby making the material tougher.

The level of stress in the y direction necessary to induce yielding is dependent on the transverse stresses. Tresca [12] proposed that yielding occurs when the sum of the principal stress minus the transverse stress equals the tensile yield stress

$$\sigma_o = \sigma_1 - \sigma_3 \qquad [2.48]$$

where:

σ_o = yield stress

σ_1 = principal stress

σ_3 = transverse principal stress

Yielding occurs when σ_1 equals σ_o, where the magnitude of the transverse stress is zero. The magnitude of the principal stress necessary to induce yielding however increases as σ_3 increases. Thus the minimum σ_y necessary to induce yielding in a notched specimen occurs at the notch tip (Figure 12d). As you move away from the notch tip, σ_y increases due to increases in σ_x

When the value of σ_y for the elastic case equals the value of σ_y for the plastic case, the limits of the plastic zone are reached. The stresses from this point on are equal and decrease. Materials which have a relatively low yield stress, have large plastic zones, since σ_y for the elastic and plastic cases would become equal at a lower stress and therefore further from the notch.

The size and shape of the plastic zone is dependent on its location within the sample. Irwin[10] viewed the zone as having a circular shape with respect to the xy cross sections, Figure 13, with its radius increasing as it moved away from the center of the sample along the z axis. This increase was attributed to the change from plane strain to plane stress conditions:

$$r_p \simeq \frac{1}{2}\left(\frac{K^2}{\sigma_o^2}\right) \quad \text{PLANE STRESS} \qquad [2.49]$$

$$r_p \simeq \frac{1}{6}\pi\left(\frac{K^2}{\sigma_o^2}\right) \quad \text{PLANE STRAIN} \qquad [2.50]$$

where;

r_p = radius of the zone

K = stress intensity

σ_o = yield stress

Irwin expected that the plastic zone near the edges would have a radius 3 times that of the center.

This theory was later modified by Hahn and Rosenfield[13] who believed that the plastic zone was more like an ellipse than a circle. The distance the zone extended from the notch tip was dependent on the angle between the direction vector and the notch on the xz plane.

$$r_y = \frac{K^2}{2\pi\sigma_o}\left(\cos^2\frac{\theta}{2}\right)\left(1+3\sin^2\frac{\theta}{2}\right) \quad \text{PLANE STRESS} \qquad [2.51]$$

where:

r_y = distance from the notch tip

θ = angle off the notch plane

Dugdale[14] proposed that in selected materials the plastic zone was neither elliptical nor circular, but rather a strip (Figure 14). The length and shape of the strip was dependent on the material's yield stress and the applied stress intensity,

$$\frac{c}{a} = \cos\frac{\pi\sigma}{2\sigma_o} \qquad [2.52]$$

$$R = \frac{\pi K^2}{8\sigma_o^2} \qquad [2.53]$$

where:

c = one half the length of the crack

a = one half the length of the crack plus the plastic zone

σ = applied stress

R = length of the plastic zone

2.2.6 Modes of Fracture

Three modes of loading exist for a partially cracked material (Figure 15). Modes I, II, and III are referred to as the tensile or opening mode, the inplane shear mode and the anti-plane shear mode, respectively. Failure can occur by one or more modes. Modes II and III are more resistant to crack propagation than Mode I since failure in the former is produced by a shearing stress. Consequently, Mode I is the failure mode found in the majority of fractures since cracks generally propagate along the path of least resistance. Pure Mode II fracture is rarely found. It does, however, produce failure in combination with Mode I in materials under tension possessing an inclined crack. Mode III loading causes failures in notched round bars undergoing torsion.

2.2.7 Fracture Toughness Testing

2.2.7.1 Toughness Testing

Standardized testing methods for measuring the fracture toughness of various metals under the various modes of loading are not well established. Currently, only one testing method has been certified by the ASTM (ASTM E-399). This method is designed to measure Mode I fracture in metals and uses either a three point bend or a compact tension specimen. This method has been applied (with a few modifications) successfully to polymeric materials. Several other methods are currently being used to measure either the critical stress intensity

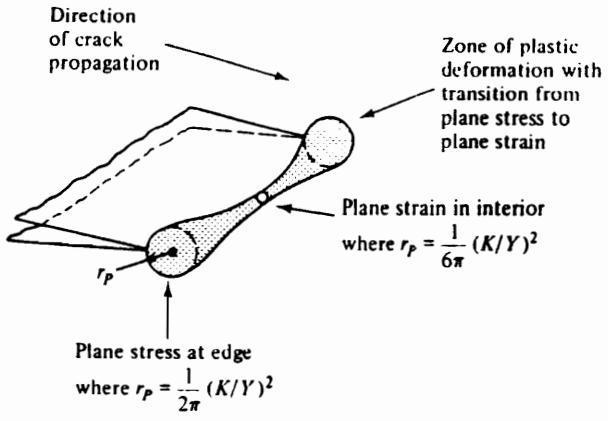

Figure 13. Shape of Irwin's plastic zone [4]

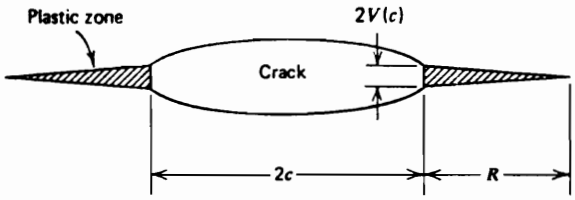

Figure 14. Dugdale strip plastic zone [3]

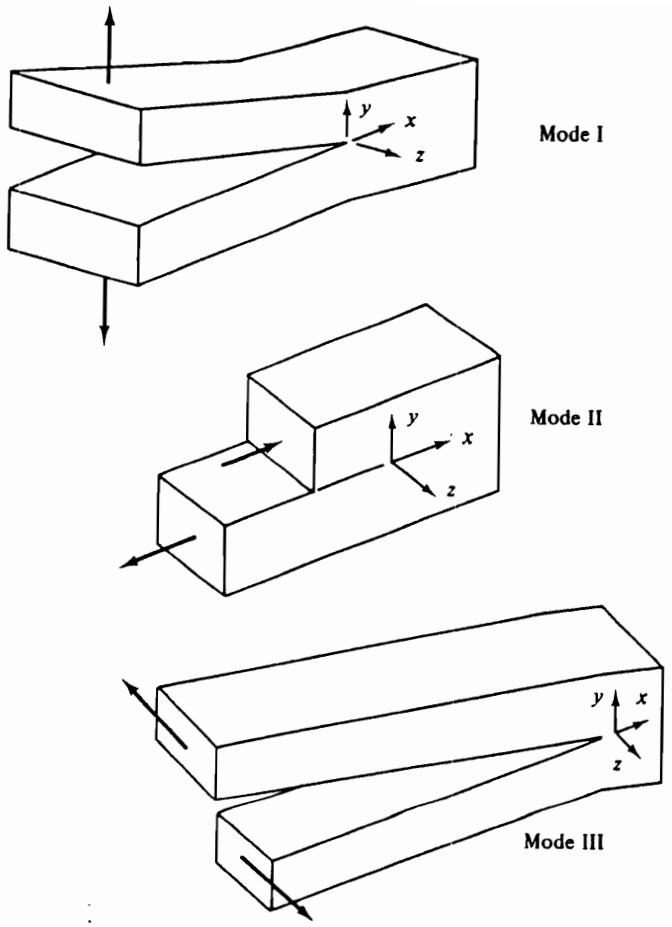

Figure 15. Modes of fracture [4]

or strain energy release rate in plastics. Ellis[15], Ting[16], and Kambour[17] have reported that critical conditons can be measured using a double cantilever beam specimen (Figure 16). A modified double cantilever beam specimen has been used by Hunston [18] to obtain a plastic's G_c from an adhesive joint. Hinkley[19] has reported the use of miniature compact tension and three point bend specimens. An Outwater torsion test has been used by Cho and Gent[20] in the determination of G_{1c} for stiff materials and adhesive joints.

The number of publications reporting Mode II or Mode III failure is quite limited. Ritchie et al.[21] have measured Mode III failure in metals using a torsionally loaded notched bar. Mode II failure has been obtained in polymethyl methacrylate by using an Arcan specimen. Brinson[22] has suggested Mode II or a combination of Mode I and Mode II failure can also be achieved using either an Iosepescu, Grant or BMC specimen (Figure 17).

2.2.7.2 Thickness Effects on Mode I Fracture

Fracture toughness of a plastic undergoing Mode I failure can increase by as much as a factor of 3 with decreasing sample thickness (Figure 18). This increase can be attributed to a transition from plane strain fracture in thick samples to plane stress fracture in thin samples. Plane stress occurs along the sides of a specimen where the surfaces are free to contract or expand. Molecular motion is less restricted than under plane strain, thereby giving the material greater ductility and toughness. As the thickness increases, the contribution from the free surfaces decreases, which lowers the material's overall toughness. The surface effect becomes negligible at the thickness labeled B. The critical stress intensity beyond this point is independent of thickness and is, therefore, only related to the material's mechanical behavior. It is referred to as the plane strain stress intensity, denoted by K_{1c}. The thickness required to obtain this plane strain condition can be calculated, theoretically, using K_{1c} and the material's yield stress,

$$B \geq 2.5\left(\frac{K_{1c}}{\sigma_o}\right)^2 \qquad [2.54]$$

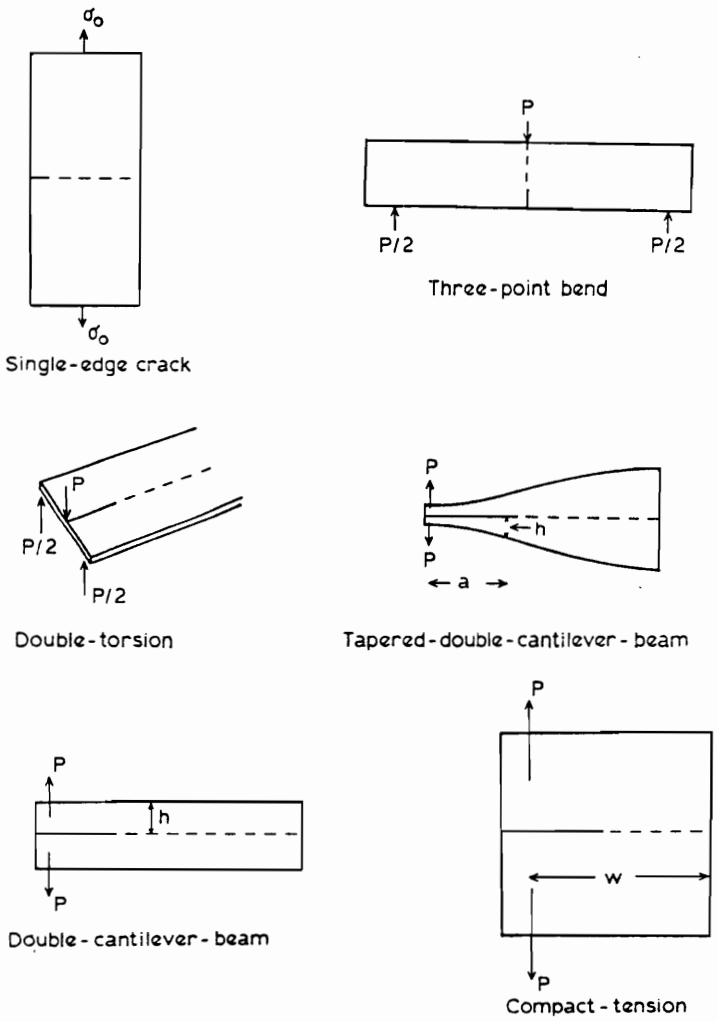

Figure 16. Various mode I fracture toughness specimens [23]

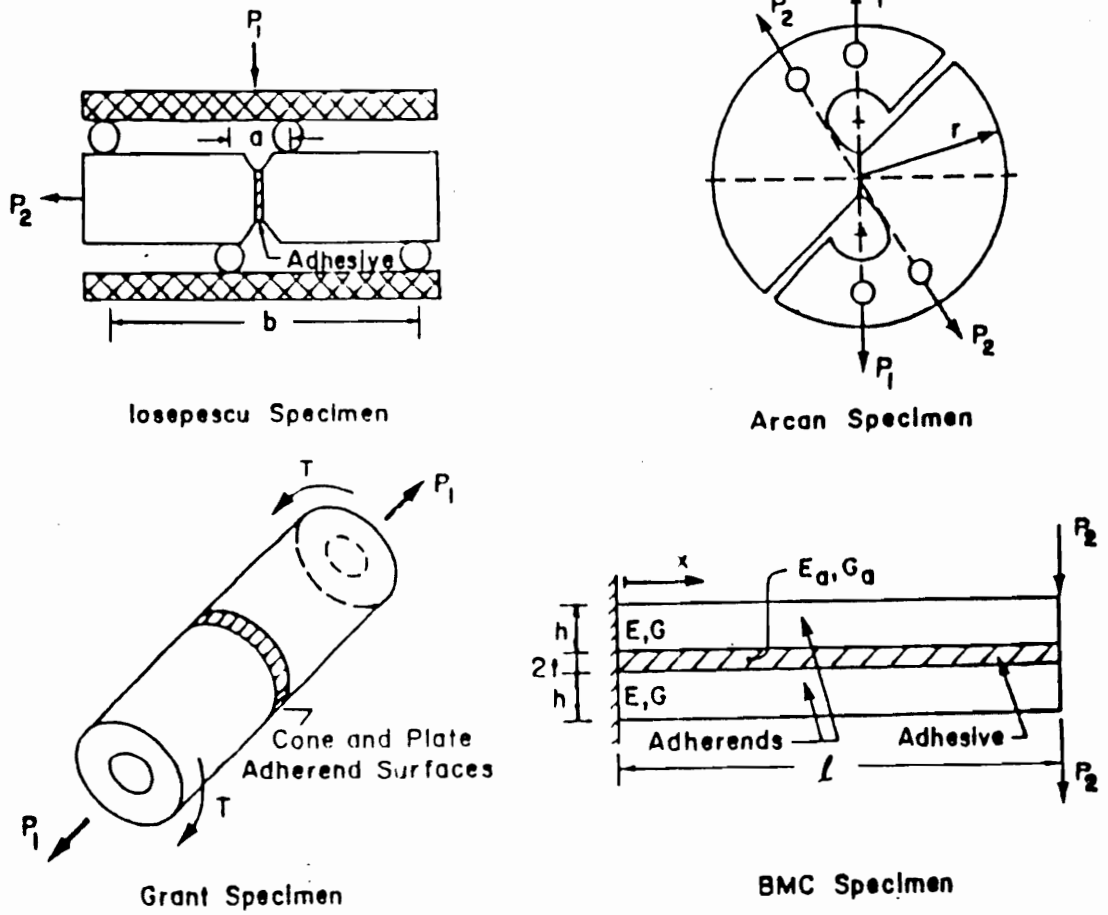

Figure 17. Iosepescu, Arcan, Grant and BMC specimens [22]

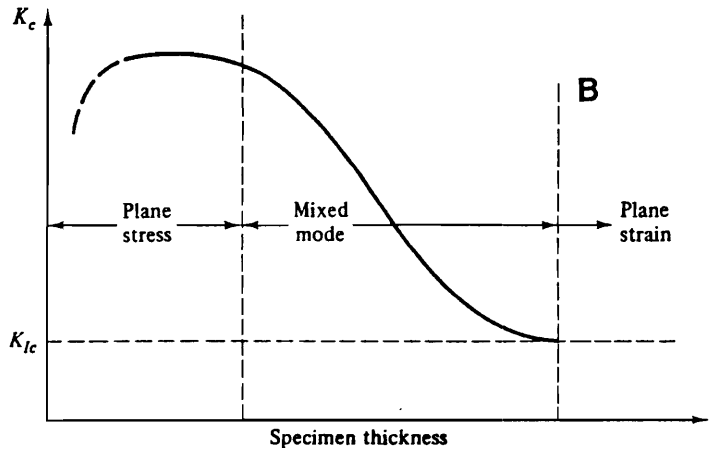

Figure 18. Critical stress intensity versus sample thickness [4]

Chapter 3. Mechanical Properties of Polymers

This chapter reviews the basic mechanical behavior of polymers. Tensile and creep tests for polymers are presented, along with discussions of the effects of topology, morphology and testing conditions on each region of the polymer's response. Also, the various molecular theories describing modulus, yielding and fracture are discussed.

3.1 Tensile Behavior of Polymers

The tensile behavior of plastics can generally be classified as either rigid and brittle, rigid and ductile, or soft and ductile (Figure 19). For room temperature testing, rigid and brittle behavior is exhibited by glassy thermosets such as most epoxy and phenolic resins, and in brittle thermoplastics such as polystyrene and polymethylmethacrylate. Stress is seen to increase linearly with strain until the material under goes brittle failure, usually at less than 10 percent strain.

Rigid and ductile response is found in tough, glassy thermoplastics such as polycarbonate and polysulfone as well as semi-crystalline rubbers as polyethylene. These materials also exhibit a pronounced elastic region where stress increases linearly with strain.

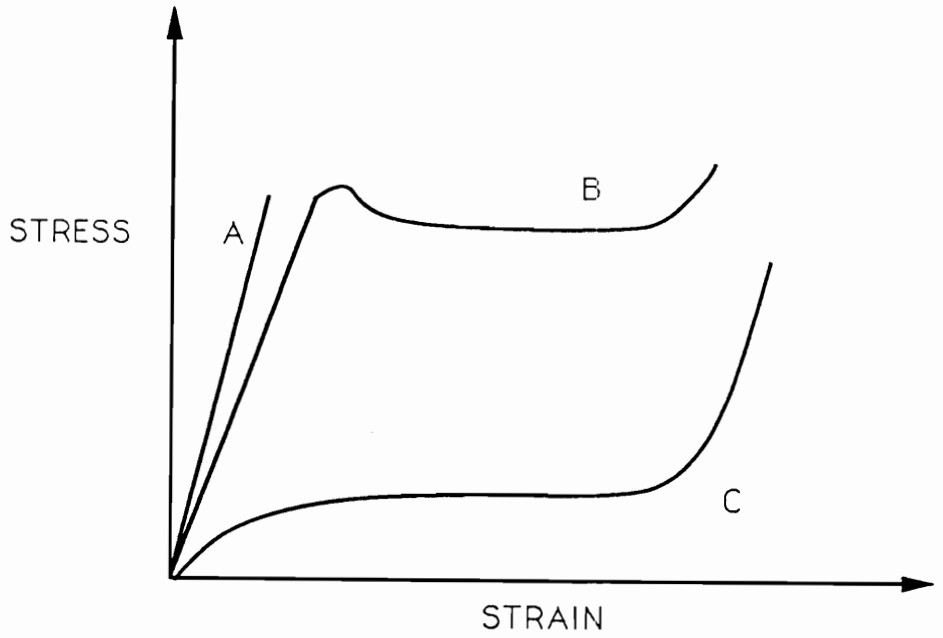

Figure 19. Load displacement curves for polymers exhibiting various behaviors: A, rigid and brittle; B, rigid and ductile; C, soft and rubbery.

However at 5 to 15 percent strain, stress goes through a localized maximum known as the yield point. This point marks the approximate initiation of plastic deformation. Beyond the yield point, the polymer undergoes a drawing process which may extend the sample up to several hundred percent strain before failure. Quite often a small decrease in stress, known as strain softening, takes place at the start of the drawing process. A dramatic increase in stress is also usually seen before failure. This phenomenon is referred to as strain hardening.

Soft and ductile polymers include thermoplastic elastomers and crosslinked rubbers such as natural rubber. These polymers generally do not exhibit a well defined elastic region or a yield point. They do, however, exhibit a long drawing zone followed by a region of strain hardening similar to the rigid and ductile polymers. Elongation at break can range from 30 to several thousand percent strain.

The tensile behavior of any polymer can be changed by altering temperature or strain rate. Increasing temperature or decreasing the strain rate promotes ductile and rubbery behavior whereas decreasing temperature or increasing strain rate promotes rigid and brittle behavior. An example of this would be an epoxy resin which exhibits rigid and brittle behavior at room temperature but soft and rubbery behavior above 200 °C.

3.2 Elastic Modulus

3.2.1 Typical Modulus Values

The tensile moduli of thermoplastics and thermosets are presented in Table 1. The polymers exhibiting rigid and brittle, and glassy rigid and ductile behavior possess the highest moduli for unoriented polymers, 300 to 700 ksi (2000 to 5000 MPa). The semi-crystalline low modulus thermoplastics such as polyethylene possess moduli siginificantly below the glassy

polymers, 50 to 200 ksi (350 to 1400 MPa). Amorphous rubbers possess the lowest modulus values, 0.1 to 10 ksi (7 to 70 MPa).

Oriented fibers of semi-crystalline or liquid crystalline thermoplastics such as Kevlar, possess moduli exceeding 5,000 ksi (35,000 MPa). The stiffness of these materials is comparable to metals such as aluminum and titanium alloys.

3.2.2 Molecular Theories

A number of researchers[24-26] have associated rigidity of a glassy polymer to the intermolecular forces which bond the chains together. They believe, that initially, it is these bonds which carry the majority of the load. Stachurski[27] has implied that it is the strongest of these forces which determines the modulus.

Bowden[28] has proposed that intermolecular forces only partially account for rigidity. He concluded, in studying polyethylene, that part of a polymer's rigidity was attributed to bond rotation. This, he believed, explained why modulus increased with the degree of crystallinity. The high packing density of the crystals increased the resistance to bond rotation. This forced the chains inside the crystals to extend by the much stiffer processes of bending or stretching of the covalent bonds. Therefore, this process required a higher level of stress leading to an increase in the modulus.

The extremely high moduli associated with highly oriented semi- crystalline fibers is also believed to be due to covalent bond bending and stretching. It is believed that after orientation, the stress is carried primarily by the polymer backbone instead of secondary bonding. Consequently, the modulus is increased.

Table 1. Summary of the stress strain behavior for various polymers and metals.

	Tensile Strength (psi x 10^3)	Tensile Modulus (psi x 10^3)	Yield Stress (psi x 10^3)	Elongation at Break (% strain)
Rigid and Brittle				
Epoxy Casting Resin	4 - 13	350	-	3 - 6
Phenolic Casting Resin	5 - 9	400-700	-	1.5 -2.0
Polymethylmethacrylate	7 - 11	325-470	-	2 - 10
Polystyrene	5.2 - 7.5	330-475	-	1.2 - 2.5
Rigid and Ductile (Glassy)				
Polycarbonate	9.5	345	9	110
Polyetheretherketone(PEEK)	10.2 - 15	550	13.2	30-150
Polyethersulfone	9.8 - 13.8	350	12.2 - 13	6 - 80
Polysulfone(UDEL)	-	360	10.2	50-100
Polyetherimide(ULTEM)	14	430	15.2	60
Nylon 6,6	11.2 - 13.1	410-480	-	60-300
Rigid and Ductile (Rubbery)				
High Density Polyethylene	3.2 - 4.5	155-158	3.8 - 4.8	10-1200
Teflon	2 - 5	58 - 80	-	200-400
Rubbery				
Natural rubber(Gum Vulcanized)	-	0.3	-	-
Natural rubber(vulcanized)	8 - 11.6	290-435	-	3 - 6
Polysulfone/ Polysiloxane copolymer	0.9	0.3	-	550
Fibers				
Kevlar	-	15,000	-	-
Polyethylene	-	5800-7100	-	-
Metal Alloys				
Aluminum	35-88	10,200	21-78	10-23
Titanium	125-185	16,800	117-175	8 - 16
Tungsten	-	59,600	-	-

psi x 10^3 = ksi
1 psi = 6895 Pa
10^5 psi = 689.5 MPa

3.2.3 Thermodynamic and Structure Effects

The elastic modulus of a polymer is dependent on thermodynamic variables such as temperature, annealling time and hydrostatic pressure as well as structural variables such as topology, morphology and molecular weight.

The dependence of elastic modulus on temperature for a typical thermoplastic can be divided into four regions; glassy, leathery, rubbery, and flow (Figure 20a). For the region of glassy response, $T < Tg$, modulus decreases slowly with increasing temperature. As the temperature nears Tg, the polymer becomes leathery over a narrow temperature range of as little as 10 °C. Modulus, during this range, can drop by several orders of magnitude. Above Tg, the polymer transforms into a rubber. The modulus becomes independent of temperature over a sometimes broad temperature range referred to as the rubbery plateau. Beyond the rubbery plateau, the polymer begins to flow causing a further decrease in the modulus.

Glassy modulus, as mentioned above, is believed to be determined by the intermolecular forces between the chains, and therefore dependent on the spacing of the molecules. Variables which decrease the spacing between the molecules, such as annealing [31] or the application of hydrostatic pressure [32], have been reported to increase modulus. Structural variables such as molecular weight, molecular weight distribution and crosslink density are not believed to significantly affect molecular packing and therefore do not significantly affect modulus [31].

The structural parameters of topology, morphology and molecular weight however, do not significantly effect the magnitude of the rubbery modulus, (Figure 20b-d). Changes which restrict chain motion, such as increasing crystallinity, molecular weight, or crosslink density, increase the rubbery modulus.

The temperature range of the plateau is dependent upon the polymer's thermal stability and molecular weight. Semicrystalline polymers exhibit a sharp decrease in modulus at their melting transitions[33]. Often, this is preceded by a slow decrease in modulus due to the melting of imperfect crystallites. Amorphous thermoplastics maintain mechanical integrity

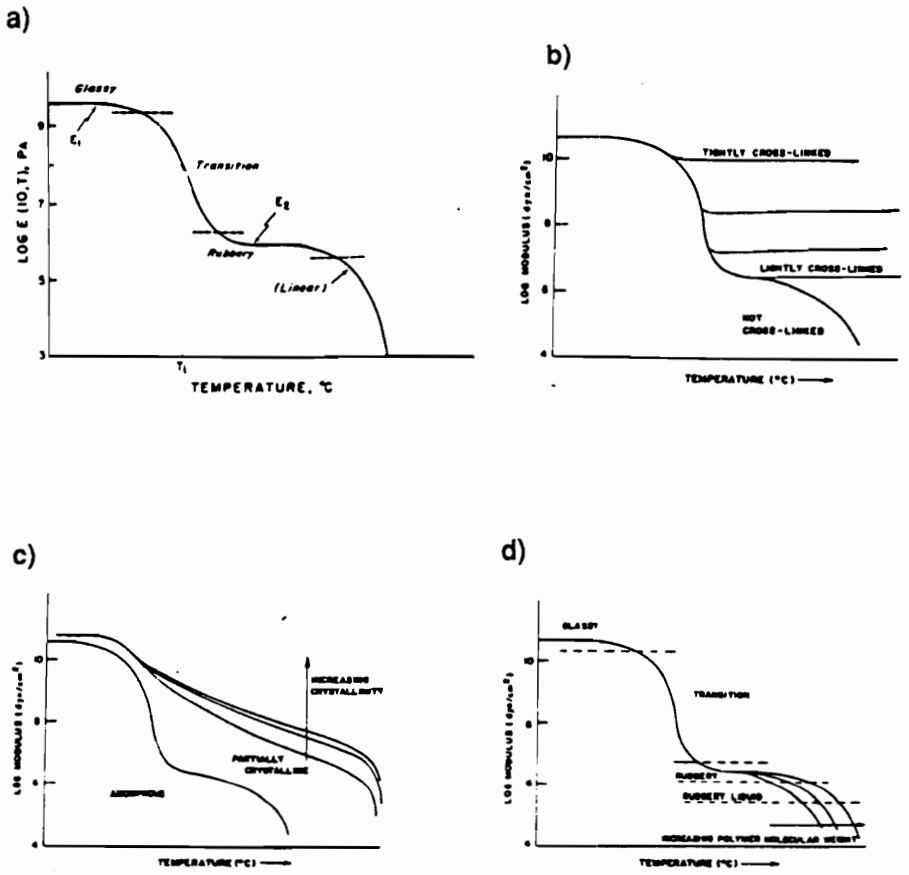

Figure 20. Effect of a)temperature b) crosslink density; c) crystallinity; and d) molecular weight on storage modulus versus temperature behavior [33,34]

above Tg due to the entanglement of their chains. As the temperature increases, the entanglements disentangle and the integrity is lost, decreasing the modulus and producing flow. An increase in the entanglement density due to an increase in molecular weight, increases the temperature range of the plateau and decreases the rate at which modulus decreases. A polymer whose molecular weight is low, will not have a significant number of entanglements and therefore, display no rubbery plateau. Thermosets do not melt or undergo disentanglement. However, modulus can decrease due to the degradation of the polymeric chains.

3.2.4 Time Effect

The effect of time on modulus is determined through a creep experiment. This test is initiated by quickly applying a tensile load to a sample. The load typically does not exceed the elastic limit of the material. The polymer elongates to a strain equal to the applied stress divided by the modulus. As the load is held constant, the material slowly elongates over time. This behavior is known as creep.

Results from a creep test is typically displayed as elongation (applied stress divided by modulus), versus time. Figure 21 shows the creep behavior for a glassy thermoset and thermoplastic. For the sake of simplicity, it is assumed that both polymers possess identical backbone structures and glass transition temperatures. Each curve mirrors its associated modulus response to temperature, with extension being divided into three stages.

The first stage is the elastic extension of the glassy material. The second stage is viscoelastic extension and occurs in association with the transition of the polymer from a glass to a rubber. The third stage involves flow and/or permanent plastic deformation.

The last stage is generally not seen in a thermoset. In a thermoplastic however, flow always occurs and eventually leads to the critical failure of the specimen. The rate at which the log of the extension increases during flow is approximately proportional to the change in

log time. Lightly crosslinked thermosets have also been reported to this third extension stage. Nielsen [35] has attributed this stage of extension in lightly crosslinked polybutadienes to the slow disentanglement of trapped dangling ends. The three stages of extension are divided by two regions of constant extension which are associated to the relatively constant glassy modulus and the rubbery plateau described above.

Thermodynamic and structural effects which would be associated with increasing the temperature required to produce a glass transition or flow, would increase the amount of time required to produce stage two and three of creep extension. When the stress is removed, the material slowly attempts to revert back to its original dimensions. The loss of creep strain during this process is defined as recovery. Figure 22 displays the creep recovery for a thermoplastic and a thermoset. Initially, polymers display a sharp but small reduction in strain as the material recovers the elastic portion of creep. At temperatures above Tg, this decrease may be obscured by viscoelastic deformation. This initial decrease is followed by a slower recovery, similar but opposite to the creep extension. At infinite time, thermosets display complete recovery while thermoplastics possess a permanent elongation. This permanent deformation can be attributed to chain disentanglement which occurs during the flow stage of creep extension.

3.3 Yielding

The term yielding, when used to describe the mechanical behavior of a material, refers to the generation of plastic or plastic-like deformation. For the case of an ideal elastic plastic material, as was discussed in the previous chapter, yielding refers to permanent plastic deformation. Plastics however do not behave as ideal elastic plastic materials. A plastic's response and recovery from an applied stress is often time dependent. Deformation which is initially considered to be plastic, can often be recovered after extended periods of time. Since

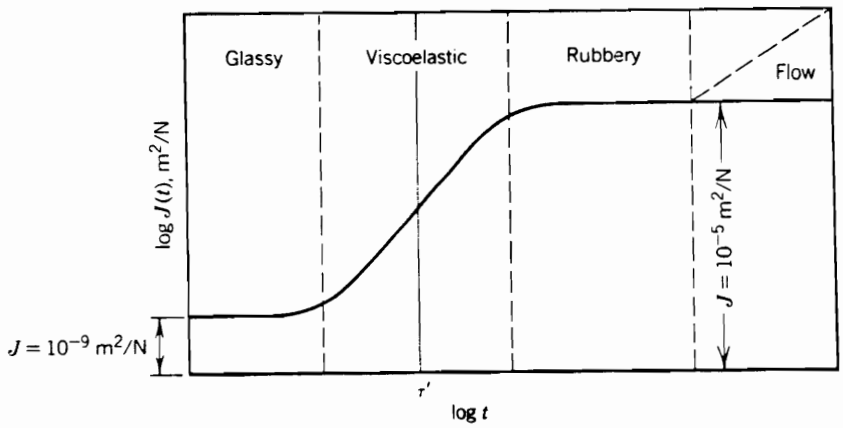

Figure 21. Creep compliance versus log time for a glassy thermoplastic and thermoset [37].

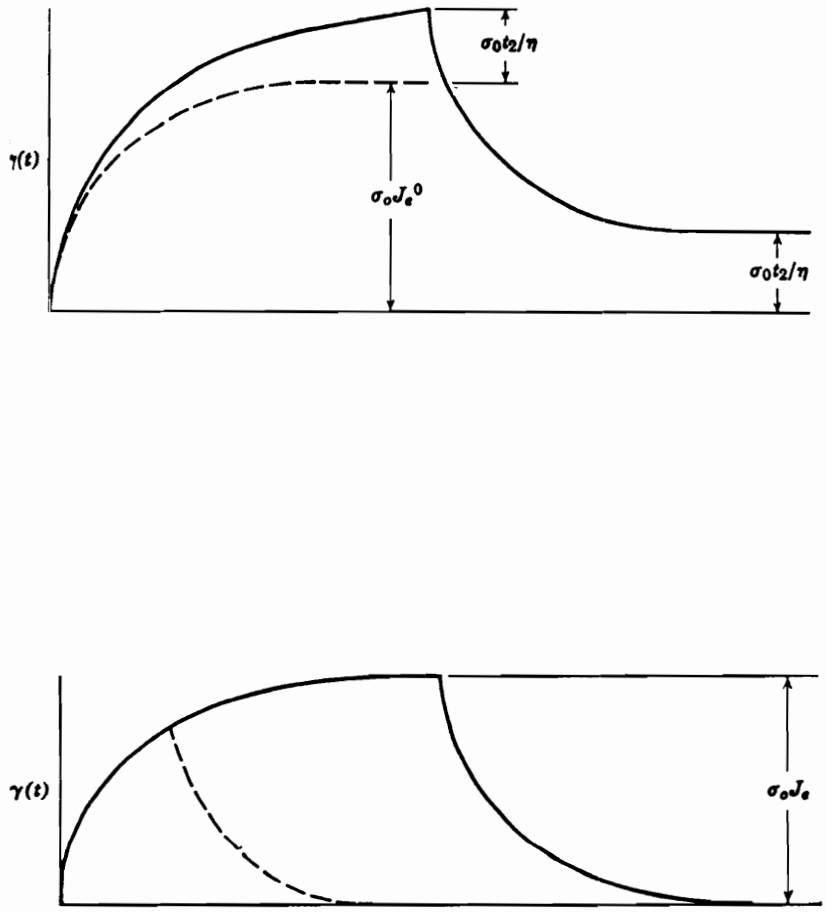

Figure 22. Creep recovery for a) glassy thermoplastic and b) thermoset [38]

it is usually difficult to separate true plastic deformation from this time dependent plastic-like deformation, the term yielding usually can be used to describe either.

3.3.1 Yield Stress

The yield point marks the location on a stress strain curve where yielding initiates. For the case of the ideal elastic plastic material, the yield point occurred at the pronounced transition between elastic and plastic deformation. For an actual polymer, the transition from elastic to plastic-like behavior is far more gradual, thereby making it difficult to pinpoint its exact position. Therefore, in order to have a point of reference so as to compare the yield stress of various polymers, most material scientist define the local stress maximum following the material's elastic response as the yield point (Figure 19).

Yield stress for a glassy rigid and ductile thermoplastic usually falls in the range from 8,000 to 15,000 psi. Rubbery thermoplastics possess yield stresses below this range. Rigid and brittle polymers as well as rubbery thermosets do not exhibit a yield point.

3.3.2 Viscoelastic and Structural Effects

Yield stress has been shown to be dependent upon chain mobility. Increases in strain rate, pressure or annealing have all been shown to increase yield stress. Rabinowitz and his coworkers[36] have shown that yield stress for polymethylmethacrylate increases proportionally with pressure

$$\tau = \tau_0 + \alpha\rho \qquad [3.1]$$

τ = yield stress at high pressure

τ_o = yield stress at atomospheric pressure

ρ = hydrostatic pressure

α = proportionality constant

The yield stress has been shown to increase from 33 x 10^6 N/m^2 at a atmospheric pressure to 60 x 10^6 N/m^2 at 450 MPa[32].

However, an increase in temperature decreases yield stress. Lefebvre[39] has reported that the yield stress of polymethylmethacrylate decreases from 400 MPa to 50 MPa as the temperature was raised from -100 °C to 50 °C.

Changes in yield stress with pressure[40] or temperature[41] have also been shown to be proportional to changes in the shear modulus of the polymer. This indicates a correlation between shear resistance and yielding. Increasing crystallinity or crosslink density also increases yield stress, to a point where at high levels of either, yielding is not seen for either glassy or rubbery systems. Increased molecular weight has also been reported[42,43] to increase yield stress. This has been attributed to an increase in chain entanglements. It is believed that during fast deformation, entanglements can restrict chain mobility, similar to crosslinking. However, entanglements are often considered necessary for yielding to occur. Several scientists[44,45] have reported that at molecular weights less than that of the chain entanglement molecular weight, Me, yielding is not observed.

3.3.3 Yielding Theories

A number of theories have been published over the past 50 years attempting to describe and predict yielding in polymeric materials. Yielding, as usually implied by these theories, encompasses both viscoelastic and plastic deformation. Currently, no one theory has found widesqread acceptance. This section will review a number of these theories and attempt to point out their similarities and discrepancies.

3.3.3.1 Activated Yielding

The first major work on plasticity was published by Eyring in 1936[46]. He proposed that the mechanism of plastic deformation for a glass was identical to the mechanism of shear deformation for a viscous liquid. Eyring pictured a material as being made up of a series of planes stacked on top of one another. Each plane contained a number of low energy positions which were isolated from one another by high energy barriers caused by the close proximity of molecules in the adjacent planes. Upon application of a shear stress, the planes are shifted relative to one another causing the molecules to jump over the barriers to adjacent energy well positions. The rate at which the energy bariers could be overcome would increase with increasing stress.

Eyring extended this work in 1945[47] to describe creep and stress relaxations of thermally activated processes. He assumed these viscoelastic phenomena were caused by either inter or intramolecular changes in or between the polymeric chains. The frequency of these changes was temperature dependent and could therefore be described by an Arrhenius type equation.

$$U = \frac{KT}{h} e^{-\Delta G/RT} = \frac{KT}{h} e^{\Delta S/R} e^{-\Delta/RT} = U_o e^{-\Delta H/kT} \qquad [3.2]$$

where:

U = frequency

k = Boltzman's constant

h = Planck's constant

T = temperature

R = gas constant

ΔG = change in free energy

ΔS = change in free entropy

ΔH = change in enthalpy

The applied stress could alter the change in enthalpy between two positions to favor the position which promoted flow in the shear direction. The frequency of this change was equal to the rate of strain

$$\dot{e} = \dot{e}_o e^{-\Delta H/RT} \sinh \frac{V\sigma}{RT} \qquad [3.3]$$

where: $\dot{e}$ = change of strain with respect to time

$\dot{e}_o$ = constant

V = activation volume

σ = applied stress

At high levels of stress, equation 3.3 can be converted to

$$\dot{e} = \dot{e}_o \exp\left[-\left(\frac{\Delta H - v\sigma}{RT} \right) \right] \qquad [3.4]$$

Equation 3.4 implies that when stress reaches a critical level, resistance to conformational changes is eliminated. This permits the chains to uncoil and elongate as quickly as the applied strain rate. Since stress varies significantly, due to fluctuations in density, the critical stress will only be reached initially in a highly localized volume.

The yield stress could be determined by the rearrangement of equation 3.4

$$\frac{\sigma}{T} = \frac{R}{V}\left[\frac{\Delta H}{RT} + \ln \frac{2\dot{e}}{\dot{e}_o} \right] \qquad [3.5]$$

where: σ = yield stress

Equation 3.5 shows that the yield stress increases with decreasing temperature or increasing strain rate.

This activated volume is approximately 5-10 nm^3, for most polymers, as determined by Haward and Thackray[48]. This suggests that yielding involves the cooperative motion of a large number of segments of the polymer chains. Bauwens and coworkers[49] determined that the initiation of yielding in polyvinylchloride and polymethylmethacrylate involved a minimum of 25 repeat units.

Hoffman[50] later applied a similar theory, the site model, to describe viscoelastic behavior in polymers. He proposed that upon the application of a stress, a portion of the bonds along the polymer's backbone would shift from gauche to the more extended trans conformation. Each bond conformational change led to an increment of strain

$$\varepsilon = \varepsilon_U + n\bar{\varepsilon} \qquad [3.6]$$

where: ε = total strain

ε_U = instantaneous elastic strain

n = number of shifts from gauche to trans conformation

$\bar{\varepsilon}$ = incremental strain per conformational shift

The theory proposed by Robertson[25] is also based on the concept that plastic deformation is caused by intramolecular motions in the polymer chains. Robertson believed that intermolecular forces determined the rigidity of a polymer. These forces were dissipated by the disruption of chain packing associated with changes in chain conformation.

Upon the application of a shear stress, the bonds would try to align themselves with the stress by changing their conformation. Since bonds in a glassy polymer existed in both low and high energy conformational states, the rearrangement would involve high to low energy shifts as well as low to high energy shifts. The jump to a high energy or flexed state was rapid since Robertson believed that the stress lowered the energy barier between the different conformational states. However, he believed that the jump from the higher state to the lower state occurred slowly due to thermal restrictions. This produced a transient maximum in the number of flexed bonds which existed initially after the application of the stress. Yielding oc-

curred when the maximum number of flexed bonds was equal to number of flexed bonds of the polymer in liquid state. The free volume, and the density of the solid and molten polymer, would also be equal since Robertson related the free volume of the polymer to the number of flexed bonds in the polymer. Robertson concluded that yielding would be highly localized since density heterogeneities existed in glassy amorphous polymers.

His theoretical calculations of yield stress for polystyrene closely matches the data for temperatures greater than 100° below the Tg. However, at the Tg the theoretical calculations are much higher than experimentally determined result. For PMMA, for a large temperature range, the calculations are consequently higher by 10^8 dyne/cm^3. Robertson reasoned that the higher theoretical values were partly due to the hydrostatic effect of the tensile test measurements.

The direct application of Robertson's theory has been limited since it only considers trans and gauche conformations. Also, there are several questions concerning the foundations of his theory. Firstly, he has concluded that the differences between the calculated yield stress and those obtained experimentally, were caused by the hydrostatic component of the tensile stress. This is in contradiction with his original theory which stated that only the shear component of the tensile stress could endure yielding. Secondly, Haward[51] has reported that bond rotations only occur at high levels of strain. Stachurski[27] believes that this observation along with the fact that most polymers yield after just 5-10 percent strain, renders Robertson's theory invalid for most polymers. These arguments aside however, Robertson's theory is still a cornerstone for many other theories on polymeric yielding.

3.3.3.2 Free Volume

Newman and Strella[52] have suggested that resistance to yielding may be dependent upon a material's free volume. Studying the yield behavior of rubber modified glassy polymers, they reported that the yield stress decreased with the addition of rubber. They concluded that this decrease was related to localized increases in free volume, caused by the formation of triaxial stresses in the polymer directly adjacent to the rubber particles.

Golden, Hammant and Hazell[53] have also associated yield stress to a polymer's free volume. They concluded that increases in the yield stress of polycarbonate, caused by thermal annealling, were due to the increase in packing of the polymer chains leading to a reduction in free volume.

Bauwens and coworkers[49,54-56] attempted to relate this proposed association between free volume and yielding with Eyring's activation model. This relationship was based on the assumption that both plastic deformation and thermal annealing are produced by chain conformational motions. This would imply that both processes would be identically influenced by changes in enthalpy and entropy during annealing. Assuming that the activation enthalpy for both processes was equal, the frequency of conformational change should be described by an expanded form of the equation used by Eyring

$$U = U_o e^{\Delta S/R} e^{-\left(\frac{Q}{RT} + \frac{\Delta H}{RT}\right)} \qquad [3.7]$$

where: Q = activation enthalpy for conformational changes

ΔH = (Tg - Tgo) ΔC_p

Tgo = glass transition of the non annealed polymer

Tg = glass transition of the annealed polymer

ΔC_p = difference in heat capacity of the polymer above and below its Tg

Substituting this expression into Eyring's prediction of yield stress they obtained

$$\frac{\sigma_y}{T} = \frac{R}{V}\left[\ln 2C\dot{\varepsilon} - \Delta S + \frac{1}{RT}(Q + \Delta H)\right] \qquad [3.8]$$

where: V = activation volume

C = constant related to the frequency of conformational changes

They concluded from their experimental results, that ΔH was the dominant factor in the increase in yield stress with annealing.

3.3.3.3 Dislocation

Bowden[28] proposed that yielding was associated with the dislocation of molecular segments. He believed that segments of a glassy polymer situated themselves with respect to one another similar to the atoms of a crystalline solid (Figure 23). These segments, over time, would position themselves in energy wells so that their internal energy would be minimum. Configurational energy barriers, similar to that proposed by Eyring, separated these energy wells. Upon the application of a shear stress the height of the barriers decrease. This allowed the segments to shift, via thermal activation, with the stress to the next adjacent energy well. Bowden believed this shifting or dislocation of the molecular segments was the mechanism of plastic deformation.

The yield stress could be determined from the strain required to dislocate a segment to the maximum of an energy barrier. The magnitude of this strain was equal to the polymer's Burgers vector. The Burgers vector was an intrinsic polymer characteristic and was dependent upon the width of the polymer, the length of its links, the spacing of its side groups and the displacement needed to cause kinks in the chain.

Bowden proposed that plastic deformation was initiated by the nucleation of small, disc shaped regions. He determined the activation energy needed to nucleate and propagate these regions using a mathematical model proposed by Kelly[57]. This model was based on the changes in elastic energy of the matrix surrounding the plastic zone and was only dependent upon the applied stress, shear modulus, size of the plastic zone and the Burgers vector

$$\Delta H = 2\pi R\left(\frac{Gb^2}{4\pi}\right)\ln\left(2\frac{R}{r_o}\right) - \pi R^2\tau b \qquad [3.9]$$

where: b = Burgers vector

τ = applied shear stress

G = shear modulus

R = radius of the plastic zone

r_o = initial radius of the plastic zone

The entropy term to the activated rate equation was assumed negligible.

Bowden's theory has only obtained limited attention in the literature, possibly due to its lack of a molecular understanding of yielding. It is, however, quite unique.

Argon[58,59] proposed that plastic deformation is caused by the development of kinks along the polymer backbone. These kinks serve to rotate segments of the chain which are not aligned with the stress. This orients the chains as well as producing strain in the stress direction (Figure 24). Initially, the formation of kink in the chain is reversible. A kink produces an elastic strain in the surrounding matrix which in turn exerts pressure on the kink. Upon removal of the stress, the stored elastic strain energy forces the kink to flip back to its original configuration Argon proposed that this unkinking was responsible for the recovery effect seen in polymers.

The kink becomes irreversible when the stress is maintained for a sufficient amount of time for the adjacent polymer chains to also undergo kinking, and thus relieving the elastic strain. The kinking is an activated process described by the Arrehenius equation. The change of enthalpy to form the kinks was predicted by Li and Gilman[60].

$$\Delta H^* = \frac{3\pi G w^2 a^3}{16(1-\nu)}[1 - 8.5(1-\nu)]^{5/6}(\tau/G)^{5/6} \qquad [3.10]$$

where: ΔH^* = change in enthalpy

G = shear modulus

ν = poisson's ratio

τ = applied shear stress

w = angle of the wedge

a = radius of the polymer chain

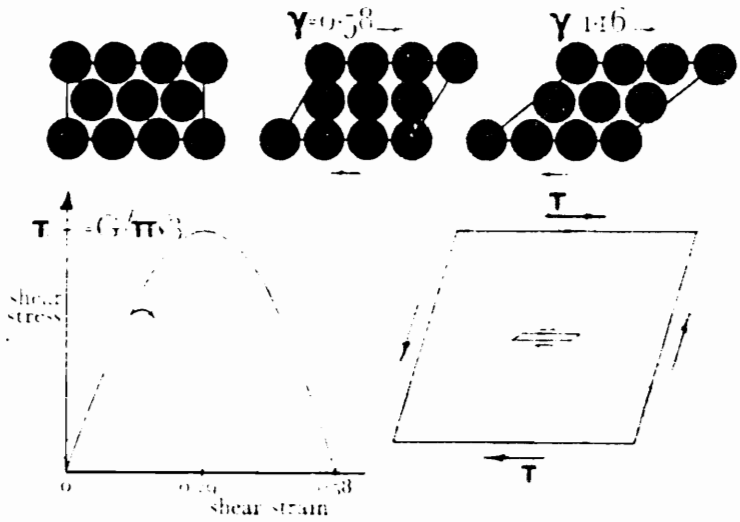

Figure 23. Bowden's image ofthe effect of shear on the packing of polymeric segments [28].

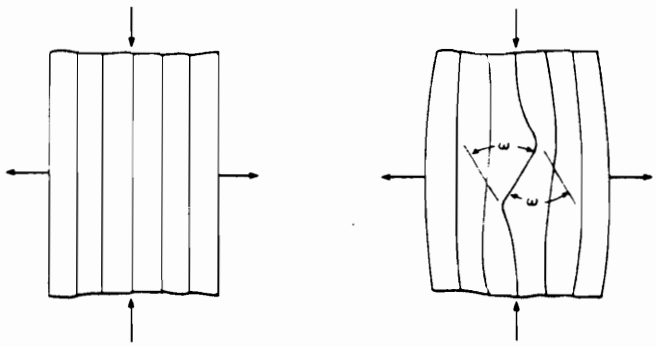

Figure 24. Schematic representation of the kinking of polymeric chains producing plastic deformation [59].

The dependence of shear modulus and poisson's ratio implies that this theory is based on elastic or intermolecular forces between the chains. The shear stress at yield is therefore also dependent upon these variables.

$$\tau = \frac{0.077G}{1-\nu}\left[1 - \frac{16(1-\nu)kT}{3\pi G w^2 a^3}\ln\left(\frac{\dot{\gamma}_o}{\dot{\gamma}}\right)\right]^{6/5} \qquad [3.11]$$

where: $\dot{\gamma}$ = applied strain rate

$\dot{\gamma}_o$ = strain rate constant

T = temperature

Some have expressed skepticism with this theory, pointing out that the kinking process would be too isolated to involve an activated volume determined in previously to be 1-20 nm^3. The theory, however, is in good agreement with yield stress experiments of PET over a wide range of temperatures and strain rates. This has also been applied successfully to polyimide systems[61]. The theory also demonstrates, through equation 3.11, how, for high induced strain rates, yield stress is proportional to shear modulus.

There are a number of similarities between this theory and that proposed by Bowden. Both theories relate rate of strain to the development or nucleation of a plastic element(a kink for Argon and a plastic disc for Bowden). The nucleation of this element is resisted in both cases by the elastic behavior of the surrounding matrix represented by the shear modulus.

3.3.3.4 Intermolecular Yielding

A more recent theory proposed by Stachurski[27,62] bases the mechanism of yielding on the breaking of intermolecular bonds. Stachurski used amorphous polyethylene to model his theory since, its chains are bonded together only by vander waals dispersion forces. He stated that these bonds form between non covalently bonded methylene units over a distribution of distances.

Upon the application of a stress, the bonds are strained according to the Lennard-Jones potential. At a critical strain, the bonds rupture. This strain is reached first by the bonds which initially were the longest. As the stress is increased, all the bonds become critically strained and rupture. Stachurski proposed that this represented the initiation of pure plastic deformation. However, if the stress is released before this occurs, the deformation is only viscoelastic. The secondary bonds reform over time and reduce the deformation. Stachurski proposed that this represented the effect known as polymeric recovery.

This model, Stachurski argued, could also explain the experimentally observed increase in yield stress with decreasing temperature or increasing pressure, since these changes would compact the polymer. This would shorten the vander waals bonds, making them more resistant to yielding.

Brown[63] also believed that resistance to yielding came from intermolecualr forces. He proposed that atoms of an amorphous glassy polymer order themselves into a loosely packed lattice like structure. Each atom of this structure is held roughly in place by vander waals forces exerted by its neighbors. During shear, these atoms are shifted relative to one another by specific rearrangement patterns. Brown determined three basic rearrangement patterns, intermolecular shear, intramolecular shear and motion along covalent bonds which he referred to as shearon, roton and tubon motions respectively.

The stress required that led to each shift was determined by a mathematical model based on the Lennard-Jones potential. Brown claims that this theory encompasses the theories of Argon, Yannas and Lunn[64] which only describe one rearrangement pattern. However, he states that this theory only partially describes molecular motion since it neglects chain flexibility.

3.3.5 Strain Softening and Hardening

Bowden[65] has related strain softening to bond rotation. He proposed that bond rotation is initially difficult due to the high packing density of the chains. However, after a few bonds have rotated, the packing density lessens. This allows rotation at a lower stress.

Strain hardening has been attributed to strain induced crystallization in a number of rubbers and thermoplastics. When a stress is applied to the polymer, the chains are oriented and crystallization occurs. The higher packing density of the chains within the crystals causes an increase in the polymer's modulus leading to a hardening effect. The hardening effect has also been attributed to the stressing of entanglements[62]. Application of stress to the entanglements may cause bond rotation which increases stiffness.

3.3.6 Forms of Yielding

Yielding can occur in three forms, which can be seen on both the macro and microscopic level (Figure 25). The most common of these, due to its occurrence in tensile specimens, is necking.

Necking develops in samples subjected to an uniaxial tensile load where no restrictions to strain in either transverse direction exist. Necking occurs during the strain softening process. Initially, necking occurs along a cross section of maximum shear which usually occurs at a ± 45 degree angle to the applied load. The lack of strain restriction allows the material to contract along the transverse directions in proportion to poisson's ratio. This causes a loss of cross sectional area.

3.3.6.1 Microscopic Yielding

Plastic deformation in metals is caused by the movement of dislocations through the

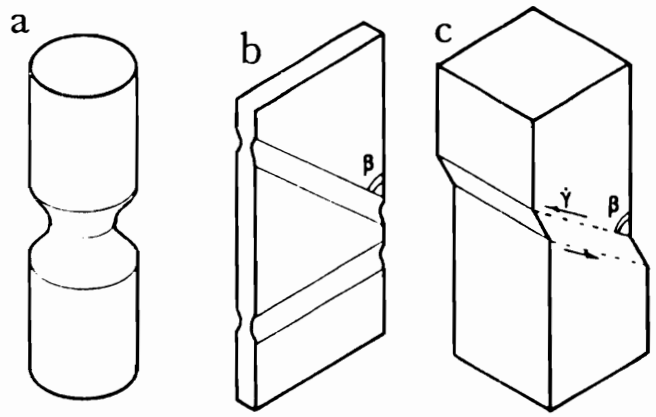

Figure 25. Forms of yielding a, necking; b, inclined necking; c, shear banding [66].

crystalline matrix. These dislocations are generally randomly spaced, producing relatively homogeneous yielding.

Plastics however, deform in very localized regions which produces inhomogeneous deformation. This is most evident in the polymer's plastic or damage zone proceeding a crack tip. Two inhomogeneous deformation processes occur within this zone, shear banding and crazing. Both are highly localized and tend to blunt the crack tip leading to a toughening of the material.

Shear banding is the stronger toughening mechanism of the two[67]. As implied by its name, shear banding involves the shifting or shearing of one cross section of material relative to another. This occurs along the plane of maximum shear. This is generally at a ± 45 degree angle to the applied stress[4]. The state of stress necessary to form shear bands is not well understood. Bowden[66] has stated that shear bands form under plain strain while Kramer[68] has reported shear banding occurring under plane stress.

Two types or sizes of shear bands are found in polymeric materials. Microshear bands are thin strips, approximately 0.5 μm in thickness, of highly deformed material. The strain in these strips can be as much as 2.5 times the strain in the bulk of the material[68,69]. These bands usually only accompany brittle fracture.

Diffuse bands or diffuse zones are much larger regions of shear, up to 0.5 mm in thickness. The strain is only a few percent greater than that of the bulk material[69]. This shearing is associated with ductile behavior and is usually responsible for the majority of energy dissipation during crack propagation of tough plastics.

The conditions necessary to form shear bands, as well as the conditions which determine the size of the bands, are directly related to the polymer's ability to strain soften. Conditions which inhibit molecular motion and increase the yield stress promote microshear banding. However, conditions which increase molecular motion and thus decrease the yield stress, such as quenching the polymer from the melt, high temperatures, or low strain rates, promote the more uniform shear as seen in the diffuse bands[66,70].

Kramer[71,72] has suggested that diffuse zone deformation is viscoelastic in nature. Kramer[68] has further reported that disentanglement of polymeric chains could not be detected in microshear bands of polystyrene.

3.3.6.2 Crazing

Crazing is a viscoelastic form of deformation which precedes crack propagation in most glassy thermoplastics. Shear banding and crazing are generally considered competitive forms of yielding, but have been reported to occur in conjunction with one another[73,74].

Crazing initiates by the cavitation of material surrounding microsized dirt particles at or near a crack tip. The cavitation is caused by the high hydrostatic stresses which are formed in front of the crack tip. Gent[75] has proposed that cavitation is proceded by a transition from glassy to rubbery behavior. The cavitation produces a thin sheet of microvoids, usually within the plane of fracture, normal to the applied load (Figure 26).

Polymers which have low yield stresses, usually yield by shear banding before the critical hydrostatic stress for cavitation is reached. Variables which lower yield stress, such as an increase in temperature, will suppress crazing. Increased pressure, which counterbalances hydrostatic tensile stress, also suppresses crazing[76,77].

After cavitation, the stress state of the material between the voids transforms from plane strain to plane stress due to the formation of free surfaces. This change allows the material to neck and creep under the applied stress, forming polymer filaments known as fibrils[78]. As the fibrils creep, polymer from the surrounding bulk interface is drawn into the fibrils[79,80]. At maximum extension, the fibrils may elongate 400 percent with the surrounding bulk material elongating up to 200 percent[68,82]. Near the crack tip, the craze may reach a thickness of 5 to 10 μm[3,79] with the fibrils having a diameter of 50 nm[80].

The cavitation and fibrillation processes also extend the microvoids to create large surface areas. At maximum extension, a craze may consist of 60 percent voids[82] and have a surface area of $10^9\ m^2/m^3$ [83].

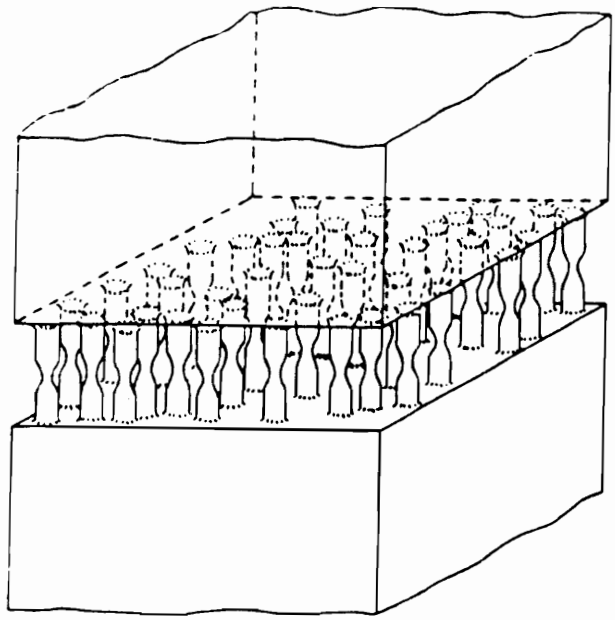

Figure 26. Craze possessing voids from cavitation and fibrils [81]

Kramer[68,80] has proposed that the large extension ratios of the fibrils can only be achieved by the chain scission or disentanglement of entangled polymeric chains. For polystyrene[68] he reports a breakdown, mainly from chain scission, of 25 to 50 percent of entangled chains. Pentice[84] has proposed that variables which reduce chain mobility, lead to chain scission over disentanglement. These include high creep rates, low temperatures, high crosslink and chain entanglement densities.

As the fibrils reach their maximum extension, they begin to fail thereby linking up the microvoids. When a sufficent number of microvoids are combined, crack propagation occurs[68].

The drawing and creeping process absorbs large amounts of strain energy, toughening the material. Pang and coworkers[85] have reported that a crazed region in polystyrene or polycarbonate dissipates 50 times more energy during crack propagation than a non-crazed region. The energy is mainly dissipated in the form of heat generated by the viscous flow of the polymer chains. Doll[82] has reported that 60 percent of the energy loss occurs from drawing with the remaining 30 to 40 percent occuring during creep. The magnitude of the energy dissipated depends on the extent to which the chains can flow past one another. Variables which restrict flow such as high strain rates, low temperatures, or high entanglement and crosslink densities, decrease the extension of the craze and lessen its toughening mechanism.

Prentice[84] proposed that this relationship between flow and energy dissipation could be determined utilizing the reptation theory. Reptation theory predicts that flow rate decreases with increasing molecular weight due to the increase in entanglement density. At relatively high strain rates the entanglements are frozen into position, forcing the chains to undergo scission reducing energy dissipation. At relatively slow strain rates or high temperatures, disentanglement is allowed. This maximizes the elongation and energy dissipation. However, entanglements are needed, since they stabilize the fibrils by generating mechanical integrity[80]. Truong, Allen and Williams[86] have reported a decrease in three orders of magnitude in the fracture energy as the molecular weight was decreased below Me..

3.4 Tensile Strength

3.4.1 Molecular Weight Effect

The stress at break of material fracturing in the realm of elastic response, is referred to as the tensile strength. For polymeric materials, tensile strength has been shown to increase and then plateau with molecular weight. Below the chain entanglement molecular weight, Me, the rate of increase is slow. However, as molecular weight increases above Me, the rate at which tensile strength increases, increases dramatically. This large increase in rate has been attributed to the formation of entanglements[87]. At high molecular weights, tensile strength levels off to a constant value. Typically, polar polymers reach this plateau level at a lower molecular weight than non-polar polymers[88]. The plateau tensile strengths for various polymers is shown in Table 1.

3.4.2 Tensile Strength Theories

Most modern theories on the molecular behavior of a polymer during fracture relate the polymer's tensile strength to the number of load carrying polymeric segments crossing the fracture plane. This was first proposed by Vincent in 1972[24].

He had previously reported[89] that bulky side groups lowered a polymer's tensile strength. He concluded that the side groups broke up the packing of the chains and lowered the number of chains per unit area crossing the fracture plane. Extending this theory to 13 high molecular weight polymers of various structures, he demonstrated that the polymer's molecular cross sectional area (MCSA)

$$\text{MCSA} = \frac{\text{weight of a repeat unit}}{(\text{sample density})(\text{length of a repeat unit})} \qquad [3.12]$$

was proportional to the critical tensile strength.

Adolf, Tirrell and Prager[90] expanded Vincent's work to include a molecular weight dependence upon tensile strength. They proposed that only the chain segments which were anchored on both sides of the fracture plane by entanglements could effectively support part of the load. Since they assumed that only chain scission caused fracture, the fracture stress had to be directly proportional to the number of these crossings. This number would depend upon the density of entanglements which was related to the polymer's molecular weight.

They derived an equation, based on the random walk theory, which determined the ratio of anchored segment crossings for a given molecular weight polymer to the number of segment crossings for an infinite molecular weight polymer. They asserted that this ratio was proportional to the ratio of the tensile strength of the two polymers.

$$\frac{N_{eff}}{N_{eff}(\infty)} = K \frac{\sigma_F}{\sigma_F(\infty)} \qquad [3.13]$$

where:

N_{eff} = number of anchored crossings for a given molecular weight

$N_{eff}(\infty)$ = number of anchored crossings for an infinite molecular weight

K = proportionality constant

σ_F = fracture stress for a given molecular weight

$\sigma_F(\infty)$ = fracture stress for an infinite molecular weight

The number of effective crossings was determined as

$$N_{eff}(\infty) = \frac{\rho l}{3N_e^{1/2}} \qquad [3.14]$$

where:

ρ = polymer density

l = statistical step length

N_e = number of step lengths between entanglements

Mikos and Peppas[91] used a similar approach to Adolf et al. in obtaining the number of anchored segment crossings

$$N_{eff}(\overline{Mn}) = N_{eff}(\infty) \exp(-2Me/\overline{Mn}) \qquad [3.15]$$

where:

$$N_{eff} = \frac{\sqrt{2/3\pi}\ \rho b N a}{Ms^{1/2} Me^{1/2}}$$

ρ = polymer density

Na = Avogadro's number

Ms = link molecular weight

Me = entanglement molecular weight

$b = \sqrt{3/2}\ C_\infty$

C_∞ = characteristic ratio

l = bond length

For high molecular weight polystyrene, $N_{eff}(\infty)$ came to be 1.46 x 10^{17} crossings per meter squared. The tensile strength was directly related to the number of crossings so that

$$\sigma_F(\overline{Mn}) = \sigma_F(\infty) \exp(-2Me/\overline{Mn}) \qquad [3.16]$$

where: σ_F = fracture stress

The total energy at break was assumed to be equal to the energy required to strain and rupture the bonds within the anchored segments.

$$G_F = N_{eff} N_e \varepsilon_s \qquad [3.17]$$

where: N_e = length between entanglements

ε_s = energy to rupture a statistical segment (includes conformational energy changes)

Conformational energy changes were included into G_F since they discovered that extension of the chains at break was greater than 99 percent maximum elongation.

For high molecular weight polymethylmethacrylate, ε_s was determined to be 3.8×10^{-18} J/bond. This is an order of magnutude greater than the bond dissociation energy. This suggests that conformational energies absorb the majority of the energy at fracture.

3.5 Ductile Brittle Transition

The failure mechanism of a polymer can be classified as either brittle or ductile. Brittle failure occurs when a polymer's yield stress exceeds its tensile strength, $\sigma_o > \sigma_F$ while ductile failure occurs when the tensile strength exceeds the yield stress, $\sigma_F < \sigma_o$. As has been discussed in previous sections, yield stress and tensile strength can be altered, independently of one another, by changes in temperature, strain rate or topology. For example, yield stress for most polymers is seen to decrease dramaticly with increasing temperature or decreasing strain rate, while tensile strength decreases slowly (Figure 27). At low temperatures, $\sigma_o > \sigma_F$, so the material fails brittlely. However, as the yield stress crosses over the tensile strength, $\sigma_B > \sigma_o$, and ductile failure occurs. The point of transition, $\sigma_F = \sigma_o$, is referred to as the ductile/brittle transition. In regards to topology, ductile polymers have been shown to fail brittlely as molecular weight is decreased below Me. Above Me, the failure mechanism of glassy polymers has been related to the polymer's chain contour length between entanglements and the chain's cross sectional area[92]. Sharp notches can also induce brittle fracture from a ductile polymer since they have been reported to increase yield stress by a factor of three.

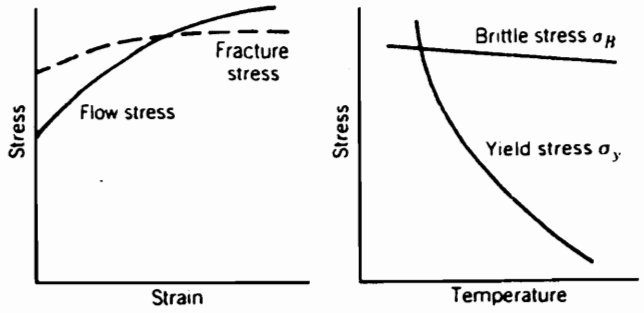

Figure 27. Stress versus temperature curves demonstrating ductile brittle transition [37].

3.6 Fracture Toughness

Table 2 shows the critical stress intensities along with some critical strain energy release rates for a number of polymers tested at room temperature using moderate strain rates. The fracture toughness values for a few metal alloys and glass are included.

Rigid and brittle polymers such as the epoxy resins, polymethylmethacrylate and polystyrene exhibit the lowest toughness values, ($K_{1_c} < 1.5$ MPa $m^{1/2}$). Ductile thermoplastics such as polysulfone and polycarbonate possess significantly higher toughness values, ($K_{1_c} > 1.5$ MPa $m^{1/2}$). In comparison to metals, however, such as aluminum and titanium alloys, even the ductile polymers are relatively brittle.

3.6.1 Viscoelastic Effects

Fracture toughness, like many of the other polymeric mechanical properties, is dependent on viscoelastic parameters. Bitner and coworkers[93] have reported that increasing test speeds decrease fracture toughness of adhesive bonds. The reason behind this decrease is the reduction in the magnitude of plastic deformation which accompanies increased strain rates. Prentice[84], studying the toughening effect of crazes in PMMA, reported that toughness decreased with increased strain rate due to the reduction in time allowed to form the crazes. He believed that fast strain rates greatly limited the disentanglement of chains thereby reducing the magnitude of plastic deformation and forcing the chains to undergo chain scission.

The effect of temperature on fracture toughness is inconclusive. Ward[94] reported that the critical strain energy release rate for polycarbonate under a plane strain condition modestly decreased with increasing temperature. Under a plane stress condition, however, G_{1_c} remained constant between -30 °C to 20 °C. Hunston[95] has presented data which implies a maximum in fracture toughness can exist with respect to temperature for adhesive bonds.

Table 2. Fracture toughness values for various polymers and metals

Materials	K_{1_c} (MPa $m^{1/2}$)	G_{1_c} (KJ/m^2)
Epoxy	0.5	0.1
Glass	0.7	0.007
PMMA	1.1	0.5
Polystyrene	1.1	0.4
Rubber toughened Epoxy	2.2	2
HIPs	-	15.8
Polyethylene	-	20
Polycarbonate	2.75-3.3	4.0
Steel mild	37	20
Aluminum Alloys	16-44	-
Titanium Alloys	75-125	-

1 MPa $m^{1/2}$ = 1 MN x $m^{-3/2}$
= 0.9101 ksi $in^{1/2}$
= 910.1 psi $in^{1/2}$
1 KJ/m^2 = 1000 J/m^2
= 5.709 in lbf/in^2
=0.476 ft lbf/in^2

Fracture toughness has also been shown to be dependent on molecular weight. Kramer[96] reported that for molecular weights less than Me, the fracture surface energy is proportional to the square root of the molecular weight

$$\gamma \propto MW^{1/2} \qquad MW < Me \qquad [18]$$

where:

$$\gamma = \text{fracture surface energy}$$

Above 2Me, the dependence on molecular weight increases[97,98]

$$\gamma \propto MW^{2.5} \qquad MW > 2Me \qquad [19]$$

The fracture surface energy finally plateaus off at some ceiling molecular weight. Prentice[84] explains the increase of toughness with molecular weight by the increase in viscous energy needed to overcome frictional drag. The increase in the molecular weight exponent as molecular weight increases beyond Me describes the added frictional drag induced by the formation of entanglements.

Annealing has also been shown to decrease fracture toughness[73]. This decrease has been attributed to the increase in yield stress which accompanies annealing[99].

3.6.2 Geometry Effects

Fracture toughness is also dependent on specimen geometry such as thickness, crack length and crack tip radius. Variations on any on these alters the state of stress on the material, possibly effecting the material's fracture toughness. Ward[94] reported that G_{1_c} for polycarbonate increases from 0.7 kJ/m² to 16 kJ/m² as specimen thickness is decreased thereby transforming the state of stress from plane strain to plane stress.

The effect of crack length on toughness is unclear. The ASTM standard of fracture toughness testing of metals state that the ratio of crack length to width must be between 0.3 and 0.7 for the test to be valid. This implies that outside of these limits the value of fracture toughness may not remain constant. Ward[100] however reports for razor notched polycarbonate, G_{1_c} is independent of crack length, even outside the ASTM limits.

The effect of the initial crack tip radius on toughness is also unclear. Increases in crack tip radius has been reported[100] to increase the extent of plane stress (shear lips) fracture thereby increasing toughness due to increased yielding. Others, however, have reported that sharp crack tips, promote ductile tearing failure thereby increasing G_{1_c}. They reason that with an increase in crack tip radius, the stress concentration in front of that crack tip is reduced. This forces the applied stress to be increased before failure can be initiated. This in turn generates a larger amount of stored elastic strain energy than would be generated in a material containing a sharper crack tip. The larger amount of stored energy promotes critical crack propagation. The sharper crack, with less stored elastic energy, is less likely to propagate critically, thereby promoting tearing.

Chapter 4 Review of Materials

Engineering thermoplastics and thermosets and their composites are slowly replacing metals in many areas such as the railway, automobile, and aerospace industries. The driving force behind this change has been the need for lighter structural materials to reduce operating fuel costs. Engineering polymers have greater strength to weight ratios than metals which allows design engineers to reduce vehicle weight.

The military aerospace industry has been a leader in innovation in this field. Engineers have been utilizing composites in fighter aircraft, not only for fuel savings, but to increase the plane's speed and maneuverability. For example, the F-15, built in the early 1970's, contains just 2 percent by weight composites. The F-18, built during the 1980's contains 10 percent composites. The advanced tactical fighter, not yet under commercial production, will contain nearly 40 percent composites.

The utilization of new matrix resins has increased the use of composites in fighter aircraft. Epoxy resins, initially utilized as aerospace composites, are limited in their applications due to their brittle nature, low glass transition temperatures and poor hot wet mechanical properties. The new engineering thermoplastic and thermoset matrix resins possess greater toughness and/or higher use temperatures than epoxies. Some of these new resins include

polyarylene ether sulfones, polyphenylene sulfides, polyarylene ether ether ketones, modified epoxies and bismaleimides. Polyarylene ether ketones and bismaleimides will be discussed.

4.1 Polyarylene Ether Ketones

The first polyarylene ether ketone(PAEK), polyetheretherketone (PEEK), was commercialized in 1981 by the Imperial Chemical Industries (ICI). Since then other polyarylene ether ketones have been commercialized, such as polyetherketone (PEK) by ICI and polyetherketoneketone (PEKK) sold by Dupont. All three resins are semicrystalline thermoplastics that are thermally, radiation and oxidatively stable, chemically resistant, tough, and processable. Initially marketed as a high temperature cable insulator, PAEKs are now found in many high temperature, high performance applications. These applications include bearings for car engines, valves in high pressure steam lines, piping material in acid pipelines, pressurized parts of geothermal wells and matrix materials for aircraft composites[101,102]. The widening array of markets for PAEKs has caused the sales of PEEK for example, to double every year since its introduction.

4.1.1 Solvent and Chemical Resistance

The semicrystalline morphology of polyarylene ether ketones imparts these polymers with excellent solvent and chemical resistance[101]. PEEK is not known to dissolve in any common solvents such as chlorinated or dipolar aprotic solvents at room temperature. However solvents such as hydrofluoric acid, trifluoromethane sulfonic acid and a mixture of phenol and 1,2,4 trichlorobenzene have been reported to dissolve the polymer at elevated temperatures. PAEKs are equally hard to swell. PEEK and PEK exhibit an increase of just 0.6 and 0.4 weight percent, respectively, after 24 hours in methylene chloride[103]. However, amor-

phous PEEK swells significantly more, 15.8 percent, due to the absence of crystallinity. Table 3 lists PEEK's retention of elongation and change in weight after being exposed to a variety of solvents.

4.1.2 Thermal, Oxidative, and Radiational Stability

The all aromatic polymer backbone of polyarylene ether ketones have been shown to possess excellent thermal, oxidative, and radiation stability. PEEK for example, has been reported to withstand gamma and beta radiation of 1000 and 10,000 Mrad respectively, without embrittlement[101]. Thermally, PAEKs possess a continuous use temperature of 260 °C and one hour stability at 400 °C under nitrogen. The backbone stability of PAEK's combined with their solvent resistance enables them to withstand high pressure steam at 280 °C and 2600 psi for 3000 hours without significant loss of tensile or flexural properties. This enables PAEK to be utilized in geothermal wells where water and oil emulsions may reach a temperature of 280 °C and a pressure of 20,000 psi.

4.1.3 Mechanical Properties

Polyarylene ether ketones are often used as structural engineering thermoplastics due to their rigidity and high fracture toughness (Table 4). PEKK, for example, possesses a tensile modulus nearly that of phenoxy resins (650,000 psi), while maintaining a fracture toughness comparable to polyether sulfones (1KJ/m^2). The magnitude of both the modulus and toughness of PAEKs depend on the ratio of ether to ketone groups along the polymer backbone. Modulus increases from 550,000 psi to 650,000 psi as the ratio of ether to ketone groups decreases from 2, for PEEK, to 0.5 for PEKK. This increase is not attributable to an increase in crystallinity, as is seen in thermoplastic elastomers, since crystallinity decreases with increasing ketone content, 33 percent for PEEK to 26 percent for PEKK. Rather, the increase is

Table 3. PEEK's retention of elongation after exposure to solvents[101]

Reagent	Temp, °C	Time, d	Retention of elongation, %	Change in weight, %
benzene	23	7	94	0
trichloroethylene	23	7	110	0.8
concentrated NaOH	23	7	94	4.3
HNO_3, 40%	23	7	107	0.4
H_2SO_4, 50%	100	30	100	0.7
tetraethyllead	23	30	100	0
dimethyl sulfoxide	100	30	100	0.7
hydrogen peroxide, 30%	23	30	100	−0.1

[a] Natural grade.

Table 4. Physical and mechanical properties of poly(arylene ether) ketones[102-105]

PROPERTY	PEKK	PEK	PEEK
Density (g/cm^3)	1.3	1.30	1.32
Crystallinity (%)*	26	-	33
Swelling in CH_2Cl_2 for 24 hours (%)	0.4 15.8**	-	0.6
Tg (°C)	156	162	143
Tm (°C)	338	373	334
Modulus (psi)	650,000	580,000	550,000
Tensile Strength (psi)	14,800	15,200	14,500
Elongation at break (%)	4	5	40
$G_{1c}(KJ/m^2)$	1	-	2

*crystalline content of commercially sold material
**swelling of totally amorphous material

due primarily to the replacement of the flexible ether groups with the more rigid, planar ketone groups.

Fracture toughness decreases with increasing ketone content, from a G_{1c} of 2 KJ/m^2 for PEEK to 1 KJ/m^2 for PEKK. Elongation at break parallels the trend of toughness, 40 percent for PEEK to 4 percent for PEKK[103,105]. This reflects restriction to motion in the polymer chain due to the increase of rigid ketone groups. Crystallinity also restricts chain flexibility. The yield stress of PEEK has been shown to increase with increasing crystallinity up to 30 percent crystalline content, where no yield is observed.

A major disadvantage in polyarylene ether ketones, however, is the polymers' loss of mechanical strength above their respective glass transition temperatures. The tensile modulus of PEEK for example, exhibits a decrease in magnitude by more than a factor of 3 as temperature is raised from 125 °C to 175 °C. Flexural modulus shows an even larger decrease, dropping from 3.6 GPa at 100 °C to 0.5 GPa at 200 °C. Tensile strength also decreases from 14,500 psi at 23 °C to 5,100 psi at 150 °C.

4.1.4 Composite Applications

The application of polyarylene ether ketones as composite matrix resins is due in part to their high transverse modulus and strength which they impart to a composite lamina. These transverse properties evolve from the development of a transcrystalline morphology within the matrix surrounding the carbon fibers[106]. Carbon fibers have been shown to act as nucleating sites for crystal formation in PEEK[106-108]. Lateral growth from these sites is prevented due to presence of adjacent crystals along the fiber. This forces the crystals to grow radially outward from the fiber leading to transcrystallinity. The transcrystallinity has been reported to improve the lamina's transverse properties by first orienting the crystals in the transverse direction, and secondly, by improving the adhesion between the matrix and the fiber thus reducing delamination.

4.1.5 Synthesis of PEEK

PEEK is synthesized through an aromatic nucleophilic substitution reaction of 4,4′difluoro-benzophenone with hydroquinone, shown in Figure 28. The reaction is carried out in diphenylsulfone at 320 °C using potassium carbonate as the base[101,109]. The reaction initiates by the formation of the phenolate of hydroquinone through the exchange of potassium ions with the phenolic protons. Carbonic acid is formed as a by product which then decomposes into water and carbon dioxide.

The reaction proceeds by the attack of the nucleophilic phenolate anion on the aromatic carbon of difluorobenzophenone adjacent to the fluorine. The rate at which this intermediate is formed is dependent on the ability of the aromatic ring to disperse the negative charge[110]. Figure 29 shows the hybrid intermediate structures of the aromatic carbanion. The electron withdrawing carbonyl group attached para to the fluorine stabilizes the intermediate, allowing the reaction to proceed.

The final step of the reaction involves the loss of the fluorine anion from the ring thus forming the aromatic ether bond. This step occurs relatively quickly in comparison to the second step.

As molecular weight and the extent of this reaction increase, the polymer crystallizes. Crystallinity in PEEK is a result of symmetry which includes the planar packing between the macromolecules caused by the aromatic backbone in association with the sp_2 bonding of the carbonyl group[109,111]. This ordered packing arrangement, at higher molecular weights, reduces the ability of the diphenyl-sulfone to solvate the polymer chains. Thus, the polymer often precipitates from the solution, terminating the polymerization and limiting the final molecular weight. Higher molecular weight polyarylene ether ketones have been obtained by incorporating ortho and meta linkages into the aromatic backbone thereby reducing the packing of the polymer chains allowing the polymer to stay in solution longer[101].

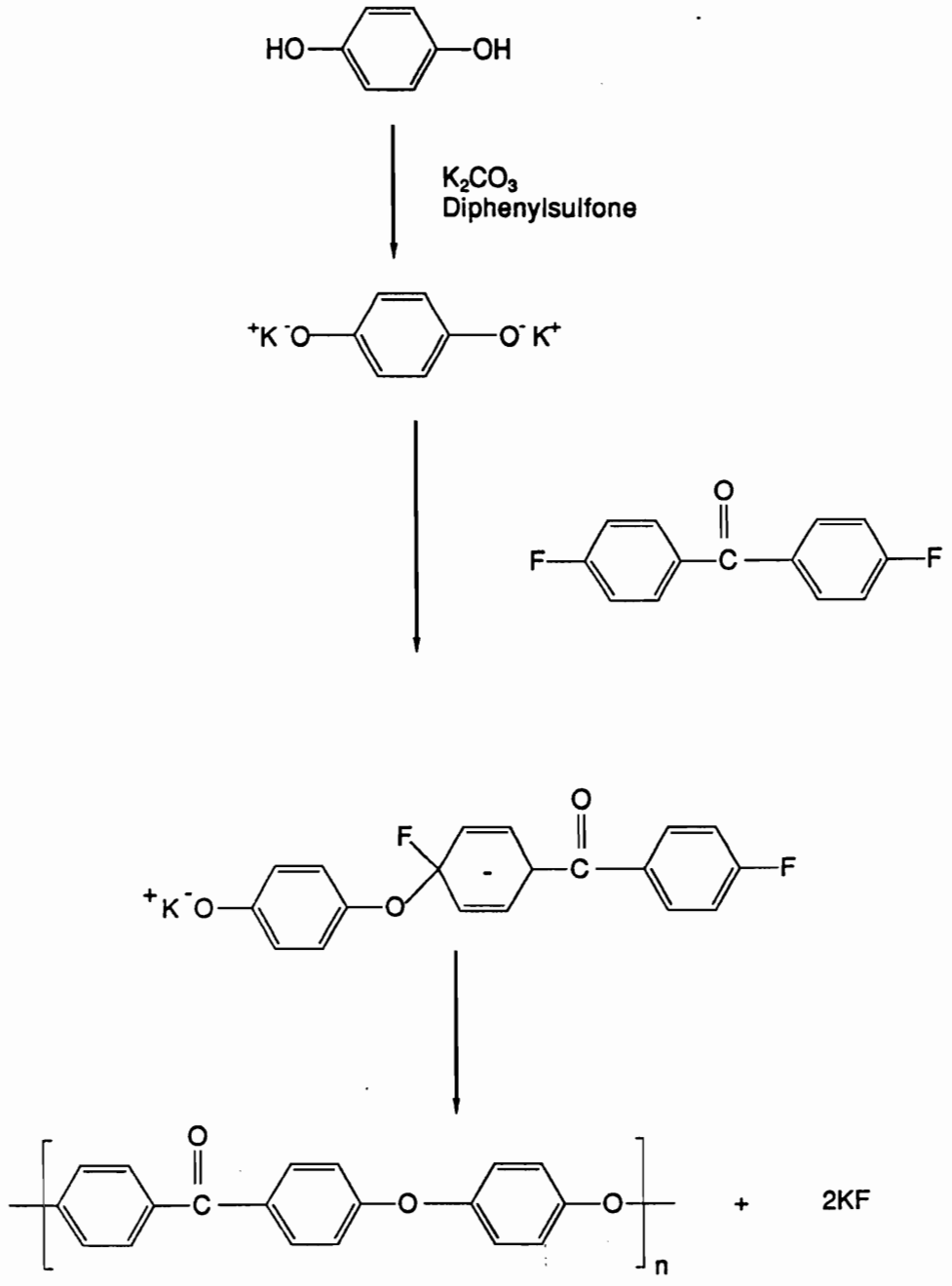

Figure 28. Synthesis of Polyetheretherketone via Nucleophilic Aromatic Substitution

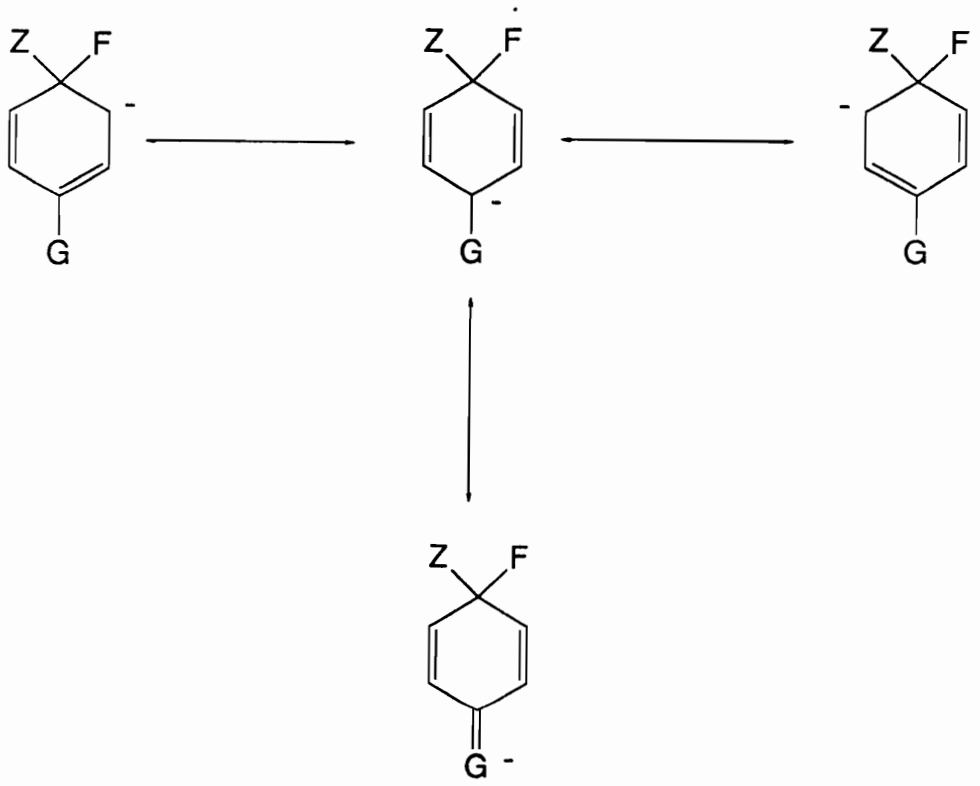

where: z = $\ddot{O}$-Ar

G = electron withdrawing group

-COR

Figure 29. Hybrid intermediate structures of an aromatic carbanion

PEK is synthesized similarly using the AB monomer 4-fluoro-4′-hydroxy benzophenone, (Figure 30) [112]. PEKK is believed to be synthesized by a Friedel-Crafts acylation using diphenylether and a mixture of iso and terephthayol chloride (Figure 31) [103].

Mohanty et al [112] reported two novel methods for obtaining crystalline PEEK without the use of high reaction temperatures. The first reaction scheme involved the use of a mixture of hydroquinone and t butyl hydroquinone. The t butyl group disrupts the packing of the PEEK molecules, thereby eliminating the crystalline morphology. This method allowed for the synthesis of high molecular weight polymers at reaction temperatures of 170 °C (Figure 32). Crystallinity could be induced to the polymer after polymerization by partial dealkylation of t butyl group under acid catalyzed high temperature reactions.

A second methodology [113] used a somewhat similar approach. By replacing 4,4′difluorobenzophenone with 4,4′-difluoro N-benzohydroxylidene aniline, crystallinity was once again broken up, allowing the reaction to take place at 150- 190 °C (Figure 33). Crystallinity was then induced by quantitatively hydrolyzing in the presence of trifluoromethane sulfonic, the ketimine linkages back to carbonyl groups. The deprotected material exhibited a melting endotherm 322 °C, just 10 degrees below that of commerical PEEK.

Wu et al [109] has reported that the Tg of PEEK could be increased by as much as 50 °C by incorporating sulfone groups along the polymer backbone. At higher levels of sulfone groups, however, crystallinity was lost.

4.1.6 Crosslinking of Polyether Ketones

Polyarylene ether ketones can be crosslinked by either physically blending a crosslinking agent with the polymer, or by incorporating reactive functional groups on the polymer chain. Oxygen has been reported to cause crosslinking of PEEK when it is blended into the polymer during processing above 400 °C[101]. Jarrett and Staniland[114] have reported that

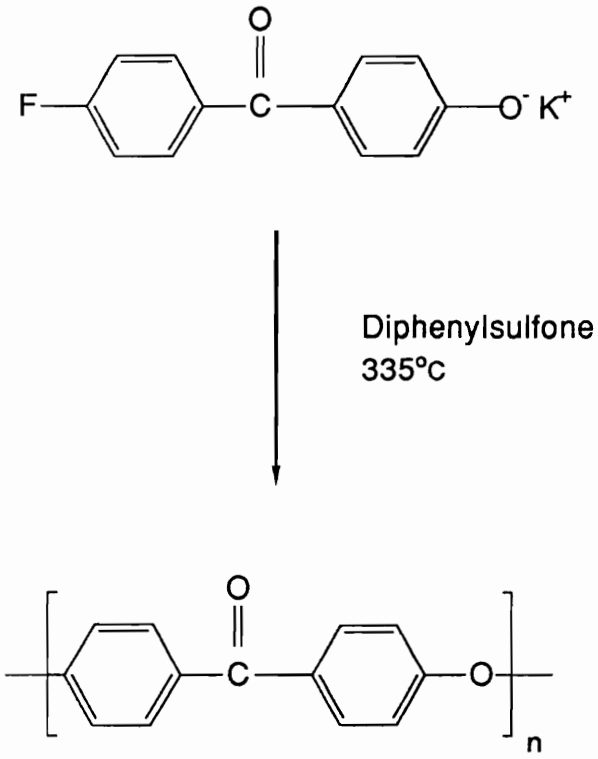

Figure 30. Synthesis of Polyetherketone [112]

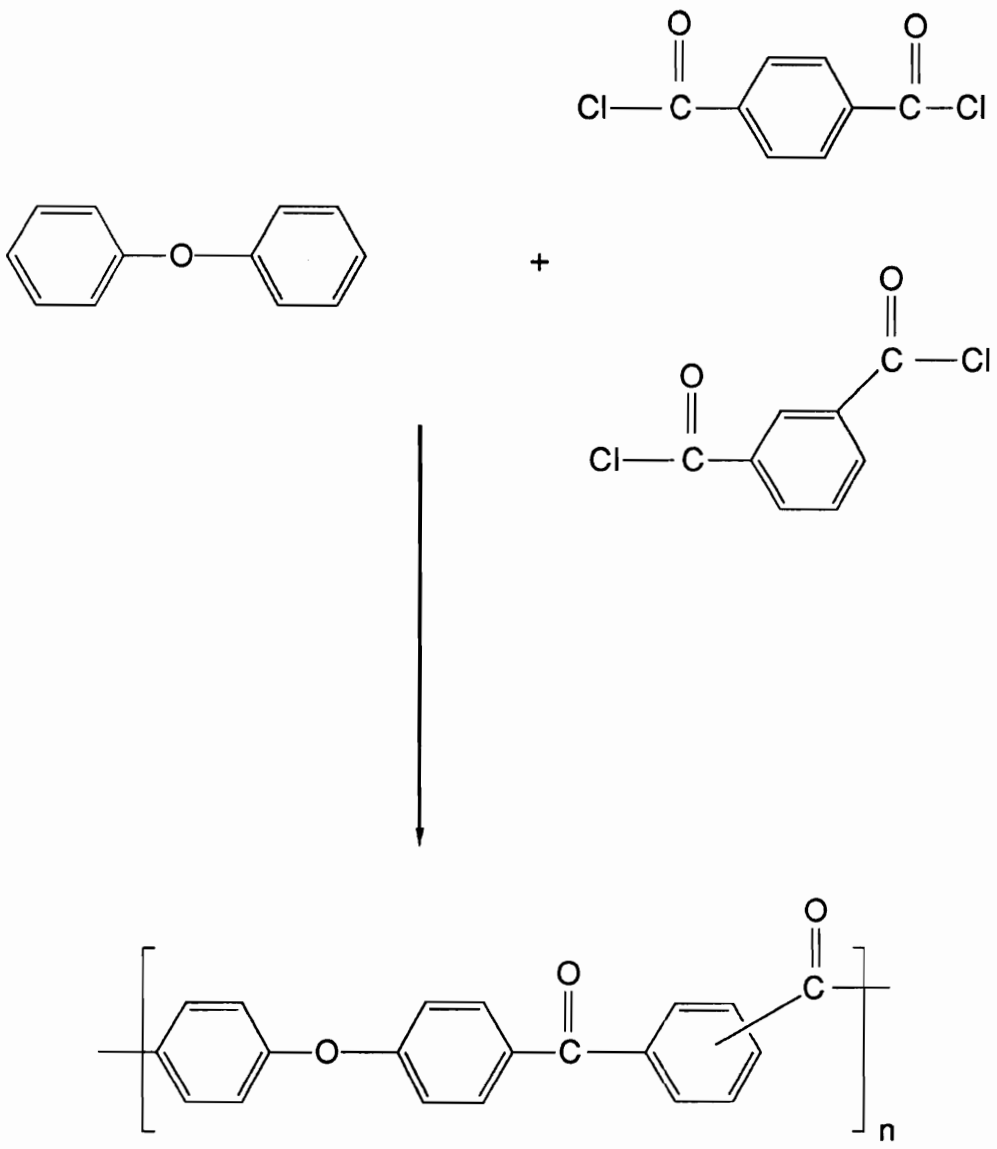

Figure 31. Synthesis of Polyetherketoneketone [103]

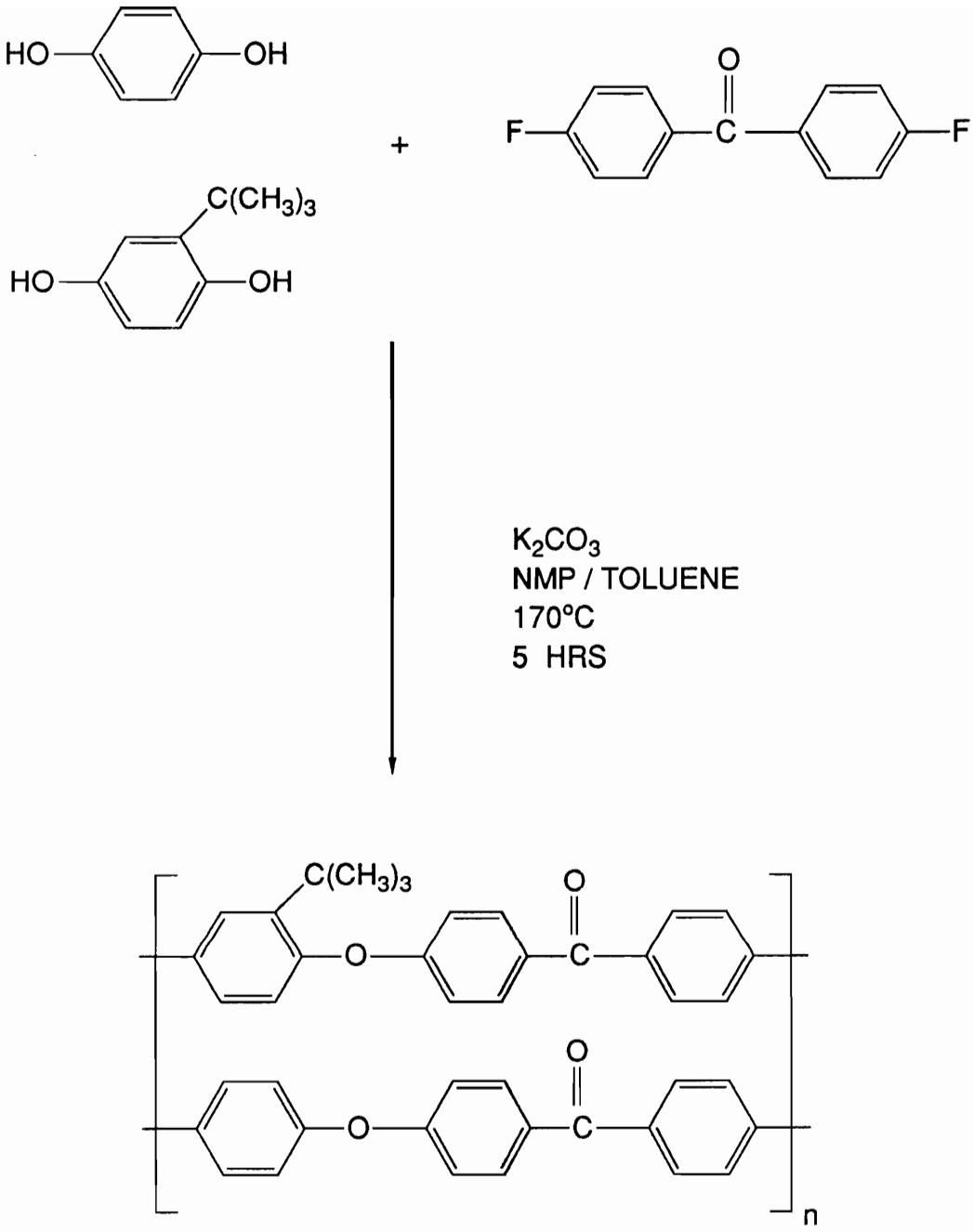

Figure 32. Synthesis of t butyl hydroquinone/hydroquinone based Polyetheretherketone [112]

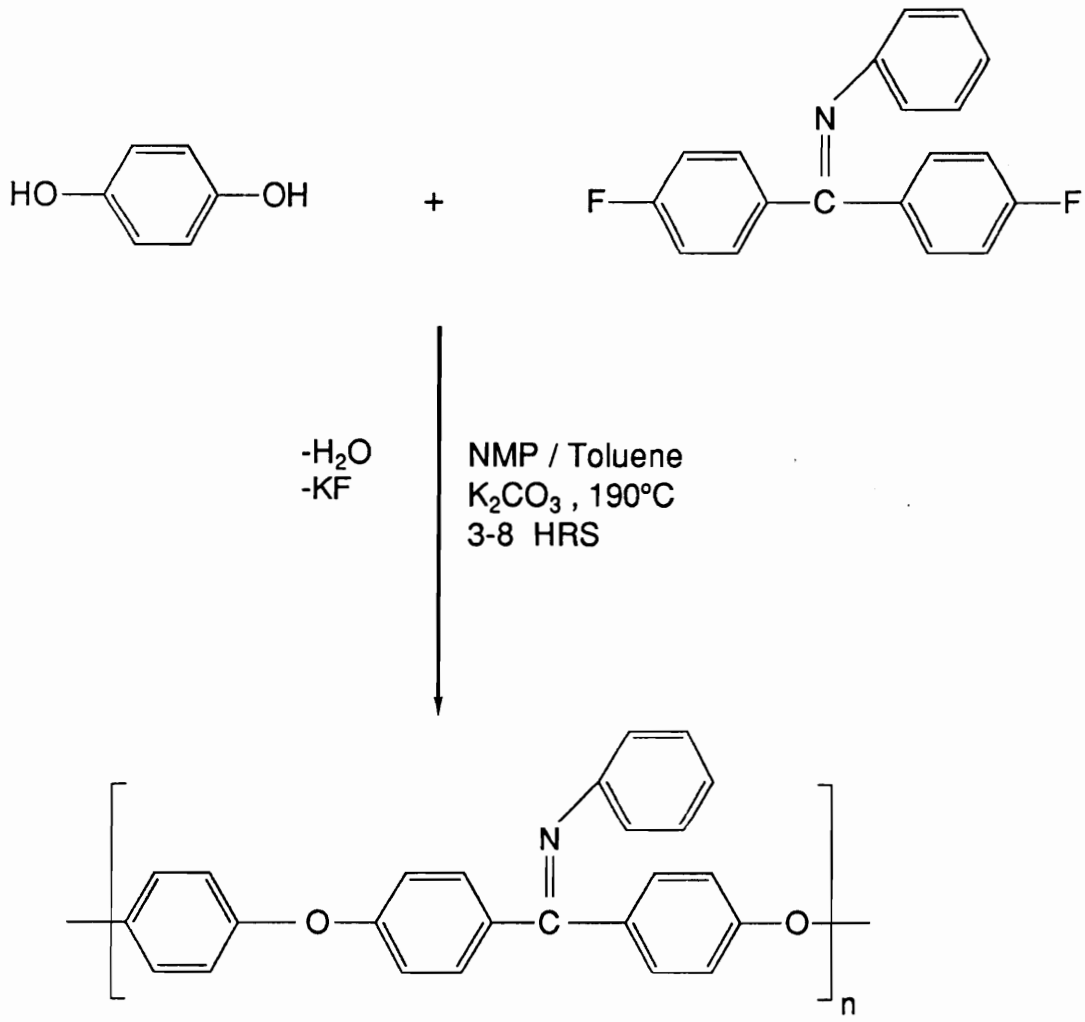

Figure 33. Synthesis of (4,4'difluoro N-benzohydroxylidene aniline) based Polyetheretherketone [113]

elemental sulfur can induce crosslinking of polyether ketone-polysulfone copolymers between 300 °C and 450 °C, by an unknown reaction.

Chan and Venkatraman[115], using elemental sulfur, altered PEK's and PEEK's physical and mechanical behavior. They demonstrated that crosslinking can be achieved by blending the reactants in an extruder at 400 °C and subsequently annealing the blend at 240 °C for several hours to several days. Although the mechanism of crosslinking is not completely understood, rheometric experiments demonstrated that chain scisson of the polymer chains occurs during blending, followed by crosslinking during the annealing process. It was also shown that crosslinking took place at a higher rate in the absence of oxygen.

Dynamic mechanical analysis of PEEK cured with two percent sulfur shows an increase in the glass transition of nearly 20 °C and a 50 percent increase in the rubbery modulus at 200 °C, compared to commercial PEEK. The percent crystallinity, determined by X-ray scattering, remains constant (40 percent). Therefore, Chan and Venkatraman concluded that sulfur induced crosslinking occurs within the amorphous regions of the polymer.

Swedo and Marvel[116] reported crosslinking polyether ketones through the reaction of biphenylene units, incorporated along the polymer backbone, at temperature of 300 - 400 °C. Glass transition temperatures of their systems were increased by as much as 100 °C.

Mohanty et al [113] reported that amorphous amine terminated polyether ketone oligomers could be thermally crosslinked above 220 °C. Upon heating, the amine endgroups react with the carbonyl groups along the polymer backbone giving imine bonds (Figure 34). Solid state C^{13}NMR of the crosslinked polymers showed the formation of a peak at 176.5 ppm which was assigned as the imine bond. The glass transition temperature of a 10K oligomer, when crosslinked, increases by only 8 °C.

Thompson and Farris[117] has also utilized the ketimine reaction in the crosslinking of PEEK with 1,4 phenylene diamine. The network was formed by reacting PEEK with a large excess of the diamine in diphenylsulfone at 230 °C for 3 hours. The material was precipitated and then pressed at 200 °C for one hour into a film and cured either in situ during dynamic mechanical or differential scanning calorimetry analysis or by a procedure which was not re-

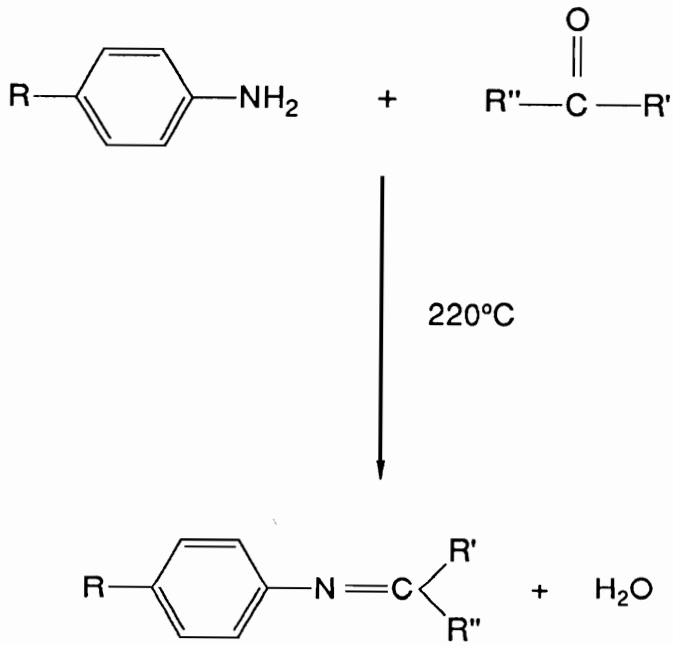

Figure 34. Ketimine formation via the reaction between an aromatic amine and a carbonyl [113]

ported. As expected, cure times increased with increasing film thickness. Thompson proposed that this was due to the reduction in the diffusion rate of water from the film. The formation of imine linkages was indicated by C^{13}NMR, showing the loss of the carbonyl signal at 192 ppm and the appearance of an imine signal at 156 ppm. The C^{13}NMR imine signal appears greater than 20 ppm higher than that reported by Mohanty (176.5 ppm). More recent measurements suggest that the difference may be related to problems with spinning side bands.

Crosslinking played a dramatic effect on the rubbery storage modulus of the material. Isothermal dynamic mechanical analysis of an in situ cure sample at 200 °C for 3 hours showed an increase in storage modulus from 10 MPa to 2 GPa. However, commercial PEEK exhibits no such increase. DSC, from room temperature to 280 °C, of the cured material does not indicate a glass transition. A melting endotherm (330 °C), however, was still detected by DSC. This indicates that the crosslinked material still has a semicrystalline morphology. The cured PEEK polymer was found to be insoluble in strong acids such as methane sulfonic acid.

4.2 Bismaleimides

Bismaleimide resins were commercially introduced approximately 20 years ago to fill the growing demand for a high temperature thermosetting composite matrix material for military aircraft applications. Bismaleimides possess superior high temperature mechanical properties compared to epoxies since they have high glass transition tempeatures, greater than 250 °C. Like epoxies however, they have excellent solvent resistance, low toxic emissions, good adhesive properties and can be easily processed. Today, bismaleimides are used in the horizontal and vertical stabilizers of the F-16 as well as parts of the AV-8B vertical take off and land fighter.

4.2.1 Synthesis and Curing of Bismaleimides

There are a number of commercially available bismaleimides on the market (Table 5). These materials, which are used as the building blocks for bismaleimide composite resins, are all crystalline solids which melt in the range of 90 to 235 °C. They are synthesized by the reaction of a bisamine with an excess of maleic anhydride at room temperature, forming a bisamic acid in quantitative yields (Figure 35) [118]. The acid undergoes cyclodehydration in the presence of acetic anhydride and fused sodium acetate at 40 to 60 °C giving a bismaleimide. The recrystallized product has a yield of approximately 70 percent. This reaction has also been used to form maleimide terminated polyether sulfone oligomers[119].

Bismaleimides are easily polymerized and can be cured in the molten state above 180 °C. The curing is thought to occur through free radical polymerization of the double bonds of the maleimide endgroups[118]. It is believed that the adjacent carbonyl group withdraws electrons from the double bond making it susceptible to radical attack[118]. The carbonyl group then stabilizes the radical after the attack by resonance. The rate of cure is a function of the mobility of endgroups. Stenzenberger reported, examining bismaleimides containing a polymethylene backbone, that the cure rate decreased with increasing melt viscosity caused by increasing methylene groups[120].

4.2.2 Bismaleimide Resins

Most commercial bismaleimide resins are formulations of various bismaleimides along with other additives such as aliphatic diamines mixed together to satisfy the requirements needed for a specific application. The base bismaleimide which is most widely used due primarily to its low price, is 4,4'bismaleimidodiphenylmethane (BMI). Prepregging formulations have been reported to contain 50 - 60 weight percent bismaleimides with the other 40 - 50 percent being a mixture of chain extenders, inorganic fillers, elastomers, reactive diluents and

Table 5. Commercially available bismaleimides[121]

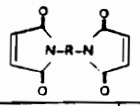

LIT	-R-	Mp (°C)	DSC Data[1]	
			T_{MAX}[2] (°C)	H[3] (J/g)
(A)	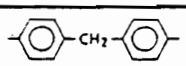	155-157	235	198
(A)	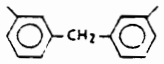	195-196	NA	NA
(A)	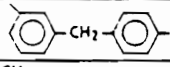	164-165	NA	NA
(A)	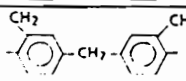	210-212	NA	NA
(A, A)	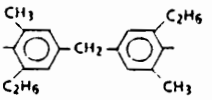	150-154	298	187
(A)	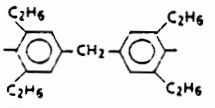	149-151	328	206
(A)	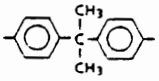	235	290	216
(A)	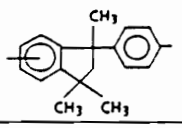	90-100	203	89

[1] DSC = Differential Scanning Calorimetry, heating rate 10°C/min.
[2] T_{MAX} = cure exotherm peak maximum.
[3] H = heat of polymerization.
(A) - Data generated by Technochemie GmbH - Verfahrenstechnik
NA - Data not published.

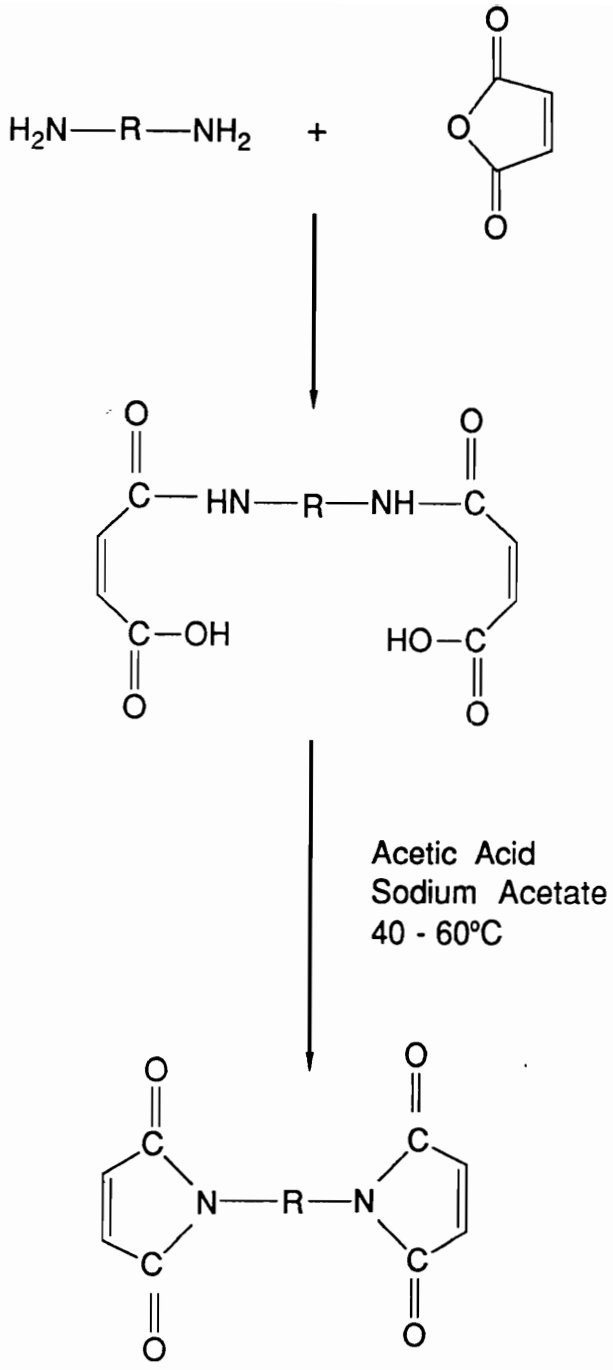

Figure 35. Synthesis of bismaleimides

comonomers[122]. The exact composition of these formulations, however, are usually proprietary information.

4.2.3 Toughening of Bismaleimides

Traditionally, inorganic fillers such as alumina, silica and glass spheres have been used in an attempt to toughen the normally brittle bismaleimide resins[123]. Recently however, attention is being paid to the toughening effects of chain extenders, elastomers and comonomers. The resin is believed to be brittle due to its high crosslink density which restricts molecular motion in the matrix. Adding elastomers, chain extenders, etc., increases the distance between crosslink points, thereby increasing the flexibility and toughness of the matrix[118]. The number of reagents available for toughening bismaleimides are limited due to the resins' high temperature performance requirements.

4.2.3.1 Comonomers and Oligomers

One such comonomer used to chain extend and toughen bismaleimides is diaminodiphenylmethane, DADPM. DADPM is incorporated into the BMI matrix through a Michael addition reaction[118]. This incorporation decreases the crosslink density of the matrix thus increasing its toughness. DADPM has been shown to improve the fracture toughness of BMI from a G_{1c} of less than 50 J/m^2 to a G_{1c} of 200 J/m^2[122]. Commercially, DADPM is used in the bismaleimide resin, Kerimide 601, from Rhone-Poulenc. Unfortunately it is recognized as a severe carcenogen.

Allyl, vinyl and propenyl terminated monomers and low molecular weight oligomers have been used as tougheners[118,122,124-126]. These materials are incorporated into the bismaleimide matrix via a Diels-Alder or an 'ene' reaction. The toughness of these networks (Table 6) exhibits a critical strain energy release rate an order of magnitude greater than that of the unmodified systems while maintaining a Tg of 250 °C or greater. Stenzenberger has

Table 6. Toughness of bismaleimide resins coreacted with allyl,vinyl, and propenyl terminated modifiers [122,124-126]

TOUGHENER	WEIGHT FRACTION (%)	G_{1c} (J/m^2)	Tg (°C)
Control/Compimide 796	100	63	> 300
4,4′bis(o-propenylphenoxy)-diphenylsulfone	18	185	285
	40	267	256
4,4′bis(o-propenylphenoxy)-benzophenone	20	191	266
	30	397	265
	40	439	249
4,4′o-methoxy-p-propenyl-phenoxy diphenylsulfone	20	234	300
	40	378	277
4,4′o-methoxy-p-propenyl-phenoxy benzophenone	20	247	252
	30	545	258
	40	466	260
2,4′bis(o-propenylphenoxy)-benzophenone	20	296	249
	30	323	252
	40	467	241
Control/Compimide 353	100	25	-
Divinylbenzene	20	180	-
o,o′diallyl bisphenol-A	24	365	-
Control/Desbimid	100	~25	
Styrene/2-hydroxy-ethyl methacrylate	50	470	250

reported that in systems containing bisallylphenyls, a maximum toughness is obtained at 30 to 40 percent modifier (Figure 36) [122]. The maximum in toughness was also observed for the 4,4'bis(-o-methoxy-p-propenylphenoxy) benzophenone/compimide 796 system (Table 7).

4.2.3.2 Blended Thermoplastics

An increase in toughness has also been achieved by physically blending thermoplastics with bismaleimide resins[123,127-129]. Table 8 shows the results of resins which have been modified by four different thermoplastics. The polyhydantoin system exhibited the greatest increase in toughness without loss of high temperature flexural modulus. Stenzenberger concluded that the retention of flexural modulus was due to the high glass transition temperature, greater than 250 °C, of polyhydantoin. Phase separation was observed in both the Ultem/Compimide system and the polybenzimidazole/matrimid system. The effect this had on the materials' toughness was not well understood.

Stenzenberger and Hergenrother have recently investigated the toughening mechanism of four different amorphous polyarylene ether ketones[123]. The PEAKs were based on 1,3-bis(4-fluorobenzoyl) benzene and the bisphenols, bisphenol-A, 1,1-bis(4-hydroxy-phenyl) 1-phenylethane, and 9-9-bis(4-hydroxyphenyl) fluorene. They discovered that the polymer backbones with the least bulkiness (bisphenol-A) had the greatest increase in toughness (Table 9). They concluded that the PAEK interpenetrated the bismaleimide matrix, leading to a toughened bismaleimide. Stenzenberger and Hergenrother also examined the effect of molecular weight on toughness. They observed no difference for two bisphenol-A based polymers which had weight average molecular weights of 122,000 and 53,800, respectively. Two types of phase separated morphologies were detected, but no correlation between fracture toughness and morphology could be concluded.

4.2.3.3 Elastomer Modification

Modification of bismaleimides with butadiene acrylonitrile rubber and functionalized oligomers has also been investigated[118,126,130]. These systems are primarily designed for

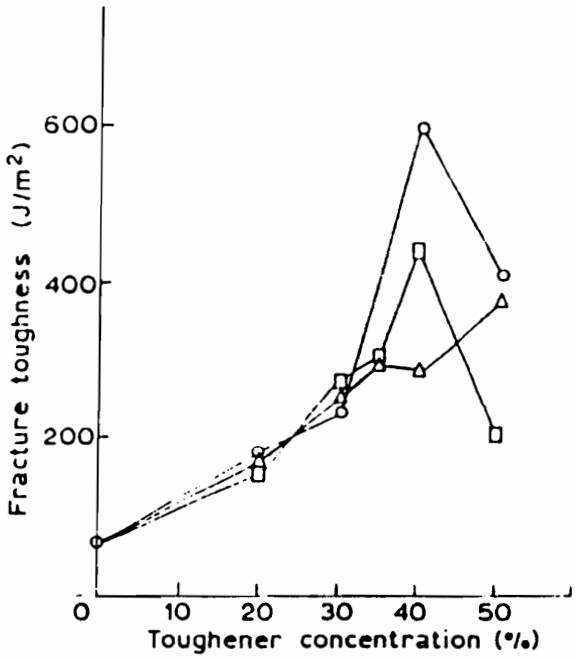

Figure 36. Bis allyl phenyl modified bismaleimide [122]

Table 7. Toughness of bismaleimide resins blended with thermoplastics [127,128]

TOUGHNER	Wt.(%)	G_{1c} (J/m^2)	FLEXURAL MODULUS 250 °C (GPa)	Tg (°C)
Control/				
Compimide 796	65	225	2.39	-
4,4'bis(o-propenylphenoxy)-	35			
Ultem	13	462	1.71	-
	26	841	0.41	-
Polyhydantoin	20	454	2.77	-
	33	1091	2.40	-
Udel	20	440	1.93	-
Control/				
Matrimid 5292B	33	128	-	251
compimide 795	67			
Polybenzimidazole	10	247		254

Table 8. Fracture toughness of poly(arylene ether) ketone modified Compimide 796/Compimide Tm123[123]

MATERIAL	Wt.(%)	K_c(MPa $m^{1/2}$)	G_{1c}(J/m^2)
Compimide 796/ Compimide Tm123 (control)	100	0.573	85
PAE-1	13 20 100	1.251 1.521 5.594	400 634 10,850
PAE-2	13 20 100	1.006 1.666 4.894	280 775 8,225
PAE-3	13 20 100	1.026 1.235 5.073	296 418 8,925
PAE-4	13 20 100	0.992 1.025 2.334	265 274 2,048

PAE =

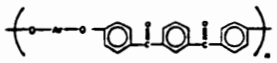

Polymer	Ar =	inh.[a] dL/g	GPC,[b] min	M_w,[c] g/mole	Tg,[d] °C.	K_{1c}, MPa/m (at 23°C)	G_{1c} J/m^2 (at 23°C)
PAE-1		0.75	29.63	122.000	156	5.594	10.850
PAE-2		0.58	31.37	53.800	152	4.894	8.225
PAE-3		1.16	28.99	203.000	175	5.073	8.925
PAE-4		0.68	30.72	110.000	223	2.334	2.048

[a] $CHCl_3$ @ 25°C
[b] Column, 10^6, 10^5, 10^4, 10^3, Å Ultrastyragel; Solvent: $CHCl_3$; Flow Rate: 1 ml/min; Detector: UV @ 254 nm
[c] Static LALLS, $CHCl_3$
[d] DSC @ 20°C/min

Table 9. Toughness of rubber modified bismaleimide resins [118,126]

TOUGHENER	WEIGHT(%)	$G_{1c}(J/m^2)$
Control/[109] Desbimid	100	470
ATBN	10	990
CTBN	10	320
VTBN	10	770
Control/[120] Compimide 353	100	30
CTBN	33	536
	43	1190
	50	776

adhesive applications, since the incorporation of the rubbery materials significantly reduces the matrix's high temperature stiffness. Table 9 shows the results for these systems. Rubber modification exhibits the greatest improvements of toughness with strain energy release rates rising to values greater than 1 KJ/m^2. These systems were all found to microphase separate except for the case of carboxy terminated polybutadiene acryonitrile, CTBN, modified Desbimid, where macrophase separation occurred due to the low reactivity of the rubber with the maleimide at the system's cure temperature of 25 °C. Stenzenberger found for the case of CTBN modified Compimide 353, a maximum in toughness was obtained at 43 percent rubber. He proposed that pendent 1,2 double bonds copolymerized with the maleimide groups.

Chapter 5. Experimental

5.1 Synthesis of Poly(Arylene Ether) Ketone Oligomers and Polymers

5.1.1 Amine Terminated PEKE Oligomers

Amine terminated Poly(arylene ether) ketone (PEKE) oligomers of controlled molecular weight were synthesized via an aromatic nucleophilic substitution reaction of bisphenol-A (Bis-A), (phenolate), 4,4′-difluorobenzophenone (DFBP) and m-aminophenol (MAP), (Figure 37). The ratios of the three monomers were calculated using a modified Carother's equation (Scheme 1). The monomers were added to the apparatus shown in Figure 38. The size of the reaction flask used ranged from 1 to 12 liters depending on the quanity of polymer desired (100 to 1300 grams). A 50 percent excess of potassium carbonate was used for all reactions. It was later discovered that only a 5 percent excess was necessary. A 1 to 2 ratio of toluene, (azeotroping solvent), to N-methylpyrrolidinone, (aprotic, dipolar solvent), was then added. Care was taken to rinse out the beaker, which was used to weigh out the starting materials, in an attempt to ensure quantitative transfer of the starting materials. The percent solids of

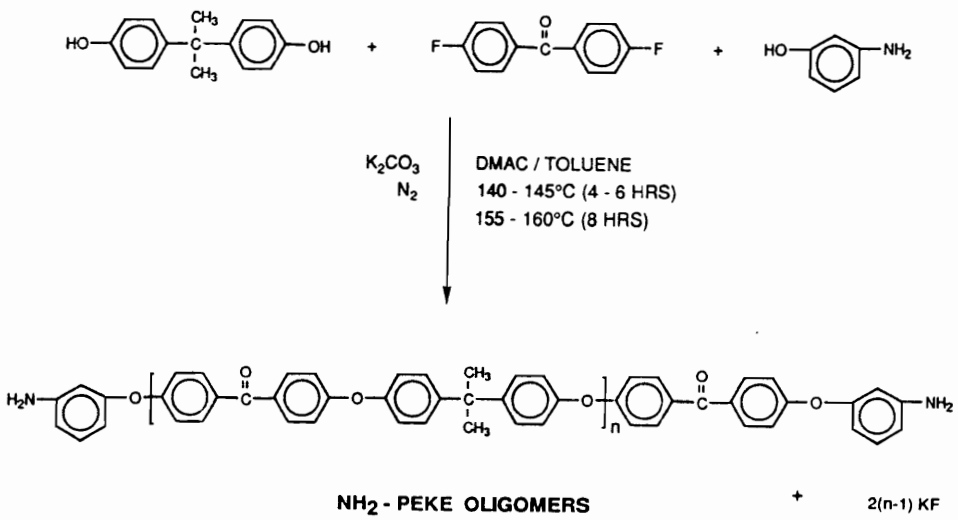

Figure 37. Synthesis of amine terminated polyetherketoneether.

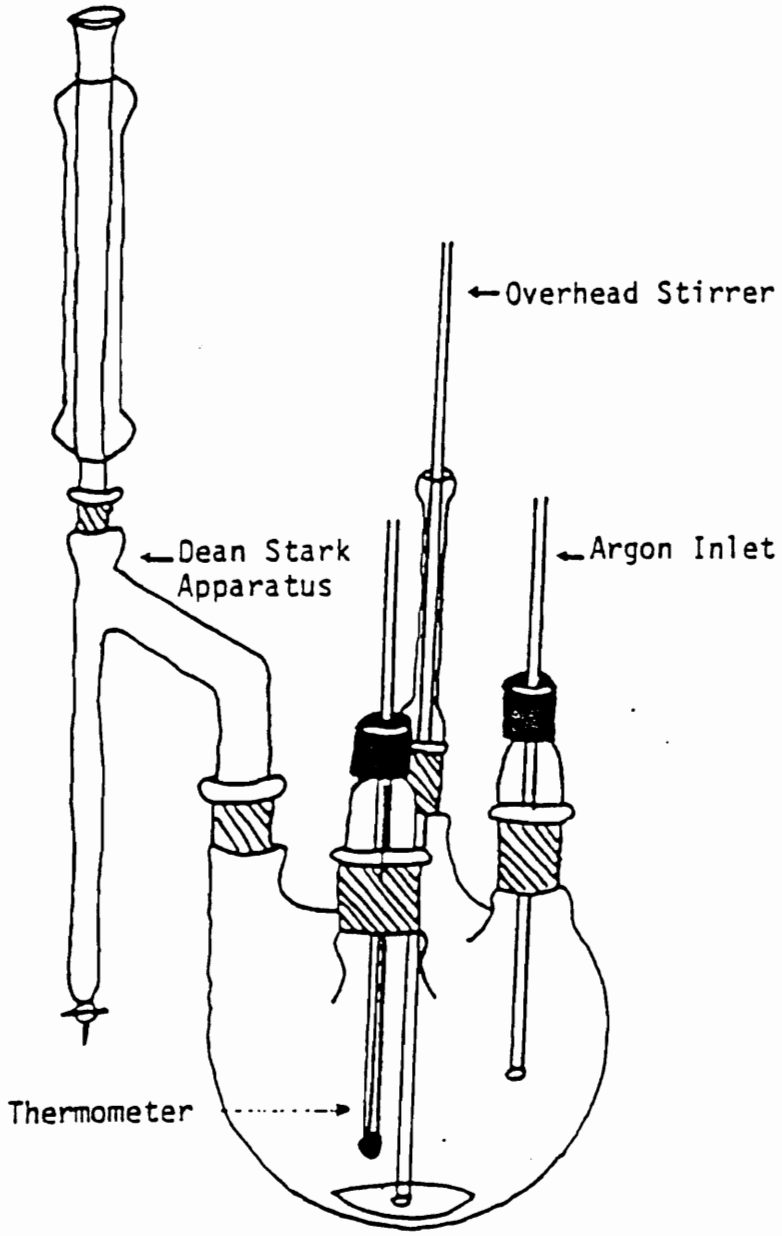

Figure 38. Apparatus for solution polymerizations[131].

monomers with respect to the volume of NMP came to approximately 20 percent. The reaction was heated by a heating mantle and purged with nitrogen.

Initially, upon heating the reaction, a greenish tint was observed, indicating the formation of the phenolate of Bis-A. The solution was allowed to reflux at 145 °C for 8 to 24 hours to azetrope off water which was generated from the reaction of potassium carbonate and Bis-A. Toluene and water were removed via a dean stark trap, allowing the reflux temperature to rise to 165 °C. The temperature was held constant for another 8 to 24 hours before the reaction was allowed to cool to room temperature. Longer reaction times were used for the larger scale reactions to ensure quantitative conversion, although, they were most likely completed within the first 8 hours.

The cooled solution was diluted with tetrahydrofuran (THF) to approximately 50 percent of the total solution volume and was filtered through a Buckner funnel. This filtration was performed to remove the bulk of the inorganic salts. The solution was then acidified with glacial acetic acid, usually 100 ml of acid for every 500 ml of NMP, and further diluted to a 10 weight percent solution with THF. The excessive amount of acid was used to produce a fine powder during coagulation. Some oligomers precipitated with the addition of acid but later would redissolve with stirring.

The oligomers were coagulated in a 70/30 mixture of methanol to water using 100 ml of methanol/water for every 10 ml of solution. The color of the filtered product varied from off white to tan. After 12 hours of air drying, the oligomers were broken up and placed in large crystallizing dishes. The oligomers were dried at 80 °C under vacuum until the evolution of acetic acid could be detected. Often, some of the oligomers flowed together during this drying process to form sticky, gummy solids. The flowing phenomena is believed to be caused by residual NMP in the powder. The oligomers were then redissolved in THF to a 10 weight percent solution and recoagulated in 100 percent methanol using 100 ml of methanol for every 10 ml of solution. The second coagulation was necessary to remove the remaining high boiling solvents trapped within the glassy oligomers. The oligomers were once again filtered and dried under vacuum at 80 °C. Final yields were 85 to 95 percent of theoretical values.

5.1.2 Maleimide Terminated PEKE Oligomers

Maleimide terminated polyether ketone oligomers were synthesized from the reaction of amine terminated PEKE oligomers with maleic anhydride, (Figure 39). The reactions were conducted in a 15 weight percent solution using either refluxing chlorobenzene or a NMP/CHP mixture as the solvent. For the NMP/CHP systems, the ratio of the two solvents was approximately 5 to 1. Chlorobenzene was preferred since its boiling temperature of 132 °C was high enough to effectively imidize the maleic acid without inducing premature crosslinking. The reactions were conducted for 12 to 36 hours. The reaction apparatus was identical to that for the amine terminated oligomer synthesis.

The solutions were subsequently cooled and then diluted with either THF or chloroform to form a 10 weight percent solution. They were then filtered and the oligomers were coagulated in methanol. The oligomers were then dried under vacuum at 80 °C, redissolved in either THF or cholroform, and recoagulated in methanol. The color of the dried product was similar to that of the amine oligomers precursor.

5.1.3 Nadimide Terminated PEKE Oligomers

Nadimide terminated PEKE oligomers (prepared by Dr. S. D. Wu) were synthesized from amine terminated PEKE oligomers and 5 Norbornene-2,3-dicarboxylic anhydride (Figure 40). The derivatizations were again done in chlorobenzene at reflux for 24 hours. The final oligomer was filtered, coagulated and dried in an analogous fashion to the maleimide terminated materials.

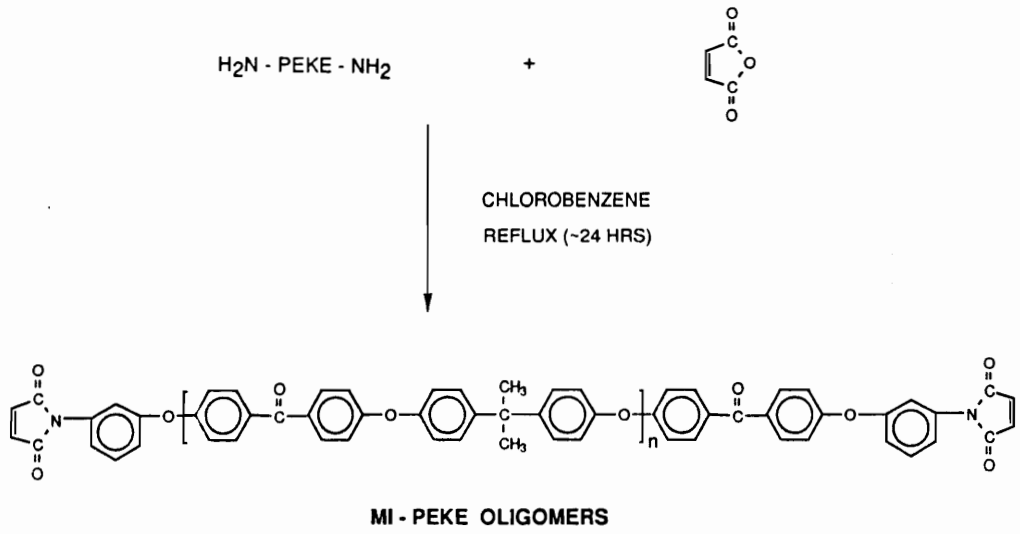

Figure 39. Synthesis of maleimide terminated polyetherketoneether.

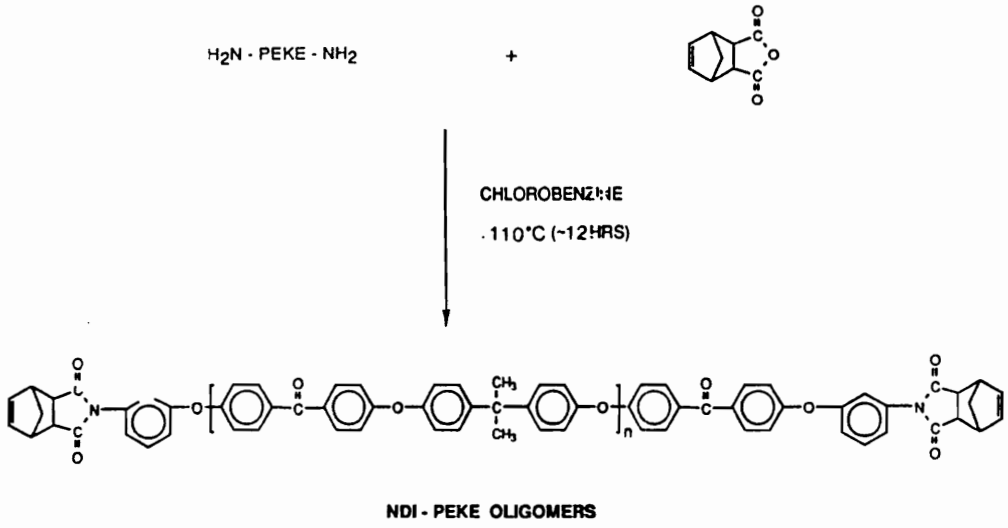

Figure 40. Synthesis of nadimide terminated polyetherketoneether.

5.1.4 Para t-Butyl Phenyl Terminated PEKE Oligomers

Para t-butyl phenyl terminated PEKE oligomers were synthesized to produce non-reactive end groups. Para t-butyl phenol was used in place of m-aminophenol as the oligomeric endcapping reagent. The polymers were isolated under identical conditions to the amine terminated oligomers.

5.1.5 Maleimide Terminated PEKKE Oligomers

Maleimide terminated polyetherketoneketoneethers, PEKKE, (prepared by G. D. Lyle), were synthesized in a two step procedure analogous to the maleimide terminated PEKE oligomers. In the first step amine terminated PEKKE oligomers were synthesized from Bis-A, bis(4-chlorobenzoyl) benzene and m-aminophenol, (Figure 41). These reactions were conducted in dimethylacetamide and toluene; using potassium carbonate as the basic catalyst. Reaction conditions and the oligomeric purification procedure were similar to those for the PEKE oligomers.

In the second step, imidizations were conducted in N-cyclohexyl pyrrolidone using only a slight excess of maleic anhydride. Reaction conditions and work up of the resulting oligomers were again similar to those for PEKE oligomers.

5.2 Molecular Weight Determination

5.2.1 Titration of Amine End Groups

Number average molecular weights of aromatic amine terminated oligomers were determined by titration of the amine endgroups using an HBr acetic acid titrant. The polymers

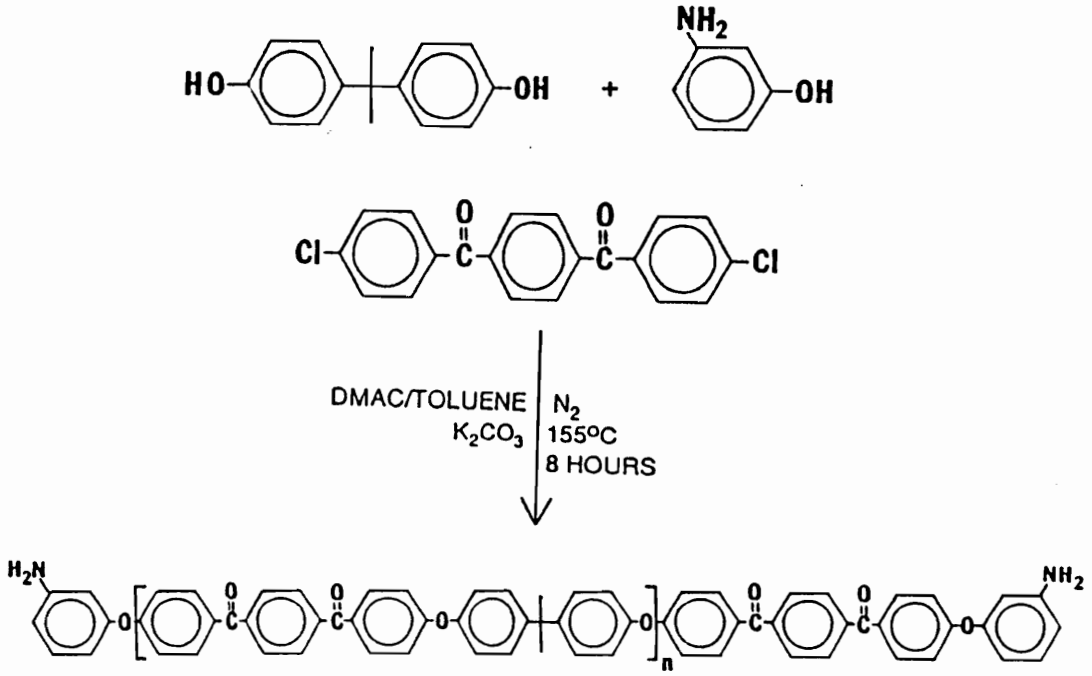

Figure 41. Synthesis of amine terminated polyetherketoneketoneether.

were weighed into a 150 ml beaker and dissolved in a mixture of 60 ml chlorobenzene and 30 ml of acetic acid. The titration endpoint was determined either by color change using crystal blue as an indicator or by a potential change using a Fisher or MCI titrator. <Mn> was calculated by equation 1. An average of three values was used as the reported result.

$$\overline{Mn} = \frac{N_{EG} * Wt}{N * V} \qquad [5.1]$$

where:

$\overline{Mn}$ = number average molecular weight

N_{EG} = number of endgroups per chain (assumed to be 2)

Wt = weight of the sample

N = normality of the titrant

V = volume of the titrant

5.2.2 Proton NMR Spectroscopy

The number average molecular weight of t-butyl phenyl terminated PEKE oligomers was determined from proton NMR by ratioing the integrated peak areas of the t-butyl group to that of the isopropylidene methyl groups (Figure 42) as shown in equation 2.

$$\overline{Mn} = 406\left(\frac{18A_{ISO}}{6A_{tBP}}\right) + 396 \qquad [5.2]$$

where:

$18\ A_{ISO}/6\ A_{tBP}$ = number of repeat units

A_{ISO} = integrated area of the isopropylidene protons

A_{tBP} = integrated area of the t butyl protons

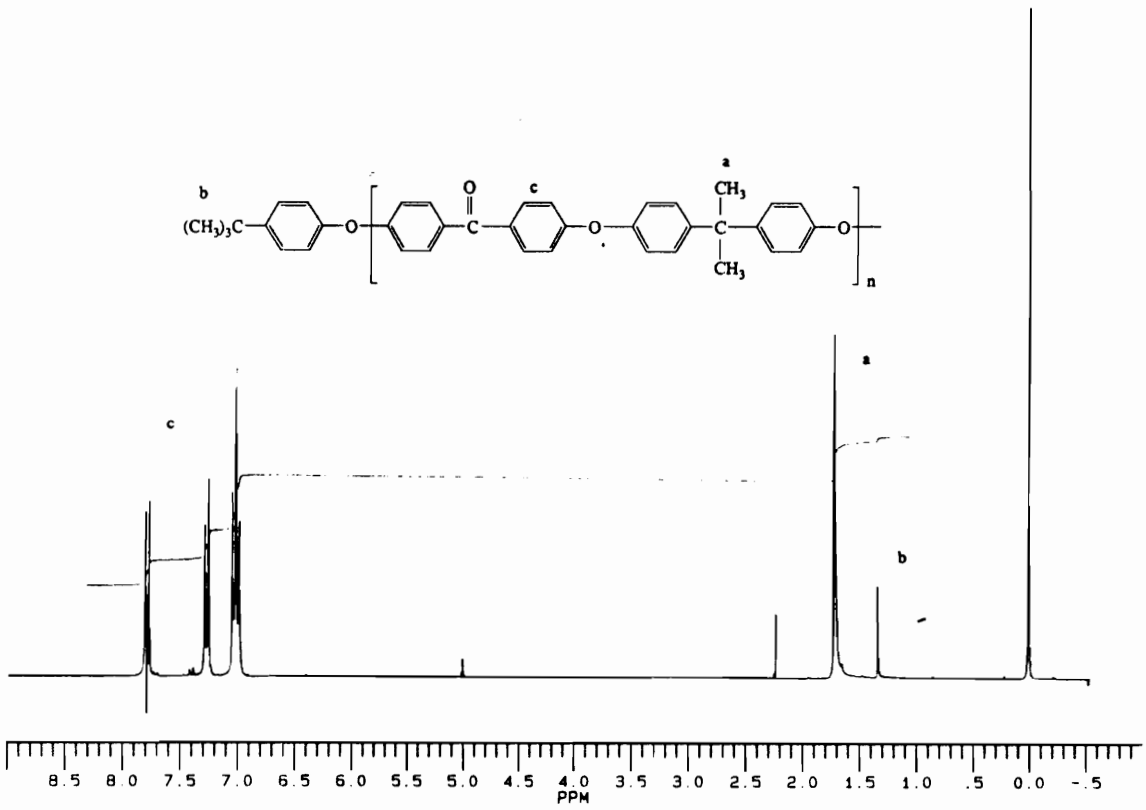

Figure 42. Proton NMR of t-butylphenyl terminated PEKE.

5.2.3 Intrinsic Viscosity

The intrinsic viscosity of the functionally terminated PEKE and PEKKE oligomers was measured using a Cannon 100 Viscometer from solutions prepared in chloroform, at 25 °C.

Intrinsic viscosities of the t-butylphenyl PEKE oligomers were determined from gel permeation chromotagraphy, differential viscosity analysis. In this analysis, a Waters 150C ALC/GPC equipped with a differential refractive index detector and a Viscotek Model 100 differential viscosity detector was used. Sample were dissolved in chloroform and filtered through a 0.5 μm millipore filter before injection. Ultrastyragel columns with pore diameters of 500, 10^3, 10^4, 10^5, and 10^6 angstroms were used. Flow rate and temperature was maintained at 1 ml per minute and 30 °C respectively.

5.2.4 Melt Viscosity

Melt viscosities of the t-butylphenyl terminated PEKE oligomers were determined on a Rheometrics model RMS 800 melt rheometer. Tests were performed using parallel plates over a range of frequencies at constant temperature of 230 °C. The data presented are the complex melt viscosities at a frequency of 1 Hz.

5.3 Blending Investigations

5.3.1 Blends of BMI with Maleimide Terminated PEKE

5.3.1.1 Precipitation Technique

Blends of BMI and maleimide terminated PEKE oligomers were prepared by weighing the materials and dissolving them in chloroform to a 10 wt/vol percent solution. The solution

was precipated in hexane using a 10 to 1 ratio of hexane to solution. They were then filtered and dried under vacuum at 60 °C. The resulting product was a light, fluffy yellow powder recovered in yields greater than 95 percent.

5.3.1.2 Evaporation Technique

Both materials were weighed and dissolved in chloroform to a 10 wt/vol percent solution. The majority of the chloroform was then removed, by rotoevaporation. Once the solution was fairly concentrated it was poured into a teflon dish and dried under vacuum at 40 °C for 12 hours. The resulting material was a hard crusty brittle material.

5.3.1.3 NMR Analysis

The weight fraction of each component of the blends was measured using proton NMR. Figure 43 shows a typical spectrum of a blend which indicates the methylene group of the BMI, and the isopropylidine group of the Bis-A based backbone of the PEKE. The weight fraction of the BMI to PEKE was calculated from the integration of these two peaks as shown in scheme 2. All sustems were found to contain weight fractions of the PEKE and BMI components to within two percent of their theoretical values.

5.3.2 Blends of Functionally Terminated PEKE Oligomers

5.3.2.1 Blending Formulation

Physical blends made from various molecular weight PEKE terminated oligomers were prepared in order to study the effect of molecular weight distribution on fracture toughness. It was necessary to obtain constant number average molecular weights within these blends while increasing distribution since many mechanical properties are dependent on $<Mn>$.

This was achieved by first assuming that the Mn obtained for each oligomer by either titration or NMR was representative for that oligomer. The exact quantity of each oligomer

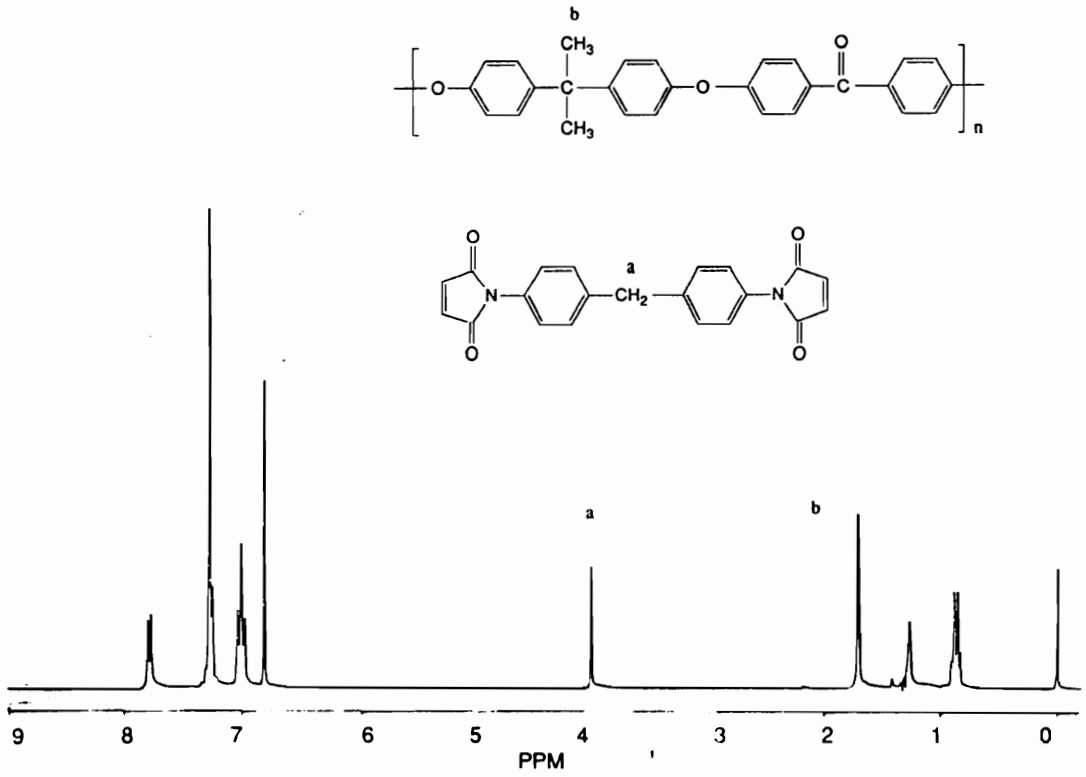

Figure 43. Proton NMR of a BMI/maleimide terminated PEKE blend.

needed for the blend of a given <Mn> was calculated as shown in scheme (3). The oligomers were then sequentially weighed out together, dissolved to a 10 wt/vol percent in chloroform, coagulated in methanol and dried.

5.3.2.2 Molecular Weight Determination

The number average molecular weights of blends prepared from t-butyl phenyl terminated oligomers were determined by proton NMR in an identical fashion as the pure oligomers. <Mn> for the blends prepared from maleimide terminated oligomers were terminated from vapor phase osmometry.

5.4 Molding and Curing of Poly (Arylene Ether) Ketones

5.4.1 Introduction

The fabrication of high quality specimens from PEKE terminated oligomers and polymers was required in order to perform mechanical and physical measurements on these systems. The fabrication involved the compression molding of the precipitated and dried polymer powder at elevated temperatures inside a metal mold. Without exception, this process was complicated by the formation of bubbles caused by the vaporization of either residual solvents trapped inside the polymer or other volatiles formed as a by product to the various cross-linking reactions. During the early stages of branching, the bubbles can be removed by a combination of various techniques, but after the material gels, the bubbles cannot easily diffuse from the specimen, rendering it useless for mechanical testing. After many preliminary efforts, a procedure was developed which eliminated the bubble problem the majority of the time, thus, permitting the preparation of useful test specimens.

5.4.2 Generalized Procedure for Test Specimen Fabrication

25 grams of the dried powder of the PEKE oligomer was first weighed onto a teflon sheet, for a plate size of 3 x 3 x 1/8 or 3 x 6 x 1/16 inches. The material was placed inside a pre-heated vacuum oven set at 160 - 170 °C for 5 min to 2 hours, depending on the terminal functional group of the PEKE. Maleimide terminated oligomers were only pretreated for 10 minutes while amine terminated oligomers were pretreated for up to 2 hours. Within 3 - 4 minutes the powder would flow as the Tg of the oligomer was exceeded. The foaming of residual solvent trapped inside the powder was observed.

The resulting material was broken up into numerous pieces and then added several pieces at a time to a metal mold. The mold consisted of a 1" wide, 8 x 8 x 1/8" metal frame, with two inserts one 3 x 6 x 1/8" and the other 3 x 3 x 1/8". With both inserts in place, a 3 x 3 x 1/8" cavity was formed. For 1/16" thick plates, a 1" wide 4 x 7 x 1/16" aluminum frame was used. The mold was usually sandwiched between two pieces of teflon coated fiberglass, two pieces of teflon sheet and two 8 x 8 x 1/8" metal press plates. The fiberglass used was a loosely woven cloth which permitted trapped gases inside the sample to escape. It should be noted that the pretreated oligomer must be molded quickly (at least within 24 hours) after pretreatment to avoid water absorption.

After several of the pretreated oligomer pieces were added to the mold, it was inserted into a hydraulic press heated to between 420 to 480 °F. The oligomers were allowed to flow and compact for 5-10 minutes to make room in the cavity for several more pretreated pieces. As the cavity became nearly full it was often found necessary to apply 1000 - 2000 pounds of load to the mold to help compact the material. Care was always taken when separating the fiberglass cloth from the plate while adding more pieces to the cavity. Ungelled material above Tg would often undesirably adhere to the cloth since the PEKE is a good adhesive. Allowing the material to first cool somewhat eliminated this problem.

When the cavity was totally full (and no signs of bubbling were detected) the teflon coated fiberglass and teflon sheets were removed and replaced by fresh pieces of teflon

sheet. This was done to give the final product a smooth surface. The plate was then cured at between 500 - 580 °F under a load of 5000 to 35000 pounds for 5 min to 12 hours. Cure temperature was mostly determined by the reaction conditions necessary for the functional endgroups of the oligomers to crosslink. The final cure temperature was sometimes raised above the needed temperature if the oligomer showed poor flow characteristics. The higher loads of 10,000 - 35,000 were also used to improve flow. Upon completion of curing, the specimen was either quick cooled inside the press under 1000 - 2000 pounds of load or quenched in water. The color of the final product varied from a transparent/translucent dark red to an opaque black.

5.5 Solubility

The gel fraction of the cured oligomers was determined through extraction experiments. Cellulose thimbles were soaked for 12 hours in chloroform, and then dried for 24 hours at 80 °C under vacuum. This procedure was performed to remove all soluble material from the thimbles. The thimbles were then cooled and weighed. A sample of the cured oligomer, approximately 0.5 grams, was then weighed and placed inside a thimble, which was then sequentially placed inside an soxhlet extractor. The soluble portion of the sample was extracted by refluxing chloroform for 4 days. The thimble and sample were then dried at 80 °C under vacuum until a constant weight was obtained, approximately 1 to 2 days. The percent gel fraction was calculated from equation 5.3.

$$\text{Percent Gel} = \frac{\text{Wt of extract. thimble \& sample} - \text{Wt of pretreated thimble}}{\text{Wt of original sample}} x100 \quad [5.3]$$

5.6 Swelling

5.6.1 Procedure

Swelling experiments were performed on the residual geled portions of samples which had undergone solubility tests by the above procedure. A sample was weighed out after it had been dried and cooled and placed in a sample bottle filled with chloroform. The sample weight was checked periodically. The percentage of swelling was determined by equation 5.4.

$$\text{Swelling } \% = \frac{\text{swollen Wt} - \text{initial Wt}}{\text{initial wt}} x100 \qquad [5.4]$$

The weighing of samples was often difficult since a number of networks broke apart to numerous pieces due to the stresses exerted on the sample by the swelling.

5.6.2 Determination of Number Average Molecular Weight between Crosslinks

The number average molecular weight between crosslinks, M_c, was calculated from swelling data for networks prepared from maleimide terminated PEKE oligomers, equation 5.5.

$$M_c = \frac{-V_s\rho_p(c^{1/3} - c/2)}{\ln(1-c) + c + \chi c^2} \qquad [5.5]$$

where:

ρ_p = polymer density (1.26 gm/cm^3)

ρ_s = solvent density (1.492 gm/cm^3)

w_o = initial polymer weight

w_{1_o} = weight of the swollen polymer after 10 days

V_s = molar volume of the solvent (80.01 cm^3/mole)

χ = Flory-Huggins constant (0.388)

V_∞ = final swollen volume = $w_o/\rho_p + (w_{1_o}-w_o)/\rho_s$

c = relative concentration = $w_o/\rho_p V_\infty$

The Flory-Huggins constant was calculated from the second virial coefficient for a 10.7K PEKE oligomer dissolved in chloroform,

$$A_2 = \frac{\rho_s}{\rho_p{}^2 m_s}\left(\frac{1}{2} - \chi\right) \qquad [5.6]$$

where:

m_s = molecular weight of the solvent

χ = Flory-Huggins constant

The second virial coefficient was determined from light scattering measurements performed on a Chromatix KMX-6 low angle laser light photometer. The light was generated from a 2 mwalt helium, neon laser operating at a wavelength of 633 nm. The change in refractive index with respect to concentration was first determined using a Chromatix KMX-16 laser differential refractometer. These measurements were performed at room temperature. Samples were filtered through a 0.2 μm acrodisc CR filter.

5.7 Annealing

Samples used for annealing studies were first quenched in ice water from 100 °C above their glass transition temperatures directly following their molding and or curing. These samples were then dried under vacuum for 8 to 10 hours at 80 °C, and divided into sections. Annealing was conducted inside a convection oven at 145 °C. All the sections of a sample

were placed inside the oven to begin the experiment and then removed at various time intervals. Upon removal, the sections were quick cooled in air. Differential scanning calorimetry was conducted on each specimen to determine the magnitude of the annealing, through the area of their associated physical aging peak.

5.8 Mechanical Testing

5.8.1 Fracture Toughness Testing

5.8.1.1 Sample Preparation

The fracture toughnesses of the cured networks were determined from a 3 point bend test. The majority of the samples tested were cut from molded plates of plastic using a scrool saw. Plates made from higher molecular weight thermoplastics or partially gelled thermosets were particularly difficult to cut to shape. Heat generated by the sawing of the plates, often caused the material to melt back together again after the blade had passed. This problem was minimized however by using a fresh saw blade and cutting the plate slowly. Samples of low molecular weight t-butylphenyl terminated PEKE oligomers were molded to specimen size in rubber molds and therefore did not need to be cut to size. For the thermosets studied, a notch was cut into each specimen using a scrool saw. A razor blade, cooled in liquid nitrogen, was then tapped into the notch until a crack was generated. This method of precracking however, could not be used for the t-butylphenyl terminated PEKE oligomers due to their brittle nature. Precracks were therefore cut into the specimens using an Exacto number 13 saw blade.

5.8.1.2 Sample Testing

Specimens were tested in an Instron model 1123 screw driven tensile testing machine

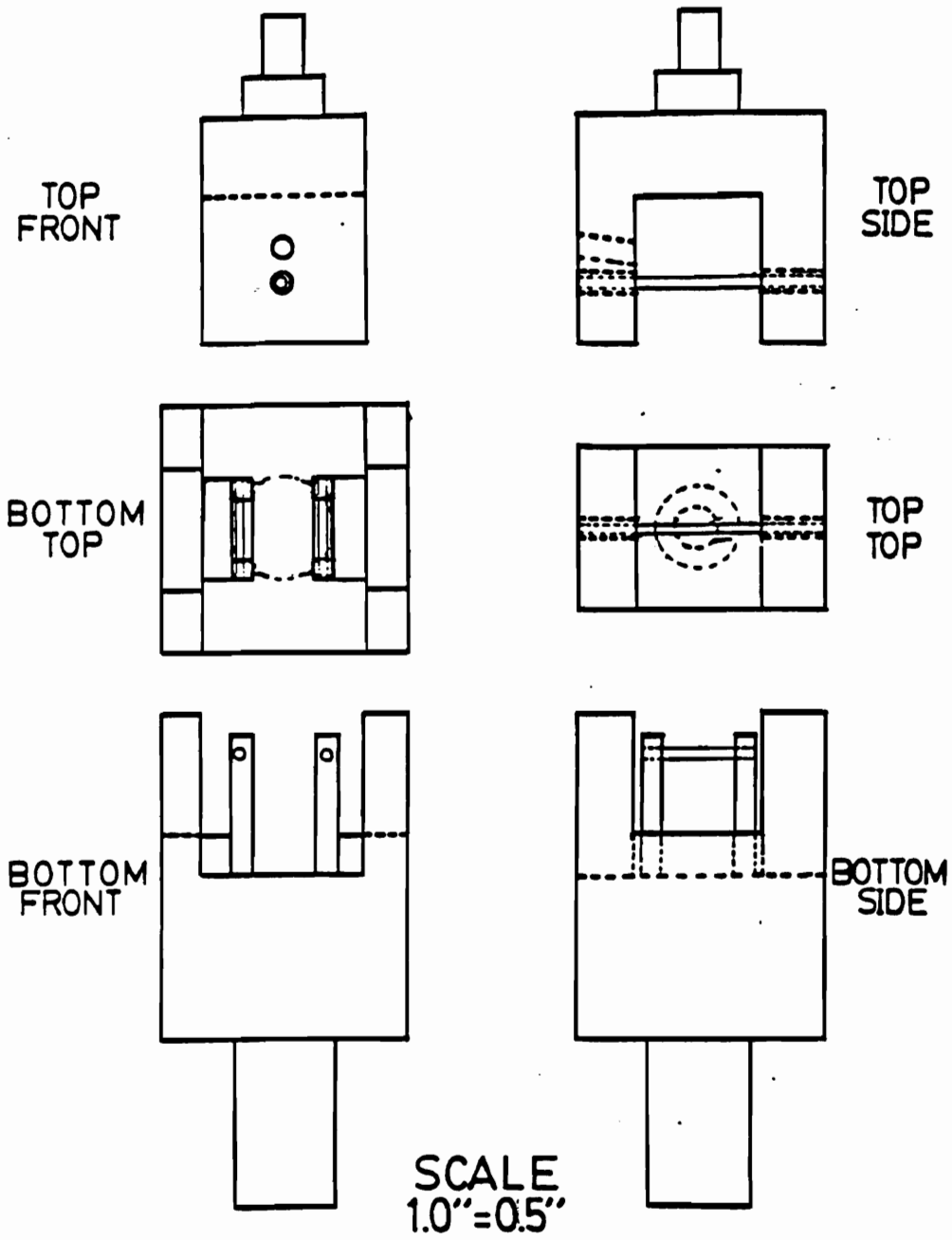

Figure 44. 3-point bend testing assembly[133].

using a three point testing assembly, (Figure 44). The tests were run under a tensile mode at a crosshead separation rate of 2 in/min. (5 cm/min.).

After the sample was fractured, the crack length, width and specimen thickness were all measured. The data from specimen whose crack length was not within 0.3 to 0.7 times sample width was not used in accordance with ASTM restrictions [132]. The shape of the precrack front often varied from a slight meniscus shape whose crack length remained relatively constant across the cross section to a off centered parabolic shaped crack front whose crack length changed as much as 50 %. For the latter samples an average crack length was taken for the toughness calculation. The toughness values for the latter crack fronts did not show any abnormal trends when compared to the rest of the data.

The critical stress intensity for the mode I, K_{1c}, loading was calculated by equation 5.7.

$$K_{1c} = \frac{\rho S}{bw^{3/2}} \left(2.9(a/w)^{0.5} - 4.6(a/w)^{1.5} + 21.8(a/w)^{2.5} - 37.6(a/w)^{3.5} + 38.7(a/w)^{4.5}\right) \quad [5.7]$$

where:

ρ = maximum load

s = span length

b = thickness

w = width

a = crack length

The critical strain energy release rate for mode I loading G_{Ic}, was determined from the chart recording of the fracture tests using equation 5.8.

$$G_{1c} = \frac{\eta U}{B(w-a)} \quad [5.8]$$

where:

η = geometry factor [134]

U = energy to failure

Irregular data was removed from the set of fracture toughness data by means of the Q test. Toughness data shown was the average of the remaining data points and was reported within a plus or minus one standard of deviation for a single specimen tested. Even though the standard of deviations for a single sample for K_{IC} data often appears quite high, the average value for a large number of samples for a specific polymer, was reproduced to within one percent of the original number on several occasions.

5.8.2 Stress-Strain Measurements

Samples for stress-strain measurements were cut from a 1/16 inch plate of material using a die meeting ASTM standard D638-1 or D638-5. The samples were tested using an Instron 1123 model material testing machine at a crosshead rate of 0.2 in/min. Strain was measured either by crosshead displacement or by an extensometer, model 2630 from Instron, containing a strain gauge of 0.5 inches.

5.8.3 Dynamic Mechanical Thermal Analysis

Dynamic mechanical thermal analysis of the various thermoplastic and thermosetting systems was obtained with a Polymer Laboratory DMTA. Samples (3 x 9 x 14 mm) were cut from compression molded specimens and mounted on a single cantilever clamp. Tests were performed at a frequency of 1 Hz and a heating rate of 5 °C/min. A large frame, N, was used for bismaleimide networks as well as for the comparison of dynamic mechanical behavior for

networks prepared from maleimide terminated PEKE oligomers. Size M frame was used for all other tests. Storage modulus (E′) and Tanδ were recorded.

5.8.4 Creep

Creep tests were performed on a Dupont model 382 dynamic mechanical analyzer. Specimens were run under a constant temperature with an initial displacement of 10 percent of the thickness.

5.9 Thermal Analysis

5.9.1 Differential Scanning Calorimetry

Glass transition temperatures along with annealing exotherms were determined from a DuPont 912 Dual Sample Differential Scanning Calorimeter, DSC. Temperature calibration was achieved by using indium which has a melting point of 156.6 °C and a heat of fusion of 6.8 cal/gm. A heating rate of 10 or 20 °K/min was used. The heating rate for annealed specimens was 5 °K/min.

5.10 Spectroscopy and Microscopy

5.10.1 Proton Nuclear Magnetic Resonance

Proton nuclear magnetic resonance spectra of PEKE oligomers and blends were obtained using a Bruker WP-270 SY Spectrometer operating at a proton frequency of 270.13 MHz. Samples were dissolved in deuterated chloroform to a 8-10 weight percent solution and examined at ambient temperature using 32 transients with a recycle time of 2.0 seconds. The resulting free induction decay was then Fourier transformed. Tetramethylsilane was used as the internal standard.

5.10.2 Scanning Electron Microscopy

Scanning electron micrographes of fracture surfaces were taken on an ISI model SX-40 SEM. Samples were first cut to size and then glued on to an aluminum base. The base as well as the sides of the sample were painted with silver paint and allowed to dry. The sample was then sputtered coated with gold using an Edwards S 150B sputter coater before being placed inside the SEM. The SEM was operated at 15 kV, at an operating distance of 8-15 mm.

5.10.3 Optical Micrographs of Cross Sections to the Fracture Plane

Optical micrographs of cross sections perpendicular to the fracture planes, within PEKE thermoplastics and thermosets, were taken to study the mechanism of plastic deformation which occurred during fracture.

5.10.3.1 Sample Preparation

A sample was prepared by first loading a precracked three point bend specimen within the Instron to approximately 90 percent of failure. The ends of the specimen were then cut off leaving the precracked region of the sample, approximately 0.25 inches in length. The sample was then placed at the bottom of a 2 oz. plastic cup and covered with 0.5 inches of a quick setting epoxy. After 24 hours, the cured epoxy block was removed.

The sample was then sanded and polished following a procedure similar to that used by Holik and coworkers at General Electric [135]. The bottom side of the block was sanded down to expose the middle cross section of the polymer specimen. The sanding was performed on polishing wheels using sand paper of decreasing coarseness, 180, 240, 320, 400 and 600 grit.

A steady stream of water was always used to wet the sandpaper so as to cool the sample and prevent any alteration of the plastic zone due to overheating. Direction of sanding was changed by 90 degrees each time the sandpaper was exchanged to the next fineness. This was done so that the sanding was performed perpendicular to the sanding scratches left behind from the previous paper. This procedure enabled the operator to determine when the previous scratches had been removed. When the scratches were removed, the sandpaper was replaced with the next greater fineness.

After sanding, the sample was polished using aluminum oxide powders which were poured as a water slurry onto a cloth laps connected to a polishing wheel. The sample was polished in the same manner as it had been sanded, using 1.0, 0.3, and 0.05 μm. The polished bottom side was then glued, using quick setting epoxy, to a stack of eight glass microscope slides. The slides were glued together by spreading some epoxy along the outside of the stack. The stack of slides was needed to improve handling of the sample as it was being sanded.

The top side of the block was sanded down until it was reduced to a wafer of 0.1 mm thickness or less. This side was then polished just as above. It was important that the final polishing direction was in a perpendicular direction to the crack so that scratches left by the

polishing would not be mistaken for deformation lines caused by the crack. After the sample was polished, the top slide was separated from the stack by sanding away the epoxy holding the stack together away.

5.10.3.2 Optical Micrograph Conditions

Optical micrographs of the polished cross sections were taken using a Spectro Tech IR-Plan Microscope. Both 4X and 10X objectives were used having numerical apertures of 0.10 and 0.25, respectively. The objectives were used in combination with either a 2.5X or 6.7X NFK lense producing a variation in magnification from 10X to 67X.

Micrographs were taken from cross polarized transmitted light using both bright and dark field illumination. Exposure times were automatically set using a PM-10AD photo micrographic exposure controller from Olympus. Kodachrome ASA 100 or Ectachrome HC ASA 25 were used for film.

5.11 Chemicals

5.11.1 Bisphenol A (Bis A)

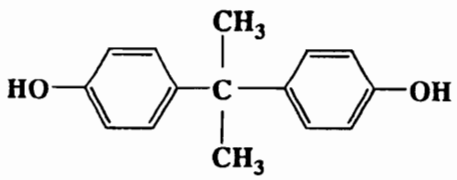

Molecular Weight:	228.7
Melting Point:	155 °C
Supplier:	Dow Chemical, USA
Purification:	Recrystallize in toluene, dried under vacuum

5.11.2 *Difluorobenzophenone (DFBP)*

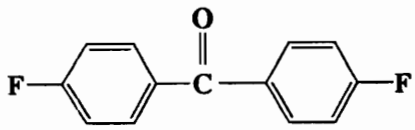

Molecular Weight:	218
Melting Point:	105 °C
Supplier:	ICI
Purification:	Recrystallize in diethyl ether, dried under vacuum

5.11.3 *m-Aminophenol*

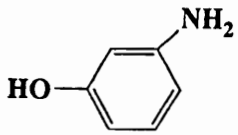

Molecular Weight:	109.13
Melting Point:	124-126 °C
Supplier:	Aldrich
Purification:	Sublimination, stored in dessicator

5.11.4 *Maleic Anhydride*

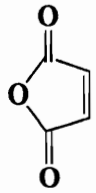

Molecular Weight:	98.06
Melting Point:	54-56 °C
Supplier:	Aldrich
Purification:	Sublimination, stored in dessicator

5.11.5 *1,1'-(Methylene-4,1-phenylene) Bismaleimide (BMI)*

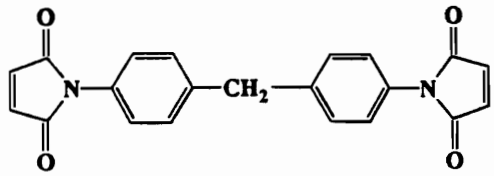

Molecular Weight:	358.36
Supplier:	BASF
Purification:	Used as received

5.11.6 N-Methyl 2 Pyrrolidinone (NMP)

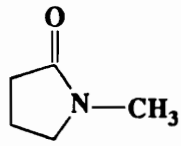

Density:	1.026 (g/cm^3)
Boiling Point:	202 °C
Supplier:	Fisher
Purification:	Vacuum distilled from calcium hydride

5.11.7 Potassium Carbonate

Molecular Weight:	138.21
Supplier:	Fisher
Purification:	Used as received

5.11.8 Glacial Acetic Acid

Molecular Weight:	60.05
Boiling Point:	116-118 °C
Supplier:	Fisher
Purification:	Used as received

5.11.9 Hexanes

Density:	0.687 (g/cm^3)
Boiling Point:	68-70 °C
Supplier:	Fisher
Purification:	Used as received

5.11.10 Chlorobenzene

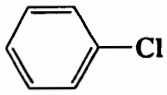

Density:	1.1058 (g/cm^3)
Boiling Point:	132 °C
Supplier:	Fisher
Purification:	Distilled from calcium hydride

5.11.11 Methanol

Boiling Point:	64 °C
Supplier:	Fisher
Purification:	Filtered

5.12.12 Tetrahydrofuran (THF)

Density:	0.8892 (g/cm^3)
Boiling Point:	67 °C
Supplier:	Fisher
Purification:	Used as received

5.11.13 Cyclohexyl Pyrrolidinone (CHP)

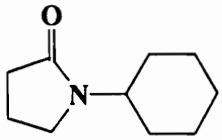

Supplier:	GAF
Purification:	Vacuum distilled from calcium hydride

5.11.14 Chloroform

Density:	1.4460 (g/cm^3)
Purification:	Used as received

5.11.15 Chloroform-d w/TMS

1 percent TMS,	99.8 percent ATM
Supplier:	Aldrich
Purification:	Used as received

5.11.16 4-t Butyl Phenol

Molecular Weight:	150.22
Melting Point:	56-61 °C
Supplier:	Aldrich
Purification:	Recrystallized in hexane, dried under vacuum

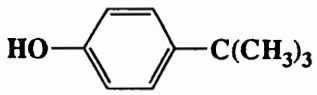

Chapter 6 Results and Discussion

6.1 Introduction

The results and discussion portion of this thesis will be divided into three chapters. In the first chapter the physical and mechanical characterization of PAEK thermoplastics and thermosets will be presented. Included will be sections dealing with the chemical characterization of the starting oligomers, the characterization of the networks by gelation and swelling experiments, dynamic mechanical tensile and creep behavior, and finally a detailed study of fracture behavior of these networks. Chapter 7 examines the same parameters as above but for bismaleimide networks modified with polyarylene ether ketone oligomers. Chapter 8 attempts to correlate the above data so as to propose a molecular scale toughening mechanism for this material.

6.2 Characterization

6.2.1 Physical and Chemical Characterization of Synthesized Oligomers

The characterization of the functionalized oligomers used in the generation of networks is shown in Table 10. The titrated molecular molecular weights and intrinsic viscosities are all reasonable values considering their theoretical molecular weights. Included are the glass transition temperatures of the final cured networks. Tg is seen to decrease slightly as the starting oligomeric molecular weight increases. This demonstrates the increase in freedom of chain motion as crosslink density decreases.

Table 11 displays the number average molecular weights, determined by proton NMR, the intrinsic viscosities and dynamic melt viscosities at 230 °C and 1 Hz for the t-butylphenyl terminated PEKE oligomers. As with the oligomers of Table 10, molecular weight and viscosities values are reasonable for their respective theoretical molecular weights. A plot of melt viscosity versus molecular weight is shown in Figure 45. Viscosity increases slowly initially as molecular weight increases. However at approximately 11,000 molecular weight, the rate at which viscosity increases, rises dramatically and remains constant. The point where this rate jump occurs, indicates the onset of entanglement formation between the chains. The molecular weight at this point, 11,000, is referred to as the chain entanglement molecular, Me, and represents the molecular weight of the chain segment between entanglement points. It should be noted that 1 Hz was chosen as the measured frequency since it was within the Newtonian responses of the various oligomers.

The composition and characterization of blends prepared from the t-butyl phenyl terminated PEKE oligomers is presented in Table 12. Several of the blends possess molecular weights approximately two thousand grams per mole greater than the theoretical molecular weight. Even though this difference is large, it is not overly excessive.

Table 10. Characterization of fundtionalized PEKE and PEKKE oligomers and their associated networks.

Oligomer	Theoretical <Mn> (g/mole)	Titrated <Mn> (g/mole)	$[\eta]^1$ (dl/g)	Network Tg (°C) DSC	DMTA
PEKE NH_2	2,500	-	-	162	166^M
	5,000	6,600	-	158	-
	10,000	11,88	0.29	156	-
PEKE MI	2,500	3,100	0.16	-	158^N
	5,000[2]	-	0.22	-	-
	5,000	5,400	0.22	-	150^N
	5,000[3]	5,900	0.27	-	-
	7,500	8,600	0.32	-	149^N
	10,000	10,700	0.48	-	149^N
	14,000	16,000	0.41	-	155^N
PEKE ∞	∞		1.4	157	153^N
PEKE NDI	2,500	2,700	0.15	174	175^M
	5,000	5,600	0.29	160	-
	7,500	8,000	0.32	159	-
	10,000	10,000	0.37	162	160^M
PEKKE MI	2,500	2,700	0.13	177	165^Q, 175^M
	5,000	5,800	0.33	175	160^Q
	10,000	11,300	0.53	169	155^Q
PEKKE ∞	∞	-	1.3		150^Q

1: $CHCl_3$ solvent at 25 °C
2: used for length of cure study
3: used for annealing study
NH_2: amine terminated
MI: maleimide terminated
NDI: nadimide terminated
∞: high molecular weight
N, M, Q: DMTA clamp size

Table 11. Characterization of t-butylphenyl terminated PEKE oligomers

Oligomer	Theoretical <Mn> (g/mole)	NMR <Mn> (g/mole)	$[\eta]^2$ (dl/g)	Melt[1] Viscosity (Pa s)
PEKE tBP	5,000	5,100	0.19	60
	7,000	8,200	0.24	142
	9,000	10,500	0.27	382
	12,000	12,700	0.32	833
	14,000	14,900	-	2364
	17,000	20,000	0.42	3263
	20,000	24,600	0.43	4679
PEKE ∞	∞	-	1.40	
PEKE OH	20,000	-		

1: dynamic melt viscosity obtained at 230 °C and 1 Hz.
2: $CHCl_3$ solvent at 25 °C
tBP: t-butylphenyl terminated
∞: high molecular weight
OH: hydroxyl terminated

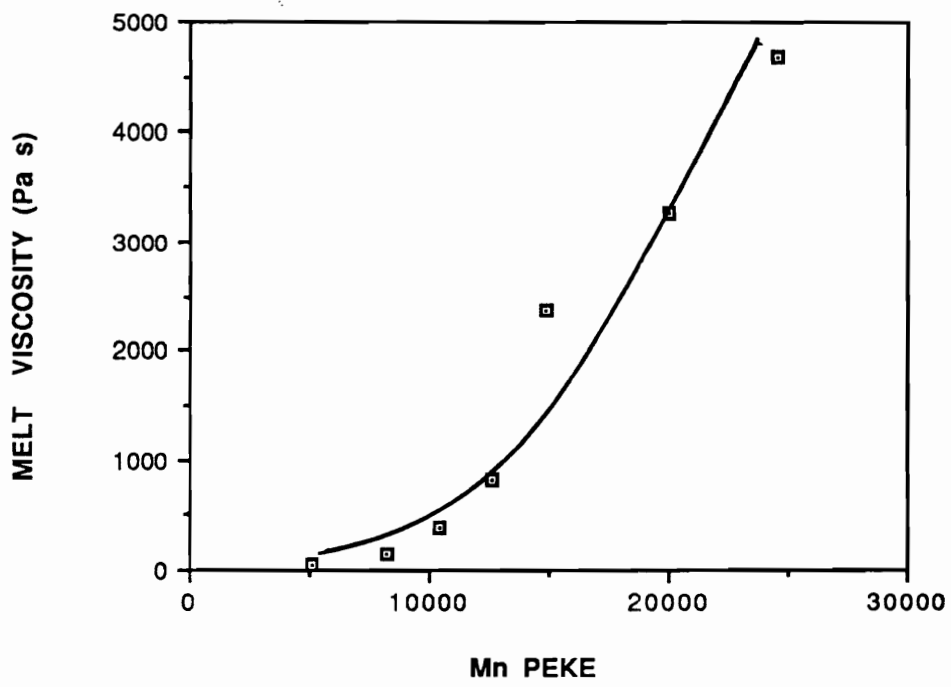

Figure 45. Dynamic melt viscosities at 1 Hz and 230 °C for t-butylphenyl terminated PEKE oligomers

Table 12. Composition and characterization of blends prepared from t-butylphenyl terminated PEKE oligomers

Oligomer	Composition (mole %)	Theoretical <Mn> (g/mole)	<Mn> NMR (g/mole)	Melt Viscosity (Pa sec.)
10.5K 14.9K	50 50	12,700	12,600	1103
8.2K 14.9K	33 67	12,700	14,600	1282
8.2K 20.0K	38 62	12,700	12.200	1006
5.1K 14.9K	22 78	12,700	15,100	1840

6.2.2 Extraction and Swelling of PAEK Networks

A number of chemical and physical characterization techniques such as NMR, FT-IR, GPC and intrinsic viscosity require that the polymer be soluble. For gelled polymeric thermosets, which are insoluble, these characterization techniques cannot be used. The characterization into the makeup of a thermoset is therefore quite limited. Two techniques which can give some indication of the makeup of a thermoset are extraction and swelling measurements.

Extraction measures the fraction of soluble material left in the network while swelling measures the absorption of solvent by the network over time. Since absorption of solvent can be related to the expansion limit of a rubbery network, swelling results can often be used to calculate the molecular weight between crosslinks, Me, for the network. As will be discussed, swelling can also give insight into the ability of the network to disentangle.

The discussion of the characterization of PAEK networks by extraction and swelling measurements will be divided into two parts. In the first part, an overview of swelling behavior of PAEK networks in chloroform will be presented along with a comparison between this behavior and creep extension overtime. The second part will include the swelling behavior of the various networks examined in this study as a means of characterizing them. Comparisons will be made between the swelling behaviors for networks prepared from various molecular weight oligomers, cured through various functional endgroups, cured for various lengths of time, and consisting of either a PEKE or a PEKKE backbone. A summary of the extraction and swelling measurements is presented at the end of this section in Table 13.

6.2.2.1 Overview of Swelling Behavior

6.2.2.1.1 PAEK Networks

The time dependent swelling behavior for a typical PEKE network is shown in Figure 46. The swelling of a network generally occurs in two stages, the first of which involves rapid

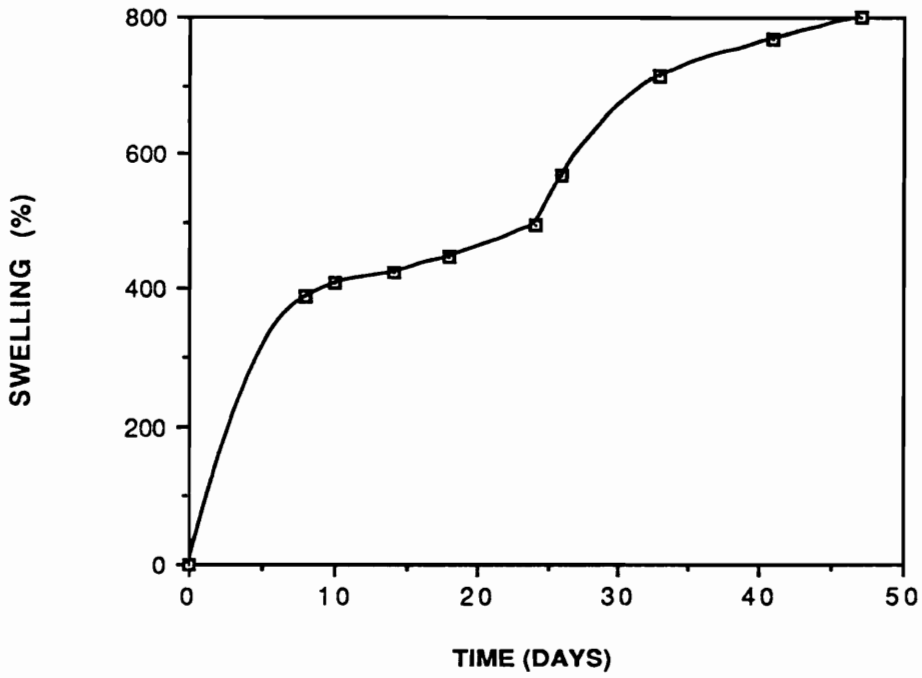

Figure 46. Percent swell versus time for a network prepared from a 5K maleimide terminated PEKE oligomer

solvent penetration within the first two days of the experiment while the second occurs days to weeks later and involves additional swelling of the sample. During the first stage, the network is transformed from a glass to a rubber as the solvent penetrates the specimen, swelling it up to 800 percent. In the majority of the specimens tested, the sample fell apart during this time generating several fragments. It was assumed that this fragmentation facilitated solvent penetration and thus maximized swelling in the first two days. The time required to thoroughly penetrate a specimen which remained intact was checked by slicing one specimen in half after two days. A visual inspection indicated that the networks was thoroughly swollen.

Following this initial stage, the networks underwent a period of little or no additional increase in swelling. The length of this dormant period ranged from several days to several weeks for the different networks. The onset of the second stage of swelling occurred abruptly in some networks (Figure 47) and gradually in others, (Figure 48). Transforming Figure 48a from a standard time to a log time scale emphasizes the transition point from the first to the second stage, (Figure 48b). The networks which exhibited an abrupt onset of the second stage also demonstrated increases in swelling up to several thousand percent within a few days while the ones that possessed the gradual transition to the second stage only swelled less than 100 percent over a few months. In was also noted that several networks which exhibited the abrupt increase to values greater than 2000 percent, later disintegrated into a few, small sticky, gelatine-like particles.

6.2.2.1.2 Comparison to Creep

The two stages of swelling increase seen in the PEKE networks parallel the various stages of creep extension observed in glassy polymers as shown in Figure 49. Since the phenomenon of swelling involves the elongation of the chains via an osmotic stress and creep involves the elongation of the chains via a tensile stress, it is plausible that the molecular motions associated with the two tests are identical. Under glassy conditions, polymers exhibit only a relatively small initial elastic extension with the application of a load due to the high restrictions to large scale chain motion. At extended periods of time under load however, the

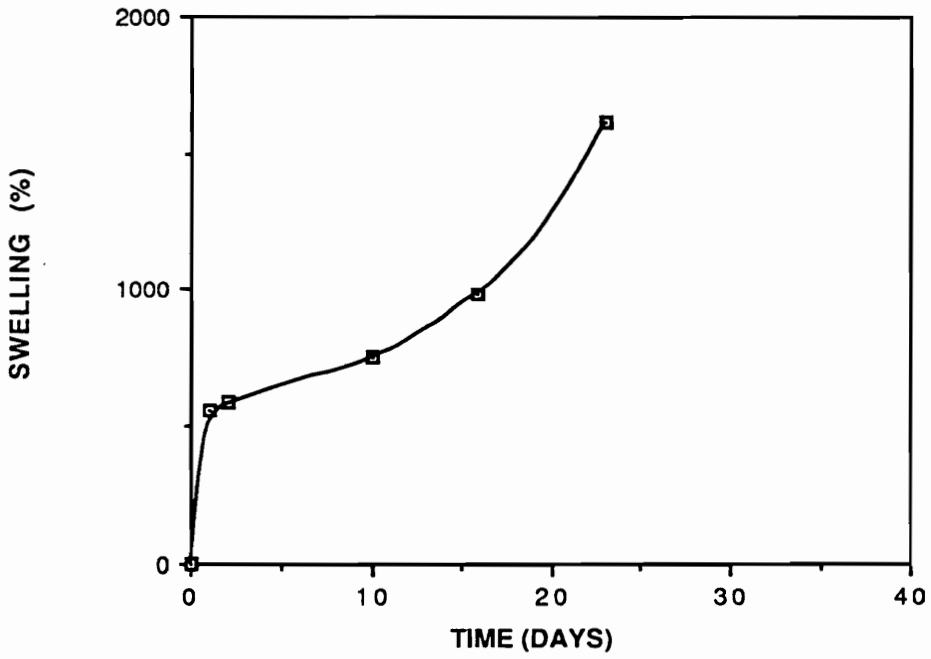

Figure 47. Swelling behavior of a PEKE network exhibiting an abrupt secondary swelling stage.

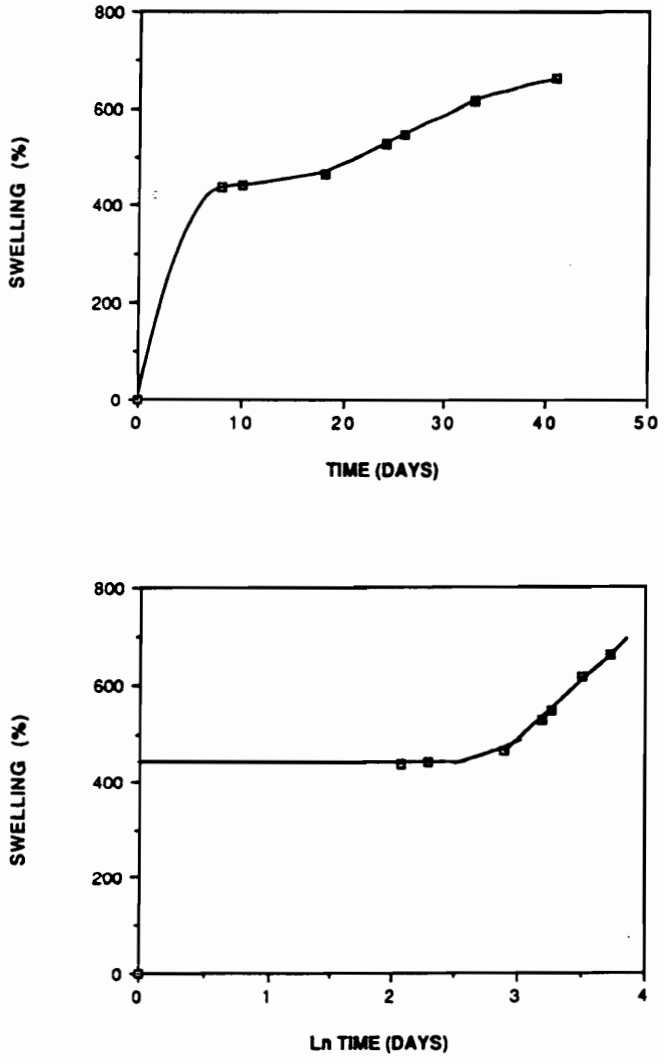

Figure 48. Swelling behavior of a PEKE network exhibiting a subtle secondary swelling stage: a) versus standard time b) versus ln time.

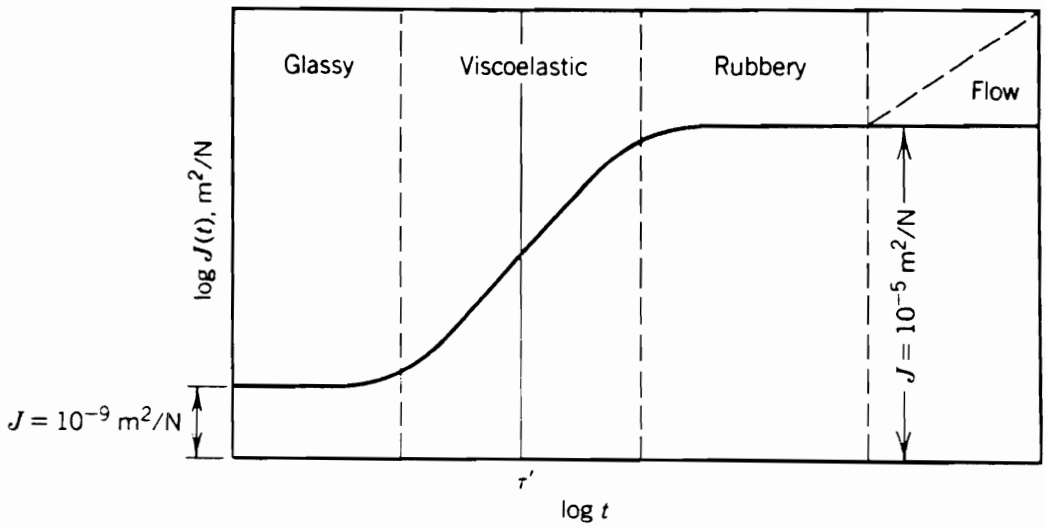

Figure 49. Creep extension versus ln time for a glassy thermoplastic and thermoset [37]

polymer undergoes a transition to a rubbery material, thus allowing large scale chain extension. This is associated with the viscoelastic jump in creep extension shown in Figure 49. The extension levels off over time due to the presence of crosslinks and entanglements which restricts further expansion of the network.

After some more time, a third jump in creep extension, referred to as flow, is observed. This jump generally only occurs in thermoplastics, although it has been reported in lightly crosslinked thermosets [35]. It has been attributed to disentanglement of polymeric chains. For thermoplastics, disentanglements can occur between any entangled chains, producing plastic deformation, flow, and eventually leading to material failure.

For lightly crosslinked networks, only dangling ends can disentangle, either from other dangling ends or from segments of the crosslinked matrix. Entanglements between chain segments which have both ends reacted into the matrix cannot be broken except by chain scission. They can therefore be considered as permanent entanglements. The disentanglement of the dangling ends permits the network to expand, but only to the limits of the crosslink and permanent entanglement points. After the maximum expansion is reached, creep extension levels off.

In highly crosslinked polymers, the density of crosslink and permanent entanglement points is too great to allow expansion of the network to occur. Therefore the third stage of creep extension is generally not observed.

The first stage of solvent uptake in a swelling experiment encompasses the elastic and viscoelastic jumps in creep extension. As the solvent penetrates the matrix, the Tg of the network is depressed below room temperature thereby transforming the glassy network into a rubber. The network expands, but only to the point of stressing the crosslink and entanglement points.

The second swelling stage coincides with the onset of disentanglement of the dangling ends and is therefore related to the third stage of creep extension. It can be speculated that the networks exhibiting an abrupt increase in swelling are probably loosely crosslinked, possessing numerous dangling ends which are relatively easy to disentangle. Those network

which disintegrate over extended periods of time, are probably not geled but rather consist of highly extended and branched chains which are highly entangled with one another but still soluble.

Networks exhibiting a more subtle increase in swelling over extended periods of time are probably more thoroughly crosslinked, thus containing fewer dangling ends. However the dangling ends in these networks are probably more difficult to disentangle since they would be further extended and branched than those of the previous networks. Also, there would be an increased likelihood that the dangling ends would be entangled with segments which are incorporated in the matrix. Since the matrix segment would have less freedom of motion than a dangling end, disentanglement would require longer times than the time required to disentangle two dangling ends. This would therefore explain the slow increase in swelling over the extended period of time.

6.2.2.2 Characterization of PAEK Networks

6.2.2.2.1 Effect of Length of Cure

The effect of dangling ends on the swelling behavior of a network was studied by varying the length of the curing cycle for a 5K maleimide terminated PEKE oligomer. Networks receiving short cure times were expected to be loosely crosslinked, possessing numerous dangling ends and a significant soluble fraction while networks receiving relatively long cure times, were expected to be tightly crosslinked, possessing only a small percent of dangling ends and no soluble fraction.

Three networks were cured at 500 °F (260 °C) for 5, 30 and 120 minutes. One other network was cured at 520 °F (270 °C) for 10.5 hours. All four networks received a 10 minute degassing stage under vacuum at 170 °C and a 30 minute molding stage at 480 °F (250 °C). The swelling behavior versus time for these 4 networks is shown in Figure 50. All networks exhibited an initial rapid rise in swelling within the first two days. The network cured for 5 minutes demonstrates the greatest initial increase in swelling of approxumately 600 percent

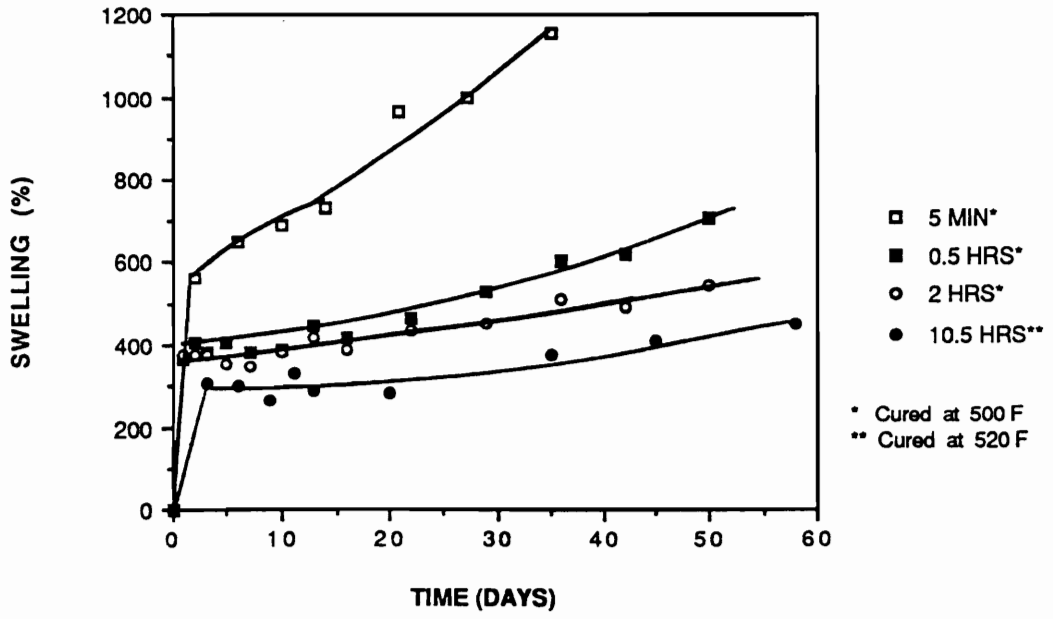

Figure 50. Swelling behavior versus cure time: for a network prepared from a 5K maleimide terminated PEKE oligomer.

along with an abrupt second stage of swelling after about 15 days. The network however did not disintegrate within the time frame of the experiment. This was surprising considering the network only received a 5 minute cure which should be insufficient to produce a gelled matrix. It was concluded therefore that the degassing and molding stages of the network induced a significant level of cure.

The degree of swelling in the 0.5, 2 and 10.5 hour networks leveled off quickly after the initial increase. The 10.5 hour network exhibited the least swelling as expected since it should contain the fewest dangling ends. Swelling appeared to begin increasing again after approximately 25 days. This increase was slow and drawn out for an extended period of time, probably due to the disentanglement of highly extended and branched chains.

Figure 51 compares the percent swelling after 10 days to the gel content for the 4 networks. The curves for gel content and percent swelling versus cure time mirror each other. For the 5 minute network, gel content was at its minimum, 65 percent, while percent swelling at its maximum, 600 percent. As cure time increased to 10.5 hours, gel content increased to almost 100 percent while percent swelling decreased to approximately 300 percent. The decrease in percent swelling corresponding to the increase in gel content may be attributed to the decrease in the number of unreacted chain ends and the increase in the network's crosslink density.

6.2.2.2.2 Maleimide Terminated PEKE's

Figure 52 shows the swelling behavior versus time for networks prepared from maleimide terminated PEKE oligomers of various molecular weights. All networks were cured for 10 to 12 hours at 500 to 520 °F and demonstrated gel contents of greater than 95 percent.

The percent swelling initially increased rapidly for all networks and then leveled off. The magnitude of swelling after the curve leveled off was dependent on the molecular weight of the starting oligomer. The networks cured from the 3.1K, 5.9K, 8.6K, 10.7K, and the 16K oligomers, possessed swelling percents of approximately 300, 400, 600, 600, and 700 respec-

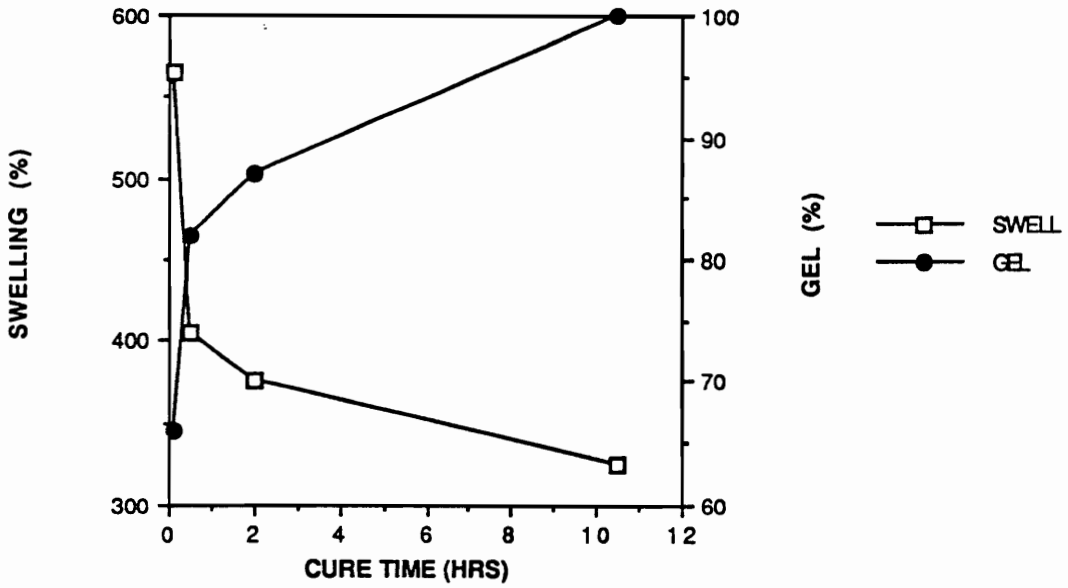

Figure 51. Gel content and swelling percent: after 10 days for a 5K maleimide terminated PEKE oligomer cured for various lengths of time.

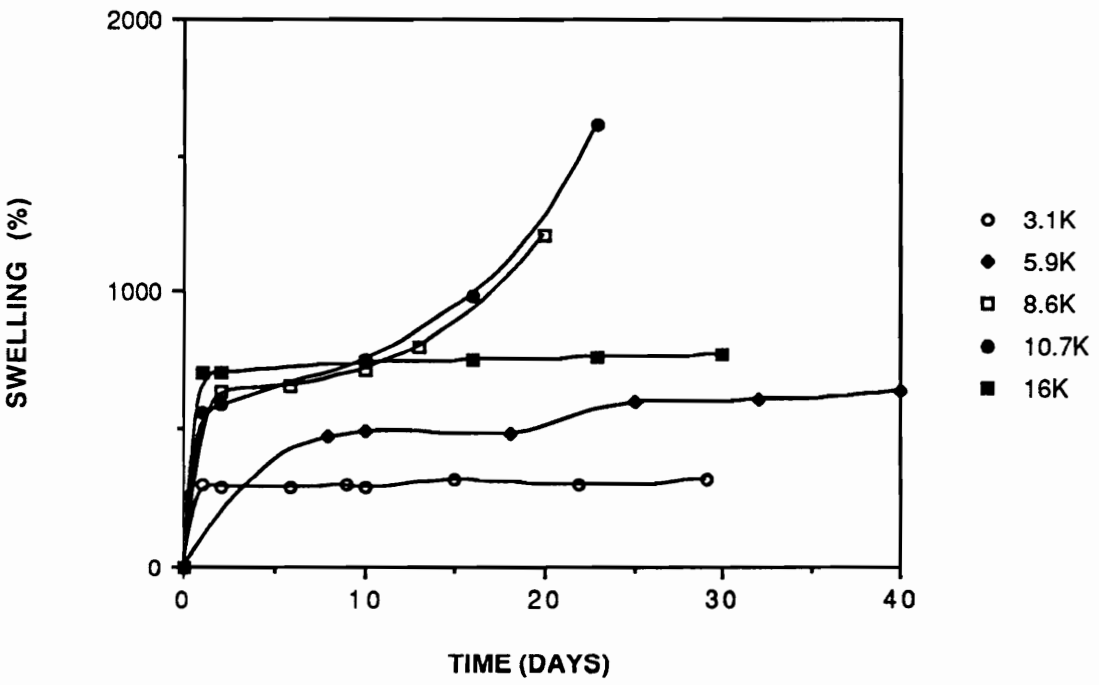

Figure 52. Swelling behavior for cured maleimide terminated oligomer: of various molecular weights.

tively. The increase in swelling with molecular weight reveals the dependence of the network's ability to expand and swell on Mc.

Only the networks from the 8.6K and 10.7K oligomers exhibited the second stage of swelling. The reason these networks exhibited a second stage of swelling while the other three did not is unclear, especially considering that all networks were cured under similar conditions. The answer may lie in the preparation of the oligomers themselves. One possible source of error could be the non-quantitative conversion of the maleic acid groups into maleimides. However, results from the titration of carboxylic endgroups of these oligomers has proven inconclusive.

The crosslink density of these networks were calculated from Flory-Huggins theory using the swelling results after 10 days (Table 14). Mc's for the 3.1K, 5.9K and 10.7K networks were all close to the titrated values of the oligomers. Mc for the 8.6K network was high while that for the 16K network was low.

6.2.2.2.3 Nadimide Terminated PEKE

Networks prepared from nadimide terminated PEKE oligomers revealed similar swelling behavior to the maleimide networks (Figure 53). All networks had a gel content of greater than 90 percent. The networks prepared from the 5.6K and the 10K oligomers exhibited both stages of swelling increase. The secondary stage of the 10K network was very pronounced while that for the 5.6K network was more gradual. The swelling behavior of the 2.7K and 8.0K networks revealed only the first stage of increase.

6.2.2.2.4 Amine Terminated PEKEs

Networks prepared from amine terminated PEKE oligomers, via a ketimine reaction, demonstrate a limitation in the extent of curing. Despite reaction times of 12 hours or better, the maximum gel content obtained was 80 percent. It has been proposed that the extent of imine bond formation is limited by its equilibrium with the reaction by product, water. Later it was discovered that post curing the network under vacuum to remove the water, success-

Table 13. Molecular weight between crosslinks for cured maleimide terminated PEKE oligomers of various molecular weights.

Theoretical <Mn> (g/mole)	Titrated <Mn> (g/mole)	Swelling % (10 days)	<Mc> (g/mole)
2500	3100	290	2560
5000	5900	415	6270
7500	8600	715	11,160
10,000	10,700	750	9770
14,000	16,000	740	12,570

constants used:

Polymer density: 1.26 g/cm^3

Solvent density (Chloroform): 1.492 g/cm^3

Molar volume of Chloroform: 80.01 cm^3/mole

Flory-Huggins constant (for a 10K PEKE oligomer in Chloroform): 0.388

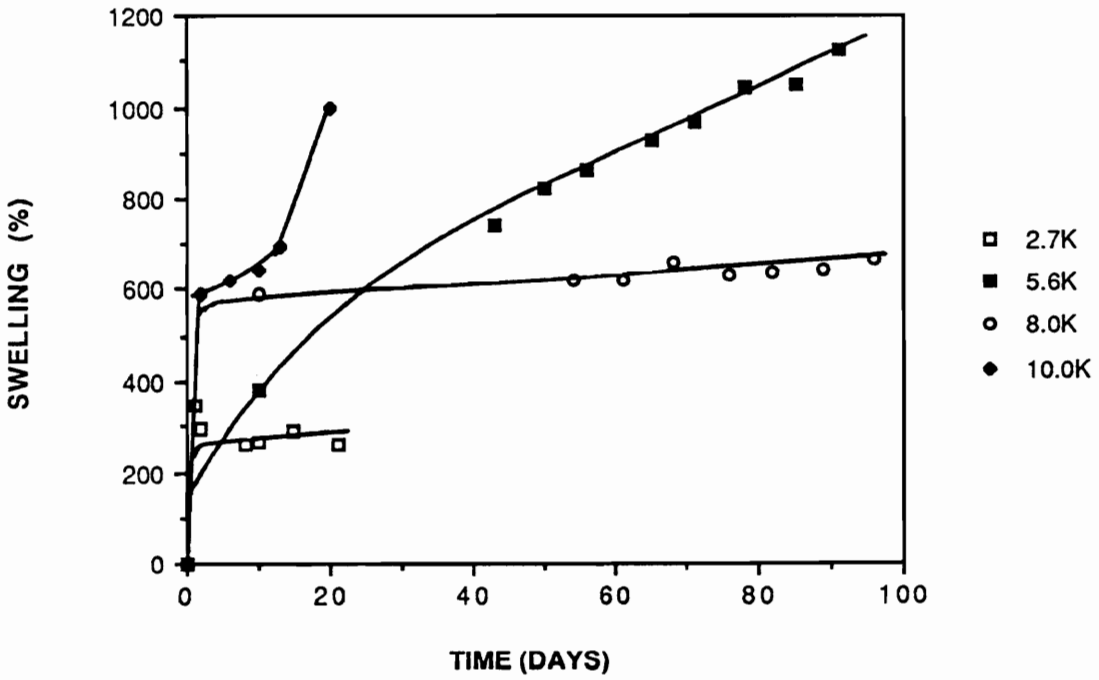

Figure 53. Swelling behaviors for cured nadimide terminated PEKE oligomers: of various molecular weights

fully produced 100 percent gelled networks. However networks used in this study only possessed gel fractions of approximately 75 percent.

The swelling behavior of the networks prepared from the amine terminated oligomers is shown in Figure 55. All three networks swelled to approximately 500 percent within the first two days. Afterwards, the percent swell of the 2.5K and 6.6K networks remained constant while the 11.8K network exhibited a slow increase.

6.2.2.2.5 Maleimide Terminated PEKKE

The swelling behavior of the networks prepared from maleimide terminated PEKKE oligomers is shown in Figure 55. The 2.7K and 11.3K networks exhibited typical behavior compared to the networks seen above. The 2.7K network exhibited only one stage of swelling to approximately 250 percent. The percent swelling of the 11.3K network leveled off at 600 percent and was followed by a slow secondary increase.

The 5.8K network however exhibited a much higher degree of swelling than expected (800 percent). This artificially high level of swelling was probably caused by insufficient curing of the network. Figure 56 is a comparison of the gel content to the percent swelling after 10 days for the three networks. The 2.7K and 11.3K networks exhibited gel fractions of greater than 90 percent while the 5.8K network possessed a gel fraction of of less than 80 percent. As was the case for the networks cured for 5 and 30 minutes, relatively low gel contents implied that the network is loosely crosslinked. This gave the network more freedom to expand and swell than networks possessing a higher gel fraction.

6.2.2.2.6 Comparison of PEKE and PEKKE Networks

A comparison of the swelling behavior of the networks prepared from maleimide terminated PEKE and PEKKE oligomers is presented in Figure 57. The 2.7K and 3.1K networks exhibited almost identical behavior over the entire length of the test while the 10.7K and 11.3K networks exhibited identical behavior up to the point where the PEKE network begins to swell further. The 5K networks are not compared here since they did not have similar gel contents.

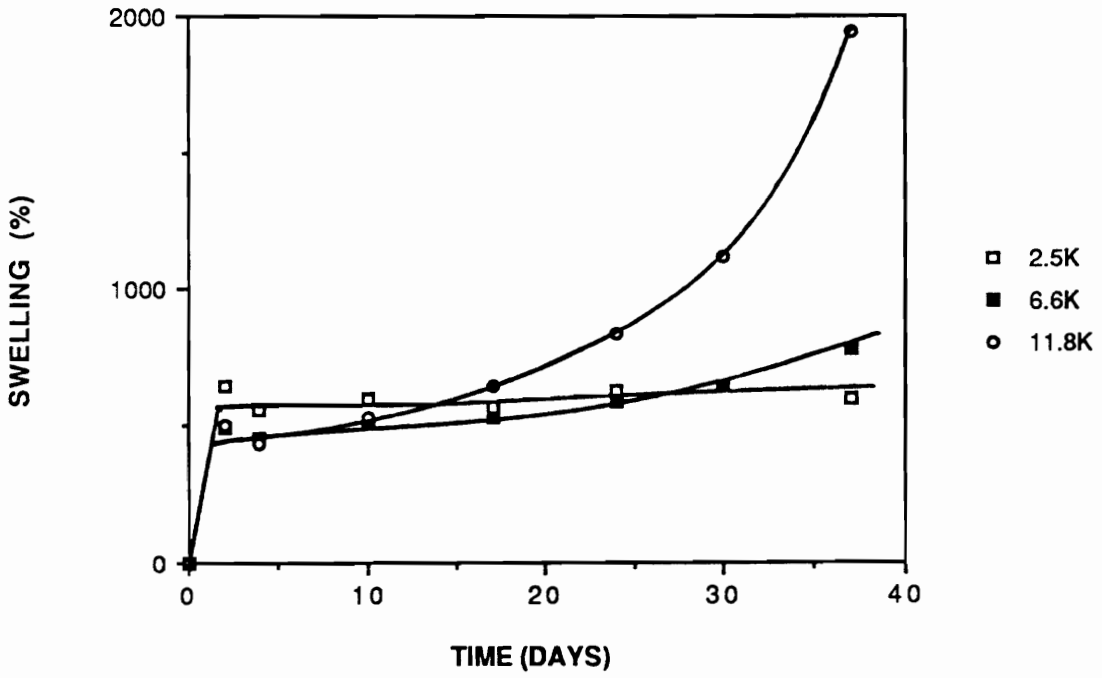

Figure 54. Swelling behavior for cured amine terminated PEKE oligomers: of various molecular weights

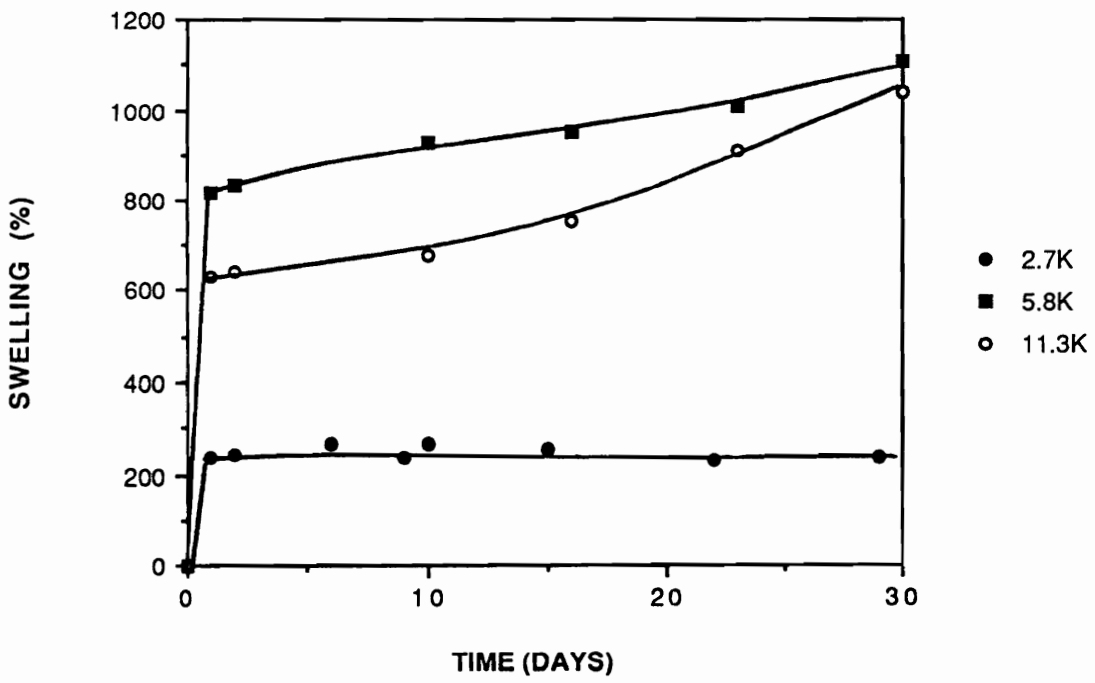

Figure 55. Swelling behavior for cured maleimide terminated PEKKE oligomers: of various molecular weights

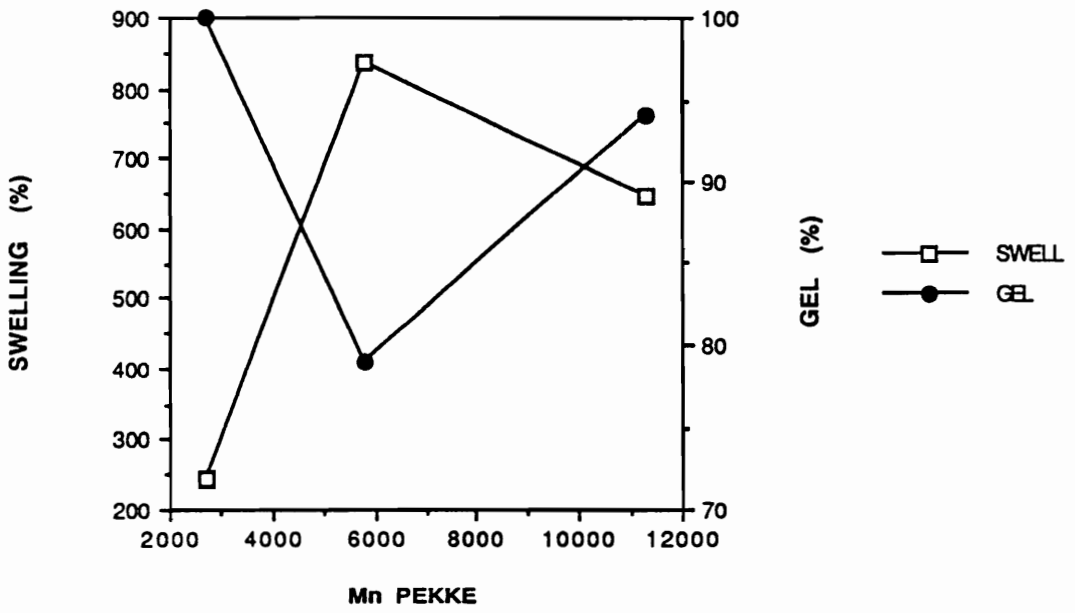

Figure 56. Comparison of gel content to % swelling after 10 days: for networks cured from varying molecular weight maleimide terminated PEKKE oligomers

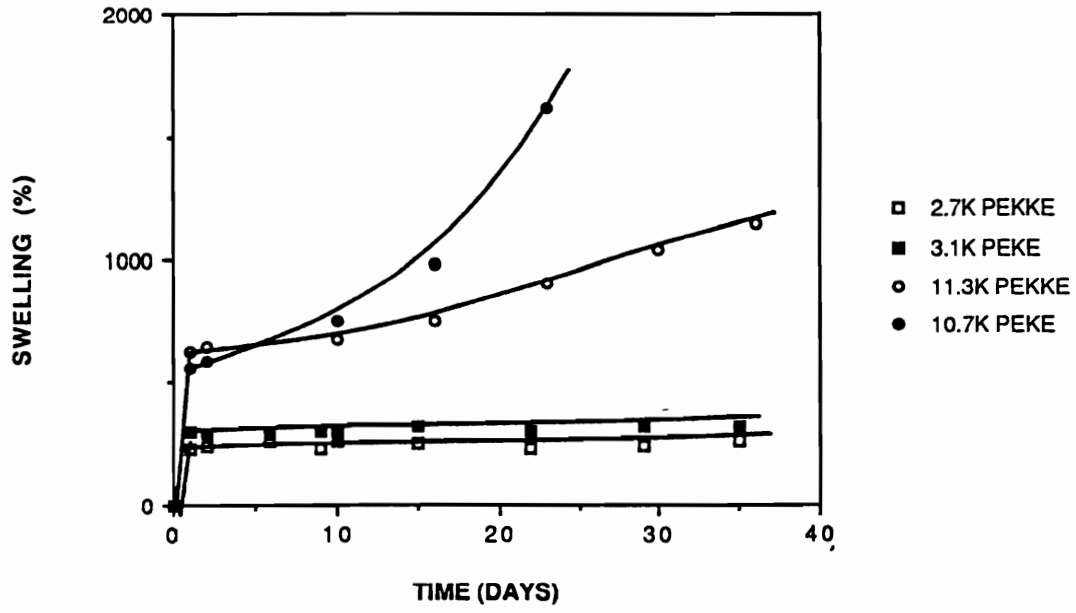

Figure 57. Comparison of the swelling behaviors for 2.5K and 10K PEKE and PEKKE networks.

Table 14. Summary of gelation and swelling results for PEKE and PEKKE networks

Comparison	Network	Variable	% Gel	Swelling[1]	Behavior[2]
length of cure	5K PEKE-MI	5 min.	66	565	abrupt
		30 min.	82	405	subtle
		2 hr.	87	375	subtle
		10.5 hr.			subtle
<Mn>	PEKE-MI	3.1K	100	290	not observed
		5.9K	100	(415)	subtle
		8.6K	95	640	abrupt
		10.7K	100	585	abrupt
		16.0K	100	705	not observed
<Mn>	PEKE-NDI	2.7K	100	295	not observed
		5.6K	92	(385)	subtle
		8.0K	100	(570)	not observed
		10.0K	100	590	abrupt
<Mn>	PEKE-NH_2	2.5K	68	650	not observed
		6.6K	77	495	subtle
		11.8K	76	505	abrupt
<Mn>	PEKKE-MI	2.7K	100	245	not observed
		5.8K	79	835	subtle
		11.3K	94	645	subtle

1: for 2 days
2: 2nd stage
( ): for 10 days

The maginitude of swelling a network undergoes should be directly related to the maximum elongation of its chains between the crosslink and entanglement points. Figure 58 compares the maximum extension of two repeat units for a PEKE and a PEKKE chain. This representation assumes the configuration of the polymer chains is restricted to two dimensions. The higher molecular weight of the PEKKE repeat unit is taken into account by dividing the maximum extension by the molecular weight. PEKE is found to have a full extension of .038 anstrom/MW while PEKKE has a full extension of 0.039 angstrom/MW. Since PEKE and PEKKE have equal extensions per molecular weight, it is logical that they possess the same magnitude of swell.

6.3 Mechanical Behavior

6.3.1 Tensile Behavior

The stress strain behaviors for networks prepared from various molecular weight maleimide terminated PEKKE oligomers and their analogus linear high molecular PEKKE thermoplastic are shown in Figure 59 and summarized in Table 15. All systems possess an apparent modulus of approximately 150,000 psi. These moduli are almost a factor of three less than the moduli values of comparable thermoplastics such as polycarbonate (350,000 psi). The artificially low moduli can be attributed to the measurement of strain by crosshead displacement. Table 15 includes the moduli of a network prepared from a 5.9K maleimide terminated PEKE oligomer using crosshead displacement to measure strain as well as an extensometer. The modulus value obtained using the crosshead displacement is comparable to that of the PEKKE systems. With the use of the extensometer, however, the modulus increases to 390,000 psi which is reasonable for these these systems. Unfortunately the extensometer was not purchased at the time the tests on the PEKKE networks were per-

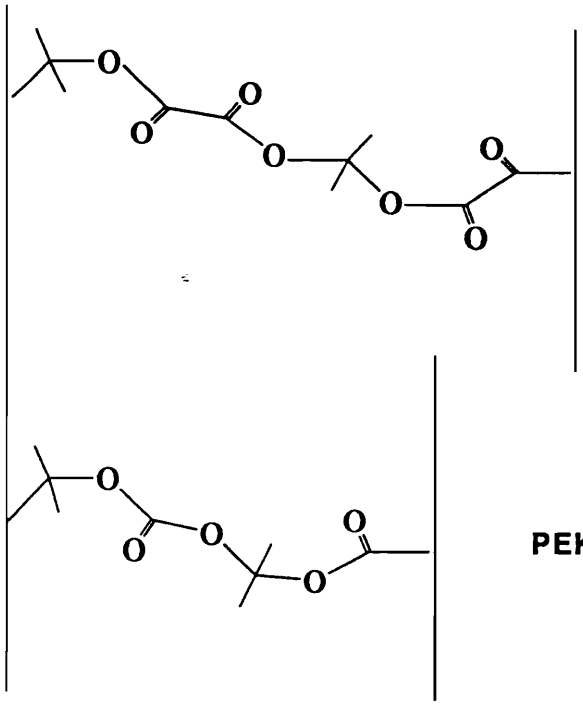

BOND	LENGTH
C-O	1.43 A
C-C=O	1.51A
C-C	1.541 A
C=C(Ar)	1.395 A

BOND ANGLE

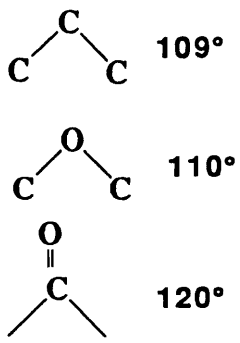

Figure 58. Comparison of the maximum extension for two repeat units: for a PEKE versus a PEKKE backbone [136].

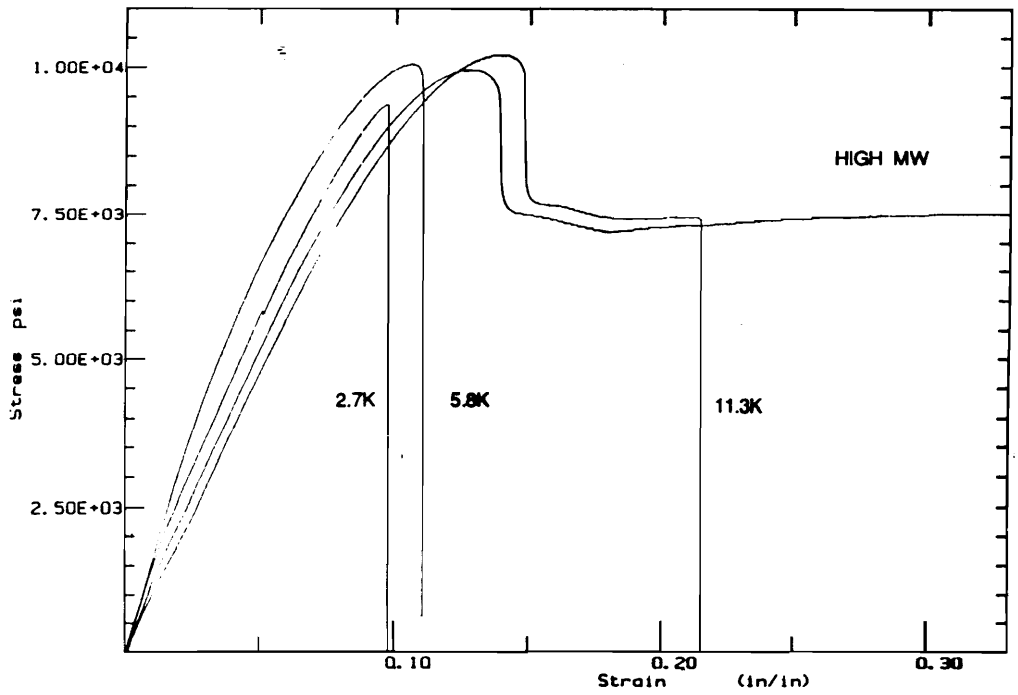

Figure 59. Tensile stress-strain behavior for networks: cured from maleimide terminated PEKKE oligomers of varying molecular weights.

Table 15. Summary of tensile behavior for PEKE and PEKKE networks

Starting Oligomer	Apparent Titrated <Mn>	Modulus (psi x 10^3)	Yield % Elongation at Break	Stress (psi x 10^3)
PEKE-NH_2	2,500	151±27	4	5.8±0.4
	6,600	144±7	11±0.5	9.6±0.3
	11,800	147±3	23	9.9±0.1
PEKKE-MI	2,700	136±7	10	9.4
	5,800	158	11	10.1
	11,300	119±22	21	10.4±0.2
	∞	123	110	10.0
PEKE-MI	5,900	108±5	29±12	11.5±0.1
	5,900[1]	390±37	38±22	10.3±0.2

NH_2: amine terminated
MI: maleimide terminated
1: strain measured by an extensometer
100,000 psi = 689.5 MPa

formed. Lack of time and material prevented the repeating of these measurements. Therefore, it is only possible to speculate that the actual moduli of these systems are approximately 400,000 psi.

The yield stress, which should be unaffected by the method of measuring strain, is shown to be approximately 9,000 psi for all systems. This value is reasonable when compared to yield stress values for similar thermoplastics. The strain softening observed in the 10K network as well as in the linear high molecular weight thermoplastic is accompanied by the formation of a neck in the test specimen. The neck initiates at an angle approximately 45° to the applied load.

The networks cured from the 2.7K and 5.8K oligomers failed before necking could occur. The elongation at break for these networks is approximately 10 percent. The ultimate elongation at break for the 11.3K network is twice that, 21 percent, while that for the linear thermoplastic is greater than 100 percent. These values again may be artificially high due to the measurement of strain by crosshead displacement.

Networks prepared from amine terminated PEKE oligomers exhibit similar stress strain behavior to that of the PEKKE systems, (Figure 60). Moduli, yield stress and elongation at break for the various oligomers are comparable to their PEKKE molecular weight counterparts. The only exception is the relatively short elongation at break of the 2.5K amine terminated PEKE network. Both specimens tested of this network are believed to have undergone premature failure caused by the presence of some type of flaw. Figure 61 shows an optical micrograph of the 2.5K fractured surface at a magnification of 25X. A flaw is observed at the side of the specimen with fracture lines radiating out from it. A similar flaw is observed in the other specimen tested. No flaws were observed in the 10K specimen. The presence of these flaws do not prove the occurrence of premature failure, but they do suggest that it is a possibility.

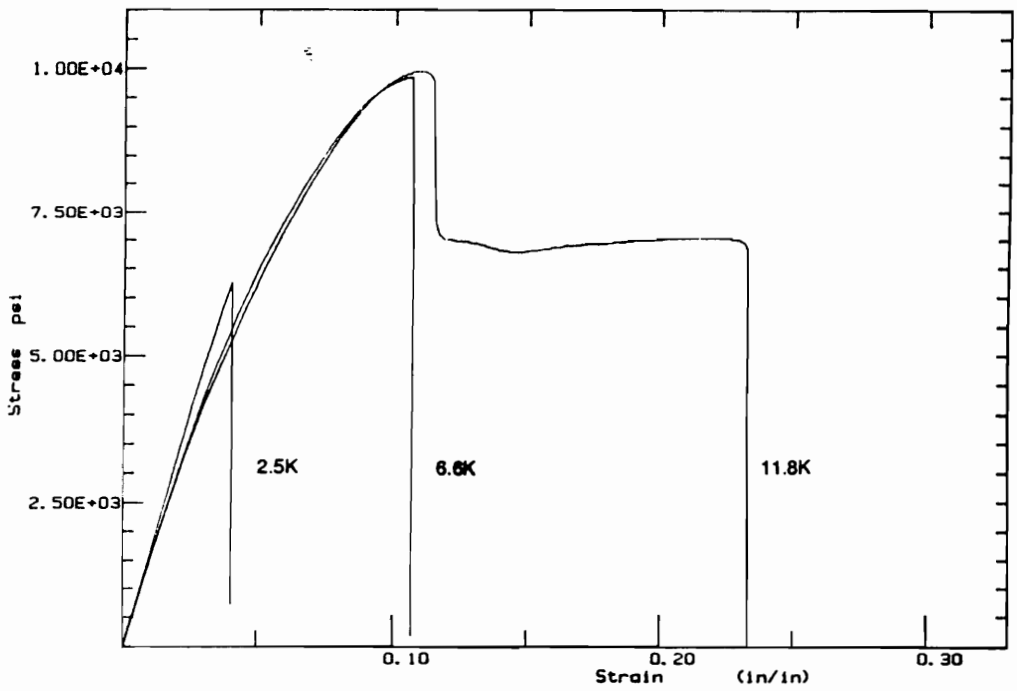

Figure 60. **Tensile stress-strain behavior:** for networks cured from amine terminated PEKE oligomers of varying molecular weights.

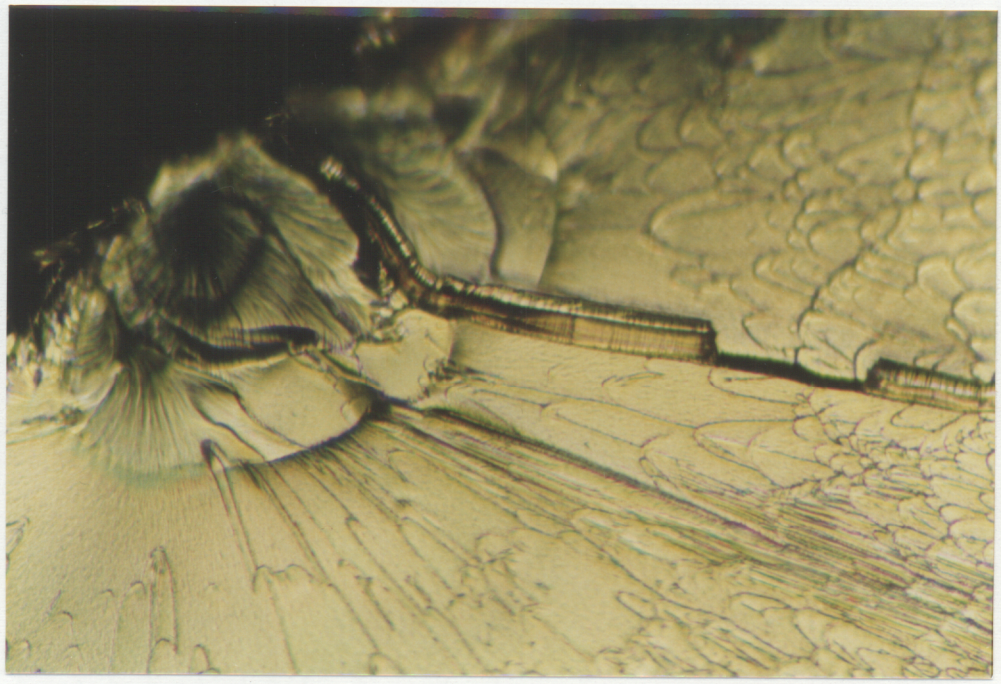

Figure 61. Optical micrograph of a fracture surface: for a tensile dogbone from a cured amine terminated 2.5K PEKE oligomer.

6.3.2 Creep Behavior

Figure 62 displays the creep behavior of networks prepared from maleimide terminated PEKE oligomers of various molecular weights. Each test was performed at 150 °C with an initial displacement of 10 percent of the specimen thickness. The rate of creep is seen to increase with chain length between crosslink points. This effect is caused by the increase in the freedom of chain motion as Mc is increased.

The rate of increase appears to decrease however as molecular weight increases. This probably is caused by the formation of entanglements between the crosslink points. These entanglements would act as temporary crosslinks thereby reducing the increase in freedom of motion generated by increasing Mc. The abrupt leveling off of the creep extension of the 10.7K and the 16K networks is caused by the maximum extension of the clamps in the DMA.

6.3.3 Dynamic Mechanical Behavior

6.3.3.1 Overview for a Cured 5K PEKE Oligomer

Figure 63 displays the dynamic mechanical behavior from -150 °C to 450 °C for a cured 5.9K maleimide terminated PEKE oligomer. PEKE possesses a large β relaxation peak ranging from -120 °C to 40 °C. A small drop in the glassy storage modulus at -75 °C is associated with this relaxation.

The glass transition of this network occurs between 120 °C to 200 °C with the tan δ maximum occurring at approximately 160 °C. Storage modulus has an associated decrease of greater than two orders of magnitude between 140 °C and 180 °C. The rubbery modulus levels off at approximately 3×10^6 Pa and remains relatively constant up to 400 °C. Above 400 °C, modulus and tan δ increases, indicating further crosslinking of the network.

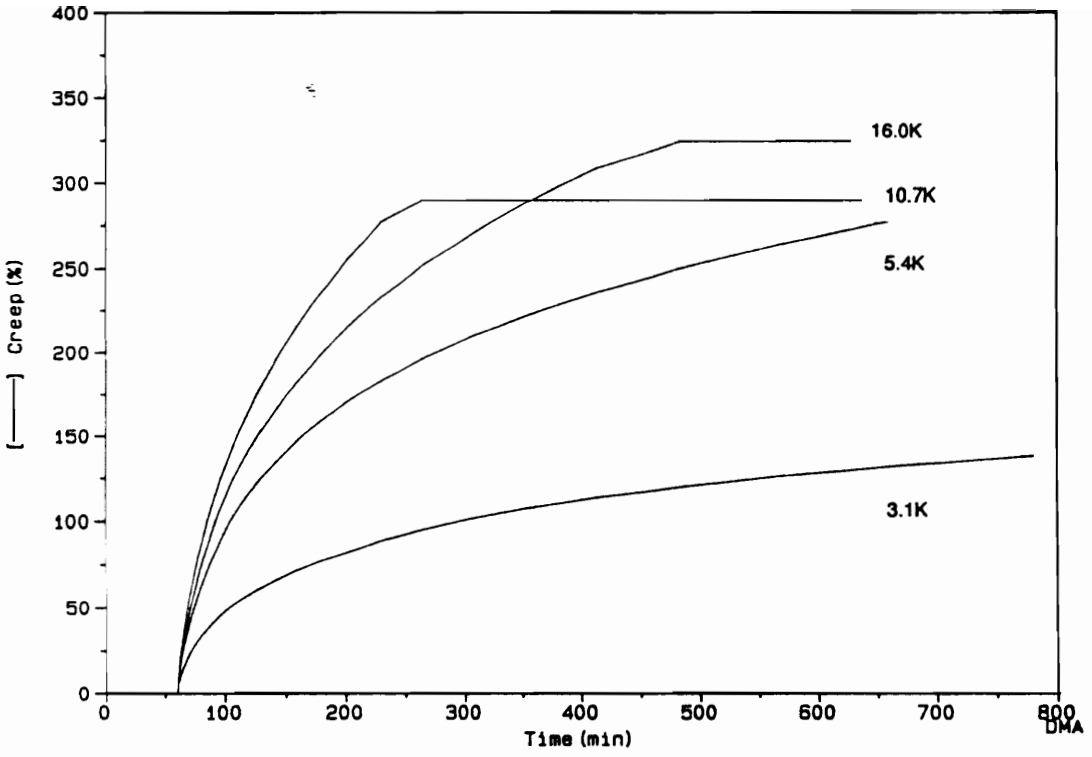

Figure 62. **Creep behavior for networks cured from maleimide terminated PEKE oligomers:** of varying molecular weights.

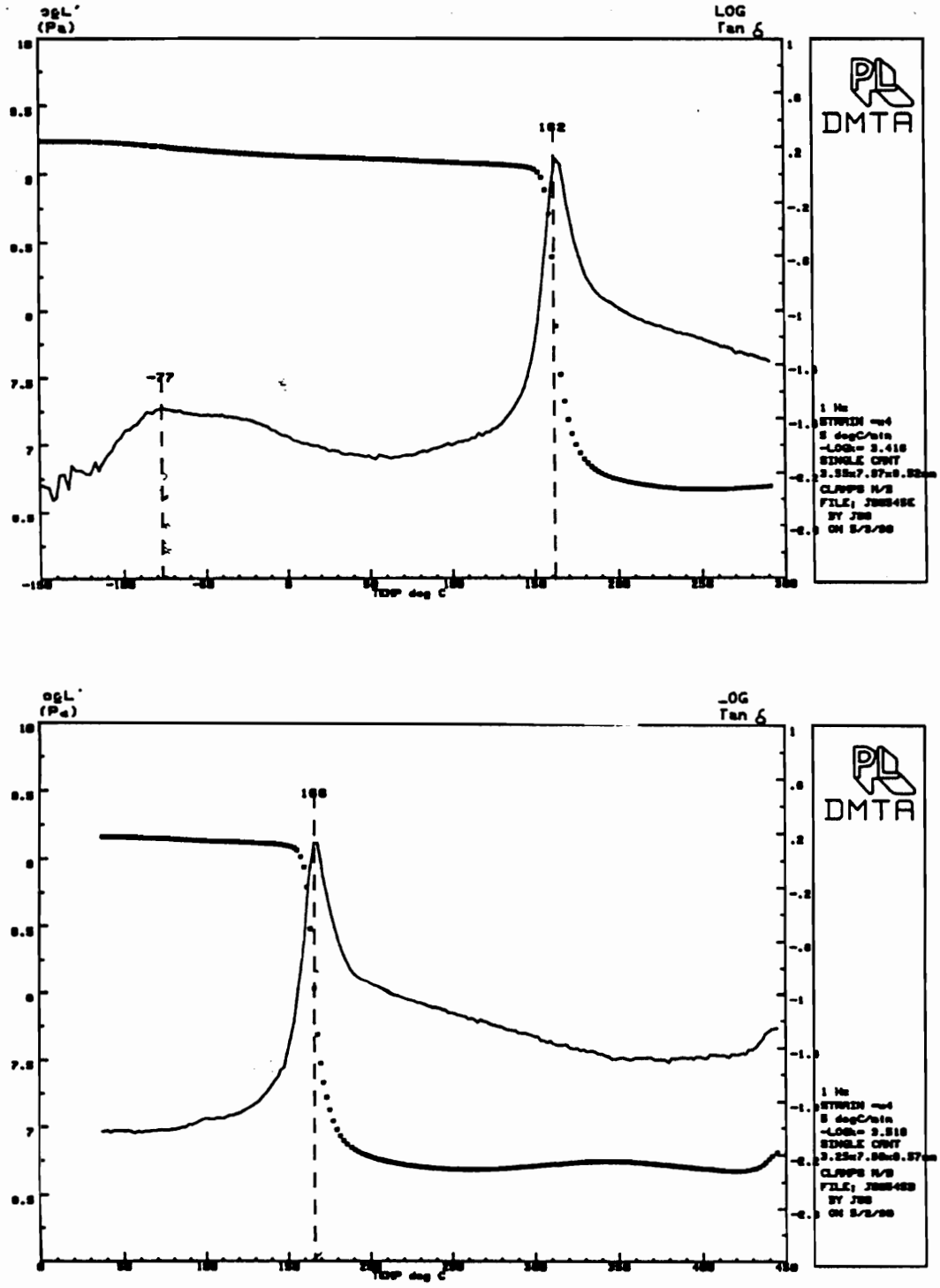

Figure 63. **Dynamic mechanical behavior for a cured maleimide terminated 5.4K PEKE oligomer:** a) -150 °C to 300 °C b) 35 °C to 450 °C

6.3.3.2 Linear, High Molecular Weight PEKE Thermoplastic

The dynamic mechanical behavior of the linear high molecular weight PEKE thermoplastic is shown in Figure 64. The polymer possesses a β transition and glass transition temperature similar to those for the cured 5.9K PEKE oligomer. However above Tg, storage modulus does not level off to a rubbery plateau, but continues to decrease until it is below the detection limits of the instrument.

6.3.3.3 Cured Amine, Maleimide, and Nadimide Terminated 2.5K PEKE Oligomers

Figure 65 compares the dynamic storage modulus versus temperature for three cured 2.5K PEKE oligomers terminated with either amine, maleimide or nadimide groups. The three networks exhibit similar dynamic behavior to one another with the nadimide network possessing the highest Tg, 175 °C, and the amine network possessing the lowest rubbery modulus. The differences in Tg and rubbery modulus are probably attributable to the different functionalities of the crosslink points. The cured nadimide terminated PEKE oligomers would be expected to possess the highest crosslink functionality since during its curing process cyclopentadiene is generated which can then react with numerous chain ends together at one junction point. The higher crosslink functionality would reduce chain freedom thereby increasing the polymer's Tg. The cured amine terminated PEKE oligomer on the other hand, possesses a crosslink functionality of only three. This allows the network more freedom to expand in the rubbery state, thus giving the network a relatively low modulus.

The tan δ curves for these networks, not shown, are nearly identical. They reach a miximum value of between 1.0 and 1.2 at the network's associated Tg which increases as the endgroup changes from amine to maleimide to nadimide.

6.3.3.4 Cured PEKE Oligomers of Varying Molecular Weight

The effect of Mc on the dynamic mechanical behavior for networks prepared from maleimide terminated PEKE oligomers of various molecular weights is shown in Figure 66. Glass transition temperature and rubbery modulus are both seen to increase slightly as Mc

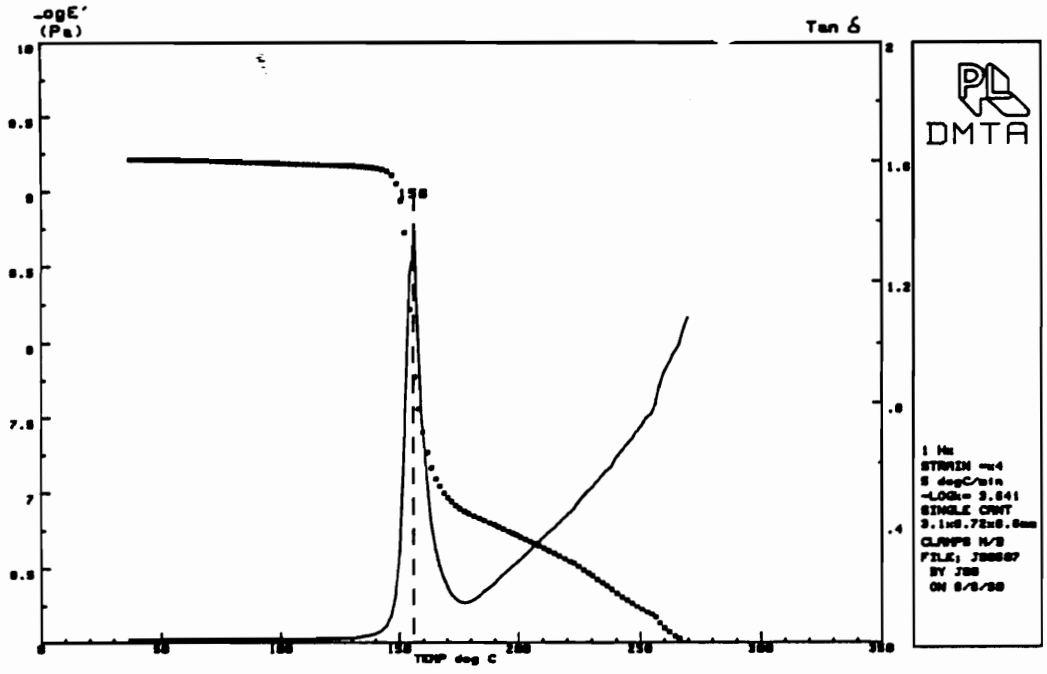

Figure 64. Dynamic mechanical behavior for a linear, high molecular weight PEKE thermoplastic

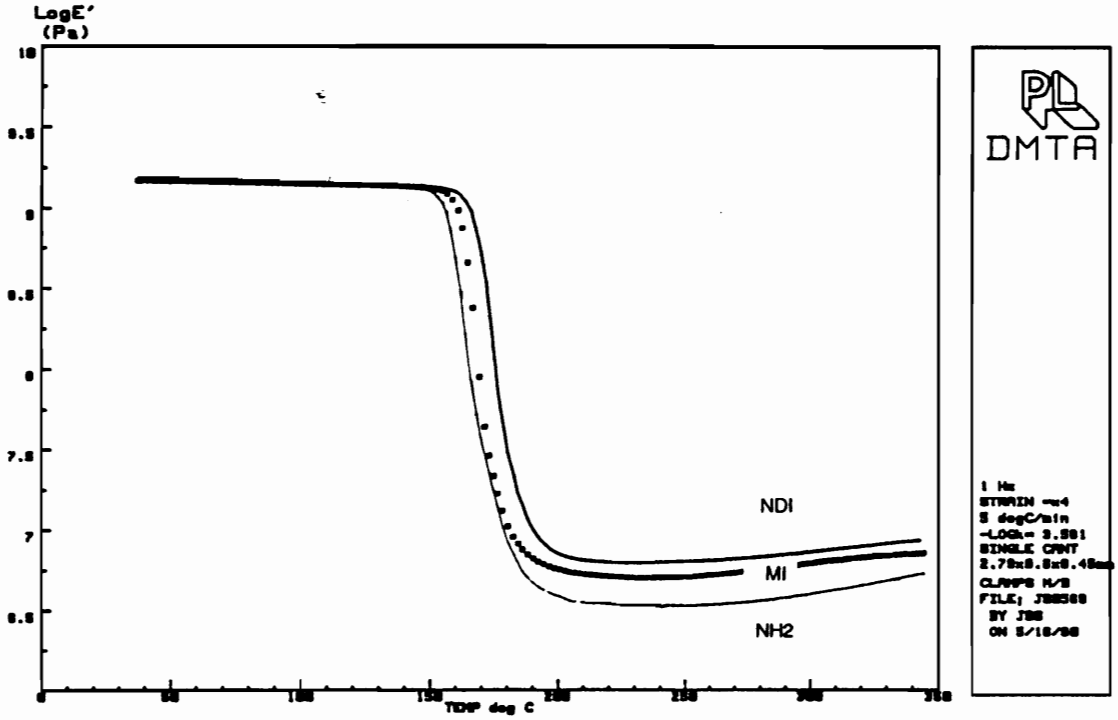

Figure 65. Comparison of the dynamic mechanical behavior: for cured amine, maleimide, and nadimide terminated 2.5K PEKE oligomers

decreases. The glass transition temperatures for 3.1K, 5.4K and the 10.7K networks were 158, 150 and 149 °C respectively. The increase in Tg and rubbery modulus as oligomer molecular weight decreases is caused by the associated increase in crosslink density. The increase in crosslink density decreases chain mobility thereby increasing Tg and rubbery modulus.

The effect of decreasing oligomer molecular weight from 16K to 3.1K on the size of the β relaxation is shown in Figure 67. Both the magnitude and temperature of the β peak are found to be independent of molecular weight.

6.3.3.5 PEKE versus PEKKE

A comparison of the dynamic mechanical behavior for cured 2.5K maleimide terminated PEKE and PEKKE oligomers is presented in Figure 68. The PEKKE network exhibits a slightly larger β relaxation than the PEKE network along with a higher glass transition temperature (175 °C compared with 167 °C using DMTA frame M). The higher Tg of the PEKKE network is probably due to the additional ketone group along the backbone which produces a stiffer chain and increases the amount of secondary bonding between the chains.

6.3.3.6 Annealing

The effect of annealing on the dynamic mechanical behavior is shown in Figures 69 and 70. Figure 69 compares the dynamic mechanical behavior of a 20K PEKE polymer which had been quenched from 100 °C above its Tg to that for an identically quenched polymer which was then annealed at 15 °C below Tg for 84 hours. Both polymers possess nearly identical behavior, possessing no differences in either the β or α transitions. The lack of a rubbery modulus is interesting since it would be expected that highly entangled polymers would possess some type of plateau. From the difficulty encountered in trying to produce flow in this polymer when it was compression molded, it is extremely doubtful that the lack of a rubbery modulus was caused by the polymer flow. Rather, it is most likely caused by the specimen slipping from the clamps as the polymer softens during its glass transition.

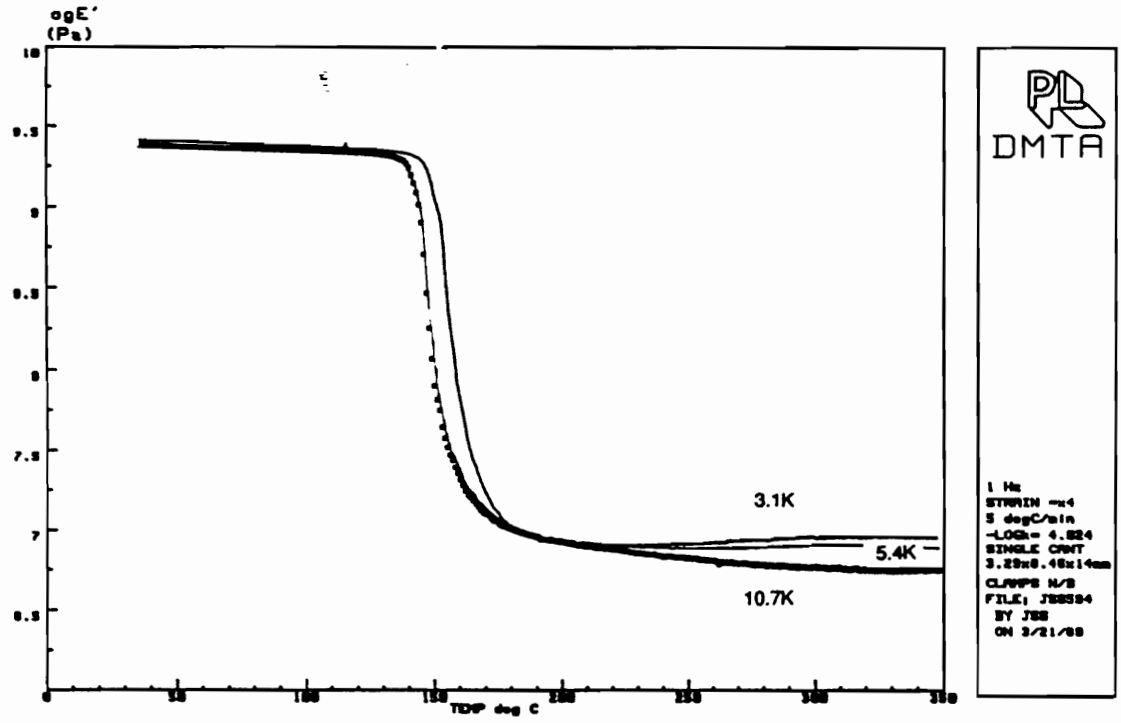

Figure 66. Comparison of the dynamic mechanical behavior for cured maleimide terminated PEKE oligomes: of varying molecular weights

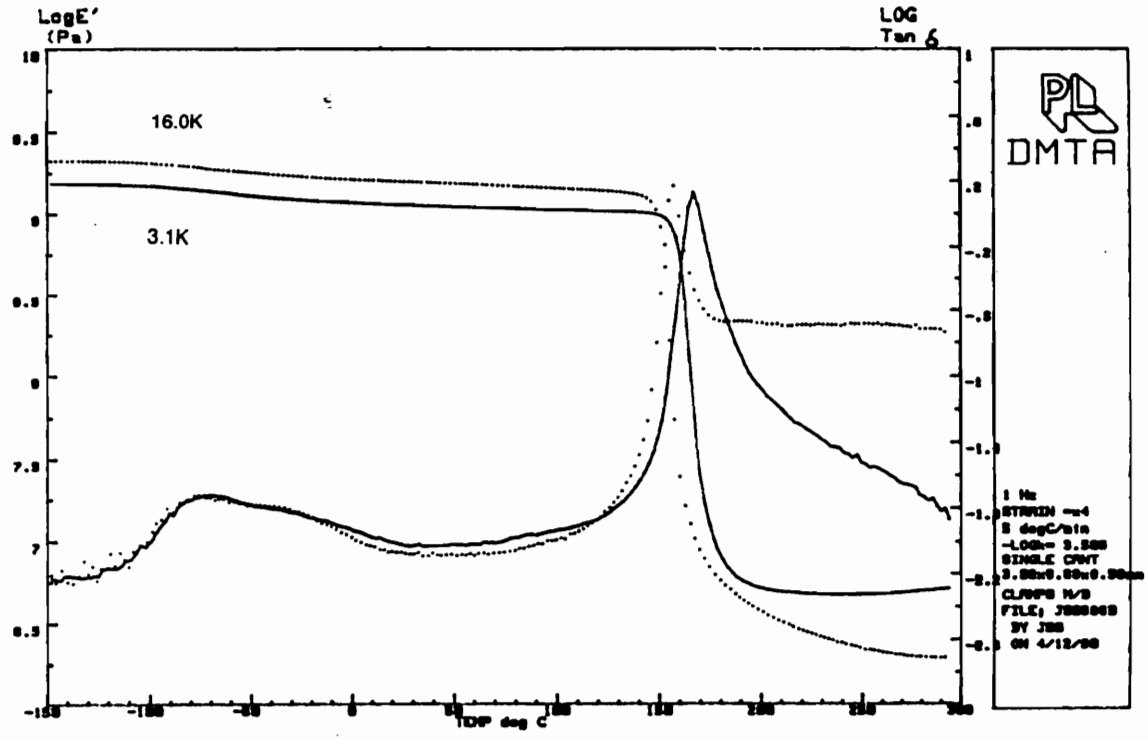

Figure 67. Comparison of the subambient dynamic mechanical behavior: for cured 3.1K and 16K maleimide terminated PEKE oligomers

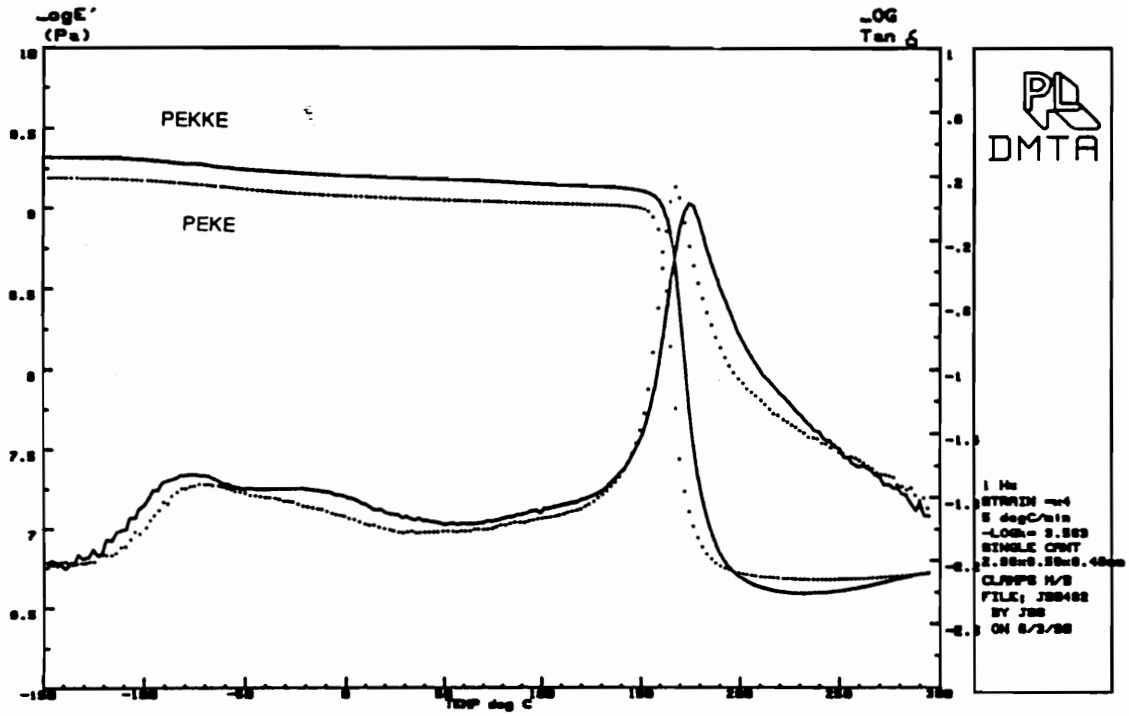

Figure 68. Sub-ambient dynamic mechanical behavior for cured 2.5K maleimide terminated PEKE and PEKKE oligomers

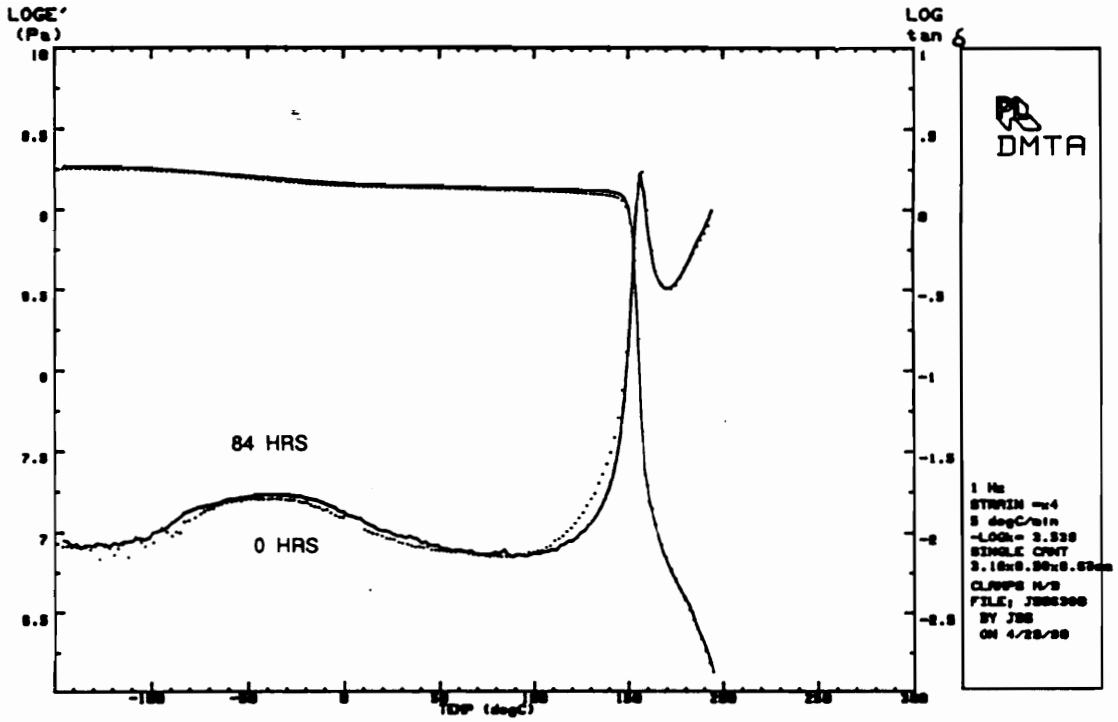

Figure 69. Subambient dynamic mechanical behavior of a quenched and an annealed 20K PEKE thermoplastic

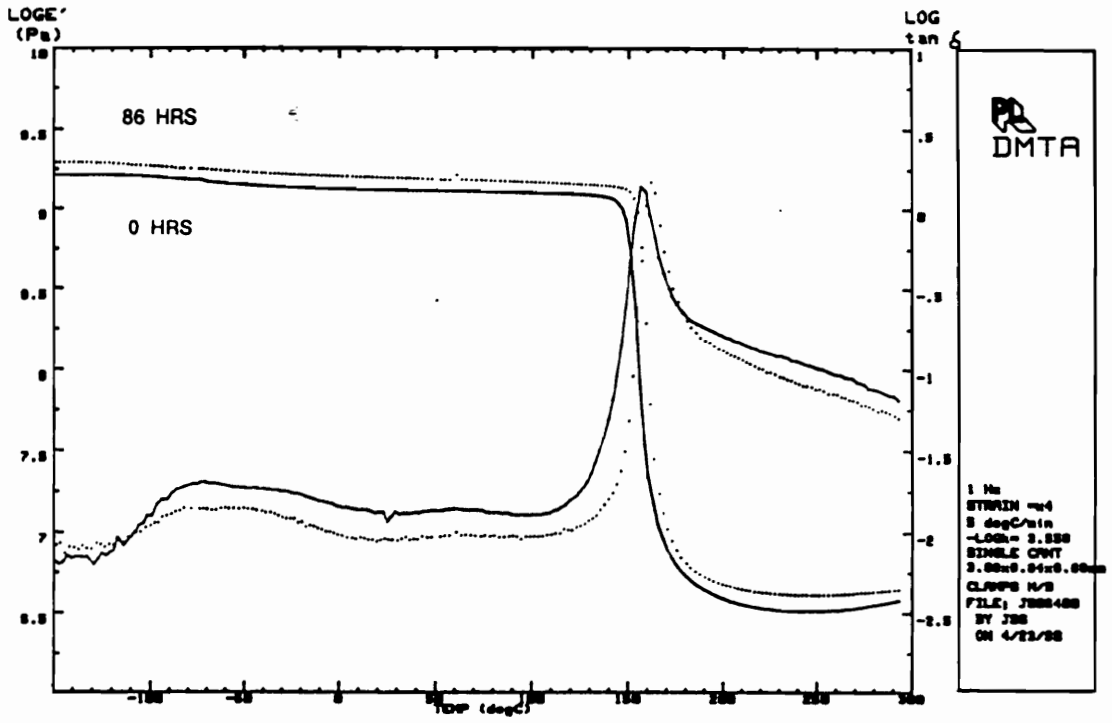

Figure 70. Subambient dynamic mechanical behavior of a quenched and an annealed 5.9K maleimide terminated PEKE oligomer.

Figure 70 compares the effect of annealing on the dynamic mechanical behavior for two networks cured from a 5.9K maleimide terminated PEKE oligomer. Both networks were quenched from approximately 120 °C above their Tg with one being annealed at 15 °C below Tg for 86 hours. Annealing decreases the magnitude of the β transition transition significantly as well as slightly increasing the network's glass transition temperature. These two changes maybe caused by the suppression of small and large scale chain motion due to the increase packing of the chains which occur during annealing.

6.3.4 Fracture Toughness

6.3.4.1 Introduction

In this section, an examination of the fracture behavior of PEKE and PEKKE thermoplastics and thermosets will be presented. This examination will be divided into four parts. The first part deals with the effect of precracking and specimen thickness on the resulting fracture toughness values. This is followed by an examination of the failure mechanisms observed for the PAEK systems. Included in this part are are scanning electron and optical micrographs of fracture surfaces. The last two parts present the fracture toughness results for PEKE and PEKKE thermosets and thermoplastics respectively. Included are examinations studying the effect of cure time, annealing, and molecular weight on fracture toughness. An indepth discussion on these effects to the overall toughening mechanisms of these polymers will not be presented here, but rather reserved to the chapter dealing with toughening mechanisms.

6.3.4.2 Geometry Effects

6.3.4.2.1 Precracks

As discussed previously, precracks were introduced into network fracture toughness

specimens by tapping a razor blade into the specimen until a crack propagated from the blade. For the PEKE thermoplastic oligomers, precracks were introduced by sawing a crack into the specimen using an Exacto saw blade.

The length of the precrack generated by the saw blade was easily controlled between 0.4 and 0.5 times the total width of the specimen. The length of the precracks produced by running a crack from a razor blade however were more difficult to control. Crack lengths ranged from 0.3 to 0.9 times the total specimen width.

The precrack fronts produced by the saw blade were a straight line perpendicular to the direction of crack growth while precrack fronts produced from the termination of a running crack were bowed like a meniscus, with the crack length in the center of the specimen being up to 10 percent longer than along the sides. The shorter crack lengths along the sides could be caused by the plane stress stress state which promotes crack termination faster than the plane strain stress state in the center of the specimen.

The bowed precrack in some specimens, were assymmetric with one side being up to 50 percent longer than the other side. These assymmetric bowed precrack fronts were probably caused by the razor not being level when it was tapped into the specimen. The length of the precrack for these specimens was measured from the center of the precrack. No abnormal scatter of the data could be detected from the K_{1c} results for these cracks compared to the symmetrically bowed cracks.

6.3.4.2.2 Thickness

K_{1c} is defined as the critical stress intensity for mode one loading producing a plane strain stress state. Under these conditions, K_{1c} is independent of specimen thickness since the state of stress is independent of thickness. For thin specimens however, thickness affects the state of stress. As thickness decreases below a critical level, the state of stress becomes a combination of plane strain and plane stress. This increases the measured critical stress intensity value above that for a pure plane strain condition. Kinloch [137] has shown that de-

creasing thickness below that required for plane strain, increases the measured fracture toughness of adhesive bonds.

The minimum thickness for obtaining plane strain conditions according to ASTM E-399 test method for metals, is shown equation 6.1

$$B = 2.5\left(\frac{K_{1c}}{\sigma_o}\right)^2 \qquad [6.1]$$

where:

B = critical thickness neede for plane strain conditions

σ_o = yield stress

For a material possessing a K_{1c} of 3.5 MPa $m^{1/2}$ and a yield stress of 9.000 psi, such as polyetherketones, B would be approximately 8 mm. The specimens used in this study were all approximately 3 mm thick, suggesting that the toughness results might be artificially high due to a significant contribution of the plane stress stress element. The level of contribution of the plane stress stress element is not certain since equation 6.1 was derived for metals and its applicability to plastics has not been verified. However in order to try to minimize any possible thickness effects in samples, tests were run at a relatively fast loading rate (2 in/min). The fast loading rate would minimize the increase in K_{1c} since it would minimize the deformation caused by the plane stress element. The effect of altering rate on the resulting K_{1c} values for PEKE systems however was not studied.

6.3.4.3 Mechanisms of Failure

The fracture surfaces of the various thermosets and thermoplastics tested, reveals three mechanisms of failure; brittle, semi-brittle, and ductile.

6.3.4.3.1 Brittle

Brittle failure is defined as fracture which produces flat, glassy, mirror-like fracture sur-

faces. This failure behavior is found in low molecular weight thermoplastics of PEKE and in PEKE modified bismaleimide networks containing at least 25 weight percent bismaleimide.

The fracture surfaces of moderate molecular weight PEKE oligomers (Mn greater than 12,000 but less than 20,000), possessed a few shear lines which ran along the surface in the direction of crack propagation. These lines appeared to be the result of small scale localized deformation. The overall failure mechanism of these materials however were still considered brittle.

Figure 71 shows a load displacement curve for a brittle failure. The material exhibits a fairly linear elastic response of stress to strain followed by a sudden decrease of load as the material fails.

6.3.4.3.2 Semi-brittle

Semi-brittle failure is associated with the fracture surfaces which contain a thin zone, up to 2 mm in thickness, of deformed material in front of the precrack tip followed by a relatively flat and glassy region of brittle fracture. This failure mechanism is seen in most of the polyetherketone networks tested.

The mode of failure is believed to change from ductile to brittle due to the increasing hydrostatic stresses. Referring to chapter 2, the normal stresses in the x, y and z directions all increase as the distance from the crack tip increases. All three stresses reach their maximum in magnitude at the limits of the plastic zone. Since the hydrostatic stress is an average of these three stresses, it too reaches a maximum at the edge of the plastic zone. If the hydrostatic stress reaches a critical level, as is believed to occur in these systems, brittle failure occurs.

The deformed zone is made up of large strands of deformed polymer running normal to the precrack front, (Figure 72). They are similar in appearance to the deformation described in diffuse zones in chapter 3.

Figure 73a shows an optical micrograph of a polished cross section of a crack front of a linear high molecular weight PEKE thermoplastic after the 3 point bend specimen had been

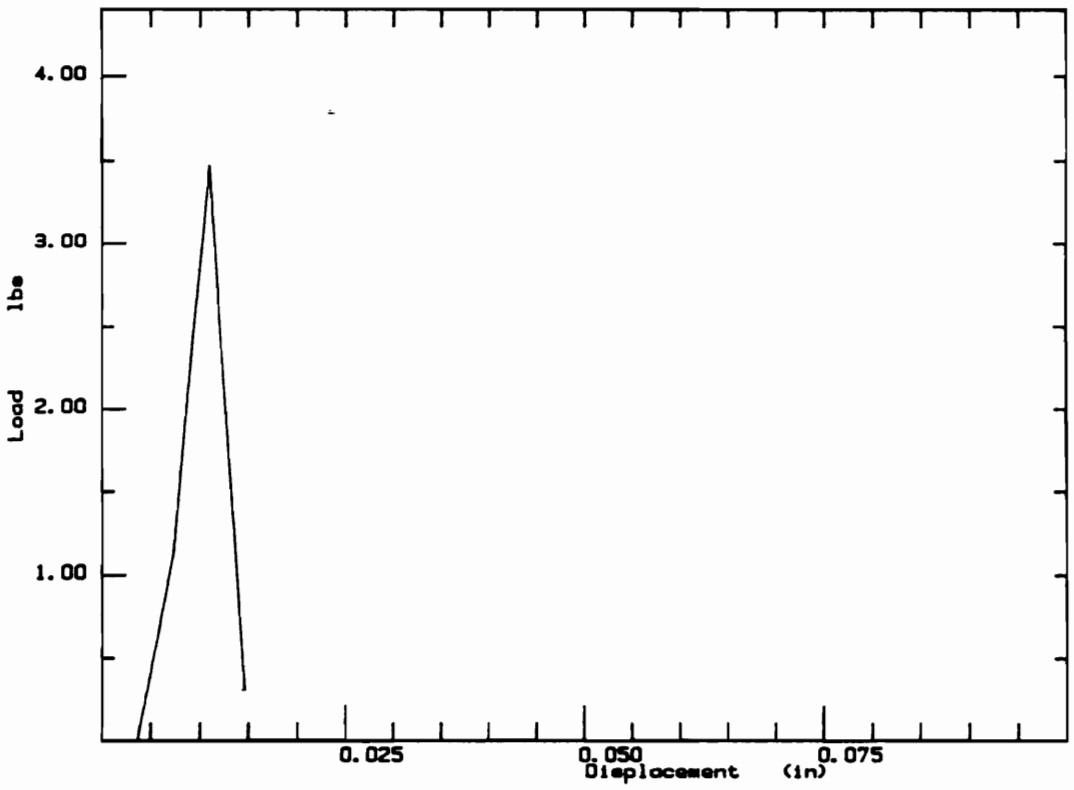

Figure 71. Load versus displacement for a 3 point bend toughness test: of a 9K t-butylphenyl PEKE oligomer exhibiting brittle behavior

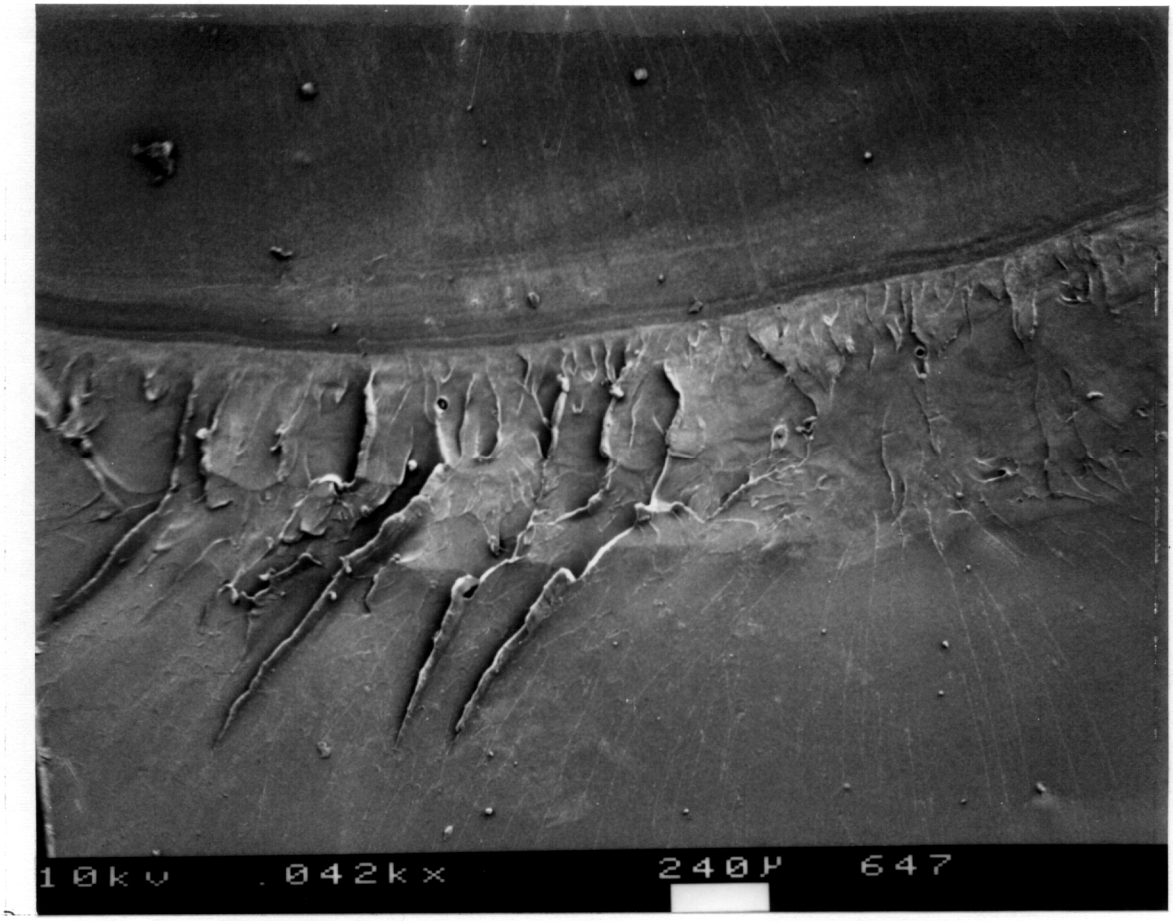

Figure 72. Scanning electron micrograph of the fracture surface: of a cured 5K PEKE oligomer at 42X, exhibiting a diffuse zone of deformation in front of the precrack tip

loaded to approximately 85 percent of the load to failure. Under cross polarized light, the cross section reveals two regions of oriented polymer chains above and below the fracture plane. These zones are similar to those predicted by Theotokoglou and Tsamasphyros [138]. Surrounding the crack tip a small diffuse zone of deformation is observed. Magnification of this region (Figure 73b) indicates a large number of shear bands radiating from the crack tip at angles of 10 to 40 degrees to the fracture plane. Shear bands for a network cured from a 5K maleimide terminated PEKE oligomer are more well defined (Figure 74). It is logical to assume that these shear bands once fractured, produced the deformed zones seen in front of the precrack tips on the fracture surfaces.

Within the region of brittle crack propagation, the size of the deformation lines decreases by approximately an order of magnitude. These lines appear as either a ribed pattern (Figure 75) or as parabolas (Figure 76). Sometimes both patterns will be present on the same surface (Figure 77).

The rib pattern has been observed in annealed samples of polycarbonate [139]. These lines are believed to be caused by the pulling up and tearing of sheets of polymer. Others[140] have explained the generation of this pattern by a continual stop and go motion of the crack. The crack, once propagation begins, is believed to run faster than the crossheads of the testing instrument can move apart to maintain a critical load on the specimen. The crack therefore stops or slows down until the crossheads can take up the slack and re-establish a critical load. During the stop or slow down periods, the materials deforms generating a rib line.

The parabolas are seen in almost all semi-brittle failures. They all contain a focus point, close to the top of the parabola, usually at a dirt particle or an indentation. They extend in the direction of crack propagation with the top closest to the precrack. Similar fracture features have been shown for polystyrene [139]. These patterns, which are described as U or V shaped, are believed to be produced by a tensile tearing stress. The material within the U is stressed so that it forms an elevated plane above the plane of the fracture surface. In the samples examined in this study, no increased elevation was observed. Rather, it only appears

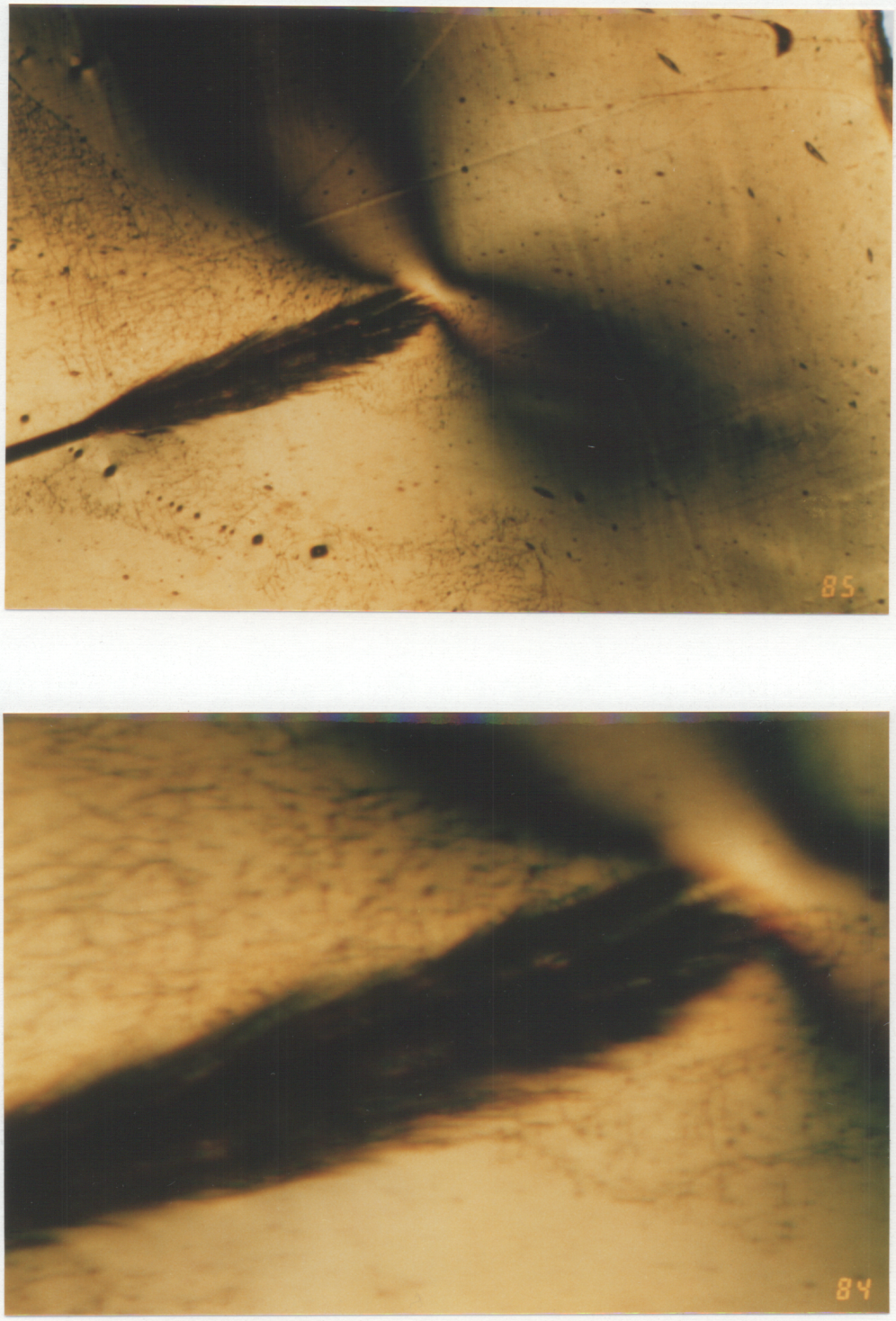

Figure 73. Optical micrograph under cross polarizers of a crack tip cross-section: for a linear, high molecular weight PEKE thermoplastic a) 25X b)60X

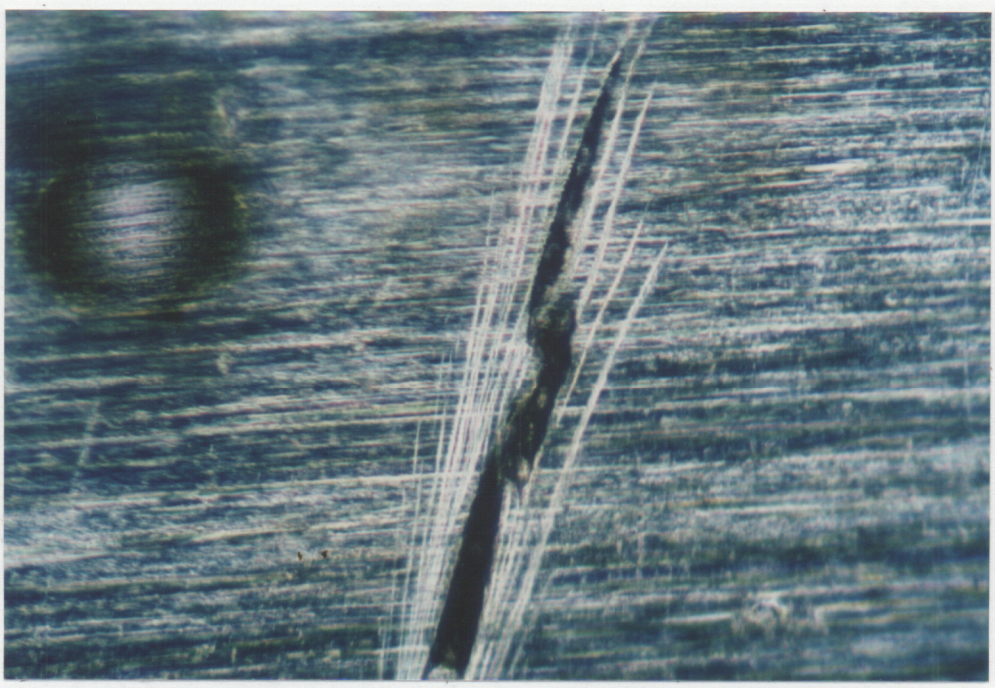

Figure 74. Optical micrograph of a cracktip cross-section for a cured 5K PEKE oligomer: at a magnification of 25X

Figure 75. Scanning electron micrograph of a fracture surface of a cured 5K amine terminated PEKE oligomer: at 201X exhibiting ribed deformation

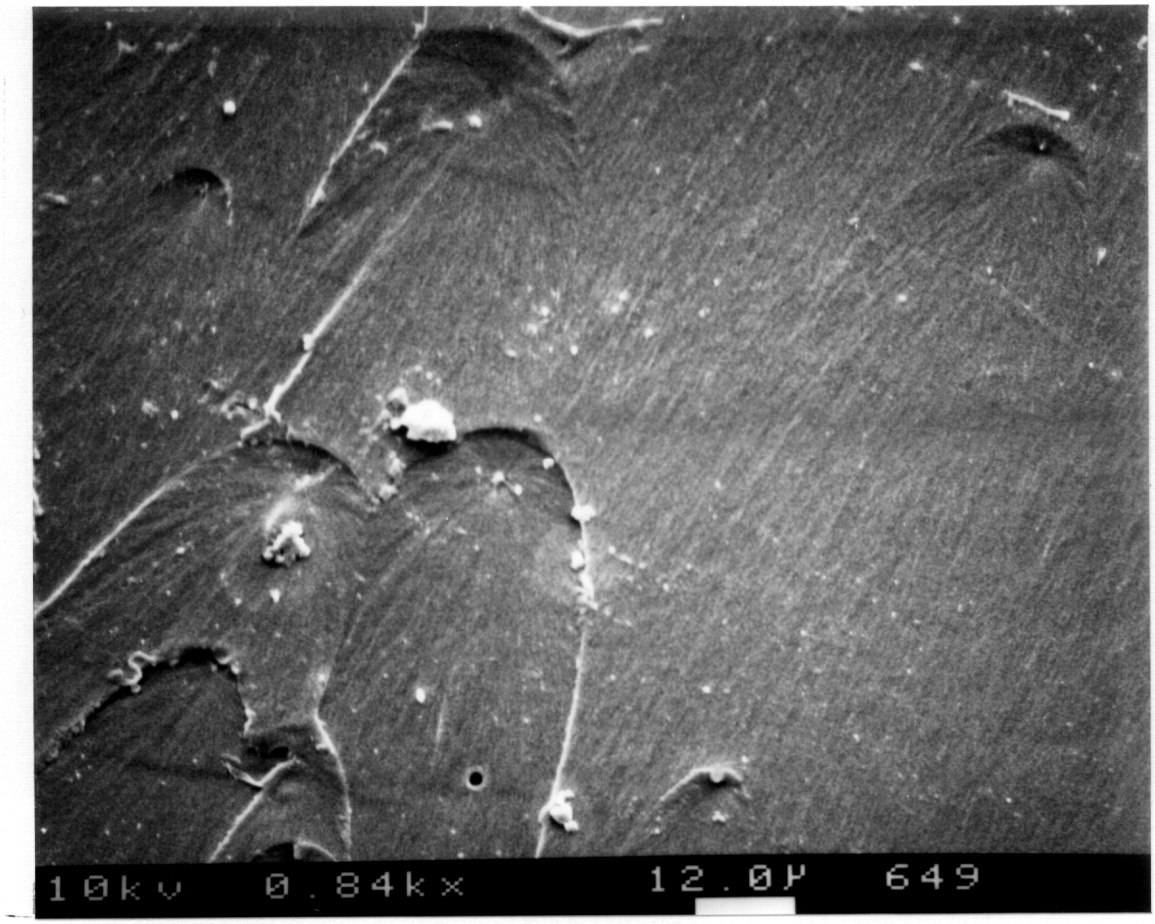

Figure 76. Scanning electron micrograph of a fracture surface of a cured 5K maleimide terminated PEKE oligomer: at 840X exhibiting parabola shaped deformation

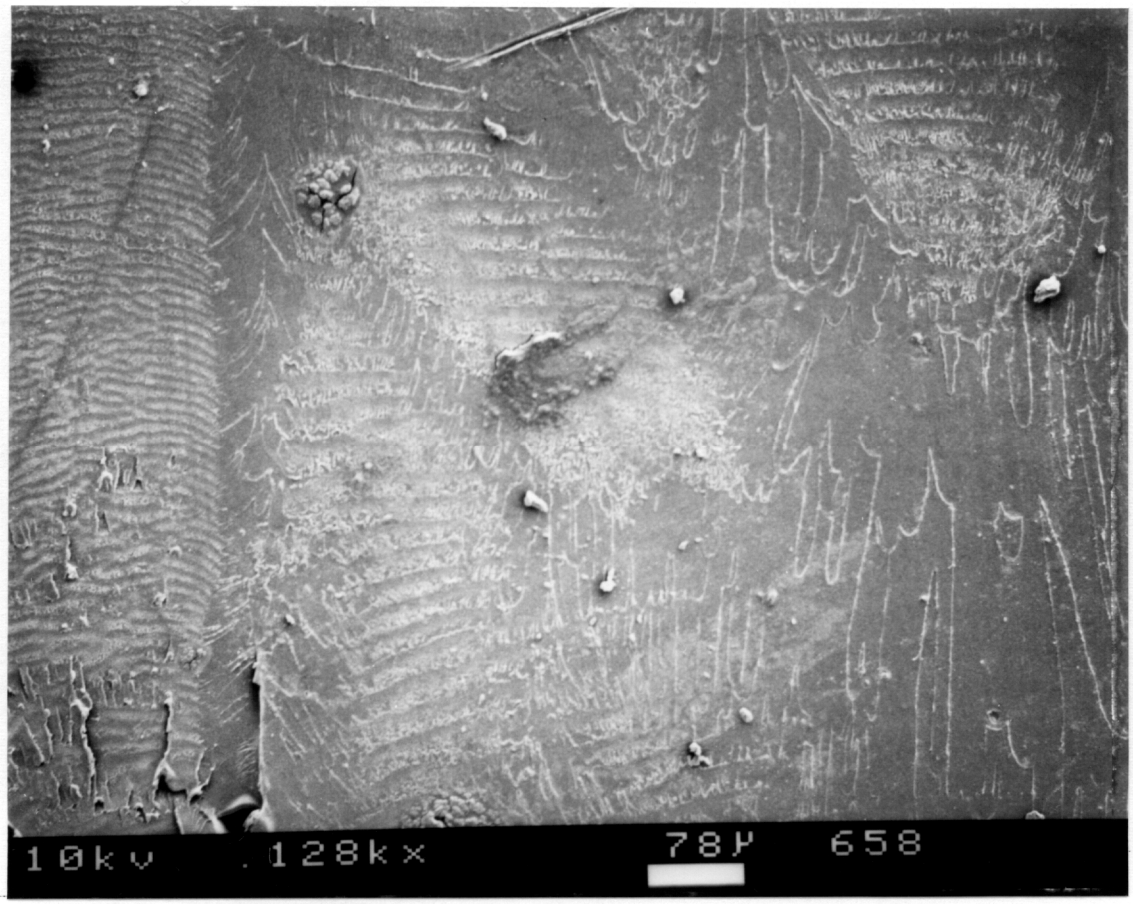

Figure 77. Scanning electron micrograph of a cured 5K maleimide terminated PEKE oligomer: at 128X exhibiting ribed and parabola shaped deformation

that the rim of parabola has been pulled up and torn. No explanation for the generation of this shape can be given at this time.

The load displacement curve for a specimen failing by a semi-brittle mechanism is shown in Figure 78. The behavior is similar to that for brittle failure. The material exhibits a linear elastic load response to displacement reaching a maximum load with 5 seconds. This is followed by a rapid critical crack propagation, within approximately 0.1 seconds, indicated by the sharp drop in load.

6.3.4.3.3 Ductile

Ductile failure produces large scale deformation and tearing of the polymer. The deformation spans the entire width of the specimen in front of the precrack tip and therefore is not confined to a thin strip as in the case of semi-brittle failure.

Ductile failure is seen in networks prepared from oligomers of molecular weights greater than 5K and in the linear high molecular weight polyetherketone thermoplastics. Figure 79 is a scanning electron micrograph of a ductile fracture surface. The specimen is drawn in from the sides narrowing the thickness of the specimen and forming two parallel ridges, shear lips, along the edges of the specimen. Within the lips, the specimen contains large deformation bands which run from the precrack tip to the bottom of the specimen. Figure 80 shows the load displacement curve for such a failure. The material exhibits an elastic region followed by a slow decrease in load as the sample tears. In most specimens tearing takes place within 10 seconds.

6.3.4.4 Fracture Toughness Results for PAEK Networks

6.3.4.4.1 PEKE versus PEKKE

Figure 81 compares the fracture toughness values for PEKE and PEKKE networks prepared from maleimide terminated oligomers of various molecular weights. The data from this figure is summarized in Table 16. The critical stress intensities for the linear high molecular

weight thermoplastics of PEKE and PEKKE are included in Figure 81 at an assigned molecular weight value of 50,000.

Over the entire range of molecular weights, PEKE systems are seen to have superior fracture toughness to PEKKE. The networks from both backbones exhibit an initial rapid increase in K_{1c} with increasing molecular weight. K_{1c} however, levels off as the molecular weight increases beyond 10,000. This leveling off is believed to be caused by the formation of entanglements along the chain segments lying between crosslink junctions. These entanglements act as psuedo crosslink points thereby limiting the network's freedom of expansion.

6.3.4.4.2 Endgroup

The fracture toughness versus molecular weight of the networks prepared from PEKE oligomers capped with amine, maleimide or nadimide groups are shown in Figure 82 and summarized in Table 17. The networks from all three crosslinking mechanisms exhibit an initial rapid increase in toughness as molecular weight increases. This is again followed by a leveling off of the toughness as molecular weight increases beyond Me. The unusually high K_{1c} values for the maleimide system at 8.6K molecular weight and for the nadimide system at 10K could be related to their lightly crosslinked structure since both networks exhibited an abrupt second stage of swelling. However this was not proven.

Over the range of molecular weights, maleimide terminated PEKE oligomers produce the toughest networks. This could be caused by some type of chain extension reaction which does not take place in the other other crosslinking mechanisms. This would therefore give the maleimide network a larger Mc and thereby more freedom of expansion. A larger Mc, however, is not indicated by swelling results. Another explanation could be the different functionalities of the associated crosslink points. The amine endgroups after reacting with a carbonyl group along the PEKE backbone, produces imine crosslinks which possess a functionality of 3. The maleimide endgroups react with one another forming ladder-like crosslink junctions of various functionalities. The nadimide endgroups are believed to de-

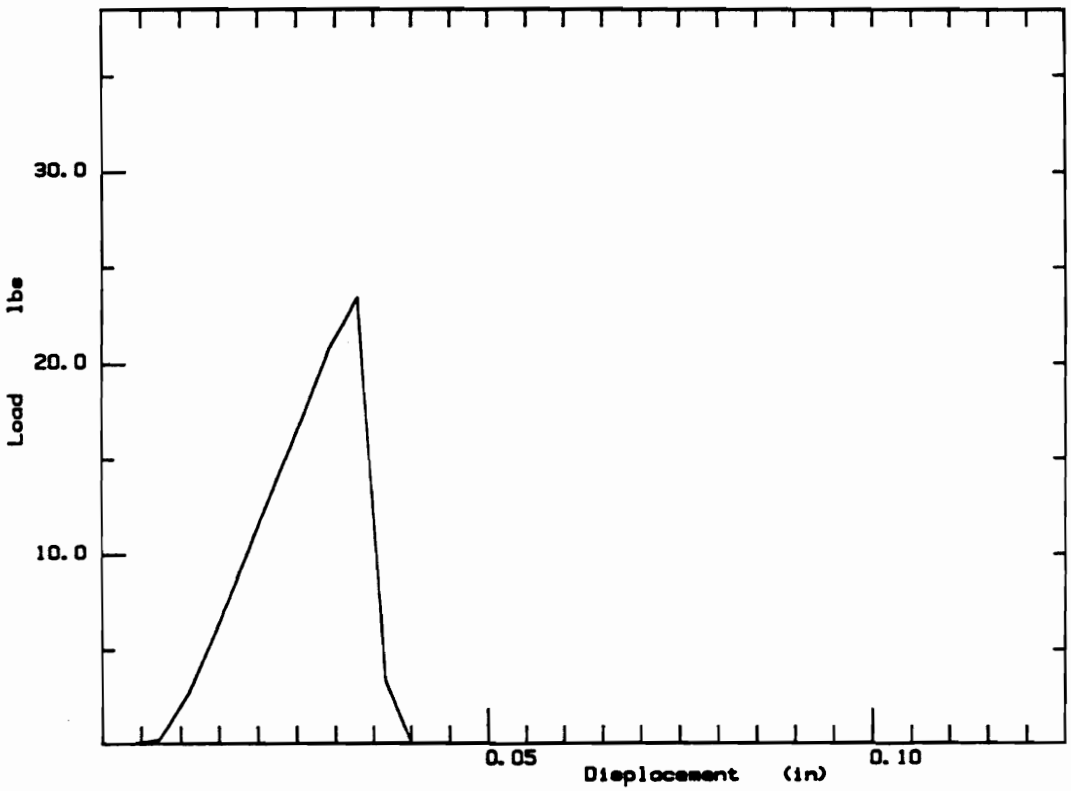

Figure 78. **Load displacement curve for a 3 point bend toughness test:** of a cured 5K PEKE oligomer exhibiting semi-brittle behavior

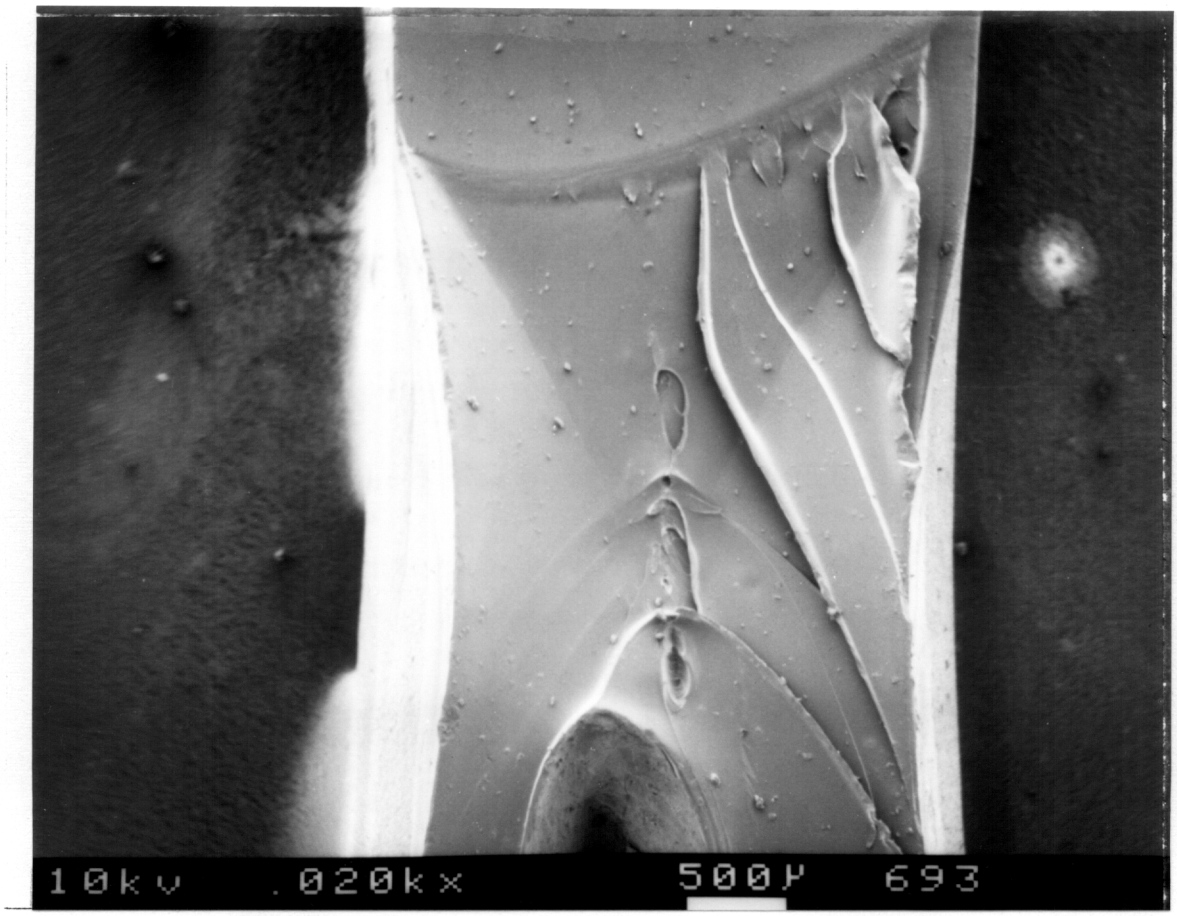

Figure 79. Scanning electron micrograph of a fracture surface of a linear high molecular weight PEKE thermoplastic: at 20X exhibiting shear lips and other large scale deformation

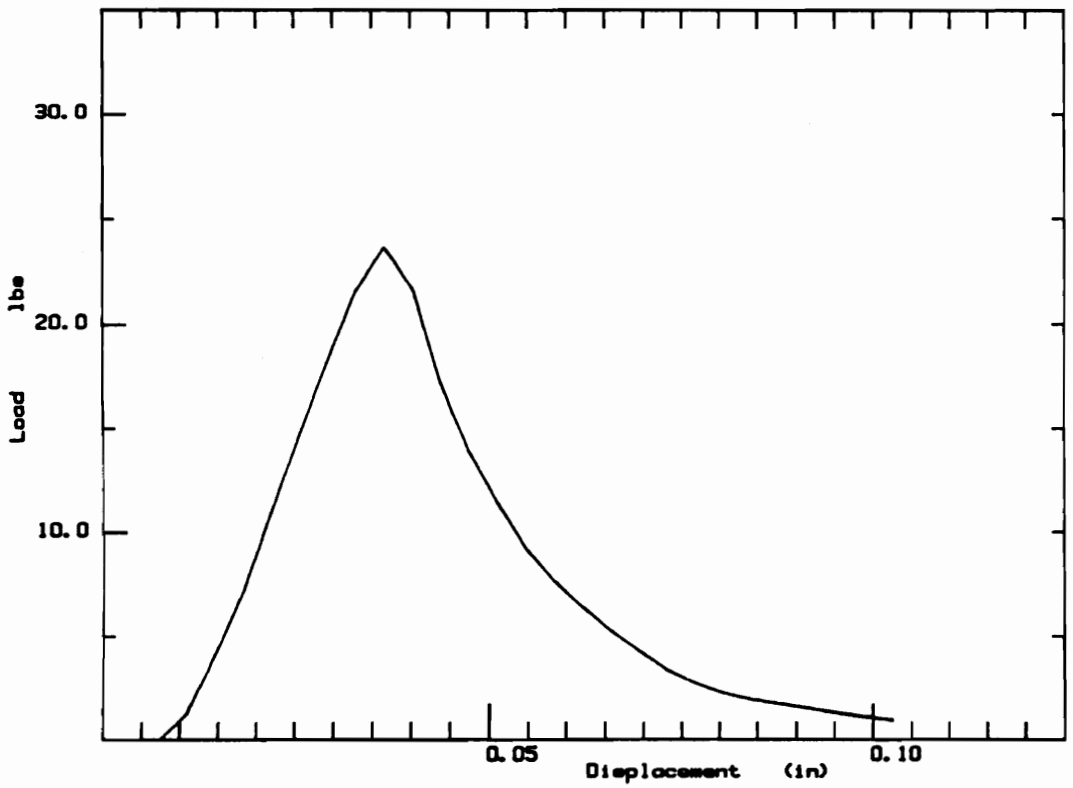

Figure 80. Load displacement curve for a 3 point bend toughness test of a cured 5K PEKE oligomer exhibiting ductile behavior.

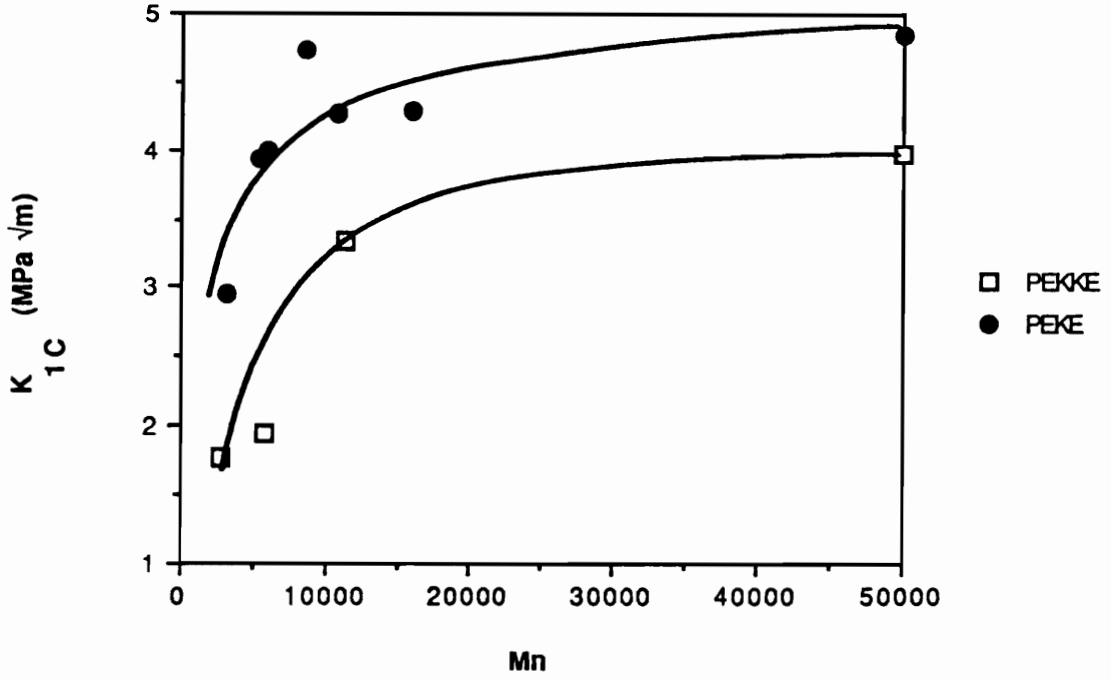

Figure 81. Comparison of fracture toughness versus molecular weight: for cured maleimide terminated PEKE and PEKKE oligomers

Table 16. Summary of the fracture toughness results for cured maleimide terminated PEKE and PEKKE oligomers of varying molecular weight

Backbone	Titrated <Mn> (g/mole)	K_{1c} (MPa $m^{1/2}$)	G_{1c} (KJ/m^2)
PEKE	3100	2.95±0.28	4.83±1.60
	5400	3.93±0.19	8.91±1.26
	5900	3.99±0.54	9.32±1.66
	8600	4.72±0.62	-
	10700	4.27±0.40	12.64±1.98
	16000	4.28±0.23	13.01±1.57
	Thermoplastic Control	4.84±0.54	-
PEKKE	2700	1.77±0.26	-
	5800	1.94±0.21	-
	11300	3.34±0.10	-
	Thermoplastic Control	3.98±0.51	-

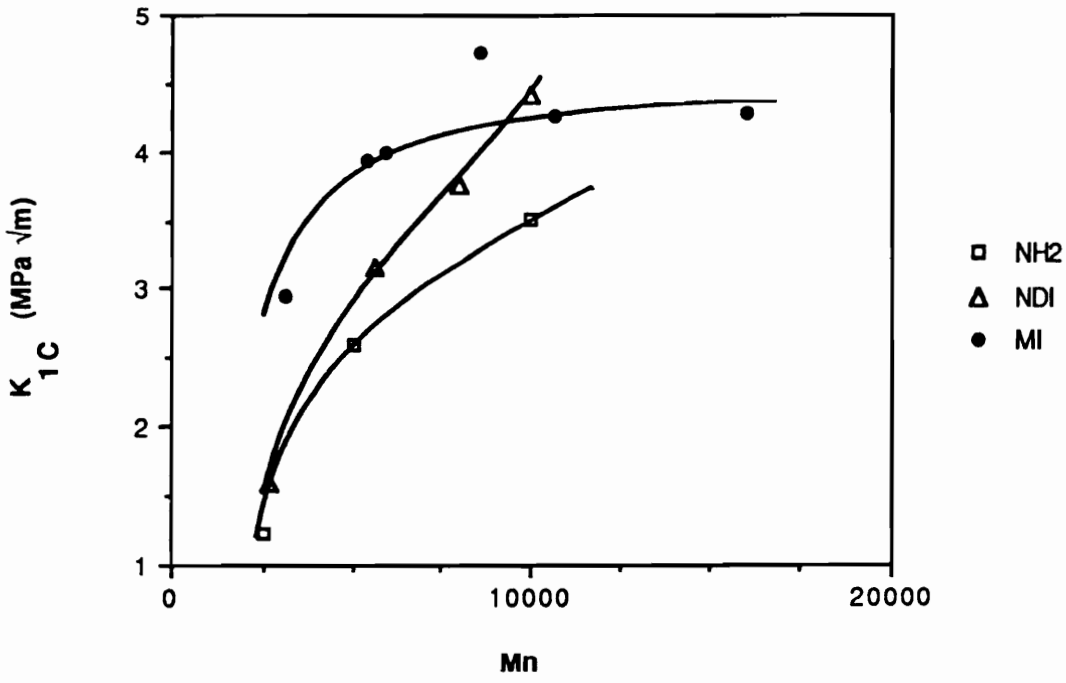

Figure 82. Comparison of fracture toughness versus molecular weight: for cured amine, maleimide and nadimide terminated PEKE oligomers

Table 17. **Summary of the fracture toughness results for cured amine, maleimide and nadimide terminated PEKE oligomers**

Endgroup	Titrated <Mn> (g/mole)	K_{1c} (MPa $m^{1/2}$)	K_{1c} (ksi $in^{1/2}$)
amine	2,500	1.23±0.36	1120±325
	6,600	2.61±0.21	2370±190
	11,800	3.52±0.35	3200±320
maleimide	3,100	2.95±0.28	2680±255
	5,400	3.93±0.19	3570±175
	5,900	3.99±0.54	3630±490
	8,600	4.72±0.62	4270±565
	10,700	4.27±0.40	3880±365
	16,000	4.28±0.23	3890±210
nadimide	2,700	1.59±0.16	1450±145
	5,600	3.17±0.25	2880±225
	8,000	3.77±0.23	3430±210
	10,000	4.42±0.37	4020±335

compose to a maleimide endgroup and cyclopentadiene before they can react. The maleimide endgroups and the cyclopentadiene can all react with one another producing various crosslinking junctions of various functionalities. Unfortunately, it is difficult at the present to characterize the functionalities of these crosslink points without working with a more well defined network. Therefore, it is only possible at this time to speculate as to the reason why the various endgroups produce different fracture toughness.

6.3.4.4.3 Annealing

Figure 83 illustrates the effect of annealing on fracture toughness of a crosslinked 5.9K maleimide terminated PEKE oligomer. The cured networks were quenched from approximately 120 °C above its Tg (150 to 160 °C) and then annealed at 145 °C for 0, 5, 24, and 60 hours.

The annealing effect on K_{1c} can be broken down into 3 regions. The first region shows a rapid decrease in K_{1c}, from 4 to 3.4 MPa $m^{1/2}$, within the first 5 hours of annealing. This is followed by a region of relatively constant K_{1c}, from 5 to 24 hours. Finally K_{1c} exhibits a modest decrease from 24 to 60 hours.

The decrease in fracture toughness with annealing is mirrored by the increase in the size of the physical aging peak which accompanies the glass transition in a DSC scan (Figure 84). The data presented in Figure 84 is for a thin film cured and annealed under the same conditions as for the fracture toughness specimens. The DSC scans on the annealed fracture toughness specimens also exhibits the three regions of annealing. This data was not presented however since only four annealing times were examined.

The cause of the step decreases in toughness and the step increases in physical aging maybe identical to the cause of the step increases in percent swelling over time. The polymer undergoes an initial relaxation as it recoils back to a less extended configuration. The amount of recoiling is limited, however, due to the presence of entanglements. Over an extended period of time, these entanglements break up, allowing the polymer to further relax.

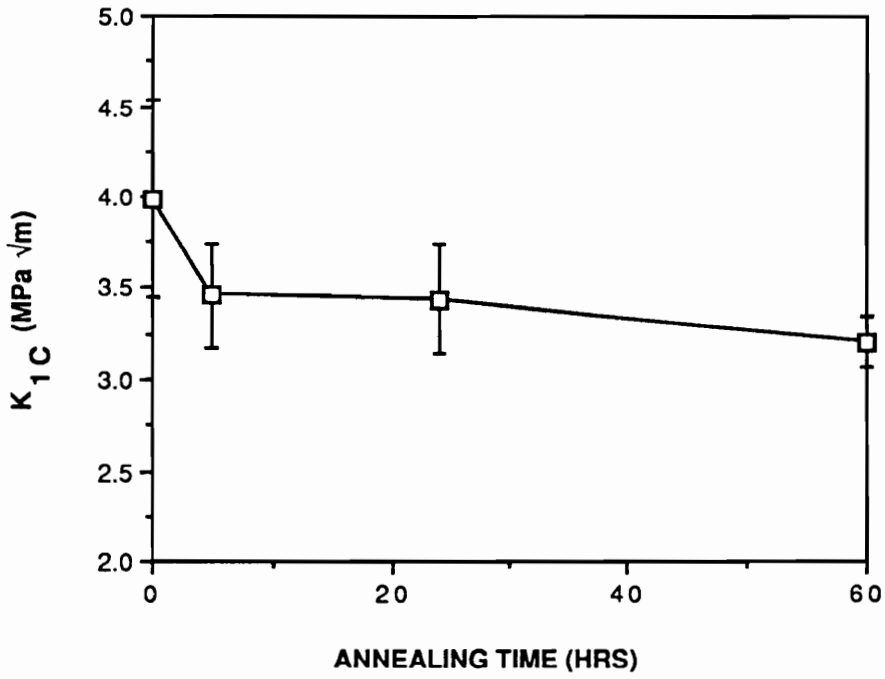

Figure 83. Effect of annealing time at 145 °C on the fracture toughness: of a cured 5K PEKE oligomer quenched from 120 °C above its Tg

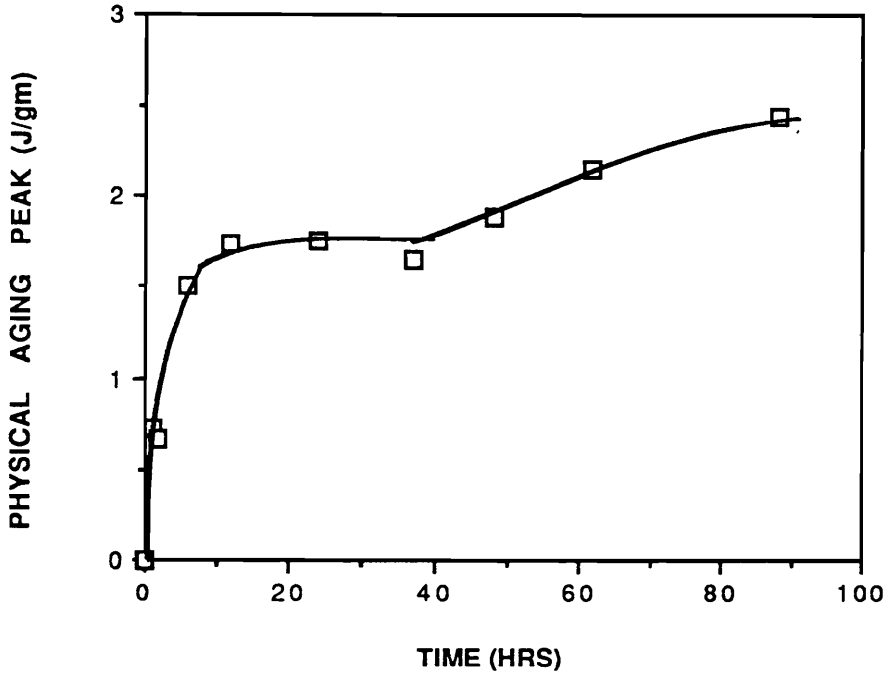

Figure 84. Magnitude of the physical aging peak from DSC measurement versus annealing time: at 145 °C for a cured maleimide terminated 5K PEKE oligomer

Table 18. Summary of the effect of annealing on fracture toughness and the magnitude of physical aging of PEKEs

System	Annealing Time (hrs)	K_{1c} (MPa $m^{1/2}$)	Physical Aging Peak (J/gm)
5.9K PEKE-MI network	0	3.99±0.40	0
	84	3.57±0.27	0.48
20K PEKE-OH Thermoplastic	0	5.11±0.47	0
	86	5.50±0.62	0.32

This experiment was repeated in order to obtain specimens for dynamic mechanical analysis. Due to lack of polymer only two blocks of material was prepared. The first was quenched from 120 °C above its Tg, as was done previously. The second was quenched and then annealed at 145 °C for 86 hours. The resulting fracture toughness as well as the area of the physical aging peak are presented in Table 18. The decrease in toughness is less than half that found for the previous specimen annealed for 60 hours. Likewise the size of the physical aging peak is significantly reduced.

The effect of annealing on fracture toughness was also conducted for a 20K hydroxyl terminated PEKE thermoplastic, (Table 18). After 84 hours of annealing at 145 °C (glass transition temperature approximately 155 °C), fracture toughness does not decrease but rather shows a slight increase. The DSC scan reveals a relatively small aging peak (0.32 J/gm) when compared to the cured 5.9K PEKE oligomer (2.4 J/gm).

6.3.4.4.4 Length of Cure

The effect of length of cure on the fracture toughness of a network cured from a maleimide terminated 5K PEKE oligomer is shown in Figure 85. Each network shown was initially subjected to degassing stage under vacuum at 170 °C for 10 minutes followed by a molding stage at 250 °C for 30 minutes. The time displayed in Figure 85 is the amount of time the network was allowed to cure at 270 °C after the initial two stages. K_{1c} is seen to be independent of cure time, implying that fracture toughness is independent of gel content and crosslink density. As was previously discussed on the characterization of these networks by extraction and swelling experiments, it is apparent that the degassing and molding stages of network preparation, induced a significant level of curing of the oligomers. Therefore even the oligomer cured for only 5 minutes possessed substantial chain extension, branching and crosslinking. It is conceivable then, since the overall topology of the networks would be similar, that their fracture toughness behavior would also be similar.

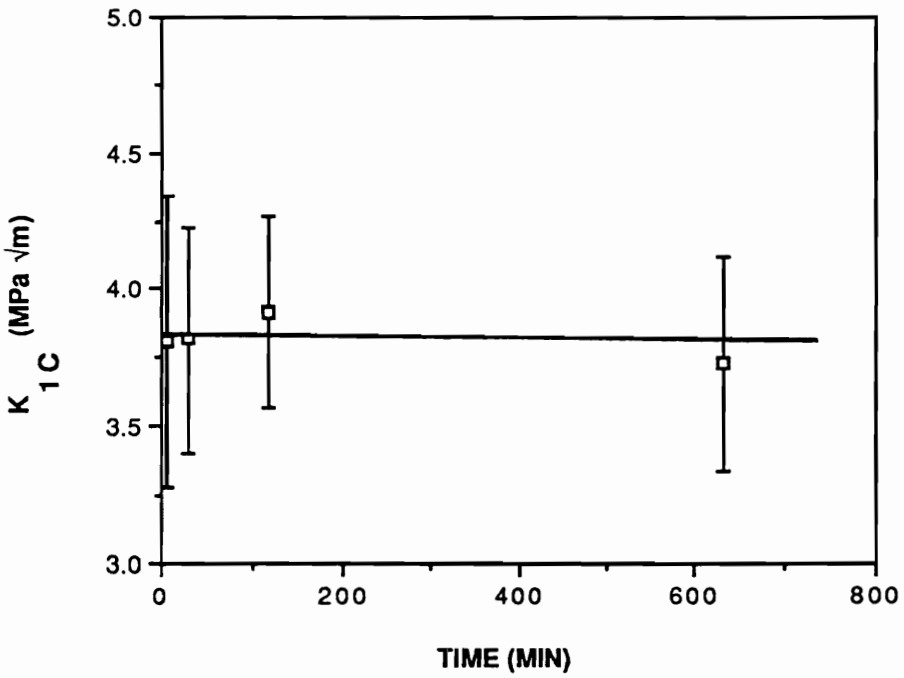

Figure 85. Fracture toughnes versus cure time at 270 °C: for a 5K maleimide terminated PEKE oligomer

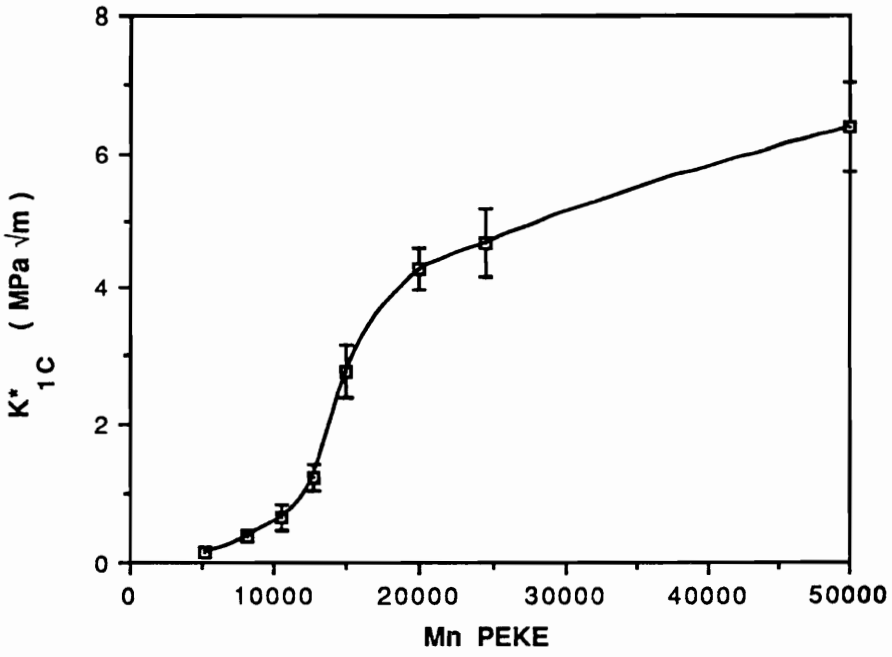

Figure 86. **Fracture toughness versus number average molecular weight:** for t-butylphenyl terminated PEKE oligomers

6.3.4.5 Fracture Toughness Results for PEKE Thermoplastics

6.3.4.5.1 Oligomers

Figure 86 illustrates the dependence of fracture toughness on number average molecular weight for t-butylphenyl terminated PEKE oligomers. Initially, for Mn less than 10,000, toughness increases slowly with respect to molecular weight but then rises dramatically for Mn's greater than 10,000 but less than 20,000. Above 20,000, the rate of increase in fracture toughness decreases to a level approximately equal to its initial rate.

The initial increase in toughness is due primarily to an increase in the ratio of intermolecular bonds to chains. As this ratio increases, the chains all more thoroughly linked together. However only a modest increase in toughness can be obtained due to the relative weakness of the intermolecular forces.

As molecular weight increases above 10,000, the polymeric chains begin to entangle. Entanglements link the chains more strongly together than intermolecular bonds thereby dramatically increasing the polymer's strength and toughness. The rate of increase in toughness however begins to decrease again as all the chains become linked through entanglements, Mn approximately equal to 20,000.

Above this second transitional molecular weight value, tensile strength [88] and fracture toughness [84] have been reported to level off to a constant value. However, for this system, toughness continues to increase, though slowly, with Mn.

Two items should be noted about these tests. First, the molecular weight value of 50,000 was assigned to the linear high molecular weight PEKE thermoplastic so it could be used as a reference. This polymer did not possess t-butylphenyl endgroups so that its Mn could not be determined by NMR. A number averaged molecular weight of over 100,000 was obtained for this polymer using GPC equipped with a differential viscosity detector.

Second, as mentioned previously, precracks were not introduced through tapping a razor blade into the specimens as was done for the PEKE thermosets. The low molecular oligomers proved to be far too brittle for this procedure. Instead, precracks were introduced

by sawing a thin notch, approximately 0.4 mm wide, into the specimens. Since these pre-cracks were far more blunt than those introduced by a razor blade, their associated fracture toughness values are artificially greater.

6.3.4.5.2 Comparison to Melt Viscosity

A comparison of the fracture toughness results for the PEKE oligomers to their associated dynamic melt viscosities at 230 °C and 1 Hz is shown in Figure 87. The parallel behavior of the two curves for molecular weights below 20,000 is striking. This suggests that the molecular scale mechanism which resists melt shear flow is identical to the mechanism which resists crack propagation.

The comparison of fracture toughness to melt viscosity was extended to four blends prepared from the t-butylphenyl terminated PEKE oligomers, (Figure 88). The make up and characterization of these blends is presented in Table 12. The four blends are found to follow the identical relationship between toughness and viscosity as was found for the pure oligomers.

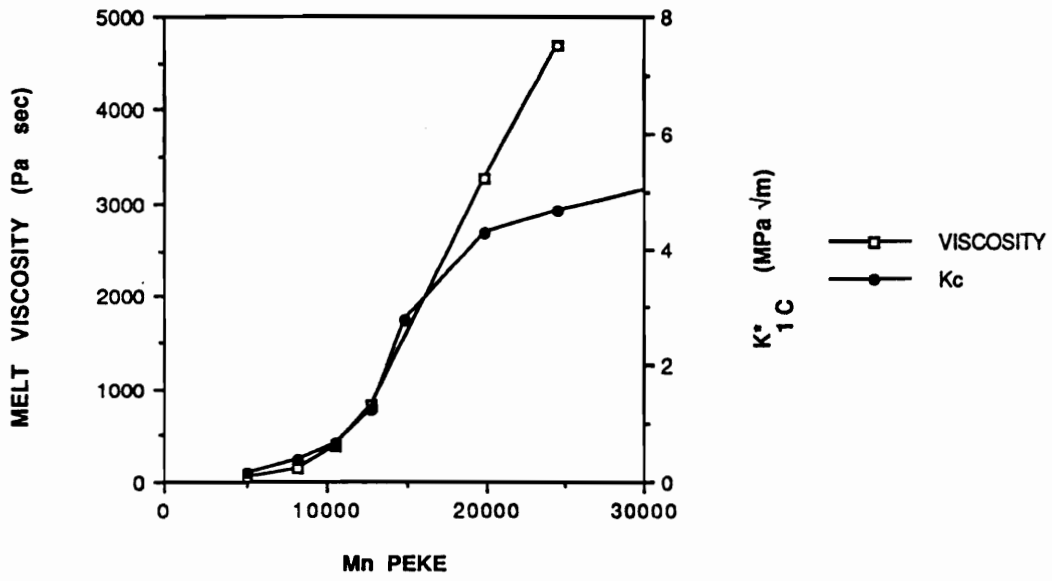

Figure 87. Comparison of fracture toughness and dynamic melt viscosity: at 230 °C and 1 Hz for the various molecular weight t-butylphenyl terminated PEKE oligomers

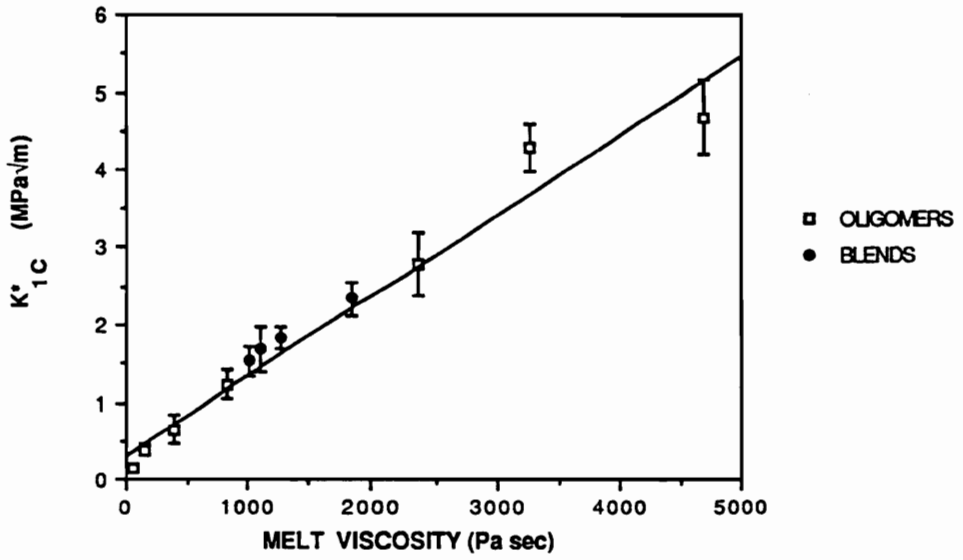

Figure 88. **Fracture toughness versus melt viscosity for various molecular weight PEKE oligomers and their blends.**

Chapter 7 Bismaleimide Networks

Bismaleimide resins are useful electronic and aerospace materials due to their high glass transition temperatures and ease of processing. Their applicability, however, is often limited due to their brittle nature. Polyetherketones are useful structural materials due to their excellent thermal stability and toughness but, they possess low glass transition temperatures. Thus, if these two materials could be cocured, it might be possible to combine the high glass transition of bismaleimides with the toughness of polyetherketones. These two material were cocured by utilizing maleimide terminated PEKE oligomers, whose synthetic preparation was described earlier in Chapter 5.

In this study, two different series of polyetherketone modified bismaleimide networks were prepared. In the first series, the molecular weight of the PEKE was held constant while its weight pecent incorporated into the network was varied. In the second series, the weight ratio between the polyetherketone and the bismaleimide was held constant (1:1), while the molecular weight of the PEKE was varied.

7.1 Blending

Bismaleimide and polyetherketone oligomers were blended, before curing, by the co-precipitation method described previously (section 5.3.1.1). A second procedure, involving the blending of the materials in solution and then evaporating the solvent (section 5.3.1.2), was also performed to test the effectiveness of the first blending procedure. The test of blending effectiveness was performed to determine whether adequate mixing had occurred between the bismaleimide and polyetherketone. Inadequate mixing would produce abnormally high amounts of phase separation, which could possibly alter the network's mechanical properties.

Figure 89 compares the dynamic mechanical behaviors of 50/50 by weight cocured networks of a 5K maleimide terminated polyetherketone oligomer with bismaleimide blended by two different procedures. The behavior of both procedures is almost identical. The fracture toughness results of the two systems are identical, $K_{1_c} = 0.91$ MPa $\sqrt{m}$. It was concluded, therefore, that the coprecipitation blending procedure, produced an adequate degree of mixing.

7.2 Maleimide Terminated Polyetherketones

7.2.1 Swelling

Figure 90 displays the swelling behavior of a 5K polyetherketone modified bismaleimide network versus time. The network swells quickly in the first two days, after which however, the percent of swelling remains constant for an indefinite amount of time. This behavior is typical for all polyetherketone modified bismaleimide networks that were tested. The networks do not exhibit any delayed swelling as was seen with the polyetherketone networks.

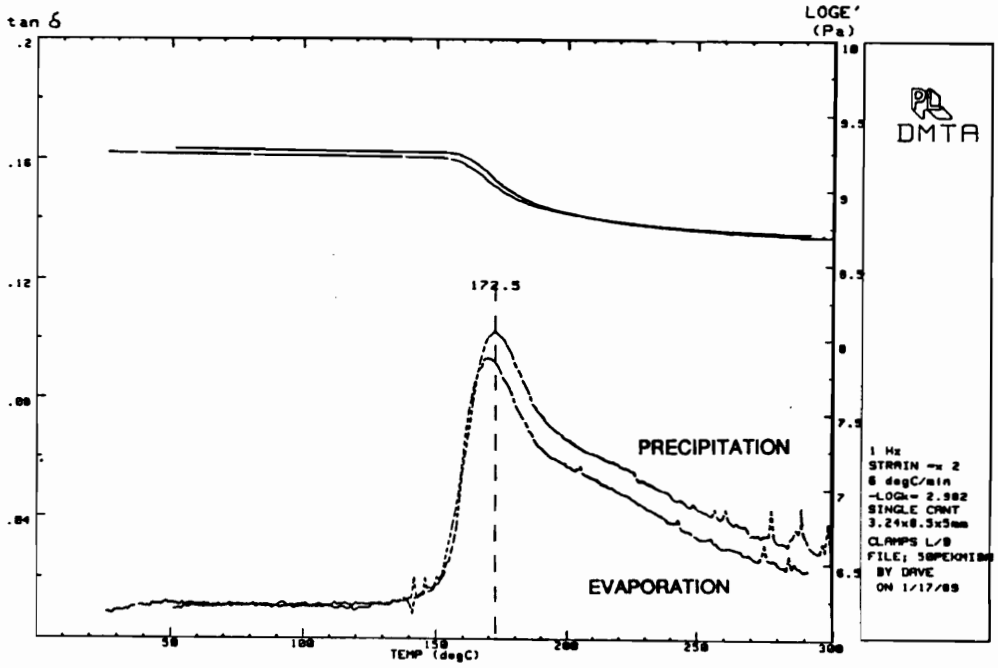

Figure 89. Comparison of blending procedures on the dynamic mechanical behavior: for a 5.4K PEKE modified BMI network of 50/50 by weight composition

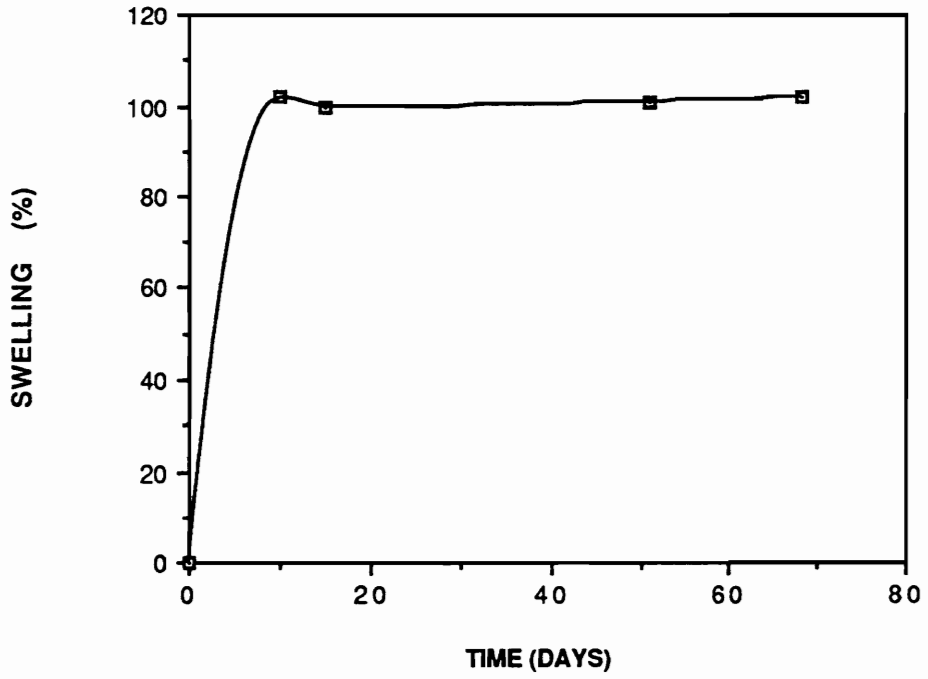

Figure 90. Percent swelling versus time for a 5.4K 25/75 by weight BMI/PEKE

Figure 91 exhibits the swelling results after 10 days for the molecular weight series of PEKE modified bismaleimide. Below 6000 molecular weight, the networks swell less than 10 percent. Above a molecular weight of 6000, swelling increases proportionally to the molecular weight.

The weight ratio series of bismaleimide networks demonstrates similar swelling behavior (Figure 92). Below 50 weight percent PEKE, the networks exhibit almost no swelling. Above 50 percent, swelling increases rapidly to greater than 350 percent for the 100 percent PEKE network. Networks for both series exhibit 100 percent gel content.

Both series exhibit significantly less swelling than would be predicted by multiplying the swelling percent seen in each component separately, by their respective weight percent and then adding the two adjusted swelling components together.

$$S(BMI/PEKE) = x^{*}S(BMI) + y^{*}S(PEKE) \qquad [7.1]$$

where:

S(BMI/PEKE) = percent swelling for the PEKE modified BMI network

S(BMI) = percent swelling for the BMI network which is negligible

S(PEKE) = percent swelling for the PEKE network

x = weight fraction of BMI

y = weight fraction of PEKE

The 5.4K PEKE network, for example, swells to 360 percent in 10 days. The BMI network modified with 50 weight percent 5.4K PEKE would be predicted to swell to approximately 180 percent. However, the actual network swelled to less than 5 percent.

The decrease in swelling is probably caused by the increased concentration of maleimide endgroups due to the large mole ratio of bismaleimide molecules. This high concentration of maleimide endgroups reacts with dangling ends of the PEKE network and, con-

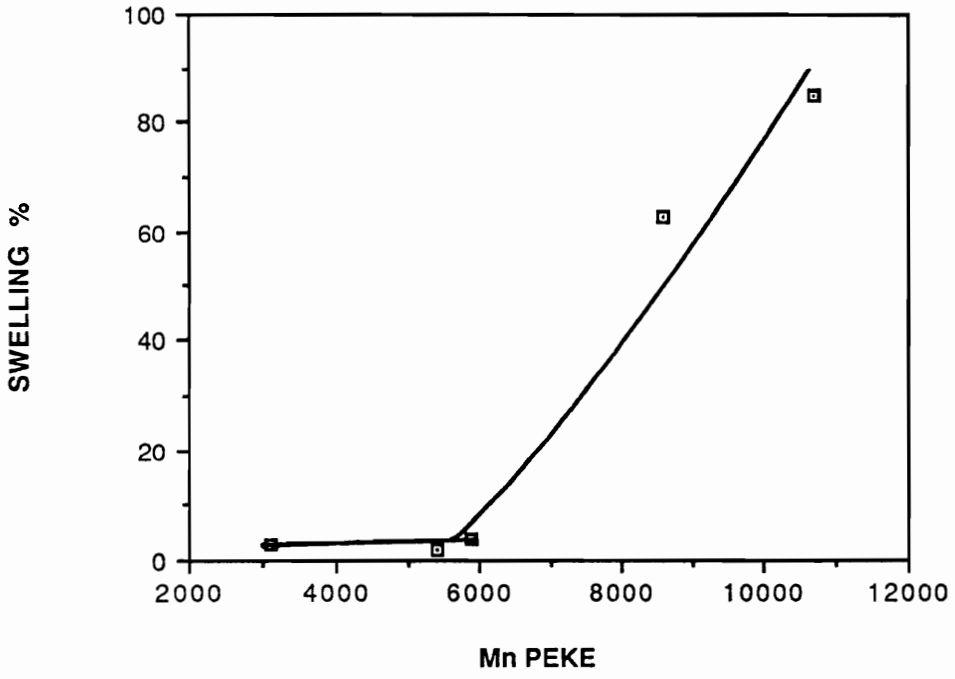

Figure 91. Percent swelling after 10 days versus number average molecular weight for 50/50 by weight BMI/PEKE network

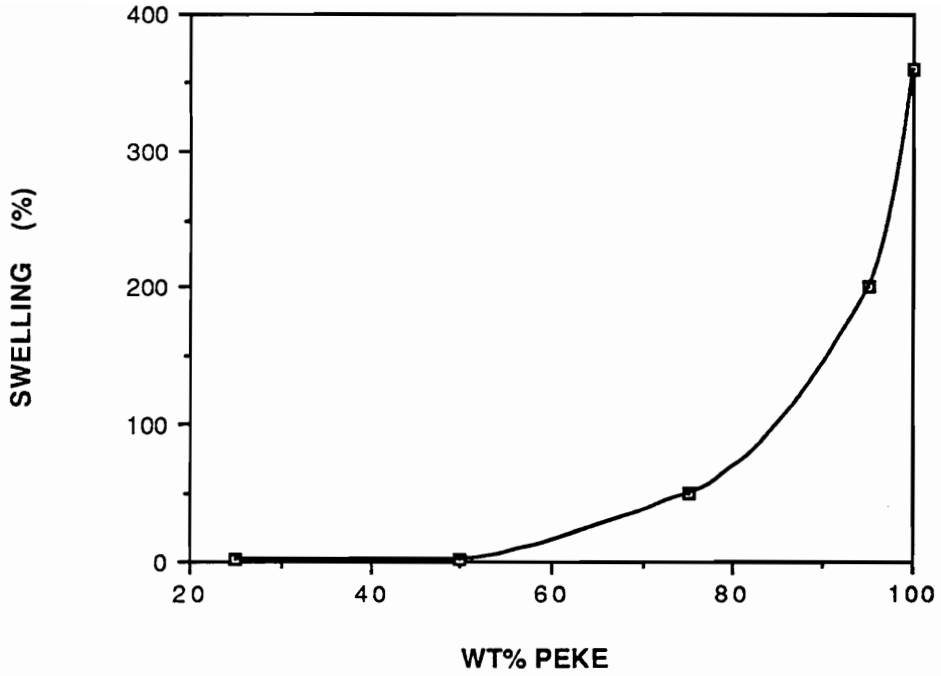

Figure 92. Percent swelling versus weight percent PEKE incorporated for BMI/5.4K PEKE networks

sequently, incorporates them into the matrix. This would greatly tightens up the crosslinking of the network, significantly reducing it ability to expand and swell.

7.2.2 Toughness

The fracture toughness results for the polyetherketone modified bismaleimide networks using either various molecular weight ratios of the polyetherketone to bismaleimide, are illustrated in Figures 93 and 94, respectively. The plot for the series networks of various molecular weights, shows a linear relationship between fracture toughness and molecular weight. For the 3.1K oligomer, the network possesses a critical stress intensity 5 times greater than unmodified bismaleimide (K_{1_c} = 0.5 MPa $m^{1/2}$). For the 10.7K oligomer toughness is increased to a value close to that for polysulfone (K_{1_c} = 1.7 MPa $m^{1/2}$).

The fracture toughness for the weight ratio series increases parallel to the network's swelling behavior. Below 50 weight percent PEKE, K_{1_c} increases slowly, with values less than 1.0 MPa $m^{1/2}$. Above 50 percent, toughness increases more rapidly to greater than 2.0 MPa $m^{1/2}$.

7.2.3 Dynamic Mechanical Behavior

A comparison of the dynamic mechanical behavior for the weight ratio series is presented in Figure 95. All the networks exhibit approximately equal glassy storage moduli and glass transition temperatures. The rubbery modulus, however, shows a strong dependence on composition, decreasing by two orders of magnitude as the loading level of polyetherketone is increased to 100 percent. This drop in modulus can be attributed to the increased contribution of a rubbery thermoplastic material, polyetherketone, and a decrease in the contribution of high modulus glassy material, bismaleimide.

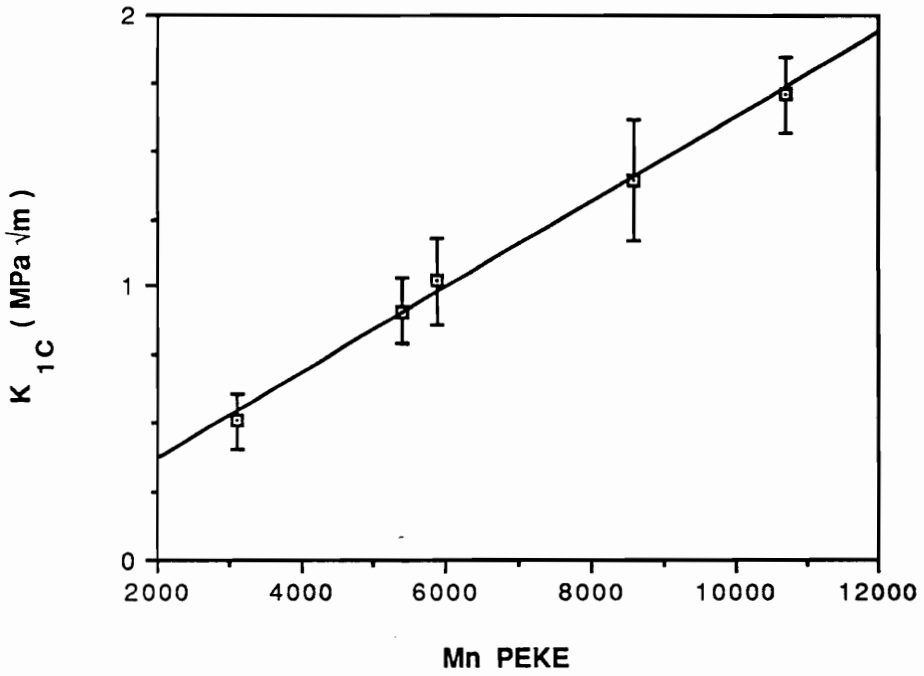

Figure 93. Critical stress intensity versus Mn for a 50/50 by weight BMI/PEKE network

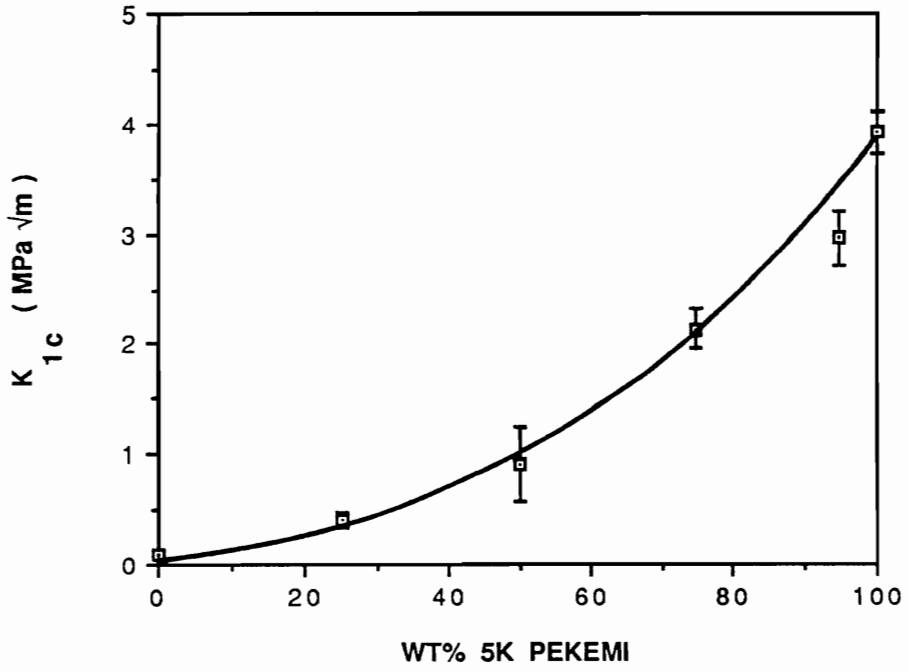

Figure 94. Critical stress intensity versus weight percent PEKE for a BMI/5.4K PEKKE network

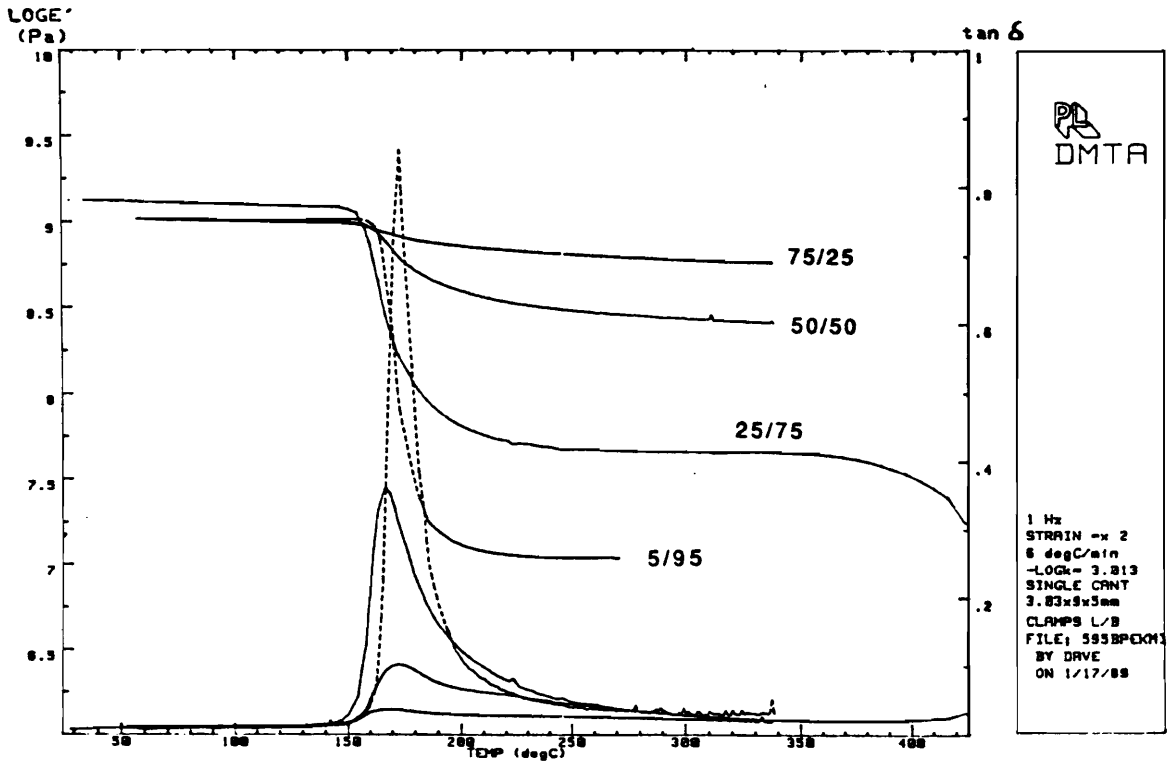

Figure 95. Comparison of the dynamic mechanical behavior of varying weight percent of a 5.4K maleimide terminated PEKE oligomer

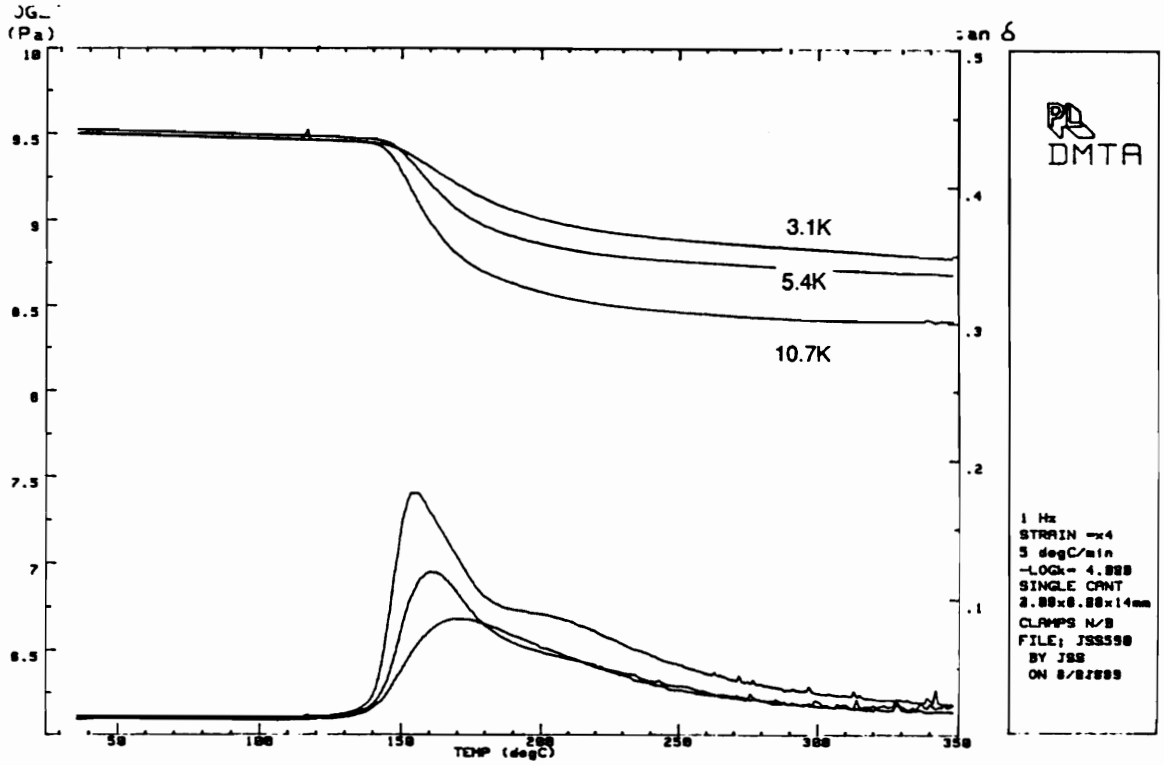

Figure 96. **Dynamic mechanical behavior of BMI networks cocured, 50/50 by weight, with maleimide terminated PEKE oligomers:** of varying number average molecular weight

Similar behavior is found for the bismaleimide networks modified with various molecular weight polyetherketones (Figure 96). The rubbery modulus is seen to decrease as molecular weight is increased from 3.1K to 10.7K. The decrease is not as significant as found when varying the weight percent of polyetherketone incorporated, but it is larger than the decrease found for the simple polyetherketone networks as molecular weight increased. The decrease cannot be attributed to the weight fraction of PEKE chains since the weight fraction remains constant. Also, the decrease cannot be attributed to the mole fraction of PEKE oligomers incorporated into the network, since the 3.1K network possesses the greatest mole fraction of PEKE oligomers as well as the highest rubbery modulus. If modulus was solely dependent on mole ratio, it would be expected that the network possessing the highest mole fraction of PEKE would possess the lowest rubbery modulus.

A summary of glassy transition temperatures obtained from DMTA as well as the swelling and the fracture toughness results are presented in Table 19.

7.2.4 Scanning Electron Micrographs

Scanning electron micrographs of the fractured surfaces for some selected modified bismaleimide networks are shown in Figures 97 through 99. The network containing 50 percent by weight 5.4K polyetherketone, appears homogeneous (Figure 97). No phase separation was observed on the fracture surface up to 8000X magnification.

Phase separation, however, was observed in the network containing 25 percent polyetherketone (Figure 98). The flat oval regions are believed to be phase separated regions of bismaleimide, since their fracture surfaces would be expected to appear much smoother than the ductile polyetherketone surface. The effect that this phase separation has on mechanical properties is unclear.

Phase separation is also seen in the network containing 50 percent of 10.7k polyetherketone (Figure 99). These phase separated regions are more elongated than those

Table 19. Summary of the physical and mechanical properties of PEKE modified BMI networks

Oligomer <Mn>	Incorporated Weight (%)	Gel (%)	Swell (%)	Tg(°C) DMTA	Tg(°C) DSC	K_{1c} (MPa $m^{1/2}$)	G_{1c} (KJ/m^2)
3,100	50	97	0	171	-	0.51±0.10	0.57
5,400	50	98	2	161	-	0.91±0.12	0.76
5,900	50	98	2	-	-	1.02±0.16	-
8,600	50	100	63	155	-	1.39±0.22	-
10,700	50	100	85	157	-	1.71±0.14	3.27
5,400	25	100	1	169	166	0.40±0.07	0.38
5,400	50	98	2	160	170	0.91±0.12	0.76
5,400	75	100	74	168	169	2.14±0.18	3.68
5,400	95	100	200	-	173	2.96±0.25	-
5,400	100	100	360	150	168	3.93±0.19	8.91

Figure 97. Scanning electron micrograph of BMI network cocured, 50/50 by weight, with a 5.4K maleimide terminated PEKE oligomer

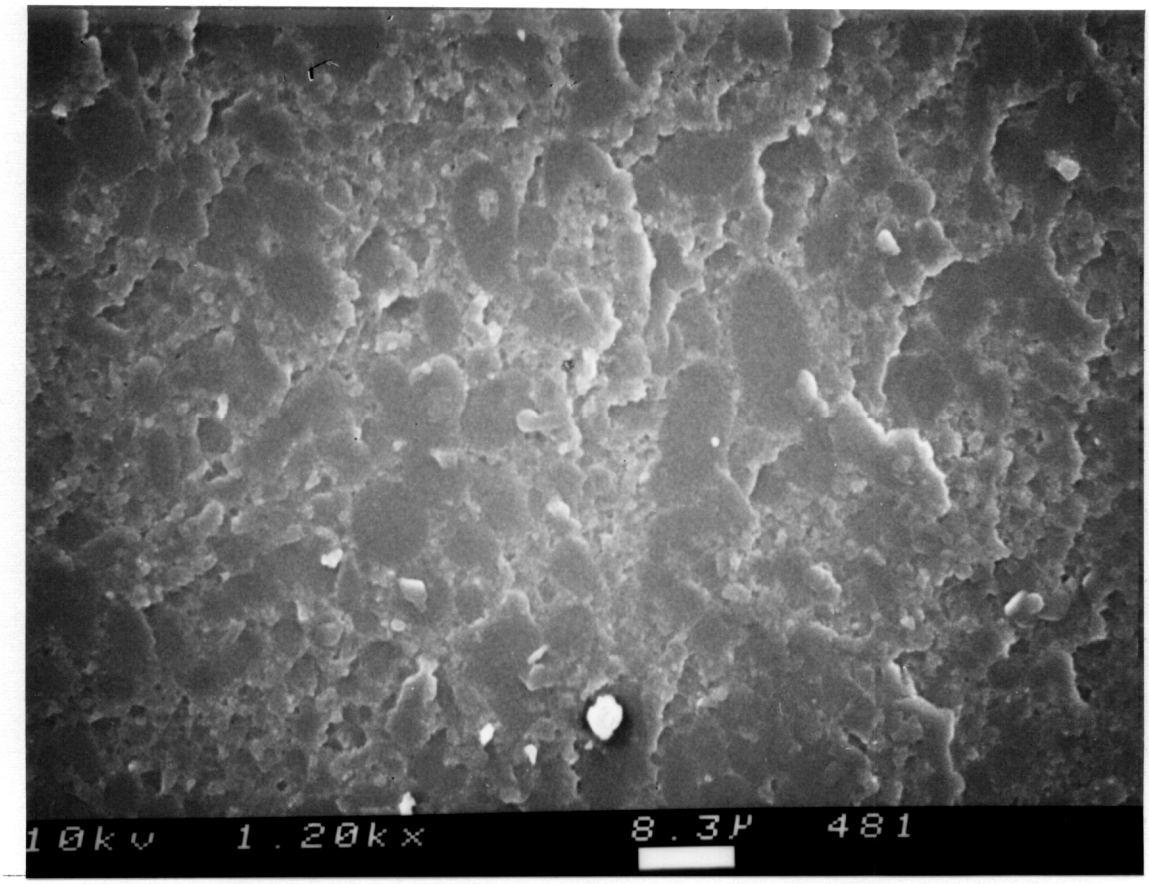

Figure 98. Scanning electron micrograph of a 75/25 by weight BMI/5.4K PEKE network

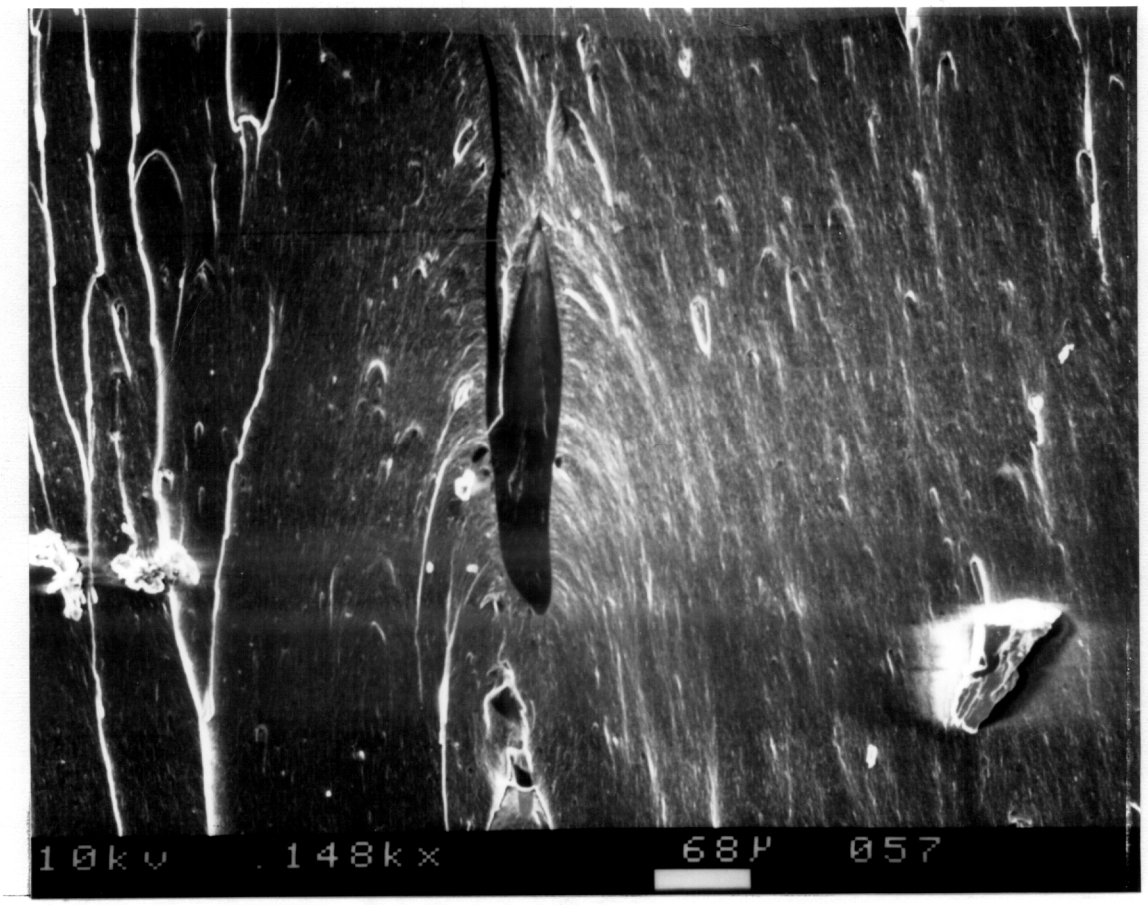

Figure 99. Scanning electron micrograph of 50/50 by weight BMI/10K maleimide terminated PEKE network

seen in Figure 98. This elongation is believed to be induced by the compression molding of the material before curing. These regions have a glassy surface, similar to Figure 98, which implies that they are rich in bismaleimide. Also, the matrix surrounding these regions possess shear lines, which indicates ductile behavior that could only be generated in polyetherketone rich regions.

7.3 t-Butylphenyl Terminated Polyetherketone

Modifying the bismaleimide with a 5.1K t-butylphenyl terminated PEKE oligomer produces a network possessing an unusual morphology. The t-butylphenyl terminated oligomer differs from the maleimide terminated oligomer in that it cannot be cocured with the bismaleimide. The PEKE oligomer therefore is physically blended into the network. Figure 100 shows an optical micrograph of a fracture surface at 25X magnification. The material is an opaque yellowish solid with brownish lines running through it. After extraction with chloroform the network becomes white. The physical and mechanical behavior of this network is shown in Table 20 and Figure 101 respectively.

The non-reactive incorporation of the t-butylphenyl terminated PEKE is exhibited by weight percent gel after extraction (Table 20). All of the non-reactive PEKE oligomer is removed during extraction, leaving only the crosslinked bismaleimide gel fraction. This is in contrast with the maleimide terminated PEKE which is essentially 100 percent gelled. The percent swelling also exhibits a difference in reactivity between the t-butylphenyl and the maleimide terminated modifiers. The chain flexibility of the maleimide terminated PEKE oligomers is restricted by the rigid bismaleimide matrix which surrounds it. This prevents the chains from uncoiling and, therefore, allows only minimum of solvent uptake. For the case of the t-butylphenyl terminated PEKE network, the removal of the PEKE oligomer during extraction, most likely creates voids in the network where solvent molecules can rest during

Figure 100. Optical micrograph of a 50/50 by weight BMI/5.1K t-butylphenyl terminated PEKE network

swelling, producing a swell of 150 percent. The presence of voids is also suggested by the observation that no sample expansion occurred during swelling.

The t-butylphenyl PEKE modified network possesses a K_{1_c} equal to that of a pure bismaleimide network. This value is an order of magnitude less than the K_{1_c} for the maleimide PEKE modified network. This suggests that the non-reactive PEKE oligomers contribute little if anything to the overall toughness of the network.

A comparison of the dynamic mechanical behavior of the two networks is shown in Figure 101. Three points of interest are observed. First, the t-butylphenyl PEKE modified network possesses a transition at 100 °C which is not seen in the maleimide PEKE/BMI network. This transition is probably caused by the relaxation of a low molecular weight or cyclic tail of the polyetherketone. Figure 102 shows the presence of the tail in the GPC of the polyetherketone. The t-butylphenyl terminated PEKE modified network exhibits a Tg 20 °C less than that of the maleimide terminated PEKE modified network as well as a significantly larger tan δ peak and a greater decrease in the storage modulus. These differences are caused by the increase in restrictions to chain motion, which are associated with the cocuring of the PEKE chains into the bismaleimide matrix.

The last point is the increase in rubbery modulus and tan δ above 300 °C. These increases most likely indicate some type of crosslinking taking place. Since this crosslinking is not seen to this extent in any of the maleimide terminated PEKE modified networks, it is possible that the crosslinking is occurring through the t-butyl endgroups, possibly via an unknown free radical reaction.

Table 20. Comparison of the physical and mechanical properties of BMI networks modified with 5.1K t-butylphenyl or 5.4K maleimide terminated PEKE oligomer

Oligomer	<Mn>	Incorporated Weight (%)	Gel (%)	Swell (%)	Tg (°C) DMTA	K_{1c} (MPa $m^{1/2}$)
PEKE-tBP	5,100	50	50	150	142	0.09
PEKE-MI	5,400	50	98	2	161	0.91

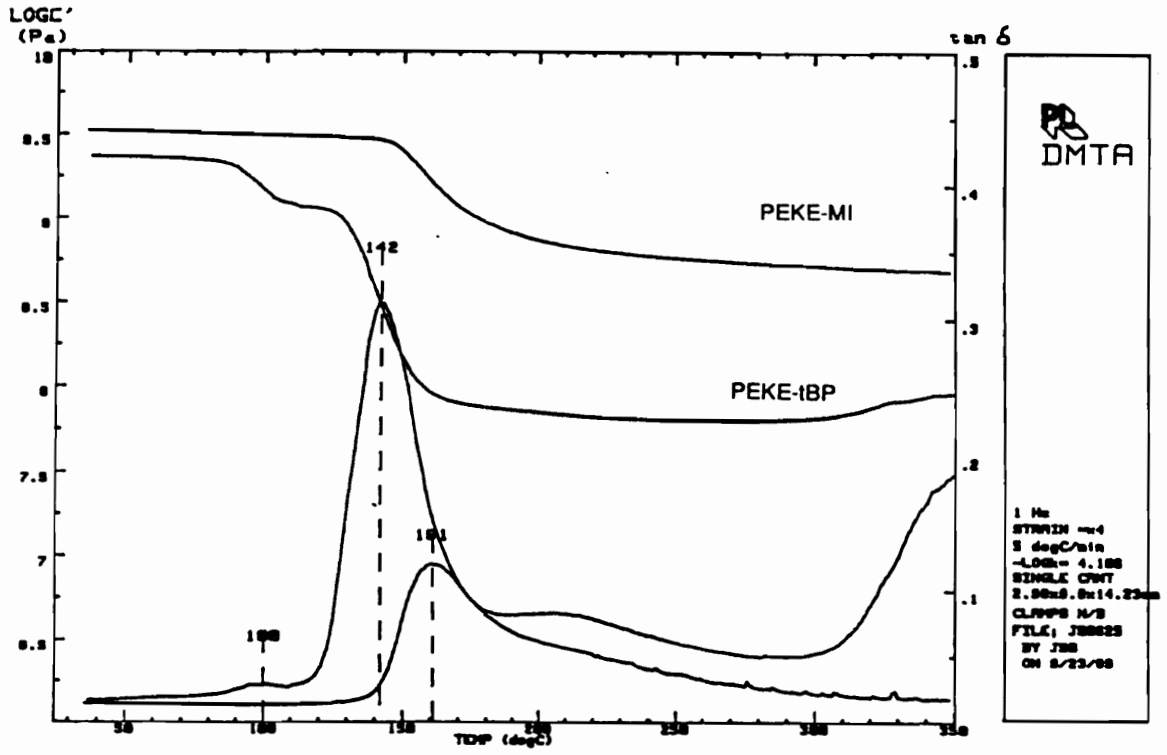

Figure 101. Comparison of the dynamic mechanical behavior of BMI networks modified with 5.1K t-butylphenyl or 5.4K maleimide terminated PEKE oligomer

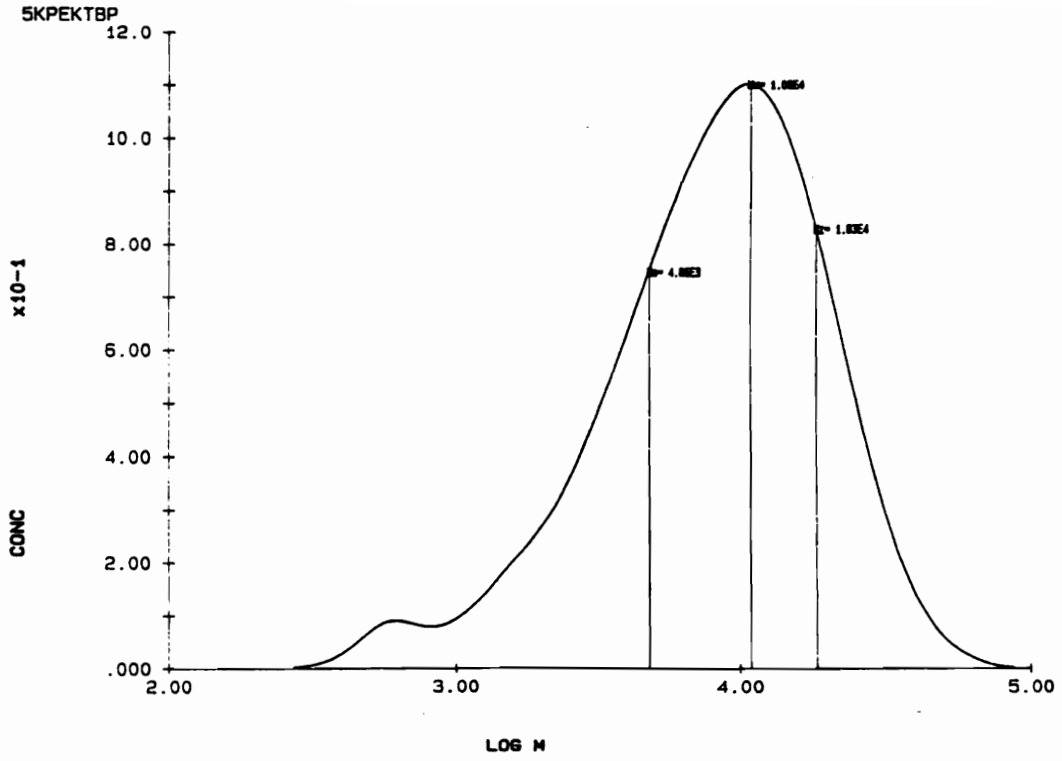

Figure 102. Gel permeation chromotography of a 5.1K t-butylphenyl terminated PEKE oligomer

Chapter 8 Analysis of Fracture Results

8.1 Introduction

This chapter will attempt to deduce the molecular scale toughening mechanism or mechanisms in poly(arylene ether)ketones so as to explain the trends in fracture toughness data. A systematic examination of the various possible mechanisms of toughening a polymer will be presented. The contribution of each mechanism to the overall toughening mechanism will be evaluated by comparing the expected results from the occurrence of that mechanism to the actual data obtained. For this, assumptions will often be made as to which matrix variables, such as the number of entanglements or the strength of the intermolecular bonds, are most effected by changes in factors such as annealing or length of cure. Since matrix variables are often interrelated with one another, the process of deducing the actual toughening mechanism will at times be questionable. It is for this reason that this chapter is presented more as a speculation than proven fact. Fracture data on the modified bismaleimide will not be included in this discussion due to the possible added effect of morphology.

As discussed earlier, a material's fracture toughness can be represented by either its critical stress intensity, K_{1_c} or its critical strain energy release rate, G_{1_c}. These terms are interrelated with one another and are both determined from the geometry of the specimen, the

geometry of the test fixture and the maximum load before failure. Assuming all geometry factors constant, it is the maximum load a material can support before failure which determines the final toughness value. Therefore, when trying to deduce molecular scale motions or interactions which would toughen a polymer, it is necessary to examine those motions or interactions which would effect the maximum load a toughness specimen can support. These motions and interactions can be divided into two categories; those which strengthen the polymer matrix, and those which blunt the precrack tip.

The first portion of this chapter will therefore be divided into two sections. The first will examine whether the trends observed in the toughness behavior of the PAEK systems can be explained by the strengthening of the polymer matrix by the load carrying capacity of intermolecular and covalent bonds. The second section will examine the toughening of the matrix by blunting the crack tip via the three sequential stages of matrix extension; intermolecular bond stretching, chain uncoiling, and disentanglement.

In the second portion of this chapter, an examination of the transition from semi-brittle to ductile failure will be presented as well as the possible relationships between α and β relaxations and fracture toughness.

8.2 Toughness Through Strength

8.2.1 Strength of a Polymer Matrix

The theoretical strength of a polymer matrix is determined in part by the strength of its intramolecular and intermolecular bonds. These bonds act together, either in series or in parallel, to support an applied load. The stability of any of these bonds is maintained as long as the load it is carrying remains below a critical value. If the load exceeds this value, the bond ruptures.

The rupture of one bond forces the other bonds to accept a greater load. As more bonds rupture, the increase in load on the remaining bonds finally becomes too great and the matix fails. Strengthening the polymer matrix so that it could carry a greater load and therefore be tougher could be accomplished by increasing the strength and/or the number of intramolecular and intermolecular load carry bonds.

8.2.2 Chemical Modification

Increasing the strength and number of the load carrying bonds maybe attempted by two procedures. The first involves chemically altering the structure of the polymer to either replace or strengthen existing weak covalent and secondary bonds or to incorporate groups along the backbone which would produce stronger interactions between the chains. One example of this would be incorporating pendant carboxylic acid groups along the backbone to produce ionic bonding between the chains. With the systems used in this study however, the overall structure of the polymer remained constant. The only variation was between the PEKE and PEKKE backbones. Therefore this procedure of toughening a polymer did not apply to this study.

8.2.3 Efficiency Improvement

A matrix can also be strengthened by increasing the number of intra and intermolecular bond carrying a load. It is obvious that the more load carrying bonds which exist per unit area, the less load each bond will be forced to carry.

8.2.3.1 Intermolecular Bonds

The number of intermolecular bonds can be increased by either greater ordering or tighter packing of the chains. Chain ordering will not be considered here since it was not

examined in this study. The effect of increased chain packing however was examined by annealing a cured 5K maleimide terminated PEKE oligomer for various lengths of time. It could be expected that packing would increase with increasing annealing time thereby strengthening the matrix and increasing its toughness. However, toughness was found to decrease with annealing. This suggested that intermolecular strength does not contribute significantly to the toughening mechanism in PAEK networks.

This conclusion was further verified by comparing the toughness results of PEKE and PEKKE based networks. Assuming intermolecular strength did contribute significantly to a polymer's toughness, it would be predicted that PEKKE networks should possess greater toughness since its backbone contains one more carbonyl group per repeat unit than the PEKE backbone. The extra carbonyl would act as an additional site for intermolecular bonding with other chains. However, actual data demonstrates that PEKKE networks possess lower fracture toughness values than PEKE networks. Therefore it is concluded that the number of intermolecular bonds does not significantly contribute to the fracture toughness of the polymers examined in this study.

8.2.3.2 Covalent Bonds

Increasing the load carrying contribution of the covalent bonds of the polymer backbone can also increase matrix strength. Since covalent bonds are significantly stronger than intermolecular bonds, they have the potential of carrying a much greater load. However in many circumstances their strength is not used efficiently. Chains which are joined together by just a few intermolecular bonds can only contribute a fraction of their total covalent bond strength to support the load. Before their full potential could be reached, the intermolecular bonds would fail. Thus by increasing the number of chains which are joined by entanglements or crosslinks, the tensile strength of the polymer matrix can be increased. For the majority of systems studied, chains were thoroughly joined together by crosslinks so that the load carrying contribution of the covalent bonds were already near its maximum, from a practical point of view. Therefore this procedure could not be applied to explain the differences in

toughness values for these networks. However the effect of increasing strength by increasing the number of chains joined by entanglements is clearly seen in the t-butylphenyl terminated PEKE oligomers. Below the chain entanglement molecular weight, the oligomers are weak and brittle. Toughness increases by a factor of 5 however as molecular weight increases above Me and the chains become entangled.

The load carrying contribution of the covalent bonds can also be increased by increasing chain packing density. Vincent [24] demonstrated that large bulky pendant groups reduced the packing density of the polymer thereby reducing its tensile strength. Again, since the chemical structure of the polymers used in this study remained constant, this procedure did not apply. The only change in packing density would have been generated in the annealing study and as mentioned previously, this decreased, not increased, the network's toughness.

8.3 Toughness Through Crack Tip Blunting

8.3.1 Stress Concentration and Material Toughness versus Crack Tip Radius

The effect of blunting the crack tip on a polymer's fracture toughness can be determined by examining the effect of blunting on the stress concentration generated by that crack tip. As discussed previously, the presence of a crack causes a magnification or concentration of an applied load in the material directly in front of its tip. This magnification causes the critical load necessary to induce failure to be reached well below the load that would have been required in the absence of the crack. The magnitude of this decrease in the critical load increases with crack length and sharpness of the crack tip (equation 8.1).

$$\sigma_c = \sigma\left(1 + 2\frac{a}{b}\right) \qquad [8.1]$$

where:

a = crack length

b = width of the crack tip

In regards to the measured fracture toughness of the polymer, the effect of crack length on the maximum load is accounted for in the geometry factors for K_{1_c} and G_{1_c}, (equation 5.7 and 5.8). The sharpness of the precrack tip however is assumed to be infinite for the fracture toughness calculations and therefore is not accounted for. Blunting the crack tip causes a decrease in the stress concentration thereby toughening the material. Plati and Williams [142] compared the sharpness of the precrack tip to the impact toughness for several polymers, (Table 21). As the crack tip radius increases from razor blade sharpness to 1 mm, toughness dramatically increases.

One approach to alter the sharpness of the precrack tip, is through the procedure used to introduce it into the specimen. A diamond tipped circular saw, for instance, can produce much sharper crack tips than a band saw. The procedure which is believed to generate the sharpness precrack tips is the one used in this study, tapping a cooled razor blade into the specimen until crack propagation occurs.

It can be speculated that crack tip blunting can also be produced by the extension of the polymer matrix directly in front of the precrack. This mechanism is in opposition to toughening the polymer through strengthening its matrix since a matrix which would be easier to extend would be weaker. This view on opposing toughening mechanisms has similarly been proposed by Yoon [141] to explain the strength of adhesive bonds.

8.3.2 Crack Tip Blunting Through Molecular Extension

8.3.2.1 Stages of Molecular Extension

As was discussed in the section on swelling, extension of a polymeric matrix occurs in three sequential stages. The first stage involves the straining of intermolecular bonds such

Table 21. Impact toughness versus precrack tip sharpness for several thermoplastics [142]

Polymer	G_{1c} $(KJ/m^2)^1$	G_{1c} $(KJ/m^2)^2$
Polyvinylchloride	1.4	7.0
Polycarbonate	4.9	62
Polymethylmethacrylate	1.3	8.5
High Density Polyethylene	3.4	6.4

1: razor blade
2: ρ = crack tip radius = 1 mm

as van der waals dispersion forces and dipole-dipole interactions. These bonds have a mechanical behavior similar to an elastic spring, meaning they can elongate and recoil instantaneously without permanent deformation upon the loading and unloading of a stress. For this reason stage one extension of the matrix due to this stage is quite limited since the strength of these bonds decreases rapidly upon straining.

The second stage of extension involves the uncoiling of chains through bond rotation. This stage has the potential to produce large scale extension since unperturbed chains usually lie in a coiled up configuration. In order for bond rotation to initiate however, two energy barriers must be overcome. The first barrier is the energy of activation for bond rotation. The covalent bonds of a polymer backbone align themselves at various angles to one another. Each bond angle possesses a particular magnitude of conformational energy which is imparted to the polymer. Since molecules prefer to lie in the lowest energy state possible, bonds align themselves at the angles which possess a local minimum in conformational energy. For a bond to rotate from one localized minimum energy position to the next, it must first pass through angles which possess greater conformational energy.

The second barrier is the energy required to disrupt the close packing of the polymer chains. If the polymer chains are tightly packed, insufficient free space would be available between the chains for a bond to rotate. A bond must therefore have sufficient enough energy not only to change conformation, but to disrupt the intermolecular bonds which maintain the tight packing thereby creating enough free space for it to rotate.

The second stage of extension is assumed to be associated with viscoelastic deformation since the rotation of covalent bonds is an activated process and therefore dependent on time and temperature. This implies that stage two extension is also associated with the polymer's glass transition. The glass transition temperature would mark the point where sufficient thermal energy was available to overcome the inter and intramolecular energy barriers. The association between stage two extension and glass transition can only be an assumption at this time since the molecular scale motions which occur at Tg are not well defined in the literature. It is a logical speculation however since the decrease in modulus and in-

crease in creep extension which accompanies the glass transition would be generated with a decrease in the restriction of bond rotation.

The third stage of extension is a continuation of the second stage. During the second stage, entanglements between the chains limit the magnitude of extension. Upon disentanglement of the chains however, an additional stage of extension occurs. Disentanglement most likely occurs via a series of bond rotations along the backbones of the entangled chain segments. This series of bond rotations is more complex than the bond rotations required to initiate stage two extension. Disentanglement therefore requires higher temperatures and/or longer transition times to occur than the temperatures and transition times required for stage two extension. This makes stage three extension a separate stage of extension. In thermoplastics, chain disentanglement is associated with permanent plastic deformation or flow. In thermosets, stage three extension is usually not observed.

8.3.2.2 Toughness versus Intermolecular Extension

If blunting is caused by the ease which intermolecular bonds can be stretched, then increases in fracture toughness must be caused by the decreases in the number or strength of the intermolecular bonds in those networks and vise versa. For the case of decreasing fracture toughness with annealing this conclusion seems logical. It would be assumed that as the annealing time increased, the number and strength of the intermolecular bonds would also increase. This would generate a stiffer matrix thus producing less blunting of the crack tip and decreasing fracture toughness.

For the case of the networks prepared from various molecular weight PEKE and PEKKE oligomers however, the intermolecular bonding argument does not seem to apply. Networks whose only differences were the molecular weight between crosslink points, would be expected to possess similar stiffnesses, since they would possess similar numbers and strengths of their intermolecular bonds. This is indicated by their associated moduli which are found to remain relatively constant as molecular weight increases (Table 15). However, fracture toughness significantly increases with increasing molecular weight. This suggests

that the stretching of intermolecular bonds is not a major contributor to the blunting of the crack tip.

8.3.2.3 Toughness versus Chain Uncoiling

The examination into the effect of the second stage of polymeric extension on fracture toughness can be simplified by dividing the extent of motion into two categories; maximum extension of the network, and partial or rate dependent extension.

Maximum extension under stage two motion, requires that entanglements act as permanent crosslink points. Chains are allowed to uncoil, but only up to the extent of placing a stress on the entanglements and crosslinks. As discussed previously, the magnitude of this extension should be related to the first swelling plateau. Figure 103 compares the magnitudes of the first swelling plateau for the networks cured from various molecular weight maleimide terminated PEKE oligomers to their associated fracture toughness values. There appears some correlation might exists between the two variables for the 3.1K and 5.9K networks but not for the 8.6K, 10.7K and 16K networks.

Comparing the first swelling plateau for the networks cured for varying times to the fracture toughness results suggests no correlation between toughness and the first swelling plateau (Figure 104). The network cured for 5 minutes exhibits a swelling plateau significantly greater than the other three networks but possesses equal toughness. This conclusion is confirmed by the comparison of the swelling plateau and toughness of networks cured from maleimide terminated PEKE and PEKKE oligomers. The 2.5K and 10K PEKKE networks exhibit identical swelling plateaus to their PEKE networks counterparts, but possess significantly lower toughness values.

Crack tip blunting due to partial uncoiling of the chains implies a relationship between toughness and the rate at which a chain can uncoil. Since a chain segment must first disrupt the intermolecular bonds it has to the surrounding chains before it can uncoil, rate of uncoiling would be dependent on the packing density of the chains. Annealing, which would increase

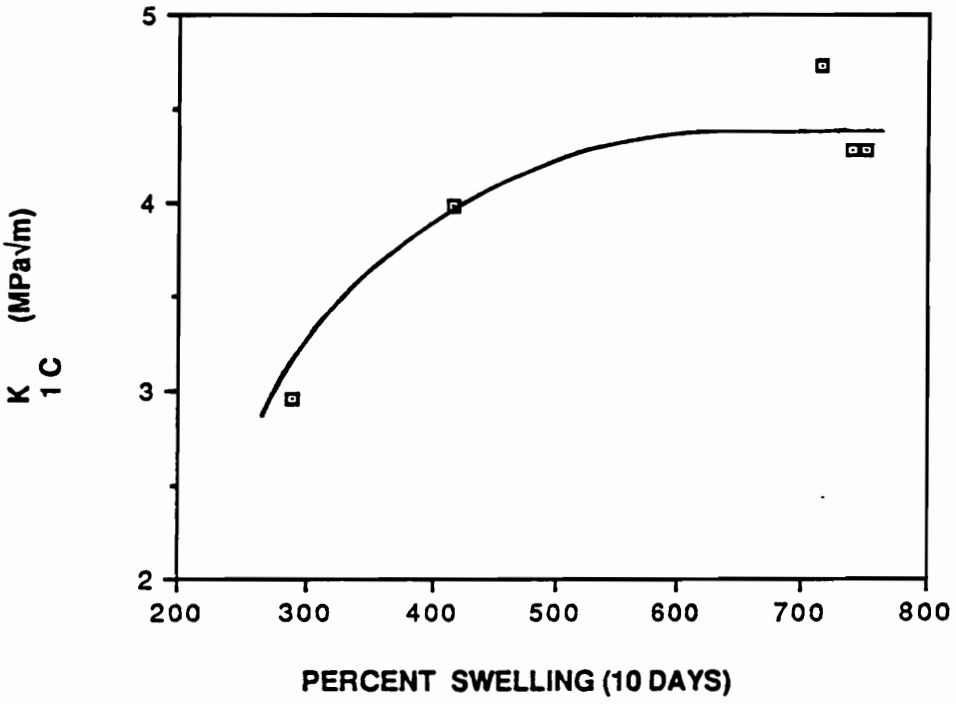

Figure 103. Fracture toughness versus swelling after 10 days for cured maleimide terminated PEKE oligomers of various molecular weight

packing density, should therefore decrease fracture toughness of the network. This is what is observed.

Networks consisting of a PEKKE backbone would be expected to exhibit fracture toughness values less than PEKE based networks since the PEKKE backbone contains an extra carbonyl which would increase intermolecular bonding strength and also produces a stiffer backbone chain than that of the PEKE. Again this is what is observed.

The rate of chain uncoiling could also be effected by the molecular weight between crosslink points. It would be predicted that as Mc increased, freedom of chain motion would also increase thereby allowing a higher rate of uncoiling. However this increase in freedom of chain motion would level off at high Mc's due the formation of entanglements between the crosslink points. This behavior of increasing chain freedom of motion with Mc followed by a ceiling value to this freedom is exhibited by the toughness data for all PEKE and PEKKE thermoplastics and thermosets examined. This behavior is also exhibited by the creep behavior of the maleimide terminated PEKE networks (Figure 62). Rate of creep increases rapidly with Mc initially, and then begins to level off as Mc reaches 10,000.

It would appear therefore from the above data that fracture toughness is strongly dependent on the rate at which chains can uncoil. Further studies into the creep behavior of the various networks however is needed before this can be proven conclusively.

8.3.2.4 Toughness versus Disentanglements

The third stage of extension can also be divided into two categories; total disentanglement of dangling ends allowing maximum extension of the polymer matrix, or partial disentanglement producing a rate dependent extension.

For a network to possess maximum extension (without the breaking of covalent bonds), all restrictions to chain motion due to intermolecuar bonds, intramolecular bond rotations, and chain entanglements would be eliminated. This would imply that identical networks possessing different thermal histories should exhibit identical K_{1_c} values. This of course, is not

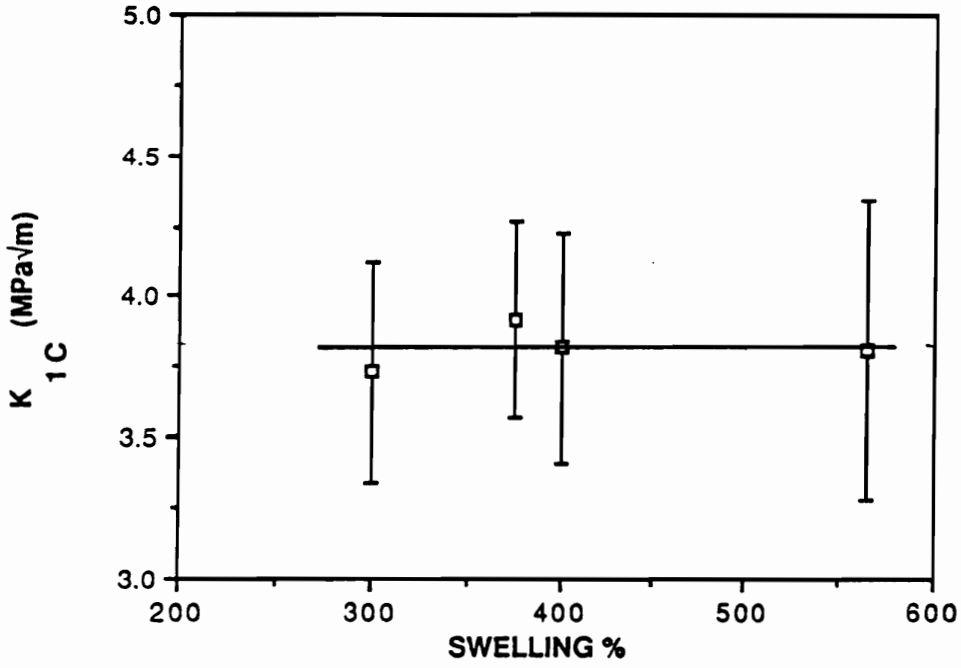

Figure 104. **Fracture toughness versus swelling after 10 days for a 5K maleimide terminated PEKE oligomer cured for various lengths of time**

what is observed for the networks annealed for various lengths of time. Therefore maximum extension of the network during fracture toughness testing is unlikely.

If toughness was dependent on rate of disentanglement, then this would be indicated by comparing K_{1_c} to the rate of disentanglement observed in swelling experiments. For the series of networks cured for various lengths of time, swelling data has shown that the rate of network expansion decreases with increasing cure time. This decrease in the rate of expansion was attributed to a decrease in the rate of disentanglement. If toughness was related to rate of disentanglement, it would be expected that toughness would decrease as cure time increased. This however is not the case. Toughness is independent of cure time suggesting that the third stage of polymeric extension does not significantly contribute to the blunting of the precrack tip.

8.4 Ductile Extension

This section will examine the implications of the conclusion that toughening is dependent on the rate of stage two extension. A discussion on the time of initiation of the three stages of extension will first be presented. This will be followed by an examination of the similarities between the molecular motions associated with ductile deformation and stage two extension as well as possible explanations of these similarities. Lastly, the transition between semi-brittle and ductile failure found in the PAEK networks will be compared to the above discussion.

8.4.1 Time Scales of Molecular Extension

From the plot of the creep extension of glassy polymer, Figure 49, the time of occurrence of the three stages of molecular extension can be obtained through the associated stages of

creep extension. The first stage of creep extension occurs instantaneouly upon the application of a load and is therefore independent of time. The second stage is associated with the glass transition of the polymer. Its time of occurrence is dependent upon the difference between the test temperature and the polymer's Tg. For temperature differences of 10 °C or less, the second stage may commence within days of the application of the load. For larger temperature differences, the time of occurrence may be many orders of magnitude greater. The time necessary to initiate stage three is most likely dependent on the complexity of the entanglements between the chains. Stage three for loosely entangled chains could occur within days of stage two extension while extension of highly entangled chains may not commence till years later.

8.4.2 Molecular Scale Motion

As concluded from the data, K_{1c} appears to be dependent on the rate of stage two extension. This conclusion seems questionable when considering the fact that the tests were performed at greater than 125 °C below the polymer's Tg and at a rate which produced failure within 5 seconds. Under these conditions it might have been expected that only stage one extension could be generated. From the examination of the fracture surfaces however, it is evident that large scale deformation did occur.

Large scale deformation of polymers under glassy conditions is quite common in glassy thermoplastics such as polysulfone and polycarbonate. Materials such as these can elongate 100 percent or more beyond their elastic limits. The deformation occurring beyond the elastic limits is referred to as ductile deformation.

The ability of a polymer to undergo ductile extension is dependent on temperature and strain rate. At relatively low temperatures or high strain rates, ductile extension is prevented from occurring thus making the polymer brittle. At higher temepratures however, a transition in the behavior of the polymer chains occurs, which enables the polymer to undergo ductile

deformation. The temperature of this transition is below the Tg of the polymer and is referred to as the ductile/brittle transition.

The fact that large scale deformation is possible at temperatures below Tg brings forth two questions. Is ductile deformation and stage two extensions generated by the same types of molecular motions? And if yes, then how can ductile deformation be generated at a significantly lower temperature than stage two extension?

Upon reexamining the molecular theories of yielding (ductile deformation), it is found that a number of similarities, concerning the inter and intramolecular restrictions to chain motion, exist between ductile deformation and stage two extension. Argon [58] believed that polymeric yielding was associated with the formation of kinks along the polymer backbone. These kinks, which were generated from bond rotation, disrupted the packing order of the chains thereby creating free volume, (Figure 24). The kinking process was opposed by the elastic nature of the surrounding matrix which attempted to maintain packing order. Robertson [25] proposed that yielding was also generated through bond rotation which thus produced free volume. However he believed that the opposition to bond rotation came from intramolecular restrictions.

Bowden's [28] explanation of strain softening is also in line with the proposed model for stage two extension. He proposed that at the yield point molecules begin to have large scale motion. The restriction to this motion is initially high due to the close packing of the molecules. However, upon the rotation of a few bonds, this packing order is disrupted, reducing the resistance to large scale motion. The stress necessary to extend the polymer therefore drops as demonstrated with the associated drop in stress with strain softening.

Since it appears from the above theories that the molecular motions associated with stage two and ductile extensions are similar, how is it then that stage one extension occurs at Tg, for creep and dynamic mechanical experiments, while ductile deformation occurs at temperatures below Tg? Two possible solutions are; the temperature of the specimens were increased to approximately the polymer's Tg during the test, or the Tg of the polymer was depressed to approximately the test temperature.

Increases in the temperature of the specimen can be produced through chain motion and the disruptions of intermolecular bonds. For the polymers used in this study, these motions would have to increase the temperature 100 °C or more to reach the polymer's Tg. Upon handling the specimens however, no temperature increase was ever detected. Since a temperature increase of 100 °C or more, even if it had been extremely localized, would have been detected upon handling, it can be concluded that this was not the mechanism which produced large scale extension.

The depression of Tg during a fracture toughness test, could be produced by the complex state of stress involved in such a test. Gent [75] has proposed that the depression of Tg is necessary to produce the cavitation stage of crazing. He believed that the hydrostatic stresses which form in front of the crack tip depress the Tg of the polymer below the test temperature thus transforming the glassy polymer into a rubber. For some polymers this would imply a depression of 100 °C or more. Others however have proposed relationships between Tg depression and hydrostatic stress which predict only a modest depression of Tg, less than 20 °C, is conceivable. The effect of deviatoric stresses on Tg have never been examined. Therefore it is unclear whether a complex state of stress can significantly depress Tg.

A third possibility is that even though ductile deformation and stage two extension appear to be very similar in regards to molecular motion, there may exist a subtle difference which would explain the difference in the temperatures at which they are generated. One obvious difference is the fact that ductile deformation occurs at stresses greater than yield stress while stage two extension associated with creep and dynamic measurements, occurs under elastic stresses.

This difference in the level of stress produces a difference in the type of deformation generated. Ductile deformation is inhomogeneous while elastic deformation is homogeneous. It is a possibility that since this difference in the type of deformation exists on the macroscopic scale, it might also equally exist on the molecular level. The inhomogeneous deformation of the polymer chains could be generated by a broad distribution of an applied load amongst the

chain segments. Under a relatively small elastic load, the stress distribution is relatively narrow thereby producing a relatively homogeneous molecular extension. As the level of stress is increased however the distribution of stress broadens. At the yield point, the start of ductile deformation, a portion of the chain segments have enough energy to overcome the energy barriers of bond rotation and intermolecular interference so as to undergo chain extension. The rest of the chain segments however remain in their original conformations thereby producing inhomogeneous deformation.

If the above proposal is correct, so that the only difference between elastic extension at the Tg and ductile deformation below Tg was the homogeneity of the extension with respect to the polymer chain segments, and if molecular motion for a rubbery chain segment could be defined through the criteria of stage two extension, then it could be argued that those chain segments undergoing ductile deformation had undergone a transition to rubbery behavior. This transition to rubbery behavior requires the Tg of the individual extended chain segments to have been depressed below the temperature of polymer matrix. This depression of Tg could be generated by the applied load on these chains. Of course it could be argued that the glass transition of a polymer involves the alteration of the entire matrix and not just individual chains. However since glass transition is generally only loosely defined as the transition from glassy to rubbery behavior and therefore does not describe the transition in the behavior on a molecular level, it is impossible to conclude which argument is correct.

The similarities of ductile deformation to elastic extension at Tg, with respect to an individual chain segment, could possibly be proven using infrared spectroscopy. The frequency of a signal, such as from a carbonyl group along the polymer backbone, may shift as the polymer transforms from a glass to a rubber. The shift would be generated by the change in packing order of the chains. If an identical shift could be detected as the polymer underwent ductile deformation, then that would tend to prove that both extension mechanisms were identical with respect to an individual polymer chain.

The breadth of the stress distribution on the ductile sample could be determined by comparing the magnitude of the shift peak to the original peak. A series of creep experiments

could be conducted, using a range of initial loads on specimens all maintained at the same temperature, and then comparing the magnitude of the shifted peaks when extension does occur. The loads would range from zero to just below the yield stress. Each load would be maintained until large scale extension resulted. The infrared of each specimen would then be taken. It would be expected that the specimen subjected to the highest load would exhibit the smallest shifted peak and thus the highest level of inhomogeneous deformation while the specimen subjected to the smallest load would exhibit the largest shifted peak.

The breadth of the extension in terms of time might also give a qualitative measurement of stress distribution. For the specimens subjected to the highest loads, the time span of the extension should be long due to the relatively high distribution of stresses with the chains subjected to the highest loads extending first. The specimens subjected to the smallest loads, should therefore exhibit the shortest extension times.

Another experiment which would indirectly confirm the similarities between ductile deformation and elastic extension at Tg would be comparing the creep extension of two specimens of a lightly crosslinked polymer, one of which had been ductilely deformed and the other which had not. If ductile deformation was identical to elastic deformation at Tg with respect to molecular motion, then upon heating the specimens past their Tg, their creep extensions should be equal, assuming equal loads.

8.4.3 Transition from Semi-brittle to Ductile Failure

As mentioned previously, toughness specimens failed by a semi-brittle or a ductile mechanism, both of which was often observed during the fracture toughness testing of a single network. No intermediate behavior has ever been observed. The transition from semi-brittle to ductile failure however appears to be dependent on crack length and molecular weight between crosslinks (Mc), (Figure 105).

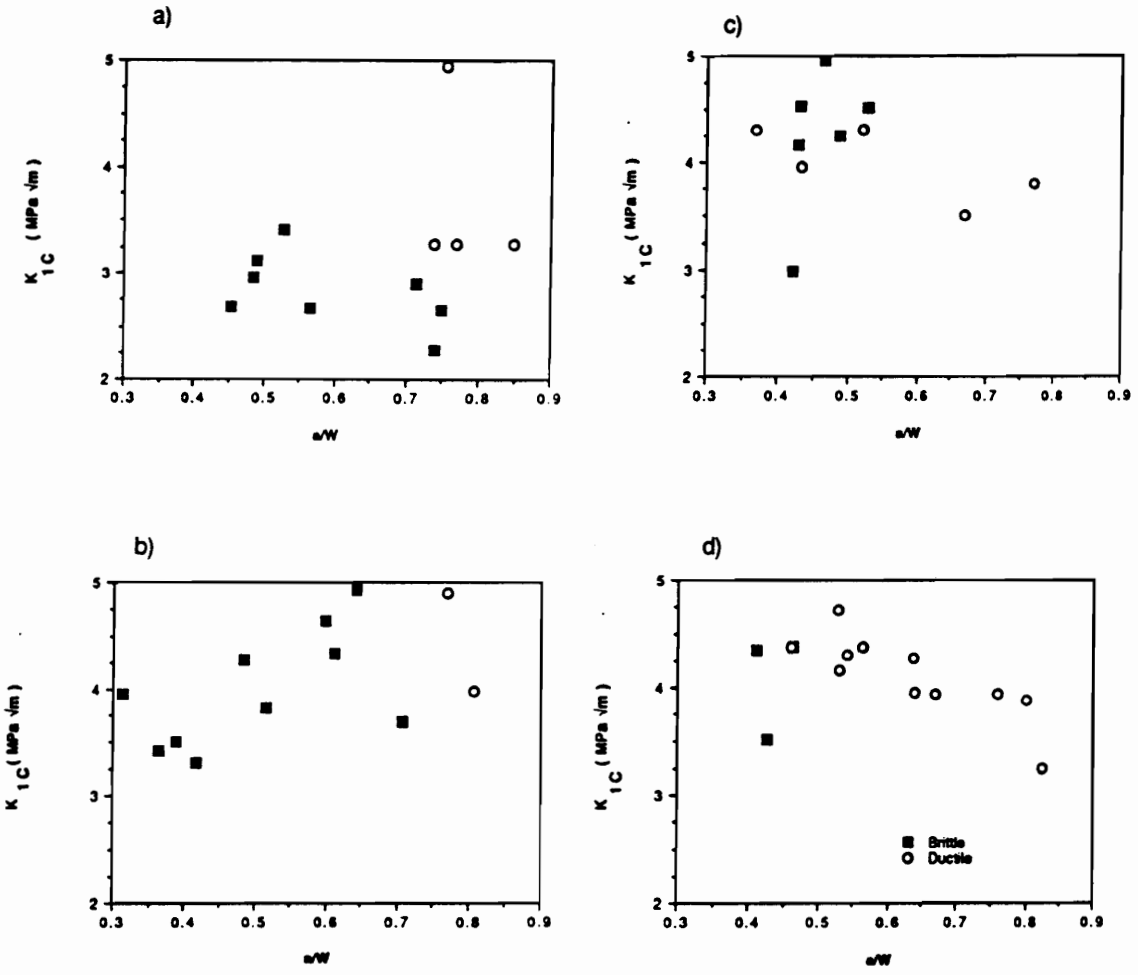

Figure 105. Fracture toughness and failure mechanism versus crack length for cured maleimide terminated PEKE oligomers: a) 3.1K b) 5.9K c)10.7K d)16.0K

For networks possessing a relatively high crosslink density, Mc less than 6,000, specimens do not exhibit ductile behavior until the crack length to width ratio reaches 0.7. Below 0.7, failure is totally semi-brittle. The network prepared from the 10.7K oligomer shows ductile failure becoming interspersed with the semi-brittle behavior for a/w down to 0.4. For the 16K network, ductile behavior dominates. Semi-brittle behavior is found only for a/w less than 0.4.

The calculated K_{1_c} value also appears to be independent of the mode of failure. Figure 106 plots a reduced fracture toughness versus crack length for several sets of toughness data chosen at random. The reduced fracture toughness values presented were the K_{1_c} values of individual specimens divided by the average K_{1_c} value for the set. Reduced K_{1_c} appears to be independent of mode of failure as well as crack length. It can be concluded therefore that molecular extension in front of the crack tip is independent of the mechanical behavior of the polymer chains away from the crack tip.

The cause of the transition is probably viscoelastic in nature. Polymeric chains in front of the crack begin to creep as a load is applied to the specimen. The slower the load is applied, the more time the chains have to respond to the stress. Figure 107 shows the load displacement curves for two theoretically identical specimens containing different crack lengths. The load increases more slowly for the specimen with the longer crack. Thus the polymer chains of the specimens containing the longer cracks would have a longer time to response to the stress. Figure 62 compares the creep behavior for the 4 networks at 150 °C. The rate of creep shows a strong dependence on Mc, with the 3.1K network deforming much slower than the 16K network. This would explain why the 3.1K network only shows ductile failure at long crack lengths.

The data which shows no change in the resulting K_{1_c} value as crack length increases, however is in opposition with this conclusion. If the chains of the specimens which possessed the longer cracks lengths had additional time to respond to the stress, it would be expected that additional blunting would result and therefore higher K_{1_c} values. One possible explanation for this contradiction is the insensitivity of the 3 point bend test to detect subtle changes in toughness.

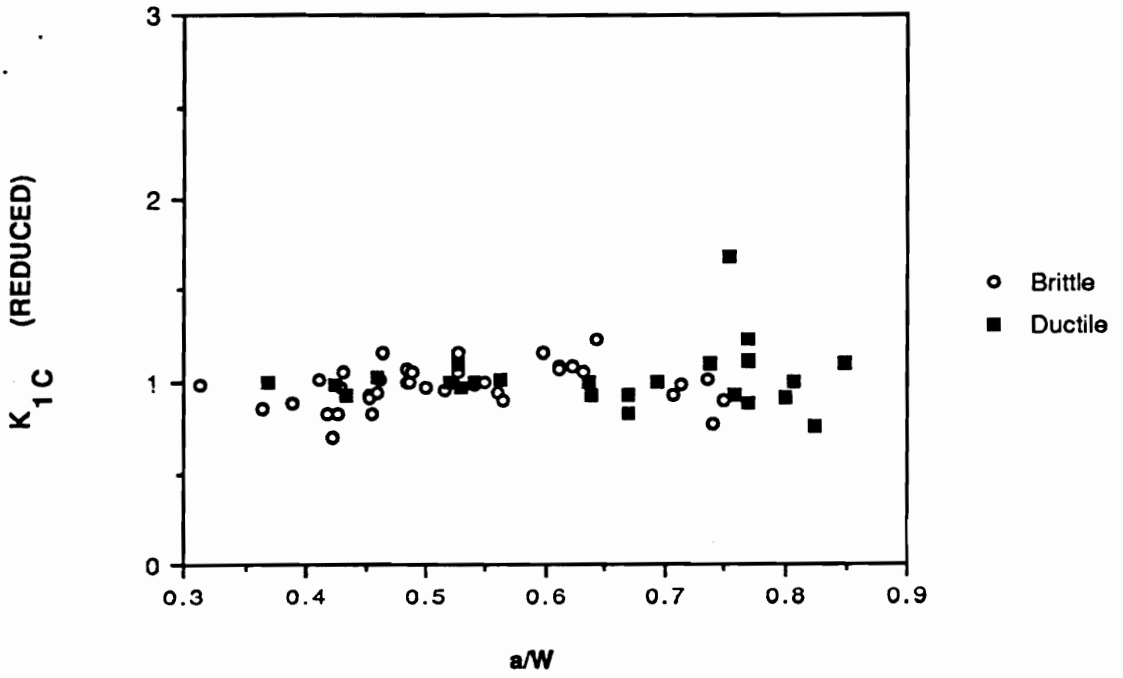

Figure 106. Reduced fracture toughness versus cracklength for various PEKE networks

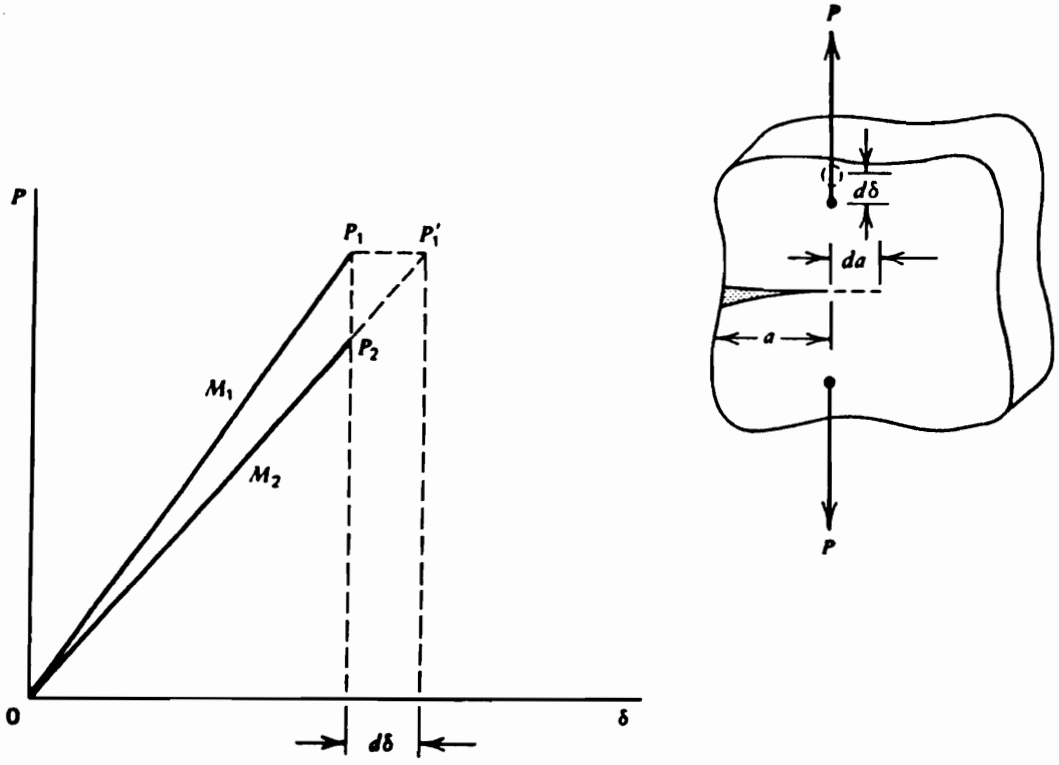

Figure 107. Load versus displacement curve for two theoretically identical specimens but possessing different crack lengths.

The reason no intermediate failure mechanism is seen is also unknown. If the transition is viscoelastic it nature, the transition must be related to an abrupt transition in viscoelastic behavior, such as a transition from glass to rubber or perhaps from brittle to ductile. This speculation is reinforced by examining the fracture mechanism of 5K network at 50 °C, (Figure 108). Out of seven specimens tested, only one broke brittlely compared to 10 out of 12 for a room temperature test. At higher temperatures, all specimens failed ductilely. No study however has been undertaken to relate this transition in failure to a viscoelastic transition.

It has been speculated that this transition could also be caused by the overlap of the plastic zone in front of the crack tip with the bottom of the specimen. This overlap would produce a plane stress stress state therefore producing ductile behavior. At first glance this conclusion seems possible since increasing crack length would position the plastic zone closer to the bottom of the specimen. Also, increasing Mc would likely increase the size of the plastic zone thereby promoting overlap. By applying the equations for plastic zone size proposed by Irwin, (equation 2.49, 2.50), it is possible to compare the size fo the plastic zone to the distance between the precrack tip and the bottom of the specimen. Assuming a K_{1_c} value of 4.2 MPa $m^{1/2}$ (3820 ksi $in^{1/2}$) and a yield stress of 55 MPa (8,000 psi), the radius of the plastic zone would be 0.31 mm under plane strain and 0.92 mm under plane stress. Since a specimen having a crack length to height ratio of 0.5 would possess a distance from the pre-crack tip to the bottom of the specimen of approximately 4 mm it is doubtful that this overlap exists.

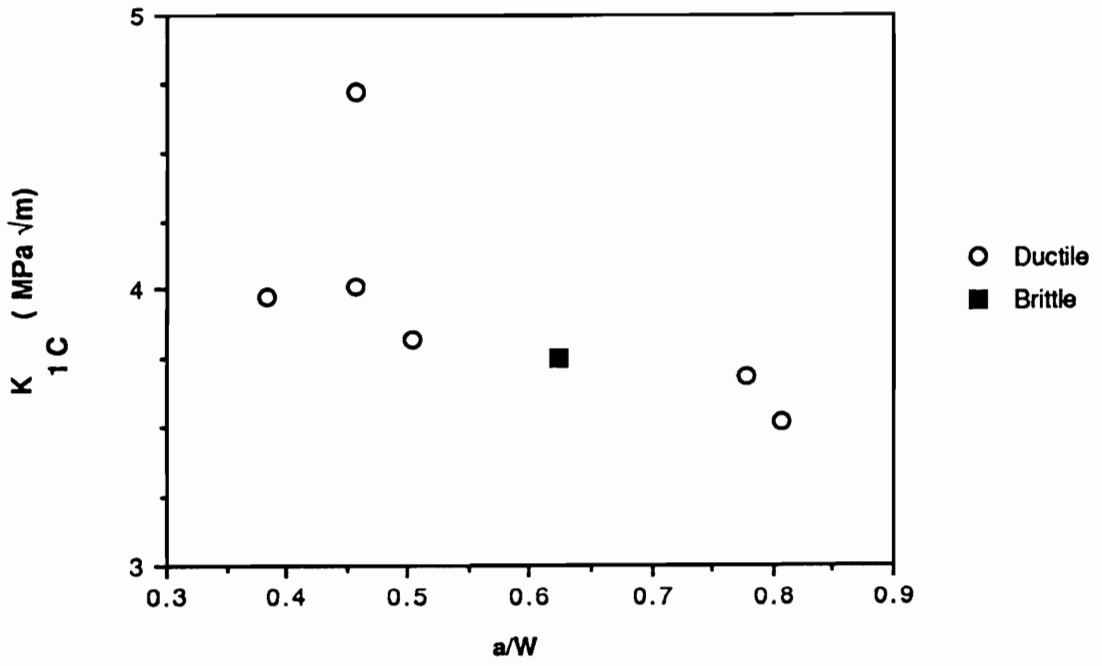

Figure 108. **Fracture toughness and failure mechanism versus crack length for a cured 5.9K maleimide terminated PEKE oligomer tested at 50 °C**

8.5 Relationship between α and β Relaxations to Fracture Toughness

8.5.1 β Relaxation

The dependence of fracture toughness on secondary or β relaxations in polymers has been speculated by a number of researchers. This speculation has not been widely accepted yet however, since β relaxations often occur at temperatures greater than 100 °C below room temperature, where most fracture toughness testing is conducted. It has been proposed, that the fast rate of critical crack propagation increases the temperature of the relaxation so that it overlaps with the temperature of the fracture test. Whether or not this overlap occurs or not, it is apparent that polymers which exhibit relatively high K_{1_c} and G_{1_c} values, possess β relaxations. For this reason the maginitude and breath of the β relaxations and the K_{1_c} values for PAEK thermoplastics and thermosets have been compared to one another using annealing time, Mc and backbone structure as variables.

Figure 70 compares the dynamic mechanical behavior of a cured 5.9K maleimide terminated PEKE oligomer which had been quenched from 120 °C above Tg to an identical network which was quenched and then annealed at 145 °C for 84 hours. The magnitude of the β relaxation is seen to decrease with annealing. Fracture toughness also decreases from 4.0 MPa $m^{1/2}$ to 3.6 MPa $m^{1/2}$.

Figure 69 compares the quenched and annealed dynamic mechanical behavior for a 20K hydroxyl terminated PEKE thermoplastic. The magnitude of the β relaxation for this system however remains unchanged. Fracture toughness also does not increase but rather remains relatively constant 5.1 to 5.5 MPa $m^{1/2}$.

These two comparisons would seem to suggest a relationship between the magnitude of the β relaxation and fracture toughness. However when comparing β relaxation to toughness for networks possessing various Mc and backbone structure a different conclusion is drawn. The dynamic mechanical behaviors of cured 3.1K and 16K PEKE oligomers are

shown in Figure 67. No difference in the β relaxation peak is observed. However fracture toughness increases from 2.95 MPa $m^{1/2}$ for the 3.1K network to 4.28 MPa $m^{1/2}$ for the 16K network. Networks composed of a PEKKE possess a slightly higher β relaxation than a PEKE network (Figure 68) but exhibits a significantly lower K_{1_C}, 1.77 to 2.95 MPa $m^{1/2}$ respectively. This seems to suggest that the data relating β relaxation to fracture toughness is still inconclusive.

The lack of correlation between β relaxation and K_{1_C} is not surprising considering the magnitude of fracture toughness is determined from the maximum load supported by the specimen, which occurs before crack propagation initiates. The increase in the temperature of the β relaxation due to the velocity of the propagating crack is therefore probably irrelevant for this type of toughness test. The temperature of the β relaxation could be increased during the loading cycle of the specimen, but due to the relatively slow crosshead displacement rate which was used for these tests (2 in/min., compared to the velocity of a critically propagating crack, approximately 10^6 in/min.), this is also doubtful. Even if this overlap did occur however, it can be argued that β relaxations can not affect fracture toughness since they can not increase matrix strength and they are not part of large scale chain extension.

8.5.2 α Relaxation

A more uniformed conclusion can be drawn if the K_{1_C} results for these polymers are compared to their associated glass transition temperatures, (Table 22). The 5K PEKE network exhibits a 5 °C increase in Tg with annealing as well as a decrease in toughness. A decrease in toughness with increasing Tg is also observed as Mc in PEKE networks is decreased from 16K to 3.1K and as the backbone is changed from PEKKE to PEKE. For the case of the annealed 20K PEKE thermoplastic, Tg remains unchanged with annealing and toughness exhibits a slight increase.

The stronger relationship between Tg and K_{1_c} than β relaxation and K_{1_c} is logical considering the large scale chain extensions which occur in front of the crack tip. It is possible however to speculate that β relaxations might act as an initiator or catalyst for this large scale chain extensions through the partial disruption of intermolecular bonds.

Table 22. Comparison of glass transition temperatures to fracture toughness for various PAEK thermoplastics and thermosets

Polymer	Conditions	Tg (°C) (DMTA)	K_{1c} (MPa $m^{1/2}$)
5.7K PEKE cured network	Quenched	157	3.99±0.40
	Annealed 86 hrs. At 145 °C	162	3.57±0.27
20K PEKE thermoplastic	Quenched	157	5.11±0.47
	Annealed 84 hrs. At 145 °C	157	5.50±0.62
16K PEKE cured network	-	156	4.28±0.23
3.1K PEKE cured network	-	167	2.95±0.28
2.7K PEKKE cured network	-	175	1.77±0.26

Chapter 9 Conclusions

The focus of this dissertation was on the physical and mechanical behavior of amorphous poly(arylene ether)ketone thermoplastics and thermosets as well as poly(arylene ether)ketone modified bismaleimide networks. Some of the physical and mechanical tests performed included swelling, fracture toughness, and tensile and dynamic mechanical analysis. These tests compared variables such as the length of cure, annealing, Mc, and backbone structure.

The increase in swelling over time for the PAEK thermosets was discovered to occur in two stages, much like the creep extension of a glassy thermoplastic. The first stage occurred within the first two days of the experiment. During this time solvent thoroughly penetrated the network, transforming the polymer into a rubber, and swelling the matrix from 200 to 800 percent. This stage was believed to parallel the elastic and viscoelastic extension stages of a creep elongation.

The second stage occurred from days to months later. Swelling increased abruptly during this stage in some networks; increasing the magnitude of absorped solvent to 1500 percent or more in a few days. This behavior was often followed by total disintegration of the network. Other networks exhibited a more subtle second stage of swelling, with the magnitude of absorbed solvent increasing an additional 100 percent over 40 days or more. It is

believed that this stage is associated with the disentanglement of dangling chain ends from the crosslinked matrix thus paralleling the flow behavior of a thermoplastic undergoing creep.

Tensile tests of networks cured from varying molecular weight amine terminated PEKE oligomers and maleimide terminated PEKKE oligomers exhibited similar responses. Modulus and yield stress for both systems were found to be independent of molecular weight while elongation at break rose rapidly with increasing molecular weight. The independence of modulus from the molecular weight of the starting oligomer is logical if the modulus is determined by the stiffness of intermolecular bonds since the number and strength of these bonds should be independent of Mc. The same logic applies to the independence of yield stress from Mc if the yield stress is determined by the stress necessary to disrupt the intermolecular bonds as long as the stress is relatively well distributed among the chains.

The dynamic mechanical analysis of the various poly(arylene ether)ketone networks indicated a significant β relaxation occurring at approximately -70 °C with a glass transition at approximately 160 °C. Tg and rubbery modulus increase slightly with decreasing Mc, increasing functionality of the crosslinks points, annealing, and increasing stiffness of the backbone.

The fracture toughness results from various molecular weight t-butylphenyl terminated PEKE oligomers was found to parallel their associated melt viscosity data for molecular weights less than 20,000 g/mole. Both curves demonstrate a dramatic increase in slope at a molecular weight of 11,000 g/moles, thus indicating PEKE's chain entanglement molecular weight. Above 20,000g/mole, melt viscosity continues to rise while fracture toughness levels off. From the data below 20,000 g/mole it was concluded that the mechanism or mechanisms which resist melt flow are probably the same mechanism or mechanisms which resist crack propagation. Since the resistance to crack propagation is not increased by the increasing ability of the polymer to flow and blunt the crack tip, it must be caused by the strengthening of the matrix by increasing intermolecular bonding and chain entanglements.

The fracture toughness values for networks cured from functionally terminated poly(arylene ether)ketone oligomers were found to be equal to or greater than the toughness

of thermoplastic polycarbonate. The toughness of the these networks increased with increasing Mc for molecular weights less than Me. Above Me, toughness leveled off, probably due to the formation of entanglements between the crosslink points. Toughness was discovered to be independent of the length of cure but dependent on the ratio of ketones to ether units along the backbone. PEKE based networks possessed significantly higher fracture toughness values than PEKKE networks. Annealing PEKE networks produced a two stage decrease in toughness over time. This decrease was mirrored by a two stage increase in the magnitude of the physical aging peak detected by DSC analysis. It was concluded that crack tip blunting, caused by the viscoelastic extension of the polymer matrix, was the mechanism of toughening for PAEK networks. Variables which decreased chain mobility such as annealing, decreasing Mc, and altering the backbone structure from PEKE to PEKKE, also decreased fracture toughness.

The transition from semi-brittle to ductile failure seen in PAEK networks was found to be dependent on crack length, temperature and Mc. The transition is therefore believed to be viscoelastic in nature. Fracture toughness results however were independent of the mechanism of failure indicating the toughening mechanism was solely dependent on the mechanical response of the chains close to the crack tip.

The swelling behavior of maleimide terminated PEKE modified bismaleimide networks exhibited a single stage of extension. This suggested that unreacted dangling ends did not exist in these networks, probably due to the high concentration of maleimide groups from the bismaleimide.

The dynamic mechanical analysis of the modified bismaleimide networks revealed only one glass transition which was associated with the relaxation of the PEKE. No indication of phase mixing, which would be demonstrated by an increase in the Tg of the PEKE portion, was ever detected, even though scanning electron micrographs revealed the majority of networks to be phase mixed. Networks which did phase separate, displayed similar dynamic behavior to the phase mixed systems. Rubbery modulus and tan δ were both strongly de-

pendent on molecular weight of the PEKE oligomer used as well as the weight ratio of PEKE to bismaleimide.

The fracture toughness of bismaleimide was greatly enhanced by their cocuring with maleimide terminated PEKE oligomers. Networks possessing 50 weight percent 10K PEKE, exhibited fracture toughness values nearing that of polysulfone. Overall, toughness increased linearly with the molecular weight PEKE oligomer and exponentially with its weight fraction.

The necessity of cocuring the PEKE oligomer into the bismaleimide matrix to improve toughness was examined by physically blending a non-reactive PEKE oligomer into the bismaleimide. This network was macrophase separated, with the PEKE portion being totally extractable. Toughness revealed no increase over the pure bismaleimide network. The dynamic mechanical analysis showed a depression of the associated PEKE Tg of approximately 20 °C from the cocured system.

Appendix A. MODEL CALCULATION

Scheme 1. Sample Molecular Weight Calculation Using a Modified Carother's Equation

Objective:

Calculate molar amounts of each starting material needed to synthesize 100 gm of 5000 <Mn>, m-aminophenol terminated PEKE oligomer.

	Molecular Weight
Bisphenol-A (Bis-A)	228
Difluorobenzophenone (DFBP)	218
m-Aminophenol (MAP)	109
Polymer Repeat Unit	406
End groups	288, 108

$$\text{Number of Repeat Units} = \frac{5000 - 288 - 108}{406} = 11.340$$

$$\text{Number of Reacted Monomer Units} = X_n = 2(11.340) + 1 = 23.680$$

$$\frac{\text{moles Bis-A}}{\text{moles DFBP}} = r = \frac{(X_n - 1)}{(X_n + 1)} = 0.9190$$

$$\text{moles of polymer} = \frac{100}{5000} = 0.020$$

$$\text{moles of Bis-A} = (\text{moles Polymer})(\text{number of repeat units})$$

$$= (0.020)(11.340) = 0.2268 \text{ moles}$$

$$\text{moles DFBP} = \frac{\text{moles Bis-A}}{r} = \frac{0.2268}{0.9190} = 0.2468 \text{ moles}$$

$$\text{mole MAP} = 2(\text{moles polymer}) = 2(0.020) = 0.040$$

Scheme 2. Sample Determination by H'-NMR of BMI Content within a BMI/PEKE Blend

PPM(TMS reference)

Methylene of BMI

Isopropylidine methyls of PEKE

$$R = \frac{\text{Integrated area of BMI methylenes}}{\text{Integrated area of PEKE methyls}}$$

$$R = \frac{2(\text{moles BMI})}{6n(\text{moles PEKE})}$$

n = number of backbone repeat units

$$n = \frac{\text{Titrated } <Mn> \text{ of amine terminated oligomer - 556}}{406}$$

$$X = \frac{\text{WT. BMI}}{\text{WT.PEKE}} = \frac{(\text{moles BMI})(\text{MW BMI})}{(\text{moles PEKE})(\text{MW PEKE})}$$

MW BMI = 358

MW PEKE = Titrated Mn PEKE

$$X = \frac{3n\ R\ 358}{\text{MW PEKE}}$$

$$\text{Wt \% BMI} = 100\left[1 - \frac{1}{(1+X)}\right]$$

Scheme 3 Sample calculation in determining molar amounts of various molecular weight oligomers to obtain a blend of given <Mn>.

Objective:

Calculate the molar amounts of a 2000, 5000, and 10,000 molecular weight oligomers needed to produce 100 grams of a blend posessing a <Mn> of 6000, letting the mole fraction for one of the oligomers be given.

$$6000 = 2000x + 5000y + 10{,}000z$$

x, y, z are the mole fractions of the oligomers

$$x + y + z = 1$$

$$\text{let } y = 0.2$$

$$x = 0.8 - z$$

$$\text{Substituting in, } 3400 = 8000z$$

$$z = 0.425$$

$$x = 0.375$$

$$\text{moles of polymer} = \frac{\text{amount of blend required}}{<\text{Mn}> \text{ of the blend}} = \frac{100}{6000} = 0.01667 \text{ moles}$$

$$\text{moles of 2K} = (0.01667)x = 6.25 \times 10^{-3} \text{ moles}$$

$$\text{moles of 5K} = (0.01667)y = 3.34 \times 10^{-3} \text{ moles}$$

$$\text{moles of 10K} = (0.01667)z = 7.08 \times 10^{-3} \text{ moles}$$

Bibliography

1. E. P. Popov, *Mechanics of Materials*, Prentice-Hall Inc., Englewood Cliffs, NJ, 1976.
2. G. E. Dieter, *Mechanical Metallurgy*, (3rd ed.) McGraw-Hill Book Co., NY, 1986.
3. R. W. Hertzber, *Deformation and Fracture Mechanics of Eng. Mat. (2nd ed.)*, John Wiley and Sons, NY, 1983.
4. R. M. Caddell, *Deformation and Fracture of Solids*, Prentice-Hall Inc., Englewood Cliffs, NJ, 1980.
5. Z. D. Jastrzebski, *The Nature and Properties of Eng. Mat.*, John Wiley and Sons, NY, 1977.
6. A. A. Griffith, *Phil. Trans. Royal Soc. London*, A221, 163, 1920.
7. E. Orowan, *Fatigue and Fracture of Metals*, MIT Press, Cambridge, 139, 1950.
8. G. R. Irwin, *Fracturing of Metals*, ASM, Cleveland, 147, 1950.
9. G. R. Irwin and J. A. Kies, *Weekley J. Res. Suppl.*, 33, 193, 1954.
10. G. R. Irwin, *Handbuch der Physiks, Vol V1*, Springer, Berlin, 551, 1958.
11. H. M. Westergaard, *Trans. ASME, J. Appl. Mech.*, 61, 49, 1939.
12. H. Tresca, *Comptes Rendus Acad. Sci. Paris*, 59, 754, 1864.
13. G. T. Hahn, A. R. Rosenfield, *Acta Met.*, 13, 293, 1965.
14. D. S. Dugdale, *J. Mech. Phys. Sol.*, 8, 100, 1960.
15. B. Ellis, A. J. Hare, R. van Noort, *J. Appl. Polym. Sci.*, 30, 4517, 1985.
16. R. Y. Ting, R. L. Cottington, *J. Appl. Polym. Sci.*, 25, 1815, 1980.

17. R. P. Kambour, A. S. Holik, S. Miller, *J. Polym. Sci. Polym. Phys. Ed.*, 16, 19, 1978.

18. D. L. Hunston, A. J. Kinloch, S. J. Shaw, S. S. Wang, *in Adhesive Joints*, K. L. Mittal ed., Plenum Press, 789, 1984.

19. J. A. Hinkley, *J. Appl. Polym. Sci.*, 32, 5654, 1986.

20. K. Cho, A. N. Gent, *Int. J. Fracture*, 28, 239, 1085.

21. R. O. Ritchie, F. A. McClintock, H. Nayeb-Hashemi, M. A. Ritter, *Metal. Transactions A*, 13A, 101, 1982.

22. H. F. Brinson, "Durability Predictions Adhesively Bonded Strts." to be published in *Mech. Behav. of Adhesive Joints*

23. A. J. Kinloch, R. J. Young, *Fracture Behavior of Polymers*, Applied Sci. Publishers, NY, 1983.

24. P. I. Vincent, *Polymer*, 13, 558, 1972.

25. R. E. Robertson, *J. Chem. Phys.*, 44, B950, 1966.

26. N. J. Mills, *Rheol. Acta.*, 13, 693, 1974.

27. Z. H. Stachurski, *J. Mat. Sci.*, 21, 3237, 1986.

28. P. B. Bowden, S. Raha, *Phil. Mag.*, 29, 149, 1974.

29. M. A. Hallam, D. L. M. Cansfrid, I. M. Ward, G. Pollard, *J. Mat. Sci.*, 21, 4199, 1986.

30. *Modern Plastics*, McGraw-Hill, 509-638, 1987.1

31. L. E. Nielson, *Mechanical Properties of Polymers and Composites*, V1,2, Marcel Dekker Inc., NY, 1974.

32. R. A. Duckett, B. C. Goswami, L. S. A. Śmith, I. M. Ward, A. M. Zihlif, *Brit. Polym. J.*, 10, 11, 1978.

33. J. J. Aklonis, W. J. Macknight, *Intro. to Polym. Viscoelasticity (2nd ed.)*, John Wiley and Sons, NY, 1983.

34. A. Rubin, *The Elements of Polymer Sci. & Eng.*, Academic Press, NY, 1982.

35. L. E. Nelson, *J. Appl. Polym. Sci.*, 8, 511, 1964.

36. S. Rabinowitz, I. M. Ward, J. S. C. Parry, *J. Mater. Sci.*, 5, 29, 1970.

37. D. W. Hadley, I. M. Ward, *in Encyl. Sci. and Eng.*, V9, John Wiley & Sons, NY, 379, 1987.

38. J. D. Ferry, *Viscoelastic Prop. of Polymers (2nd ed.)*, John Wiley & Sons, NY, 1970.

39. J. M. Lefebvre, B. Escaig, *J. Mate. Sci.*, 20, 438, 1985.

40. N. Brown, *Material Sci. Eng.*, 8, 69. 1971.

41. A. S. Argon, R. D. Andrews, J. A. Godrick, W. Whitney, *J. Appl. Phys.*, 39, 1899, 1968.

42. D. M. Shinozaki, J. Vlachopoulos, K. Woo, A. Hamielel, *J. Appl. Polym. Sci.*, 21, 3345, 1977.

43. B. Maxwell, M. Nguyen, *Polym. Eng. Sci.*, 19, 1140, 1979.

44. S. Matsuoka, T. T. Wang, *Coat. Plast. Prepr. Pap. Meet. Am. Chem. Soc. Div. Org. Coat. Plast. Chem.*, 36, 155, 1976.

45. R. J. Gardner, J. R. Martin, *J. Appl. Polym. Sci.*, 24, 1269, 1979.

46. H. Eyring, *J. Chem. Phys.*, 4, 283, 1936.

47. G. Halsey, H. J. White, H. Eyring, *Text Res. J.*, 13, 295, 1945.

48. R. N. Haward and G. Thackray, *Proc. Roy. Soc.*, A, 302, 453, 1968.

49. C. Bauwens-Crowet, J. C. Bauwens, *Polymer*, 23, 1599, 1982.

50. J. D. Hoffman, G. Williams, E. Passaglia, *J. Polym. Sci.*, 14, 173, 1966.

51. R. N. Haward, J. N. Hay, I. W. Parson, G. Adams, A. Owadh, C. P. Boxnyak, A. Aref-Azaf, A. Cross, *Coll. Polym. Sci.*, 258, 42.

52. S. Newman, S. Strella, *J. Appl. Polym. Sci.*, 9, 2297, 1965.

53. J. H. Golden, B. L. Hammant, E. A. Hazell, *J. Appl. Polym. Sci.*, 11, 1571, 1967.

54. J. C. Bauwens, *Polymer*, 25, 1523, 1984.

55. J. C. Bauwens, C. Bauwens-Crowet, G. Homes, *J. Polym. Sci.*, Pt A-2, 7, 1745, 1969.

56. J. C. Bauwens, *Polymer*, 21, 699, 1980.

57. A. Kelly, *Strong Solids*, Clarendon Press, 22, 1966.

58. A. S. Argon, *J. Macromol. Sci.-Phys.*, B8, 573, 1973.

59. A. S. Argon, *Phil. Mag.*, 28, 839, 1973.

60. J. C. M. Li, J. J. Gilman, *J. Appl. Phys.*, 41, 4248, 1970.

61. A. S. Argon, M. I. Bessonov, *Phil. Mag.*, 35(4), 917, 1977.

62. Z. H. Stachurski, *J. Mat. Sci.*, 21, 3231, 1986.

63. N. Brown, *J. Mat. Sci.*, 18, 2241, 1983.

64. I. V. Yannas, A. C. Lunn, *Polym. Prepr.*, 16, 564, 1975.

65. P. B. Bowden, *Polymer*, 9, 449, 1968.

66. P. B. Bowden, *in Physics of Glassy Polymers*, R. N. Haward ed., Halsted Press, NY, 279-339, 1973.

67. R. P. Kambour, *Polym. Comm.*, 24, 292, 1983.

68. C. S. Henkee, E. J. Kramer, *J. Mat. Sci.*, 21, 1398, 1986.

69. P. B. Bowden, *Phil. Mag.*, 22, 455, 1970.

70. J. C. M. Li, *Polym. Eng. Sci.*, 24(10), 761, 1984.

71. E. J. Kramer, *J. Macromol. Sci.*, B10, 191, 1974.

72. E. J. Kramer, *J. Polym. Sci. Polym. Phys. Ed.*, 13, 509, 1975.

73. R. A. W. Fraser, I. M. Ward, *J. Mat. Sci.*, 12, 459, 1977.

74. N. J. Mills, *J. Mater. Sci.*, 11, 363, 1976.

75. A. Gent, *J. Mat. Sci.*, 5, 925, 1970.

76. S. S. Sternstein, *Polymeric Mat. ASM*, Metals Park, Ohio, 369, 1975.

77. S. S. Sternstein and F. A. Myers, *J. Macromol.*, B8, 539, 1973.

78. E. Passaglia, *Polymer*, 25, 1727, 1984.

79. E. J. Kramer, E. W. Hart, *Polymer*, 25, 1667, 1984.

80. C. C. Kuo, S. L. Phoenix, E. J. Kramer, *J. Mat. Sci. Lett.*, 4, 459, 1985.

81. E. Passaglia, *J. Phys. Chem. Solids*, 48(11), 1075, 1987.

82. W. Doll, *Polym. Eng. Sci.*, 24(10), 798, 1984.

83. E. J. Kramer, *Polym. Eng. Sci.*, 24(10), 761, 1984.

84. P. Prentice, *Polymer*, 24, 344, 1983.

85. S. S. Pang, Z. D. Zhang, S. S. Shern, C. C. Hsiao, *J. Polym. Sci. Polym. Phys. Ed.*, 23, 683, 1985.

86. V. T. Trlong, P. E. M. Allen, D. R. G. Williams, *Eur. Polym. J.*, 23(8), 595, 1987.

87. A. N. Gent and A. G. Thomas, *J. Polym. Sci.*, A-2, 10, 571, 1972.

88. R. W. Nunes, J. R. Martin, J. F. Johnson, *Polym. Eng. Sci.*, 22(4), 205, 1982.

89. P. I. Vincent, *Polymer*, 1, 425, 1960.

90. D. Adolf, M. Tirrell, S. Prager, *J. Polym. Sci. Polym. Phys. Ed.*, 23, 413, 1985.

91. A. G. Mikos, N. A. Peppas, *J. Chem. Phys.*, 88(2), 337, 1988.

92. S. M. Aharoni, *Macromolecules*, 18, 2624, 1985.

93. J. L. Bitner, J. L. Rushford, W. S. Rose, D. L. Hunston and C. K. Riew, *J. Adhesion*, 13, 3, 1981.

94. R. A. Fraser, I. M. Ward, *Polymer*, 19, 220, 1978.

95. D. L. Hunston, J. L. Rushford, J. L. Bitner, J. Oroshnik and W. S. Rose, *J. Elastomers and Plastics*, 12, 133, 1980.

96. E. J. Kramer, *J. Mater. Sci.*, 14, 1381, 1978.

97. R. P. Kuzy and M. J. Katz, *Polymer*, 19, 1345, 1978.

98. G. L. Pitman, I. M. Ward, *Polymer*, 20, 895, 1979.

99. G. Allen, D. C. W. Morley and T. Williams, *J. Mat. Sci.*, 8, 1449, 1973.

100. G. L. Pitman, I. M. Ward, R. A. Duckett, *J. Mat. Sci.*, 13, 2092, 1978.

101. R. May, *in Ency. Polym. Sci. & Eng. (2nd ed.)*, V12, John Wiley & Sons, NY, 313, 1987.

102. R. B. Rigby, *in Eng. Thermoplastics*, J. M. Margolis ed., Marcel Dekker, NY, 299, 1985.

103. I. Y. Chang, *33rd Int. SAMPE Symp.*, 194, 1988.

104. J. F. Pratte, W. H. Krueger, I. Y. Chang, *34th Int. SAMPE Symp.*, 2229, 1989.

105. Victrex PEK Characterization Data, ICI, 1989.

106. Y. Lee, R. S. Porter, *Polym. Eng. Sci.*, 26(9), 633, 1986.

107. J. T. Hartness, *SAMPE Journal*, 20(5), 26, 1984.

108. S. Y. Hobbs, *Nature Phys. Sci.*, 234, 12, 1971.

109. S. D. Wu, J. L. Hedrick, D. K. Mohanty, B. K. Carter, G. L. Wilkes, J. E. McGrath, *31st Int. SAMPE Symp.*, 933, 1986.

110. R. T. Morrison, R. N. Boyd, *Organic Chemistry (3rd ed.)*, Allyn and Bacon, 1973.

111. H. X. Nguyen, H. Ishida, *J. Polym. Sci. Polym. Phys. Ed.*, 24, 1079, 1986.

112. D. K. Mohanty, T. S. Lin, T. C. Ward, J. E. McGrath, *31st Int. SAMPE Symp.*, 945, 1986.

113. D. K. Mohanty, R. C. Lowery, G. D. Lyle, J. E. McGrath, *32nd Int. SAMPE Symp.*, 408, 1987.

114. G. Jarret, P. A. Staniland, *U. S. Pat. 3993628*, ICI, 1976.

115. C. M. Chan, S. Venkatraman, *J. Appl. Polym. Sci.*, 32, 5933, 1986.

116. R. J. Swedo, C. S. Marvel, *J. Polym. Sci. Polym. Chem. Ed.*, 17, 2815, 1979.

117. S. A. Thompson, R. J. Farris, *J. Appl. Polym. Sci.*, 36, 1113, 1988.

118. H. Stenzenberger, *in Struct. Adhesives: Develop. in Resins and Primers*, A. J. Kinloch ed., Elsevier Appl. Sci. Pub., 77, New York, 1986.

119. G. T. Kwiatkowski, L. M. Robenson, G. L. Brode, A. W. Bedwin, *J. Polym. Sci. Polym. Chem. Ed.*, 13, 961, 1975.

120. D. O. Hummel, K. U. Heinen, H. Stenzenberger, H. Siesier, *J. Appl. Polym. Sci.*, 18, 2015, 1974.

121. H. D. Stenzenberger, M. Herzog, P. Konig, W. Romer, W. Breitigam, *34th Int. SAMPE Symp.*, 1877, 1989.

122. H. Stenzenberger, *Brit. Polym. J.*, 20, 383, 1988.

123. H. D. Stenzenberger, W. Romer, P. M. Hergenrother, B. J. Jensen, *34th Int. SAMPE Symp.*, 2054, 1989.

124. H. D. Stenzenberger, P. Konig, M. Herzog, W. Romer, S. Pierce, *32nd Int. SAMPE Symp.*, 44, 1987.

125. H. D. Stenzenberger, W. Romer, M. Herzog, S. Pierce, M. Canning, K. Fear, *31st Int. SAMPE Symp.*, 920, 1986.

126. K. F. M. G. J. Scholle, H. Winter, *33rd Int. SAMPE Symp.*, 1109, 1988.

127. M. T. Blair, P. a. Steiner, E. N. Willis, *33rd Int. SAMPE Symp.*, 524, 1988.

128. H. D. Stenzenberger, W. Romer, M. Herzog, P. Konig, *33rd Int. SAMPE Symp.*, 1546, 1988.

129. C. R. Lin, W. L. Liu, J. T. Hu, *34th Int. SAMPE Symp.*, 1803, 1989.

130. T. Abraham, *J. Polym. Sci. Polym. Lett.*, 26, 521, 1988.

131. D. Webster, *Ph D. Thesis*, Virginia Tech, 1986.

132. American Standard Testing Method E-399.

133. J. Cecere, *Ph D. Thesis*, Virginia Tech, 1988.

134. J. G. Williams, *Fracture Mechanics of Polymers*, Ellis Horwood/Wiley, 1985.

135. A. S. Holik, R. P. Kambour, D. G. Fink and S. Y. Hobbs, *Microstructural Science*, 7, 357, 1979.

136. R. C. Weast ed., *CRC Handbook of Chemistry and Physics*, CRC Press Inc., 1980.

137. A. J. Kinloch, S. J. Shaw, *J. Adhesion*, 12, 59, 1981.

138. E. E. Theotokoglou, G. Tsamasphyros, *J. Appl. Polym. Sci.*, 31, 163, 1986.

139. L. Engel, H. Klingele, G. Ehrenstein and H. Schaper, *An Atlas of Polymer Damage*, Prentice-Hall Inc., Englewood Cliffs, NJ, 1981.

140. Mike Takemori, *Private Communications*, General Electric Corporation, 1988.

141. T. H. Yoon, *Private Communications*, Virginia Tech, 1990.

142. E. Plati, J. G. Williams, *Polym. Eng. Sci.*, 15, 470, 1975.

VITA

James Steven Senger was born on December 6, 1961 and raised in a traditional American middleclass family in the suburbs of Baltimore, Maryland. In 1979 he graduated from Towson Senior High School and entered the engineering program at Virginia Tech. In 1983 he received a B.S. in Chemical Engineering. Unready to leave the security of school and enter the real world, Jim decided to continue his education by entering the graduate level polymer program at Virginia Tech., where under the direction of Professor James E. McGrath he received his M.S. degree in chemistry in 1987 and a Ph.D. in materials engineering science in 1990. Jim is currently employed as a senior engineer in the plastics divison of Ciba Geigy Corp. in Ardsley, New York.